

**GRAPHENE COLLOIDAL DISPERSIONS:
PRODUCTION AND PROCESSING FOR NANOCOMPOSITES
AND THREE-DIMENSIONAL NETWORKS**

A Dissertation

by

DORSA PARVIZ

Submitted to the Office of Graduate and Professional Studies of
Texas A&M University
in partial fulfillment of the requirements for the degree of

DOCTOR OF PHILOSOPHY

Chair of Committee,	Micah J. Green
Committee Members,	Mustafa Akbulut
	Yossef Elabd
	Jamie Grunlan
Head of Department,	Nazmul Karim

August, 2016

Major Subject: Chemical Engineering

Copyright 2016, Dorsa Parviz

ABSTRACT

Graphene, a two-dimensional layer of carbon atoms, is prized for its extraordinary properties including high electrical and thermal conductivities, surface area and exceptional mechanical strength. These supreme properties make it a promising material for applications such as electronics, nanocomposites, and energy storage devices. The scalable and repeatable production of high-quality graphene in large quantities is a challenging task. Among all the various production methods, the liquid-phase exfoliation from graphite is a promising technique due to its potential scalability, low cost, and simplicity of processing. Yet, the reaggregation of graphene sheets in the liquid, caused by the strong inter-sheets attractive forces, restricts the graphene yield of this method.

One of the main goals of this thesis is to increase the yield of liquid-phase exfoliation method without compromising on the graphene quality. Non-covalent functionalization of graphene with specific dispersant molecules prevents reaggregation of the sheets and increases the graphene concentration in dispersions, while it preserves the π -conjugated network of the nanosheets. Here, pyrene-derivatives are used as dispersants to stabilize pristine graphene in aqueous dispersions through non-covalent functionalization. We study the dependence of the graphene yield on the dispersant concentration, functional groups, counterions, solvent choice, and pH of solution. The graphene yield and graphene/dispersant ratio obtained by pyrene derivatives exceeds those obtained by polymers and surfactants.

The pyrene-graphene interactions are then exploited for designing novel copolymer dispersants which can improve the graphene dispersion in polymer

nanocomposites. Normally, the incompatibility of pristine graphene surface energy with polymers increases the interfacial tension within the nanocomposites and prevents proper dispersion of the graphene nanosheets. The pyrene-polysiloxane copolymers, synthesized through a hydrosilylation reaction, act both as graphene stabilizers in the dispersions and the host matrix of the resulting nanocomposite. The graphene/polysiloxane composite films are cast from the dispersion and their electrical properties and morphological structure is characterized by various techniques. Similar strategy is used to prepare pyrene-functional copolymers of polystyrene (PS) and poly(methylmethacrylate) (PMMA) as graphene dispersants. The graphene dispersions prepared by these dispersant are vacuum filtered to yield Janus graphene/PS and graphene/PMMA composite films with one electrically-conductive side and another electrically-insulating side.

In order to prepare aggregation-resistant graphene powder, we crumple graphene nanosheets via rapid evaporation of the dispersions in an industrially scalable spray dryer. Morphological transition of 2D nanosheets to 3D crumpled particles is directly observed by sample collection within the spray dryer. The particle size and morphology of the crumpled sheets is tuned by adjusting the Peclet number of spray drying process. The unfolding of the crumpled particles upon rewetting depends on the sheet type and the solvent choice. The crumpled GO nanosheets are then used to prepare porous 3D networks of graphene using an aqueous sol-gel technique. The high surface area and electrical conductivity of these networks can be exploited in applications such as energy storage, chemical sensing, oil adsorption and catalysis.

ACKNOWLEDGEMENTS

Dr. Green, thanks for the advice and encouragement you have given me over these years. It is amazing to have an advisor who cares about your needs, helps you with your choices and guides you through your research and career path. I have learned more than just scientific concepts from you. You taught me how to approach a problem to find practical answers and how to organize my thoughts in a systematic and presentable manner. I have applied all these skills in other aspects of my life and I am so grateful for that.

I would also like to thank Dr. Ronald Hedden, for all those brainstorming sessions that we had and his advice over our common research projects. I am also thankful to Dr. Grunlan, Dr. Elabd and Dr. Akbulut for their valuable input as my committee members. I would also like to acknowledge all of my colleagues, past and current members of the Green group. Special thanks to Sriya, Irin, Morgan, and Yueyi, it would have been impossible to complete my work without you girls. You girls were always inspirational and a great source of help. Ahmed, Tanvir, Rozana, Brandon, you guys were always available during my time of need. The new graduate students in our group: Touseef, Smit, and Martin, there was never a dull moment with you all. Whenever my experiments were not cooperating, you always raised my spirits. To the countless undergraduates who have worked in Green's group, thank you for all those joyful moments. Also, I thank the funding agencies: National Science Foundation (NSF), Airforce Office of Scientific Research (AFOSR) and DuPont.

To my parents, you are my original source of inspiration; you are the ones to fuel my thirst for knowledge and intellectual curiosity. There are not enough pages in this thesis to convey how thankful I am for all of your constant support and encouragement throughout the years. You have showered me with love, helped me to expand my horizons, and always were present when I needed you the most. Even though you always knew I would get my PhD, it still must be a surprise that it is in chemical engineering! To my lovely, fun and wise younger brother, you are my best friend and no matter what happen, I will always seek your advice, even if it is for photoshopping TEM images.

TABLE OF CONTENTS

	Page
ABSTRACT	ii
ACKNOWLEDGEMENTS	iv
TABLE OF CONTENTS	vi
LIST OF FIGURES.....	x
LIST OF TABLES	xviii
CHAPTER I INTRODUCTION	1
1.1 Motivation.....	1
1.2 Goals and outline of thesis.....	3
CHAPTER II GRAPHENE: STRUCTURE, PROPERTIES, PRODUCTION AND APPLICATION.....	8
2.1 History of graphene	8
2.2 Structure of graphene.....	9
2.2.1 Atomic structure	9
2.2.2 Electronic structure	11
2.2.3 Chemical structure	12
2.3 Graphene properties.....	14
2.3.1 Electrical properties	14
2.3.2 Mechanical properties.....	15
2.3.3 Thermal properties.....	15
2.3.4 Optical properties.....	16
2.3.5 Other properties	17
2.4 Other graphene derivatives.....	17
2.4.1 Graphene oxide (GO).....	17
2.4.2 Reduced graphene oxide (RGO).....	21
2.5 Production and synthesis of graphene	22
2.5.1 Bottom-up approach	28
2.5.2 Top-down approach	31
2.5.2.1 Exfoliation in solid phase.....	32
2.5.2.2 Exfoliation in liquid phase	34
2.5.2.2.1 Oxidation-exfoliation-reduction of graphite.....	36
2.5.2.2.2 Intercalation-exfoliation of graphite	38
2.5.2.2.3 Direct liquid-phase exfoliation	40
2.6 Conclusion.....	49

CHAPTER III GRAPHENE-BASED FUNCTIONAL MATERIALS	50
3.1 Graphene-polymer nanocomposites	50
3.1.1 Challenges and opportunities for graphene-polymer nanocomposites	50
3.1.2 Incorporation of graphene into polymer matrices.....	52
3.1.3 Modification of graphene-polymer interface	54
3.1.4 Fabrication of graphene-polymer nanocomposites.....	57
3.2 Graphene two-dimensional assemblies	59
3.2.1 Graphene-based thin films	60
3.2.2 Freestanding graphene-based papers	65
3.3 Graphene three-dimensional networks	66
3.4 Conclusion	73
CHAPTER IV GRAPHENE COLLOIDAL DISPERSIONS WITH PYRENE DERIVATIVES AS STABILIZERS	75
4.1 Introduction	75
4.2 Experimental procedures	77
4.2.1 Materials	77
4.2.2 Preparation of graphene dispersions	77
4.2.3 Preparation of graphene/epoxy composite.....	78
4.2.4 Characterization of graphene dispersions	79
4.2.5 Dispersion stability tests	80
4.2.6 Characterization of graphene/epoxy composites	81
4.3 Results and discussion	82
4.3.1 Quality of graphene sheets.....	82
4.3.2 Effectiveness of pyrene derivatives as graphene stabilizers	86
4.3.3 Graphene yield and processability	93
4.3.4 Stability of graphene dispersions.....	98
4.3.5 Graphene-polymer nanocomposites	101
4.4 Conclusion	103
CHAPTER V DESIGNER PYRENE-FUNCTIONAL STABILIZER FOR PRISTINE GRAPHENE/POLYSILOXANE CONDUCTIVE FILMS AND NETWORKS.....	105
5.1 Introduction	105
5.2 Background of the graphene/silicone nanocomposites	107
5.3 Experimental procedures	110
5.3.1 Materials	110
5.3.2 Synthesis of the pyrene-containing copolymers	110
5.3.3 Preparation of graphene dispersions	112
5.3.4 Preparation of graphene/copolymer composite films and networks.....	112
5.3.5 Characterization	113

5.4	Results and discussion	115
5.4.1	Design of pyrene-containing copolymer.....	115
5.4.2	Analysis of linear copolymers (PMPyS)	116
5.4.3	Graphene/copolymer (PMPyS-G) dispersions.....	120
5.4.4	Graphene/copolymer (PMPyS-G) films	123
5.4.5	Networks of self-crosslinking copolymer (PMPyS-N).....	126
5.4.6	Graphene/copolymer crosslinked networks (PMPyS-NG).....	129
5.5	Conclusion	131

CHAPTER VI JANUS FILMS OF PRISTINE GRAPHENE STABILIZED BY

PYRENE-FUCNTIONAL COPOLYMERS..... 133

6.1	Introduction	133
6.2	Experimental procedures	134
6.2.1	Materials	134
6.2.2	Synthesis of pyrene-containing copolymers	135
6.2.3	Preparation of graphene dispersions	136
6.2.4	Preparation of G/PMPMA and G/PSPMA Janus films	136
6.2.5	Characterization	137
6.3	Results and discussion	139
6.3.1	Analysis of pyrene-functional copolymers	139
6.3.2	Graphene/copolymer dispersion and films	143
6.4	Conclusions.....	151

CHAPTER VII CRUMPLING AND UNFOLDING OF SPRAY-DRIEDD

PRISTINE GRAPHENE AND GRAPHENE OXIDE NANOSHEETS 153

7.1	Introduction	153
7.2	Experimental procedures	156
7.2.1	Materials	156
7.2.2	Preparation of graphene dispersions	156
7.2.3	Spray drying of the dispersions	157
7.2.4	Characterization	157
7.3	Results and discussion	159
7.3.1	Crumpling of the nanosheets	159
7.3.2	Mechanism of nanosheets crumpling.....	163
7.3.3	Tuning crumpled particles morphology.....	168
7.3.4	Effect of dispersant and drying method.....	172
7.3.5	Unfolding of crumpled nanosheets	174
7.4	Conclusions.....	178

CHAPTER VIII MORPHOLOGY AND CROSSLINK CONTROL IN GRAPHENE

THREE-DIMENSIONAL NETWORKS..... 180

8.1	Introduction	180
8.2	Experimental procedures	183
8.2.1	Materials and methods	183
8.2.2	Characterization	184
8.3	Results and discussion	186
8.3.1	GO-catalyst interactions and bridging structures.....	186
8.3.2	GO morphology effects.....	190
8.4	Conclusion	194
CHAPTER IX CONCLUSION AND FUTURE WORK		196
9.1	Summary of thesis	196
9.1.1	Direct liquid-phase exfoliation of pristine graphene by pyrene derivatives .	196
9.1.2	Pyrene-based designer dispersant for graphene/polysiloxane composites .	197
9.1.3	Pyrene-functional PMMA & PS copolymers for Janus graphene films	198
9.1.4	Crumpling and unfolding of pristine graphene and graphene oxide sheets	198
9.1.5	Graphene conductive 3D networks with high surface area	199
9.2	Conclusions	200
9.3	Future research directions.....	202
REFERENCES.....		204

LIST OF FIGURES

	Page
Figure 2.1. (a) Atomic-resolution TEM image of a structurally perfect graphene sheet (reproduced from Dato <i>et al.</i> ¹⁴), (b) Atomic model of a corrugated large-area suspended graphene sheet (reproduced from Meyer <i>et al.</i> ⁹) and (c) Graphene as the building block of carbon buckyballs, carbon nanotubes and graphite (reproduced from Geim <i>et al.</i> ²).....	10
Figure 2.2. (a) Atomic model of various structural defects of a monolayer graphene sheets, (b) HRTEM image of similar structural defects on a monolayer graphene sheet (reproduced from Hashimoto <i>et al.</i> ²³), (c) The STEM image of the edge of a graphene layer (reproduced from Suenaga <i>et al.</i> ⁴¹), (d) schematic of different covalent fictionalizations of pristine graphene, and (e) schematic of different non-covalent functionalization of pristine graphene (reproduced from Rodriguez-Perez <i>et al.</i> ²¹).....	14
Figure 2.3. Most recent atomistic model of graphene oxide containing hydroxyl, carboxyl and epoxide functional groups (reproduced from Szabo <i>et al.</i> ⁷⁰).....	19
Figure 2.4. HRTEM images of (a) Pristine graphene, (b) GO, and (c) RGO. The graphitic area are shown in yellow, the oxidized regions are shown in red and holes are shown in blue (reproduced from Erickson <i>et al.</i> ⁷²).	22
Figure 2.5. Various graphene synthesis method and respective product quality and applications (reproduced from Sivudu <i>et al.</i> ¹⁰⁵).....	25
Figure 2.6. Categorization of main graphene production method based on their cost and product quality (reproduced from Ren <i>et al.</i> ¹⁰⁶).....	28
Figure 2.7. Main bottom-up graphene synthesis techniques (reproduced from Bonaccorso <i>et al.</i> ¹²³).....	31
Figure 2.8. Schematic of graphene production by (a) micromechanical cleavage reproduced from Bonaccorso <i>et al.</i> ¹²³), and (b) ball-milling (reproduced from Zhao <i>et al.</i> ¹³¹).....	33
Figure 2.9. Schematic of graphene production through oxidation-exfoliation-reduction route (reproduced from Ren <i>et al.</i> ¹⁰⁶).....	37
Figure 2.10. Schematic of graphene production through electrochemical intercalation-exfoliation route (reproduced from Ren <i>et al.</i> ¹⁰⁶)	39

Figure 2.11. Direct liquid-phase exfoliation of graphite into graphene sheets (adapted from Ren <i>et al.</i> ¹⁰⁶)	41
Figure 2.12. (a) Graphene concentration in various organic solvents vs. solvent surface tension plot reveals the optimum surface tension (40-50 mJ/m ²) for graphene dispersion, and (b) TEM image of few-layer graphene sheets in NMP dispersion (reproduced from Hernandez <i>et al.</i>).	44
Figure 2.13. Production of stable aqueous graphene dispersions in presence of dispersants.	45
Figure 3.1. Schematic of the covalent fictionalization of graphene with polystyrene using “grafting from” approach (reproduced from Fang <i>et al.</i> ²¹⁹).	56
Figure 3.2. Non-covalent functionalization of graphene by grafting pyrene-terminated PANIPAAm to its surface (reproduced from Liu <i>et al.</i> ²²²).	57
Figure 3.3. Fabrication of (a) graphene-polycarbonate nanocomposite through solution mixing and melt blending (reproduced from Shen <i>et al.</i> ²²⁷) , and (b) graphene-natural rubber nanocomposite through latex-mixing, melt mixing and hot-pressing (reproduced from Zhan <i>et al.</i> ²¹⁰).	58
Figure 3.4. (a) Typical graphene ink/solution used in the thin film fabrication, (b) a transparent graphene conductive thin film, (c) graphene-PVA composite thin film, (d) dip-coating of a substrate in graphene dispersion is another method for thin film fabrication, (e) rod-coating of graphene solution on substrate, (f) spray-caoting of graphen dispersion through air on the substrate, and (g) inkjet-printing using graphene ink (reproduced from Bonaccorso <i>et al.</i> ¹²³).	62
Figure 3.5. (a) Digital photo of flexible freestanding GO film, (b) SEM image of the cross-section of GO freestanding film (reproduced from Dikin <i>et al.</i> ²⁸¹), (c) digital photo of RGO freestanding films, and (d) SEM image of the cross-section of RGO freestanding film (reproduced from Chen <i>et al.</i> ²⁸⁵).	67
Figure 3.6. Hydrothermal synthesis of 3D graphene network, (a) digital photo of GO dispersions and GO hydrogel, (b) digital photo of the hydrothermally-reduced GO aerogels, and (c) SEM image of the microporous structure of the hydrothermally-reduced GO aerogel (reproduced form Xu <i>et al.</i> ²³³).	70
Figure 3.7. SEM images of RGO aerogels porous structure prepared by (a) sol-gel technique (reproduced from Worsley <i>et al.</i> ³¹⁴), and (b) freeze-casting technique (reproduced from Qui <i>et al.</i> ³¹⁹)	72
Figure 4.1. The molecular structure of various pyrene derivatives used in this study as graphene stabilizers.....	83

Figure 4.2. HRTEM images of the graphene sheets in Py-SASS-stabilized aqueous dispersion. Counting the number of the layers on the edge of the sheets reveals the few-layer nature of stabilized graphene. The sheet size varies between 2 to 3 μm	84
Figure 4.3. Raman spectra of expanded graphite and Py-SASS-stabilized graphene. Downward shift of the 2D band at 2675 cm^{-1} confirms the few-layer nature of the stabilized graphene. Presence of Py-SASS on the graphene surface appears in the broad shoulder bound to the 2D band.	85
Figure 4.4. Schematic of mechanism of pyrene derivatives adsorption on graphene surface.	86
Figure 4.5. Final concentration of graphene stabilized by different pyrene derivatives concentrations. The concentration of parent expanded graphite in all the dispersions was 20 mg/ml.	87
Figure 4.6. The number and position of functional groups affects the graphene concentration in the dispersions. a) Py-SASS assisted dispersion with final graphene concentration of 0.11 mg/ml and b) Py-(SO ₃) ₄ assisted dispersion with final graphene concentration of 0.04 mg/ml. The same concentration of stabilizer (1 mg/ml) was used in both samples.	90
Figure 4.7. Zeta potential changes with stabilizer concentration in Py-SASS-stabilized dispersions. The absolute value of the zeta potential decreased gradually with an increase in the Py-SASS concentration.	91
Figure 4.8. Thermogravimetric analysis of Py-SASS and freeze-dried Py-SASS/graphene powder.	93
Figure 4.9. Graphene concentration increases with addition of initial expanded graphite concentration.	95
Figure 4.10. The post-centrifugation graphene concentration in mixtures of ethanol/water. Ethanol was added to an aqueous dispersion of graphene to prepare dispersions with 10-90 vol.% of ethanol.	97
Figure 4.11. Redisperiosn of freeze-dried Py-SASS/graphene powder in water at original dispersion concentration.	98
Figure 4.12. zeta potential of graphene dispersion prepared with pyrene derivatives at different pH values. The original pH of the dispersions before any change by acid or base addition is mentioned in the parentheses in front of each pyrene derivative.	99

Figure 4.13. Flocculation and redispersion of PCA-stabilized graphene dispersion upon pH changes: a) The original dispersion at pH= 11, b) the destabilized dispersion after addition of acid at pH= 3 and c) the recovered dispersion after increasing the pH to 10.5 by addition of base. (Note that the concentration is lowered simply by dilution effects of the acid and base.).....	100
Figure 4.14. Visible stability of graphene dispersions against temperature changes.....	101
Figure 4.15. 0.5 wt % graphene/epoxy composites prepared by a) Doctor-blading and b) casting in a Teflon mold.....	102
Figure 4.16. SEM images of a) epoxy and b) Py-SASS stabilized graphene/epoxy composite.	102
Figure 5.1. Designing pyrene-based polymeric stabilizer for pristine graphene.....	109
Figure 5.2. Synthesis of PMPyS copolymer via grafting 1-ethynylpyrene to PDMS-PHMS copolymer backbone through a Pt-catalyzed hydrosilylation reaction.	116
Figure 5.3. Elution profiles of different PMPyS fractions from GPC (performed by Ziniu Yu).	117
Figure 5.4. FT-IR spectra of fraction 4 of the PMPyS sample (by Ziniu Yu)	118
Figure 5.5. GPC analysis of a fraction 4 of the PMPyS sample confirms the attachment of vinylpyrene groups to the polymer backbone (performed by Ziniu Yu)	119
Figure 5.6. UV-vis spectra of the copolymer precursors and all of the PMPyS fractions.	120
Figure 5.7. Graphene concentration variation vs. PMPyS fractions concentration; the pyrene content in the dispersions of all fractions was held constant at 1 mg/mL.....	122
Figure 5.8. HRTEM images of (a) graphene sheets stabilized by unfractionated PMPyS copolymer, the inset shows the fraction 4 graphene dispersion and (b) a graphene sheet in dispersion prepared by fraction 4 of the PMPyS copolymer, the inset shows the edge of the same graphene sheets and verifies the few-layer nature of stabilized graphene sheets.....	123
Figure 5.9. SEM images of (a) the top surface of the graphene/PDMS film (fraction 4) cast on the membrane and (b) cross section of the film on the membrane (inset shows digital image of the cast film). The average thickness of the sample is ~ 10 μm . This film has an electrical conductivity of 220 S/m.	124

Figure 5.10. DSC heating traces for fractions 2 and 6 of PMPyS and PMPyS-G samples (performed by Ziniu Yu).	126
Figure 5.11. (a) proposed mechanism of crosslinking of PMPyS-N copolymer, and (b) digital image of the crosslinked film of PMPyS-N.....	127
Figure 5.12. FT-IR spectra of the crosslinking copolymer precursors and the PMPyS-N products at various reaction times. (a) SiH peak, these peaks were present during the reaction and disappeared only after 7 days, (b) alkyne band peak, absence of this peak at 3294 cm^{-1} in the PMPyS copolymers indicated a lack of free 1-ethynylpyrene in the product, (c) a second band at 1508 cm^{-1} is indicative of a C=C: Pt complex formed after grafting of pyrene groups to the polymer chains and (d) $-\text{C}\equiv\text{C}-\text{H}$ peak which disappeared after the reaction.	128
Figure 5.13. SEM images of (a) top surface of the crosslinked graphene containing PMPyS-NG film (digital image of the sample is shown in the inset), and (b) cross-section of the graphene containing dispersion of the same sample cast on the PTFE membrane (digital image of the sample is shown in the inset).	129
Figure 5.14. (a) PDMS gel with (0.6 vol. %) and without graphene before swelling; (b) PDMS gel with and without graphene after swelling in chloroform. Scale bars are $\sim 1\text{ cm}$; (c) Soluble fraction of gel as measured from swelling study (performed by Ziniu Yu).	131
Figure 6.1. Proposed synthesis route of (a) PMPMA, and (b) PSPMA random copolymers. n and m represent the mole fractions of MMA/Styrene and pyrenemethyl methacrylate in the copolymer chain, respectively.	139
Figure 6.2. Absorbance spectra of pyrenemethyl methacrylate and the synthesized copolymers. The pyrene characteristic peak appears for all three samples at 348 nm (performed by Ziniu Yu).	140
Figure 6.3. Elution profiles of copolymers obtained from the GPC analysis (performed by Ziniu Yu).	141
Figure 6.4. Comparison of the copolymers elution profiles traced by the UV-vis and RI detectors (performed by Ziniu Yu)	141
Figure 6.5. HRTEM images of graphene sheets cast from dispersions of (a) graphene/PSPMA-15, and (b) graphene/PMPMA-15.....	144
Figure 6.6. Schematic of Janus graphene/copolymer film preparation by vacuum filtration.....	145

Figure 6.7. SEM images of the cross-section of (a and d) Janus graphene/PSPMA-10 and graphene/PMPMA-10 films, respectively (the inset shows the digital photo of the graphene/PSPMA-10 film), (b and f) polymer-rich sections of the Janus graphene/PSPMA-10 and graphene/PMPMA-10 films, respectively, and (e and h) graphene-rich sections of the Janus graphene/PSPMA-10 and graphene/PMPMA-10 films, respectively.	147
Figure 6.8. Thermogravimetric analysis of PSPMA-15 and PMPMA-15 copolymers.	148
Figure 6.9. Thermogravimetric analysis of Janus and cast films of graphene /PSPMA-10 and graphene/PSPMA-15.	149
Figure 6.10. Thermogravimetric analysis of Janus and cast films of graphene /PMPMA-10 and graphene/PMPMA-15.....	150
Figure 7.1. TEM images of nanosheets of (a) pristine graphene and (b) GO cast from the aqueous dispersions.	159
Figure 7.2. (a) SEM and (b and c) HRTEM images of crumpled nanosheets of pristine graphene. Dispersions of nanosheets were spray dried at atomizer pressure of 60 Psi and drying temperature of 220 °C. The concentration of nanosheets in dispersion was 0.1 mg/mL.	161
Figure 7.3. (a) SEM and (b and c) HRTEM images of crumpled nanosheets of GO. Dispersions of nanosheets were spray dried at atomizer pressure of 60 Psi and drying temperature of 220 °C. The concentration of nanosheets in dispersion is 0.1 mg/mL.	162
Figure 7.4. TEM images of the evolution of nanosheets during drying within the spray dryer, (a,b,c) pristine graphene and (d,e,f) GO nanosheets. Samples were collected on TEM grids which were fixed at different stages within the spray dryer. Stages were 10 cm apart from each other.....	164
Figure 7.5. HRTEM images of the edge folding phenomenon in pristine graphene nanosheets. Samples were collected directly on TEM grids at the second stage within the spray dryer.....	164
Figure 7.6. Proposed mechanism of crumpling for pristine graphene and graphene oxide nanosheets.	167
Figure 7.7. Effect of initial droplet size (varied by changing the atomizer pressure) on final morphology of the crumpled (a,b,c) pristine graphene and (d,e,f) GO nanosheets. Samples were dried at 120 °C and concentration of nanosheets in the dispersion was 0.1 mg/mL.	170

Figure 7.8. Effect of drying temperature on final morphology of crumpled (a,b,c) pristine graphene and (d,e,f) GO nanosheets. All the samples were sprayed at atomizer pressure of 40 psi and the concentration of the nanosheets in the dispersion was 0.1 mg/ml.	170
Figure 7.9. Effect of nanosheets concentration on the final morphology of (a,b) pristine graphene and (c,d) GO nanosheets. All the samples were sprayed at an atomizer pressure of 40 psi and dried at 170 °C.	171
Figure 7.10. Morphology of the freeze-dried (a) pristine graphene and (b) GO nanosheets.	172
Figure 7.11. Effect of the dispersant on crumpling of pristine graphene nanosheets. Pristine graphene nanosheets stabilized by (a) PVP, (b) PAM and (c) SDBS were sprayed at atomizer pressure of 60 psi and dried at 220°C.	173
Figure 7.12. TEM images of: a) Crumpled pristine graphene unfolding after hydration on TEM grid; b) Crumpled pristine graphene unfolding after redispersion in water; c) Crumpled GO remains crumpled after hydration on TEM grid; d) Crumpled GO remains crumpled and does not redisperse in water.	175
Figure 7.13. TEM images of (a,b) annealed crumpled GO nanosheets and (c,d) annealed crumpled GO nanosheets after rehydration on the TEM grid. Annealing of the crumpled nanosheets was carried under nitrogen atmosphere and at 600 °C.	176
Figure 7.14. We attempted to redisperse crumpled pristine graphene in (a) ethanol, (b) acetone, and (c) chloroform. Aggregation was observed for ethanol and acetone but redispersion (but not unfolding) occurred in chloroform.	178
Figure 8.1. Images of (a) as-synthesized GO hydrogel, and (b) GO aerogel dried using CPD.	187
Figure 8.2. SEM images of GO aerogels prepared with (a and b) 2 and 1 wt % of GO content, respectively,(3.6 ml of ammonia was used), and (c and d) 1 wt% GO content using 3.6 and 1.8 ml of ammonia, respectively.	188
Figure 8.3. Proposed mechanism for gel crosslinking and bridge formation. (a) high catalyst/GO ratio (0.024), (b) low catalyst/GO ratio (0.012), (scalebars ~ 1 μm in SEM images).	189
Figure 8.4. SEM images of CGO aerogels prepared using (a and b) CGO particles sprayed at 150 °C, and (c and d) CGO particles sprayed at 120 °C (the inset shows the CGO particles morphology sprayed at 120 °C).	191

Figure 8.5. SEM images of aerogels prepared using CGO/GO ratios of (a and b) 0.3
(c and d) 1, and (e and f) 3. All the CGO particles were sprayed at 120 °C. 192

Figure 8.6. Thermogravimetric characterization of GO and CGO aerogels. 194

LIST OF TABLES

	Page
Table 2.1. Property-application relationships for graphene sheets. Here, a thick indicates importance, cross indicates unimportance and square means the property is sometimes important (reproduced from Edwards et al. ⁸⁶).	23
Table 4.1. Effect of functional groups on the graphene yield. The effectiveness of the functional groups changes in the order of sulfonyl > carboxyl > amine.	88
Table 4.2. Effectiveness of surfactants, polymers and pyrene derivatives as graphene stabilizers compared by their graphene yield and graphene/stabilizer ratio.	94
Table 4.3. Average particle size in sulfonyl-containing graphene dispersions at various pH values measured by DLS technique.	99
Table 4.4. Mechanical and electrical properties of 0.5 wt% PVP- and Py-SASS-stabilized graphene/epoxy composites.	103
Table 5.1. Molar masses of the PMPyS fractions obtained from GPC analysis (performed by Ziniu Yu).	117
Table 5.2. Pyrene content of different PMPyS fractions (based on the area under UV-vis spectra of each fraction).	120
Table 6.1. Number average molecular weight (M _n) and polydispersity index (PDI) of the copolymers obtained from the GPC results, using the UV-vis and RI detectors (prepared by Ziniu Yu).	143
Table 6.2. Electrical conductivity and graphene content of the Janus and cast films of graphene/PSPMA and graphene/PMPMA samples.	151
Table 8.1. The electrical conductivities and BET surface areas of the aerogels. All these gels were prepared using 3.6 ml of ammonia as the catalyst. All the CGO particles were sprayed at 120 °C.	193

CHAPTER I

INTRODUCTION

1.1 Motivation

The scientific and technological developments over the last few decades have globally touched our life styles; nowadays, we demand faster data processing and storage systems, stronger and lighter structural materials, sustainable energy supply, precision medicines, and targeted drug delivery. Hence, the urge to create new materials with properties to satisfy the consumer demands has been the deepest motivation for scientists all around the globe. With improvements in electron and atomic microscopy techniques, it has become feasible to resolve and manipulate the materials structure at nanoscale. The discovery of fullerenes and carbon nanotubes (CNT), two carbonaceous materials with nanometer-size dimensions, is one of the main outcomes of the search for novel materials in the “era of nanotechnology”. Like some other nanomaterials, CNTs present an extraordinary combination of material properties including electrical, thermal, mechanical and optical properties. Exploring the possible synthetic routes for preparation of CNTs and developing methods to apply their properties in existing technologies have led to discovery of a new carbon nanomaterial, called “graphene”.

Graphene, a single layer of carbon atoms arranged in a honeycomb lattice, is the first two-dimensional atomic crystal that was identified in the lab in 2004 by Andre Geim and Konstantin Novoselov. The achievement was a scientific breakthrough which brought the 2010 Nobel Prize of physics to them. The theoretical studies have predicted

extremely high electrical and thermal conductivities, exceptional mechanical strength and elasticity, and high surface area for graphene. The experimental measurements performed on a single layer of graphene, exfoliated from HOPG (highly ordered pyrolytic graphite), verified the theoretical predictions. Ever since, researchers from all different scientific disciplines have explored its potential applications in preparation of electronic devices, composite materials, sensors, energy conversion and storage, and biomedical devices. Some researchers have claimed that graphene will replace the traditional materials like silicon in the existing electronic products market.

Although graphene shows a lot of promise for future applications, there are many challenges that need to be embraced and overcome before it can be adopted by the modern technologies. The main obstacle is the repeatable production of high-quality graphene in large quantities. Various methods have been developed to prepare graphene with qualities that meet the requirements of specific applications. The products of these methods are different in dimensions, defects density and electronic structure and offer a broad range of quality and properties. Yet, a scalable approach that is capable of producing graphene batches with similar properties is highly desirable. More importantly, the transition from atomic-scale graphene sheet to the bulk graphene-based products is associated with drastic changes in the properties. Thus, the lab-scale models of such products have to be precisely investigated to pave the way for design and manufacturing of graphene-based functional materials with industrial purposes. Furthermore, the graphene production and incorporation into the final products must

remain economic to meet the end-user expectations. Otherwise, the graphene products commercialization, like CNT products, will be hindered by economic considerations.

Among all the graphene production methods, the liquid-phase exfoliation of graphene from graphite is a promising approach for scalable production of larger amounts of graphene. However, this method is restrained by the strong attractive forces between graphene sheets which cause reaggregation in the liquid phase. Thus, strategies need to be developed to prevent reaggregation of the sheets and enhance their processability in the liquid phase. Also, the strong inter-sheet attraction and surface chemistry of graphene make is incompatible with many other materials such as polymers. To process graphene sheets in presence of these materials, the graphene surface has to be modified. However, the modification of graphene surface must preserve the structure and quality of the original graphene sheets. Additionally, alternative approaches that enable the production of aggregation-resistant graphene sheets and their bulk macroscale structures are highly demanded.

1.2 Goals and outline of thesis

Facile and inexpensive production of graphene that suits composite material and energy storage applications is the main theme of this thesis. Our goals can be categorized as follows: *(1) preparation of stable graphene colloidal dispersions, (2) modification of graphene sheets into a more polymer-compatible surface, (3) morphological transition of graphene to prepare aggregation-resistant sheets, and (4) assembly of the graphene sheets in a three-dimensional network.* To achieve these goals, a specific class of

dispersants was used to stabilize graphene in water. Also, graphene-philic copolymers have been synthesized and used for preparation of graphene-polymer nanocomposites. Moreover, graphene sheets have been crumpled into 3D morphology to produce aggregation-resistant particles. Finally, the graphene planar 2D and crumpled 3D sheets were used to prepare graphene hydrogels and aerogels.

Chapter II of the thesis is a review of the graphene structure, properties and production methods. The graphene atomic, electronic and chemical structure is discussed in this chapter. Electrical, mechanical, thermal and optical properties of graphene are explained. Also, other graphene derivatives including graphene oxide (GO) and reduced graphene oxide (RGO), their molecular structure and properties are introduced. Then, the main approaches of graphene production are discussed with an emphasis on the processing-structure-property relationships in their products and their suitability for various applications. The bottoms-up and top-down methods with their advantages and disadvantages are introduced. The liquid-phase exfoliation of graphene and its variation based on the starting material, processing techniques and the product quality are extensively discussed.

In *Chapter III*, the graphene-based materials for various applications along with their fabrication methods are introduced to the reader. First, the graphene-polymer nanocomposites and their current fabrication methods are reviewed. The challenges for fabrication of nanocomposites and the possible strategies to overcome those challenges are discussed. Next, the two-dimensional assemblies of graphene including graphene thin films and freestanding papers are presented. The fabrication methods and the

potential application of these materials are also explained. Finally, the three-dimensional graphene structures are introduced and their fabrication methods are reviewed in details.

In *Chapter IV*, our work on preparation of colloidal graphene dispersions using pyrene-derivatives is presented. The quality of graphene sheets is investigated and the mechanism of graphene stabilization by these dispersants is studied. The effects of various parameters such as dispersant functional groups, counterions, concentration and pH of dispersion on the graphene yield are evaluated. The yield of graphene in these dispersions proves the higher efficiency of these dispersants as graphene stabilizers compared to surfactants and polymers. Also, the stability and processability of these dispersions at various pH and temperatures are assessed. The dispersions are then used to prepare graphene-epoxy composites; the enhancement of composite mechanical and electrical properties upon addition of graphene is evaluated.

Chapter V describes the design and synthesis of a graphene-philic copolymer through grafting pyrene groups to the polymer backbone. The pyrene groups are grafted to the polysiloxane backbone via hydrosilylation reaction. The pyrene-functional polysiloxane copolymer acts as the graphene stabilizer in the dispersions, and as the host matrix in the resulting nanocomposite. This designer dispersant improves the non-covalent interactions at graphene-polymer interface to enhance the compatibility and the dispersion of graphene within the polymer matrix. The graphene dispersions are prepared in solvent and cast to form highly conductive graphene/polysiloxane films. The variation of polymer synthesis chemistry leads to formation of conductive self-crosslinking networks of graphene/polysiloxane.

In *Chapter VI*, we apply the designer stabilizer strategy to prepare pyrene-functional polystyrene (PS) and poly(methylmethacrylate) (PMMA) copolymers. These copolymers stabilize graphene through the non-covalent interactions of pyrene and graphene. Vacuum filtration of the resulting graphene dispersions leads to formation of Janus graphene composite films with an electrically-conductive side and another electrically-insulating side. We demonstrate that formation of this specific structure is feasible through leaching of the unbound polymer chains from the graphene film.

Chapter VII describes the crumpling of graphene sheets into three-dimensional semi-spherical particles via spray drying the graphene dispersions. The π - π stacking of the crumpled graphene sheets is less likely to occur and thus, these particles are prone to aggregation. The mechanism of the morphological transition from 2D sheets to 3D particles is observed by collecting samples within the spray dryer during the process. Also, we demonstrate that the crumpling behavior of the sheets depends on their surface chemistry and elasticity and differs for graphene oxide and pristine graphene. It is possible to tune the product morphology and size by adjusting the Peclet number of the drying process. Furthermore, the stability of the crumpled particles against rewetting with various solvents is evaluated.

In *Chapter VIII* we study the formation of graphene 3D networks through a sol-gel transition in graphene oxide aqueous dispersions. We indicate that the gelation occurs due to the partial reduction and simultaneous crosslinking of the sheets and. The reduction of the nanosheets triggers the π - π stacking between the reduced sections and creates physical crosslinks, whereas the covalent bond formation between functional

groups of the GO nanosheets forms chemical crosslinks. We study the effect of GO concentration and catalyst/GO ratio on crosslinking mechanism. We also assess the effect of nanosheets morphology on the crosslinks density in the aerogels by using crumpled graphene oxide particles as the GO source. To correlate the morphology of aerogels with their bulk properties, we measure their electrical conductivity, surface area and thermal stability.

Chapter IX summarizes the results of all the previous chapters. It also contains concluding remarks about the importance of graphene dispersants, the design of novel dispersants for nanocomposite applications, the mechanism of morphological transition in nanosheets, and the application of crumpled graphene in 3D networks preparation. Finally, the potential future research directions that can be followed based on the current thesis is described.

CHAPTER II

GRAPHENE: STRUCTURE, PROPERTIES, PRODUCTION AND APPLICATION

2.1 History of graphene

Graphene is the most recent addition to the carbon allotropes family consisting of graphite, diamond, carbon nanotubes (CNT) and fullerenes. It is a freestanding atomic layer of sp^2 hybridized carbon atoms which was first isolated from HOPG (highly ordered pyrolytic graphite) and indentified in the lab in 2004.¹ This achievement brought the 2010 Nobel Prize of physics to Professor Geim and Professor Novoselov at the University of Manchester. The subsequent experiments revealed its exceptional electrical, mechanical, optical, and thermal properties. Ever since, Scientists of all research backgrounds have explored its potential applications in electronics, photonics, spintronics, composites, and energy conversion and storage.

Despite the enormous recent excitement, graphene has been known since 1940s in scientific communities.² However, it was only depicted as a theoretical 2D crystal such that its existence in real world was considered to be thermodynamically unfavorable and thus, impossible. In fact, it was believed that such an atomic thin 2D crystal cannot sustain the thermal fluctuations at room temperature and its structures would collapse due to atomic dislocations and defects.² If such a structure existed, it should be embedded in a 3D structure as graphite.²⁻⁴ Many scientists tried to grow a graphene layer on a substrate, particularly by adopting the chemical vapor deposition

(CVD) technique used for carbon nanotubes growth on SiC substrate.^{5,6} Unfortunately, most of these attempts were not capable of producing a large, single layer and defect-free “pristine graphene” sheet. It was not until 2004, the year that Geim and Novoselov isolated graphene using the “scotch-tape” method (mechanical cleavage), that a single layer of pristine graphene was introduced to the world.^{1,7} Since then, enormous effort has been dedicated to devise various methods for graphene production such as epitaxial growth, organic synthesis and solid- or liquid-phase exfoliation.^{8,9}

2.2 Structure of graphene

2.2.1 Atomic structure

Graphene is a 2D monolayer of carbon atoms arranged into a honeycomb lattice. Each carbon atom is connected to three other carbon atoms with covalent σ bonds of 0.142 nm length.¹⁰ The angle between the bonds is 120° . Also, each carbon atom shares a delocalized double bond with adjacent atoms through its π orbital which is located above and below the lattice plane. Such a sp^2 hybridization of carbon atoms contributes to the delocalized network of π electrons and forms a conjugated system along the graphene layer. This 2D crystal may be a few microns in lateral size and is only terminated at the edges by sp^3 hybridized carbon atoms bonded to hydrogen atoms. Such a thin layer of graphene may be pictures as a flat sheet; however, studies have shown that some “rippling” occurs on the surface of freestanding graphene sheet.^{2,9} The rippling intensifies with an increase in the sheet lateral size.¹¹ Additionally, surface roughness of

a graphene sheet captured on a substrate is different than a freestanding one due to the interactions with the substrate.¹²

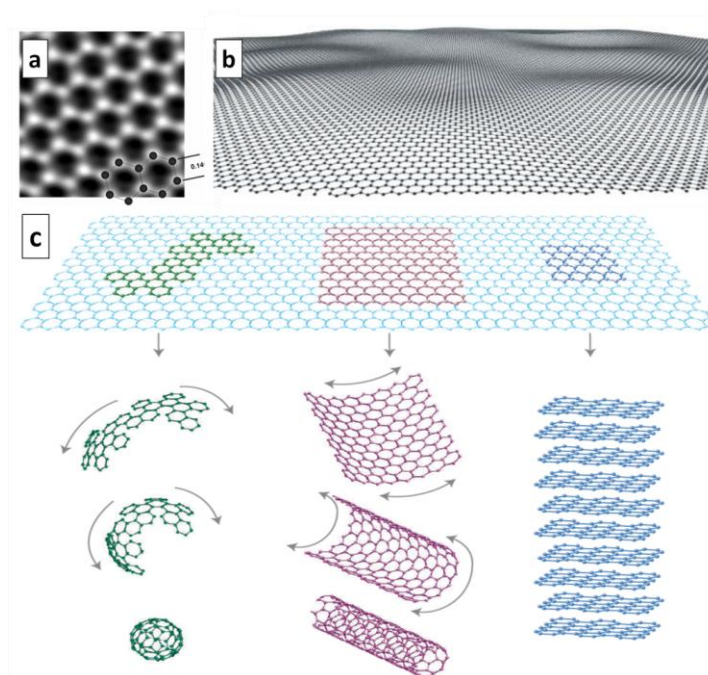


Figure 2.1. (a) Atomic-resolution TEM image of a structurally perfect graphene sheet (reproduced from Dato *et al.*¹⁴), (b) Atomic model of a corrugated large-area suspended graphene sheet (reproduced from Meyer *et al.*⁹) and (c) Graphene as the building block of carbon buckyballs, carbon nanotubes and graphite (reproduced from Geim *et al.*²).

A graphene layer can be theoretically considered as the building block of other carbon nanomaterials including fullerenes and carbon nanotubes (Figure 2.1). In reality, graphene layers stack on top of each other to make graphite with interlayer spacing of 0.335 nm.² Stacking of graphene layers occurs through sharing their π orbital electrons. Attention must be paid to this stacking phenomenon, as it draws a distinction between

graphene and graphite.² A single layer graphene sheet (SLG) poses specific atomic and material properties which will be mentioned in the next section in this text. A bilayer graphene represents almost similar properties, but further increase in the number of layers changes the properties drastically and makes the sheets with more than 10 layers of graphene to resemble graphite rather than a SLG sheet.¹³ Any graphene sheet with 2-10 layers is called few-layer graphene (FLG).²

2.2.2 Electronic structure

A graphene layer has one type of electron and one type of hole as charge carriers. These charge carriers behave as massless relativistic particles (known as Dirac Fermions) when subjected to a magnetic field.⁷ The nature of these charge carriers resembles electrons which have lost their rest mass and their behavior could be described by a (2+1) dimensional Dirac equation.^{2,7,15} The carrier mobility in single layer graphene is exceptionally high.¹ The rapid carrier transport could be attributed to the low defect density in pristine graphene, which allows the carriers to travel long interatomic distances without being scattered, a phenomenon known as “ballistic transport”.¹⁶ Defects, impurities and surface roughness (wrinkles and ridges) may act as scattering sites and reduce the carrier mean free path. Therefore, the carrier mobility measurement highly depends on the graphene quality and also its interactions with the substrates and surrounding environment.¹⁷ Carrier motilities up to $15,000 \text{ cm}^2/\text{Vs}$ have been measured at ambient conditions.^{1,7,15} Impurity-induced scattering was minimized by measurements

under vacuum for a mechanically-exfoliated freestanding graphene layer and carrier mobilities as high as $200,000 \text{ cm}^2/\text{Vs}$ were obtained.¹⁸

The other extraordinary electronic property of graphene is the fact that single layer graphene is a zero band gap semiconductor.^{1,7} The valence and conduction bands of graphene meet at the neutrality point (Dirac point). The carrier transport in such a structure is ambipolar; meaning that the charge carrier can be tuned between holes and electrons by applying a proper gate voltage. A positive gate bias promotes electrons as carriers and a negative gate bias makes holes the dominant carriers.^{2,7,18}

All the above-mentioned structural properties belong to single-layer graphene and to some extent to bilayers. Addition of more layers to graphene, as in few-layer graphene, potentially alters the electronic state, band structure and carrier transport due to the interlayer interactions.^{13,19}

2.2.3 Chemical structure

Pristine graphene sheet exhibits very low chemical reactivity due to its atomic-thin flat structure.²⁰ The lack of curvature in graphene 2D morphology hinders its reactivity compared to CNTs and fullerenes.²¹ As expected, pristine graphene is a hydrophobic material and prone to agglomeration in water. It is not soluble in most organic solvents and remains inert in presence of air at temperatures up to $\sim 250 \text{ }^\circ\text{C}$. On the other hand, the atomic structure of a graphene layer is not always perfect; it contains topological defects (pentagons and heptagons instead of hexagonal rings), vacancies (missing atoms), adatoms (extra atoms) and impurities adsorbed on the surface (Figure

2.2a and b).^{22,23} The presence of these defective sites on the graphene increases its reactivity.^{21,24} Also, the surface corrugation is expected to induce some defects and local high-energy sites which may participate in chemical reactions.²¹

Because of the difference in carbon atom hybridization at the basal plane and the edges, the chemical reactivity of these locations is not similar (Figure 2.2c). The sp^3 -hybridized edges are more reactive and open to accept covalent functionalization.²⁵ In contrary, the basal plane requires a sp^2 to sp^3 transformation to become reactive. Such a transformation is energy consuming and perturbs the π -conjugated system. Therefore, highly energetic species are needed to attack the π network of the basal plane in order to create covalent functionalization on the basal plane (Figure 2.2d). The edges of pristine graphene have been decorated by hydrogen atoms and stronger bonds with fluorine.^{21,26-}
²⁹ Additionally, nitrogen-containing groups have been covalently attached to the basal plane of graphene through the reaction of energetic free radicals such as aryl diazonium salts and benzoyl peroxide and dienophiles such as azomethine ylide with the C=C bond in the π system.³⁰⁻³² Oxidation reactions that introduce oxygen-containing functional groups to the pristine graphene surface will be discussed later in Section 2.4.1.

The non-covalent functionalization of graphene occurs through π - π interaction with other chemical species (Figure 2.2e). Small organic molecules, polyaromatic hydrocarbons such as pyrene,³³ porphyrin³⁴ and perylene,³⁵ surfactants,^{36,37} polymers,^{38,39} and electron-donors and -acceptors such as aniline and nitrobenzene⁴⁰ are a few examples of the chemical species whose adsorption and vdW interactions with graphene basal plane have been studied.²¹

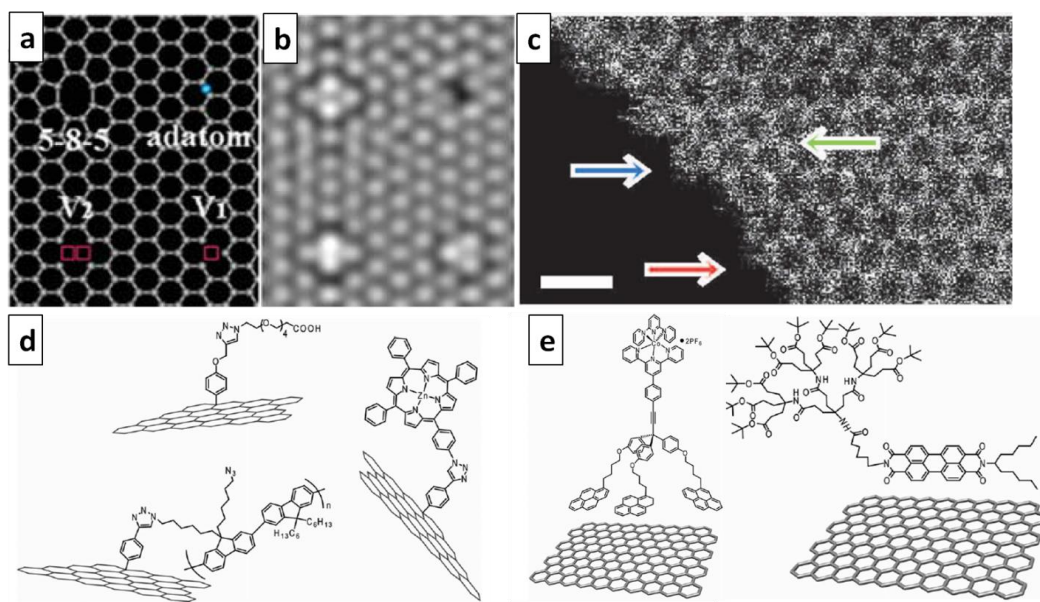


Figure 2.2. (a) Atomic model of various structural defects of a monolayer graphene sheets, (b) HRTEM image of similar structural defects on a monolayer graphene sheet (reproduced from Hashimoto *et al.*²³), (c) The STEM image of the edge of a graphene layer (reproduced from Suenaga *et al.*⁴¹), (d) schematic of different covalent functionalizations of pristine graphene, and (e) schematic of different non-covalent functionalization of pristine graphene (reproduced from Rodriguez-Perez *et al.*²¹).

2.3 Graphene properties

2.3.1 Electrical properties

As was mentioned earlier, graphene has an extraordinary electronic structure. The rapid charge transport along the basal plane is the origin of its high electrical conductivity.² The highest value of electrical conductivity that has been reported for a freestanding SLG is 6000 S/cm. The corresponding resistivity was in the range of 10^{-6} Ω .m which is 100 times lower than that of silver.¹⁶ Obviously, these values change as the number of the layers or the defects density increase in the graphene sheet.

2.3.2 Mechanical properties

Theoretical studies and simulations anticipated that a pristine single-layer graphene exhibits spectacular mechanical properties because of its sp^2 -hybridized carbon structure which provide the three-fold coordinated covalent C-C bonds along the surface.⁴² An AFM nanoindentation technique (with a diamond AFM tip) was used to measure the breaking strength and strain of a graphene monolayer suspended over a silicon wafer substrate. A fracture strain of 25% was obtained for this sample and the corresponding intrinsic tensile strength and the Young's modulus were 130 GPa and ~ 1 TPa, respectively.⁴³ This experiment and a couple of similar measurements confirmed that graphene is the strongest material ever measured and could supersede strong structural materials such as steel and Kevlar. Mechanical properties of few-layer graphene were also investigated using the same AFM technique and Young's modulus of ~ 0.5 TPa was reported for these samples.^{44,45}

2.3.3 Thermal properties

The in-plane thermal conduction in graphene is isotropic and mainly occurs by phonon transport. The large phonon mean free path in the basal plane of pristine graphene is responsible for the ballistic conduction at low temperatures.⁴⁶ The presence of impurities and defects in the structure contributes to phonon scattering and diminishes the thermal conductivity. The in-plane thermal conductivity of graphene at room temperature is among the highest values measured for a material, ~ 5000 W/mK for a mechanically exfoliated SLG.⁴⁷ Another measurement for a CVD grown sample showed

a thermal conductivity of 2500 W/mK.⁴⁸ This value is in the same range as diamond thermal conductivity (~ 2200 W/mK). The thermal conductivity of the SLG supported by SiO₂ was measured as 600 W/mK; the reduction of conductivity was attributed to phonon transfer from graphene to the substrate.⁴⁹ The cross-plane thermal conductivity of graphene is pretty low and is in the same range of graphite thermal conductivity, ~ 6 W/mK.⁵⁰ Interestingly, an increase in the number of layers of graphene sheets does not alter the cross-plane thermal conductivity drastically.⁵¹

2.3.4 Optical properties

The optical transmittance of single-layer graphene has been experimentally observed to be a constant value of $\sim 97.7\%$.^{52,53} The independence of the transmittance constant on material characteristics in graphene originates in its electronic properties and the fact that carriers are massless Dirac fermions.^{52,54} The light absorption increases linearly with the increase in number of layers of graphene and the absorption spectra is flat at wavelengths of 300-2500 nm.^{53,54} The absorption of light generates electron/hole pairs on graphene surface which tend to recombine very rapidly.⁵⁵ The separation and quick recombination of electron/hole along with electronic properties of graphene can be promising in photodetectors.⁵³ It is also possible to obtain photo luminescence in graphene by perturbation of the π system through oxidation or doping. The interrupted π system prevents the fast recombination of electron/hole pairs and allows for photo luminescence. It is a reversible process, meaning that it is possible to quench the luminescence by restoring the π conjugated network.⁵³

2.3.5 Other properties

In addition to its extraordinary mechanical, electrical and thermal properties, graphene also has a theoretical surface area of $2630 \text{ m}^2/\text{g}$.⁵⁶ Although this value is higher than the surface area of CNTs, but the experimental values reported for the graphene sheets produced in the lab is not even close to it.⁵⁷ Also, graphene has been highlighted as an efficient gas barrier material; the diffusion of small gas molecules through the graphene layer is very difficult and selective.^{58,59} Graphene also has interesting magnetic and spintronic properties.⁶⁰

2.4 Other graphene derivatives

2.4.1 Graphene oxide (GO)

Graphene oxide is an important graphene derivative that has been widely used as a precursor for graphene production through chemical or thermal reduction.^{8,61,62} Graphene oxide refers to a highly oxidized single layer of graphene in which the basal plane and the edges are heavily functionalized with oxygen-containing groups. It is produced by oxidization of graphite to form graphite oxide, followed by exfoliation of GO from graphite oxide that can be accomplished via a variety of mechanical and thermal techniques.^{63,64} Graphite flakes can be oxidized by chemical treatment in presence of various oxidizing agents such as KClO_3 , HNO_3 , KMnO_4 and H_2SO_4 . Several oxidation approaches have been developed to achieve higher degree of oxidation in the resultant graphite oxide, with the modified Hummers' method known as the most efficient and common one.⁶⁵ Like its graphite precursor, the graphite oxide obtained by

this method consists of stacks of many layers of GO that are held together by hydrogen and other type of covalent bonds between the functional groups of the adjacent layers. The interlayer spacing in graphite oxide is slightly larger than that of graphite due to the presence of functional groups on its surface. It is very common to exfoliate GO from graphite oxide in a solvent (usually water) by sonication.^{66,67} Upon exfoliation in liquid phase, single-layer GO can be obtained in the dispersion.

The atomic structure of GO has been a matter of controversy; several models have been suggested over the years to represent the atomic structures of GO. The most recent models suggest a non-stoichiometric atomic composition and amorphous structure for GO.⁶⁸⁻⁷⁰ The ambiguity associated with its atomic structure originates in the variation of synthetic approaches and the extent of oxidization reaction from one sample to the other. This makes the C/O atomic ratio of GO to be different for each sample. Various spectroscopic techniques such as NMR, XPS, XANES, FTIR and Raman spectroscopy and also, microscopic techniques including HRTEM, AFM and STM have been used to investigate the structure of the GO nanosheets.⁷¹ The results show that GO consists of small islands of sp^2 -hybridized carbon atoms and larger areas of functionalized sp^3 -hybridized carbon atoms as well as atomic defects and holes.^{70,72} The main functional groups covalently bonded to the surface of GO include hydroxyl and epoxide groups which are randomly distributed on the basal plane (Figure 2.3). Fewer amounts of carboxyl, carbonyl, quinone and phenol groups can be found at the edges of a GO sheet.^{64,73} The atomic defects mainly form under the harsh synthetic condition required for oxidation reaction.

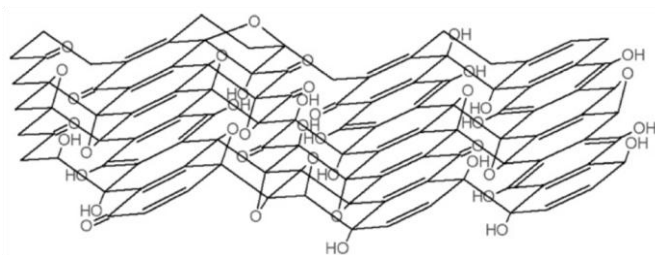


Figure 2.3. Most recent atomistic model of graphene oxide containing hydroxyl, carboxyl and epoxide functional groups (reproduced from Szabo *et al.*⁷⁰).

The presence of functional groups and defects induces higher surface roughness in GO and give rise to a highly wrinkled structure compared to pristine graphene.⁷⁰ The surface roughness along with other parameters such as density and location of the functional groups determine GO electronic structure which is quite different from that of pristine graphene. The as-synthesized GO sheet is electrically insulator with a large band gap; this is because of the high population of sp^3 functionalized carbon atoms that disrupts the π -conjugated system.^{66,74,75} Also, the carrier mobility in GO surface is very low due to the lack of a proper percolation path between the sp^2 -hybridized islands.⁶⁴ However, it is possible to tune its electronic structure by reducing the density of functional groups (particularly, epoxide and hydroxyl groups) on the basal plane through chemical or thermal reduction.⁷¹ This allows for higher carrier motilities, introduces an energy gap in the GO electron density of states and turns GO into a semiconductor. Further removal of functional groups will lead to recovery of a large portion of the network of sp^2 carbon atoms and a highly conductive sample.^{76,77}

Although the functional groups of GO withhold achieving superior electrical properties, but they can be advantageous to its chemical reactivity.⁶⁴ Due to the high polarity of the oxygen-containing groups, GO is easily dispersible in water and many other solvents. It has recently been reported that GO on its own is not soluble in water; instead, it is stabilized by anomalous oxidative debris.⁷⁸ The solution-processability of GO is important for preparation of bulk graphene products; processing of GO in liquid phase via solution casting, spin coating, and vacuum filtration is very common. Also, the functional groups are reactive sites that can be targeted in various chemical reactions for modification of GO structure into a graphene derivative with tunable properties. For example, the epoxide groups may be exposed to amine-containing groups to initiate a ring-opening reaction and nitrogen-dope the GO surface.^{71,79} The carboxyl groups can be activated by several chemical species and allow for attachment of small or large molecules (i.e., surfactants and polymers) to the GO surface.⁸⁰ Also, the hydroxyl groups are always available for hydrogen bonding and spur the possibility of non-covalent functionalization of GO.^{30,81} Most importantly, the chemical reactivity of GO stimulates various chemical and thermal routes for its reduction which will be introduced in the following section.

Like pristine graphene, the mechanical properties of GO change with addition of more layers to the sheet. The Young's modulus of single-layer GO is 156.5 GPa which is almost five times lower than that of single layer pristine graphene. The Young's modulus of bi- and tri-layers of GO have been measured and reported to be 223.9 and

229.5 GPa, respectively.⁸² It is worthy to mention that these values are prone to change with alteration of the type and density of the functional groups on the surface of GO.

2.4.2 Reduced graphene oxide (RGO)

Reduction of GO is very important for restoring the π -conjugated system in the basal plane and thus, producing graphene. The product of the reduction process is “reduced graphene oxide (RGO)” which has similarities with pristine graphene in atomic and electronic structure, but never attains the same properties of pristine graphene.⁸³ The reduction process can reconstruct the sp^2 -bonding network only partially and leaves some oxygenated species and lattice defects on the RGO surface (Figure 2.4). The residual sp^3 -functionalized atoms and atomic defects act as scattering sites and prevent the ballistic transport of charge carriers that has been observed in pristine graphene.⁸⁴ In fact, the carrier transport in RGO occurs through a percolation path which is created by restored sp^2 -hybridized domains within the basal plane.^{72,83} The mechanical properties of RGO also suffer from the inhomogeneity of its atomic structure. The Young’s modulus of an RGO sheets was measured as 185-250 GPa which is similar to modulus of 2-3 layer GO rather than that of pristine graphene.⁸⁵ The degree of sp^2 network restoration fully depends on the initial oxidation level, reduction method and the extent of reduction. The chemical reactivity of RGO is less than GO because of the loss of a large portion of functional groups. Also, RGO renders less polarity and higher hydrophobicity compared to GO and is not dispersible in water and the other solvents. The RGO sheets obtained by chemical reduction in solution phase tends to aggregate due to the increased vdW

forces between the restores sp^2 domains of their basal planes and thus, need to be reduced in presence of some surfactant or polymers to prevent reaggregation.

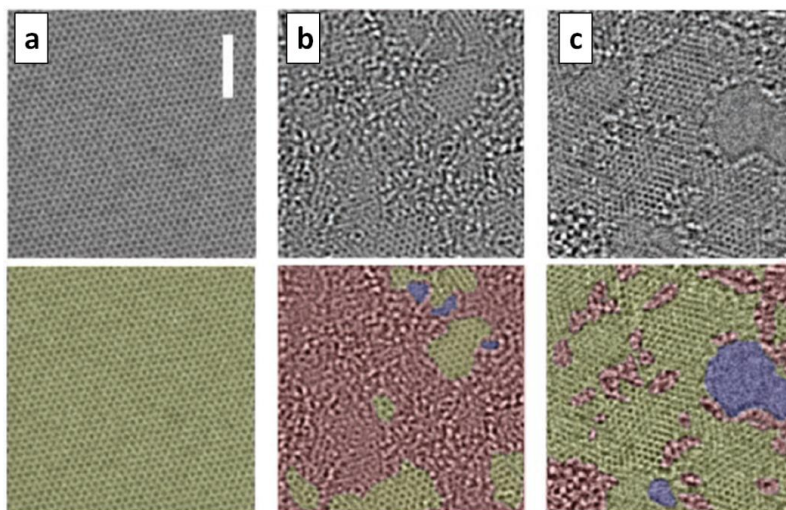


Figure 2.4. HRTEM images of (a) Pristine graphene, (b) GO, and (c) RGO. The graphitic areas are shown in yellow, the oxidized regions are shown in red and holes are shown in blue (reproduced from Erickson et al. ⁷²).

2.5 Production and synthesis of graphene

Since the first successful isolation of single-layer graphene in the lab in 2004¹, scientists have investigated numerous strategies to achieve repeatable production of high-quality graphene in large quantities. Though all these methods produce graphene, the quality, purity, quantity, form and processability of their products are extremely different. The products vary over a broad spectrum from pristine graphene to GO and present a wide range of morphological (i.e., sheet size and thickness) and compositional (i.e., sp^2 - and sp^3 -hybridized carbon, defects, oxygen-containing groups and impurities)

structures; thus, offer a various range of material properties. On the other hand, a diverse combination of material properties is required for different applications (Table 2.1). For example, the graphene used in solar cells needs to be both electrically conductive and extremely transparent, while the optical transparency is not as important as electrical properties in supercapacitors and batteries. Therefore, it is expected that each production method yields a graphene product which suits certain applications; the competency of the product for a specific application can be estimated by accurate inspection of its morphology and chemical composition.⁸⁶

	Electrical conductivity	Strength	Elasticity	Surface area	Transparency	Thermal conductivity
Transistors	✓	✗	✗	✗	✗	✗
Energy storage devices	✓	✗	✗	✓	✗	✗
Electrodes	✓	□	□	□	□	✗
Electrically conductive inks	✓	✗	✓	✗	□	✗
Polymer composites	✓	✓	✓	✓	□	✓
Sensors	✓	✗	□	✗	✗	✗

Table 2.1. Property-application relationships for graphene sheets. Here, a thick indicates importance, cross indicates unimportance and square means the property is sometimes important (reproduced from Edwards et al.⁸⁶).

Depending on the preparation strategy, the graphene sheets indicate differences in the morphological properties such as lateral size and thickness, the density of structural and compositional defects on the surface, the residual impurity content, surface chemistry and the chemical reactivity. These parameters can be used as metrics for evaluation of graphene quality since they affect the graphene properties. In this

sense, high-quality graphene with superior material properties is a single- to few-layer sheet with at least a few microns in length and minimal defects and impurities. Characterization techniques used for assessment of these parameters have to be non-destructive, have high resolution, provide both molecular and morphological information, and be applicable for all product forms.^{53,87} Raman spectroscopy is an invaluable tool that provides information about the sheet thickness⁸⁸ and structural defects⁸⁹ (i.e. sp^3 -hybridized carbon content and edge effects)⁹⁰. Microscopy techniques including HRTEM and AFM have been extensively used to determine the sheets thickness and lateral size.^{22,88,91} Also, the XPS spectroscopy has been used to assess the compositional defects by measuring the C/O atomic ratio and distinguish pristine graphene from RGO and GO.⁷¹ The necessity of using such high quality graphene depends on the application type; electronic (e.g. transistors) and optical (e.g. light emitting diodes OLED) devices, in which fast charge transportation over a micron-range distance is required, demand single- and bilayer graphene sheets with the least defects density.^{21,92,93} On the contrary, some of graphene properties like its chemical reactivity and solubility in water do not improve with the quality and even enhance with higher number of defects.²¹ Hence, graphene sheets of mediocre quality (i.e. smaller few-layer sheets with more atomic defects) are appropriate for applications such as gas storage, energy storage⁹⁴ and sensors.⁹⁵

Currently, the available techniques produce graphene in two major forms: (1) large-area graphene sheets (usually adhered on a substrate) and (2) smaller free-standing sheets (usually dispersed in a liquid). Large area graphene sheets are mainly produced

by bottom-up approaches such as chemical vapor deposition⁹⁶⁻¹⁰⁰ and epitaxial growth on a substrate^{101,102} and can be few centimeters in size. These sheets are promising candidates for preparation of thin films for flexible electronic devices and transparent electrodes for photovoltaic devices. Top-down approaches have been explored to exfoliate graphene from graphite in solid or liquid phase.^{74,103,104} These methods usually produce a few micron-sized sheets which are suitable for preparation of electrodes in batteries and supercapacitors, polymer composites and conductive inks and coatings (Figure 2.5).

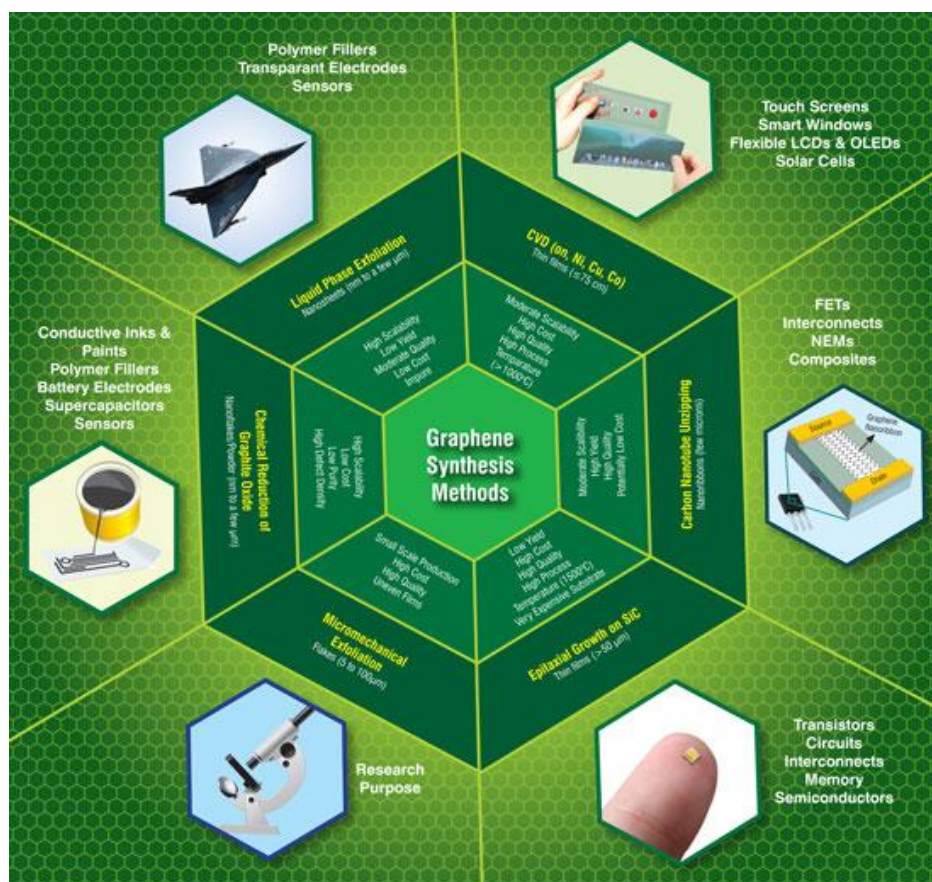


Figure 2.5. Various graphene synthesis method and respective product quality and applications (reproduced from Sivudu *et al.*¹⁰⁵).

Aside from the general quality standards of the graphene sheets, each of these product forms have to be processable in industrial procedures to make their way to the final applications. The impurities associated with the products of these approaches are from different origin; they can be metallic and catalyst particles or polymer and surfactant chains in a solution and hence, require different removal processes. The large area graphene sheets that can be transferred to other substrates, without being damaged or contaminated, are of special interest to the device manufacturers. Likewise, processing of smaller freestanding graphene sheets in liquid phase (e.g. solvent evaporation and rewetting) and its exposure to various chemicals and flow fields (e.g. during spin coating, solution casting, vacuum filtration, etc) is an inevitable step of nanocomposites, batteries and coatings preparation. These smaller freestanding sheets should be originally stable when dispersed in the liquid phase, be aggregation-resistant after drying and rewetting in the liquid phase, remain stable over time and centrifugation, have a high concentration in solution and carry the minimum dispersant content.

Not all the methods produce the same amount of graphene and not all the applications require comparable graphene quantities. Lower quantities of graphene are demanded for production of transparent graphene electrodes and sensors or for the fundamental studies of graphene properties. Lab-scale production methods are capable of providing sufficient high quality graphene for these applications. Conversely, graphene-based energy storage devices and polymer nanocomposites require bulk quantities of graphene. So far, production of larger amounts of graphene has been

associated with a dissipation of quality which arises by an increase in the number of layers and/or defects and/or reduction of the sheets lateral size. Hence, for such applications, the quality of graphene has to be compromised to obtain larger quantities of product.

It is also critical to produce these large quantities of graphene in a scalable, high-yield fashion. The yield is defined by the ratio of graphene product / graphite feedstock, and most prior studies report yields that are fairly low. One might think that yield is a less important metric, given the relatively low cost of graphite, but the associated handling and solvent usage dictates that pre-treatments and recycle streams should be used to increase yields to useful levels. In the same context, the scalability of the production methods becomes of great importance. Scalability may be understood through the scaling law for production as a function of the system size. One may undertake a scalability analysis for each separate unit operation within the graphene production, with graphene synthesis distinct from graphene separation or handling units. Some methods are more appropriate for scale up and some of them cannot be scaled up due to difficult processing and demanding operational conditions such as high temperature and pressure. Additionally, parameters such as cheap and easily accessible precursor source and the efficiency of the process play a role in choosing the graphene production method (Figure 2.6).

With all the above-mentioned points in mind, researchers have developed various methods in the laboratories, with some of them being well-suited for certain

applications. These methods include a wide range of top-down and bottom-up approaches which will be addressed in the following sections.

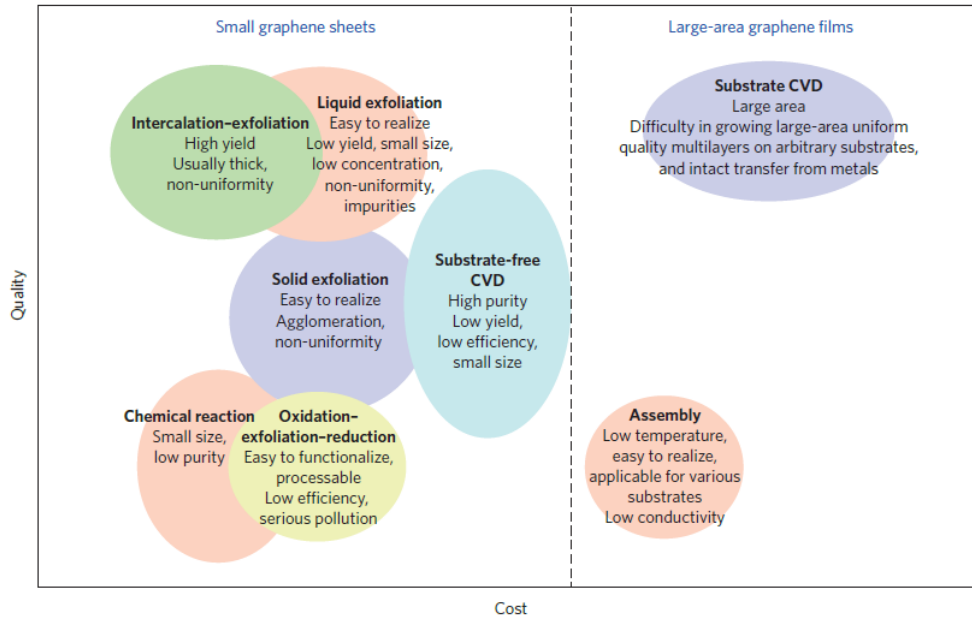


Figure 2.6. Categorization of main graphene production method based on their cost and product quality (reproduced from Ren *et al.*¹⁰⁶).

2.5.1 Bottom-up approach

This approach refers to growth or synthesis of graphene at atomic level using non-graphitic carbon sources. The main advantages of these methods include their capability of producing large-area graphene films and tuning the graphene electronic structure at the atomic level during the synthesis process. These features make the product of bottom-up methods appropriate for applications that aim to harness the

superior charge carrier mobility in a graphene sheet including electronic devices such as transistors and OLEDs.

The main bottom-up methods include epitaxial growth on silicon carbide,^{101,102,107} chemical vapor deposition (CVD) on various substrates^{96-100,108} and wet chemical synthesis of graphene (Figure 2.7).¹⁰⁹⁻¹¹¹ In epitaxial growth, sublimation of silicon atoms from SiC surface at high temperatures (>1000 °C) is followed by graphitization of remaining carbon atoms on the surface. The resultant graphene has single to few layers, but suffers from non-uniformity in crystalline structure which originates in the polycrystalline nature of the initial SiC wafer. Using CVD technique, graphene layers can be deposited from solid, liquid or gaseous precursors on a substrate through thermal, plasma enhanced, reactive and many more processes. Thermal CVD on metals is the most common method in which pyrolysis of carbon containing gases such as methane occurs at high temperature on metallic substrates. The type of metal, pressure, temperature and gas feed rate are some of the parameters that define the final structure of the product.⁹⁹ The deposition on semiconductor and insulator substrates has been recently investigated.¹¹²

The growth methods provide the opportunity to selectively dope graphene with other molecules and functional groups to create a band-gap which is vital in applications such as graphene-based field effect transistors (FETs), OLEDs, solar cells and battery electrodes.^{113,114} However, the as-grown graphene contain some atomic defects and impurities which are induced by the substrates and inhibit the charge transport along the sheets surface. Also, in most cases the large graphene films have to be transferred to

another substrate (e.g. transfer from a conductive metallic substrate to an insulating substrate in transistors); this can be challenging due to the strong interactions of the graphene and the original substrate.^{115,116} Moreover, the lack of control on the number of layers is another drawback of the CVD and epitaxial growth methods.¹¹⁷ Recently, molecular beam epitaxy (MBE) has been applied to grow graphene on insulator substrates with a considerable control over the number of layers.¹¹⁸ All these issues, as well as the high cost of the substrate materials (which are usually etched away after the synthesis), high operational temperature and pressure and the low yield of the continuous growth process make the scalability of these methods problematic.

Researchers have recently attended to alternative bottom-up approaches, mainly wet chemical methods, which let them avoid the challenges associated with using a substrate and harsh growth conditions. These approaches have not been studied as vastly as other methods and currently are in their early stages. Unzipping of carbon nanotubes¹¹⁹⁻¹²¹ and organic synthesis of graphene-like polyacyclic hydrocarbons (PAHs)^{109,122} are the two main routes of wet chemical synthesis. A controlled unzipping of CNTs in various solutions (e.g. sulfuric acids, KOH, etc.) produces graphene nanoribbons (GNR) of < 50 nm width which inherit the band-gap of the original CNT.¹²¹ The products of PAH-based organic synthesis are single layers of graphene with small lateral size (< 200 nm).¹²² The main challenges in wet chemical synthesis methods are increasing the flake size and inhibiting sheets aggregation after synthesis in liquid phase.¹¹¹ Despite all their limitation, the wet chemical approaches are promising because of the high quality and purity of their resultant graphene.

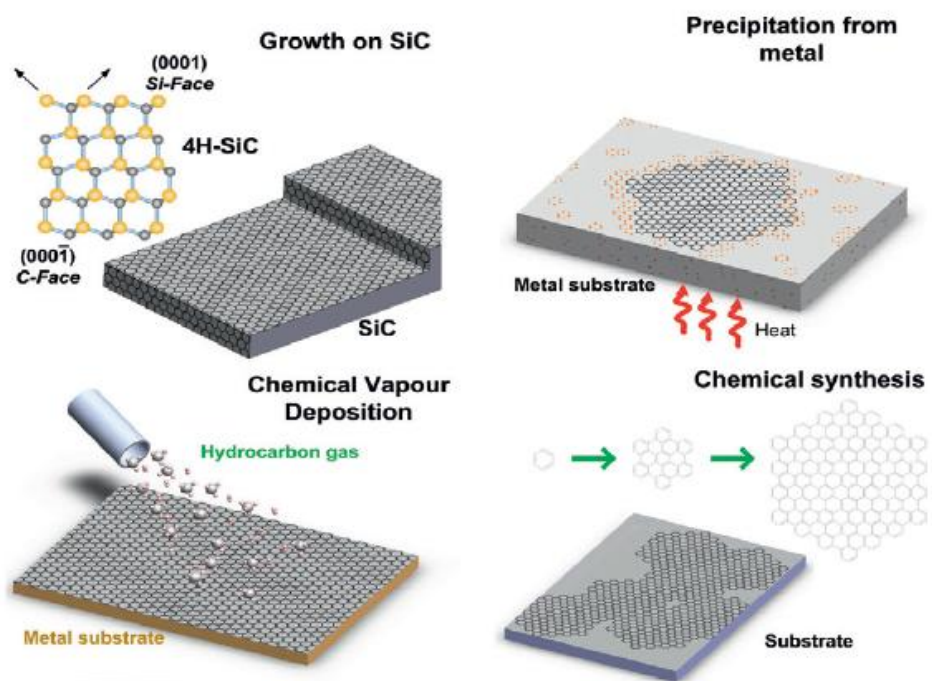


Figure 2.7. Main bottom-up graphene synthesis techniques (reproduced from Bonaccorso *et al.*¹²³).

2.5.2 Top-down approach

Graphite or its derivatives are the main carbon source in the top-down approach that aims to “exfoliate” single- to few-layer graphene sheets from the “parent” graphitic material. Since the interlayer vdW attractive forces in graphite are weak, they can be dominated by an external force, resulting in separation of adjacent layers.¹ Also, the interlayer attractive forces can be diminished by intercalation of various atoms and molecules into the graphite structure and increasing the interlayer spacing.¹²⁴ It is important to avoid disruption of the atomic structure and sp^2 bonding network of graphene layers during this process. Exfoliation may be carried out in solid or liquid

phase using various sources of external energy. Maintaining the exfoliated state of the graphene sheets requires an energy barrier which prevents the reaggregation of the sheets, especially in a medium which prompts the Brownian motion of the sheets, i.e., liquid phase. Here we briefly discuss the solid phase exfoliation and then we will review the existing liquid phase exfoliation methods in depth, as it is the focus of this thesis.

2.5.2.1 Exfoliation in solid phase

Exfoliation of graphite into graphene sheets in solid phase may be accomplished by applying mechanical forces (Figure 2.8). Micromechanical cleavage is the oldest solid-phase exfoliation method that applies normal forces to separate graphene layers from graphite source. Although this process produces very high-quality graphene sheets, but it is extremely limited by its yield and efficiency and is impractical for large-scale production of graphene.¹

Ball milling is a well-established industrial technique that applies shear force to exfoliate graphene sheets from graphite.¹²⁵⁻¹²⁹ This technique can produce large-area graphene sheets in high quantities; however, intensive milling and grinding of the sheets is necessary for production of few-layer graphene sheets. This damages the basal plane of the graphene and increases the structural defects in the final product. The ball milling has also been performed in presence of other components to modify the graphene surface for specific applications.^{129,130} Thermal annealing or washing the product with solvents is a required step for removal of the impurities (metals of the milling unit) in this method.

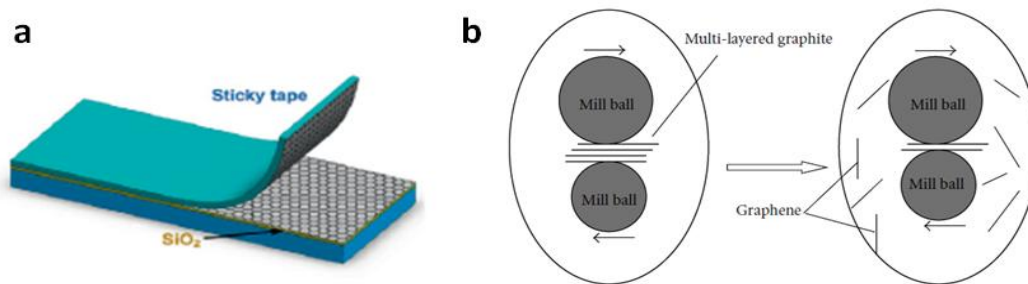


Figure 2.8. Schematic of graphene production by (a) micromechanical cleavage reproduced from Bonaccorso *et al.*¹²³), and (b) ball-milling (reproduced from Zhao *et al.*¹³¹).

Thermal expansion of graphite oxide and graphite intercalation compounds (GICs) via microwave radiation or rapid heating to high temperatures (>1000 °C) is another method to exfoliate graphene in solid-phase.¹³² First, the graphite oxide and GICs have to be synthesized in liquid phase to introduce functional groups and intercalants of various types to the graphite structure. The subsequent thermal shock leads to flash evaporation and release of the functional groups and intercalants into the interlayer spacing of graphite and ultimate exfoliation of graphene layers. The product of this method has lower C/O ratio compared to pristine graphene.

In general, the solid-phase exfoliation methods are promising candidates for large-scale production of graphene powder. Yet, the products of these methods suffer from high density of structural and compositional defects. Additional exfoliation and/or stabilization is needed to prepare the product of these methods for further liquid-phase processing.

2.5.2.2 Exfoliation in liquid phase

Exfoliation of graphite in liquids allows for simple production of liquid dispersions with high graphene content and facilitates processing of graphene in industrial techniques. Parent graphite can be mechanically or electrochemically exfoliated into graphene in a solvent; however, the high interfacial tension at the graphene-solvent interface and strong inter-sheet attractive forces promote reaggregation of exfoliated sheets, necessitating stabilization of the sheets prior or simultaneously to the exfoliation. Stabilization can be achieved either by balancing the surface energy of the sheets and the liquid phase to minimize the interfacial tension or by modifying the sheets surface to eliminate the inter-sheet attraction and make them more solvent-philic.¹³³ The main stabilization routes include covalent functionalization through oxidation prior to exfoliation, exfoliation in the solvents with surface energies similar to graphene and non-covalent functionalization using surfactants, polymers and other types of dispersant molecules.

The final products of these methods are colloidal dispersions of freestanding graphene sheets. The choice of exfoliation technique and stabilization strategy determines the graphene quality and quantity. Other than the morphological and compositional properties of the sheets that can be assessed by characterization techniques such as Raman spectroscopy,⁸⁸⁻⁹⁰ XPS spectroscopy,⁷¹ HRTEM, and AFM,^{22,88,91} the concentration and stability of graphene in the dispersion are important parameters which need to be determined precisely.¹³⁴ UV-vis spectroscopy is the common method of measuring graphene concentration; the absorption spectra of

graphene at wavelength of >500 nm is used to determine concentration according to the Beer-Lambert law.^{103,135-137} Thermogravimetric analysis (TGA) of the graphene powder cast from the dispersion may also be used for concentration measurements.¹³⁸ The colloidal stability of the dispersions has been analyzed by zeta potential measurements.^{139,140} According to DLVO theory, a charge may develop at the interface of colloidal particles and the solvent molecules. The value of this surface potential (zeta potential) directly correlates to the colloidal stability of the dispersion. When the absolute value of the zeta potential exceeds 30 mV, the dispersion is considered stable.^{134,141} The long term stability is an important parameter in post-processing of the dispersions. Proper separation of exfoliated/stabilized sheets from graphitic materials and non-stabilized sheets through effective centrifugation improves the stability of dispersion over time.¹³⁴

Stable freestanding graphene sheets can be easily processed in presence of solvents, polymers and other chemicals to produce polymer nanocomposites, printed electronic devices,^{75,76} conductive inks and coatings, batteries and supercapacitors electrodes and chemical sensors. Most of these applications require a proper electrical conductivity, but ultrafast charge transportation is not essential for them. Thus, the smaller flake size and higher number of layers of exfoliated graphene sheets is not an impasse for such applications. Moreover, the yields of these methods, which could be evaluated by measuring the graphene concentration in the dispersions, mostly exceed those of bottom-up methods. Liquid-phase exfoliation require less demanding processing conditions and has a lower cost of production due to the comparably cheap starting

material. All these characteristics make liquid-phase exfoliation methods a promising candidate for large-scale production of graphene. Here, we outline the three main graphene liquid exfoliation techniques that have been broadly investigated.

2.5.2.2.1 Oxidation-exfoliation-reduction of graphite

Chemical conversion of graphite to graphene oxide is the oldest exfoliation technique for graphene production. It starts with oxidation of graphite into graphite oxide, followed by exfoliation of graphite oxide into GO in a proper solvent via sonication and ultimately, reduction of GO sheets to form RGO (Figure 2.9).^{66,67,71} The oxidation is usually performed based on the modified Hummer's method in presence of oxidants including sulfuric acid, nitric acid and potassium permanganates.^{65,70} Oxidation introduces covalent functional groups such as hydroxyl (-OH), carboxyl (-COOH), epoxide (-O-) and carbonyl (C=O) to the layers of the resultant graphite oxide and makes it hydrophilic. Graphite oxide can be easily exfoliated and dispersed in water to form stable GO aqueous dispersions. The dispersed GO sheets are mostly single layer with several hundreds of nanometer to a few micrometers length and are stable at concentrations up to 10 mg/ml.⁷¹

As mentioned earlier in section 2.4.1, GO has a different composition and structure than graphene and has to be reduced in order to restore the sp^2 -hybridized network of carbon atoms and unique properties of graphene. Chemical reduction in solution^{77,142} or vapor phase^{143,144}, thermal annealing^{61,145} and electrochemical techniques¹⁴⁶ have been used to prepare RGO. The chemical reduction has been

performed using various reducing agents such as hydrazine^{77,142,147}, sodium borohydride¹⁴⁸ and hydroquinine¹⁴⁹ in the solution or vapor phase. Every reducing agent introduces a different reduction reaction pathway; therefore, is capable of removing specific functional groups and leaves the other oxygen-containing functionalities in the final RGO product.⁵³ It has been reported that the C/O atomic ratio of RGO can be increased to 14.9:1 by choosing the proper reducing agent and reduction conditions.¹⁵⁰ During the chemical reduction in liquid phase, the brown aqueous dispersion of GO turns black and the RGO sheets which are no longer hydrophilic aggregate and precipitate. To prevent reaggregation, the reduction has to be performed in presence of proper dispersant molecules in the solvent.⁷⁴

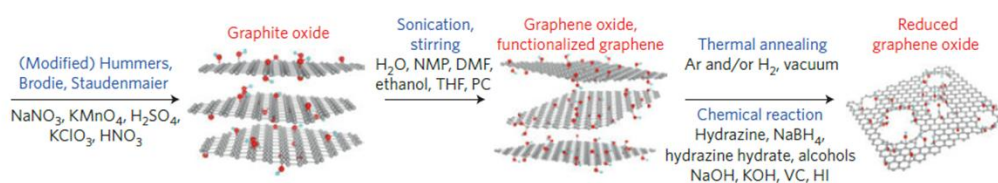


Figure 2.9. Schematic of graphene production through oxidation-exfoliation-reduction route (reproduced from Ren *et al.*¹⁰⁶).

In an alternative approach, the GO dispersions could be filtered and dried to prepare GO powder for thermal reduction. Heating GO to temperatures as high as 1050 °C removes the hydroxyl and epoxide groups in form of carbon dioxide, but leaves some stable carbonyl and ether functionalities on the basal plane.^{145,151} Electrical conductivity

of 1000-2300 S/m has been reported for thermally-reduced RGO. Electrochemical reduction is an alternative method to avoid the hazardous chemicals (e.g. hydrazine) and harsh reduction conditions (1100 °C). In this technique, a voltage is applied to a GO electrode in presence of a buffer solution.¹⁴⁶

The high yield of the process, large quantities of the product and low cost of production are the main advantages of this method. Moreover, the chemical reactivity and hydrophilicity of the GO sheets allows using wet chemistry techniques to modify the structure and properties of the sheets to prepare customized graphene for specific applications. However, the demanding processing conditions and the mediocre quality of RGO hinder the versatility of this route as a scalable graphene production method.

2.5.2.2.2 Intercalation-exfoliation of graphite

Graphene sheets can be produced quickly through electrochemical intercalation and exfoliation of graphite. This method includes electrochemical oxidation/reduction of graphite, intercalation of ions into the spacing of graphite layers and exfoliation under an electrochemical bias, followed by a subsequent ultrasonication step to complete the exfoliation (Figure 2.10). This whole electrochemical treatment of graphite can be accomplished in less than an hour.^{152,153} A simple experimental set up for this method includes a graphite working electrode, a reference electrode, electrolyte solution and a DC power supply. The graphite host material could be a graphite rod, graphite flexible foil or HOPG and common reference electrode materials are Pt, calomel and Ag/AgCl₂. The electrolyte which provides the intercalant ions can either be an aqueous solution of

acidic materials (sulfuric, perchloric, etc) and/or surfactants (SDBS, SBS, etc) or non-aqueous solutions of ionic liquids and organic solvents.¹⁵⁴⁻¹⁵⁶

Applying a potential causes the oxidation (or reduction) of the graphite which leads to intercalation of anions (or cations) from the electrolyte. The intercalation increases the interlayer spacing and results in structural expansion of the electrode. Upon completion of the intercalation, a reverse potential is applied to exfoliate the graphene layers from the electrode. The graphene flakes precipitate in the solution and form sludge at the bottom of the cell.^{152,153} In the anodic intercalation a positive potential is applied to oxidize the graphite and intercalate anions.^{132,156-159} In this case, the potential required for ion intercalation is usually higher than the potential needed for graphite oxidation.^{2,152} Thus the product is partially oxidized graphene with sp^3 carbon defects and oxygen-containing functional groups. Non-oxidative intercalation and exfoliation has been accomplished by cathodic reduction of graphite in presence of lithium ions to avoid oxidation of graphite.^{160,161} Although the product offers a high C/O ratio and minimal sp^3 defects, but the quantity of the material produced by this method is very low in the absence of acidic ions.¹⁵³

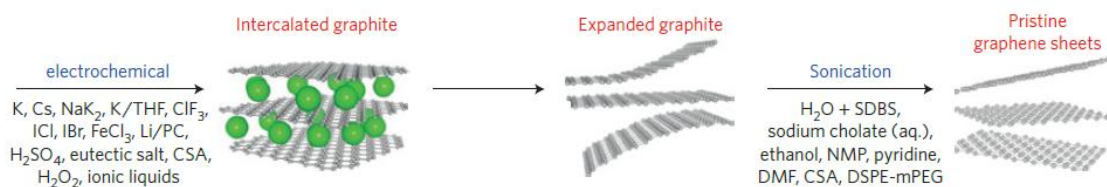


Figure 2.10. Schematic of graphene production through electrochemical intercalation-exfoliation route (reproduced from Ren *et al.*¹⁰⁶).

The graphene flakes produced by electrochemical exfoliation generally have higher sheets size (up to 50 μm) than the other liquid-phase graphene products. The number of layers of the sheets varies over a wide range from single to multiple layers and hence, require further exfoliation through ultrasonication.^{152,153} Consequently, the electrochemical intercalation and exfoliation of graphite is more perceived as a pre-processing step rather than a main method of graphene production. The poor quality of the anodic intercalation products, low yield of the cathodic intercalation products, and the difficulty of removal of the residual electrolyte ions and solvents from the final product are some issues that should be resolved before considering this method for large-scale production of graphene.

2.5.2.2.3 Direct liquid-phase exfoliation

A more recent strategy is to directly exfoliate graphite in a solvent using ultrasonication. This process involves three steps: (1) exfoliation of graphite, (2) stabilization of graphene layers and (3) separation of graphene sheets from unexfoliated and non-stabilized graphitic material (Figure 2.11). In exfoliation step, the ultrasonic waves produce cavitation bubbles in the solvent; as these bubble collapses due to the pressure increase, they generate high energy micro-jets and shock waves that act on the bulk graphite and exert compressive stress on the sheets to induce exfoliation.¹³⁰ In a secondary mechanism, the unbalanced compressive forces on two adjacent layers cause a shear-induced exfoliation. Additionally, the micro-jets may act as wedges that diffuse to the interlayer spacing of graphite and enforce exfoliation.¹³⁰ After exfoliation, the

sheet-liquid attractive forces have to exceed the graphene interlayer attractive forces in order to prevent reaggregation. This could be accomplished by reducing the sheet-liquid interfacial tension through various strategies such as usage of organic solvents, ionic liquids or aqueous solutions of dispersants molecules. After sonication, unexfoliated thick graphitic sheets are a large fraction of the solid content in the dispersion. These heavier graphitic sheets can be separated from the exfoliated graphene by centrifugation to obtain dispersions of high-quality graphene sheets with long term stability. The yield of the process could be calculated by measuring the amount of starting graphite and the concentration of graphene sheets in the centrifuged dispersions (using UV-vis spectroscopy technique). The type of the solvent and the dispersant, as well as processing parameters such as sonication time and power and centrifugation force and time are the main factors that affect the graphene quality and process yield. Here, we discuss various liquid systems and processing that have been used in direct liquid-phase exfoliation of graphite and introduce the recent improvements of exfoliation techniques.

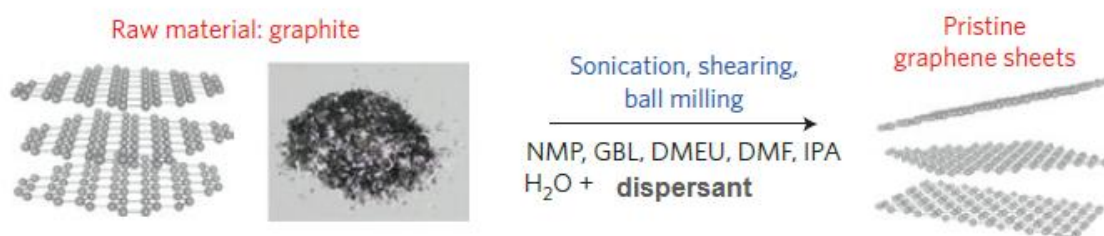


Figure 2.11. Direct liquid-phase exfoliation of graphite into graphene sheets (adapted from Ren *et al.*¹⁰⁶).

(I) Dispersion in organic solvents

From a thermodynamic point of view, direct liquid-phase exfoliation can be perceived as “dissolution” of graphene in the liquid phase for which the enthalpy of mixing should be minimized. The following expression suggested by Coleman *et al.*¹⁰³ shows the enthalpy of mixing of graphene in a pure solvent:

$$\frac{\Delta H_{mix}}{V_{mix}} \approx \frac{2}{T_{NS}} (\sqrt{E_{S,S}} - \sqrt{E_{S,G}})^2 \phi_G$$

where ΔH_{mix} is the enthalpy of mixing, V_{mix} is the volume of the mixture, T_{NS} is the thickness of graphene sheet, $E_{S,S}$ and $E_{S,G}$ are the square root of the surface energies of the solvent and graphene, respectively, and ϕ_G is the graphene volume fraction. The surface energy of graphene is defined as the energy per area required for separation of two adjacent layers. The term in parentheses represents the interfacial tension of graphene sheets immersed in the solvent. Higher surface tension in the solution increases the tendency of the sheets to adhere to each other; thus, complicates the exfoliation in first place and later, induces reaggregation of exfoliated layers. When the surface energies of solvent and graphene are equal or close, the enthalpy of mixing has its minimal value and the exfoliation and dispersion occurs spontaneously or more easily.

Coleman *et al.* measured the graphene concentration after sonication and centrifugation in a range of organic solvents to find the optimum surface tension for graphene exfoliation and dispersion which was 40 mJ/m² (Figure 2.12).¹⁰³ Solvents including N-methyl-2-pyrrolidone (NMP), N,N-dimethylformamide (DMF) and ortho-dichlorobenzene (o-DCB) have the surface energy within this desired range and have been widely used to exfoliate single- and few-layer graphene sheets. Additionally,

Hansen solubility parameters, which are the square root of dispersive, polar and hydrogen bonding components of the materials cohesive energy density, allows for more accurate prediction of solubility of the graphene sheets in various solvents.^{103,162} The concentration of graphene in organic solvents is too low (~ 0.01 mg/ml) for practical industrial applications. Several strategies were adapted to improve the yield of graphene in these solvents including longer sonication times (up to 460 hrs),¹³⁵ higher sonication powers (tip sonication instead of bath sonication) and addition of intercalants¹⁶³ and surfactant¹⁶⁴. All of these modifications increased the process yield, but led to a considerable drop in sheets size and increased defect density. Moreover, most of these solvents are highly toxic, impose health hazards, are expensive and their high boiling points (>200 °C) hinder their application in industrial techniques (e.g. solution casting) which aim to prepare transparent electrodes, solar cells, etc. To address these issues, several attempts have been made to exfoliate graphene in low boiling point solvents such as isopropanol, chloroform and acetone using longer sonication times.^{165,166} Also, solvent exchange methods have been used to transfer exfoliated graphene from original solvent (e.g. NMP) to low boiling point solvents like ethanol.¹⁶⁷ Although the graphene concentrations obtained in these solvents are comparatively high, the stability of these dispersions is a matter of controversy.

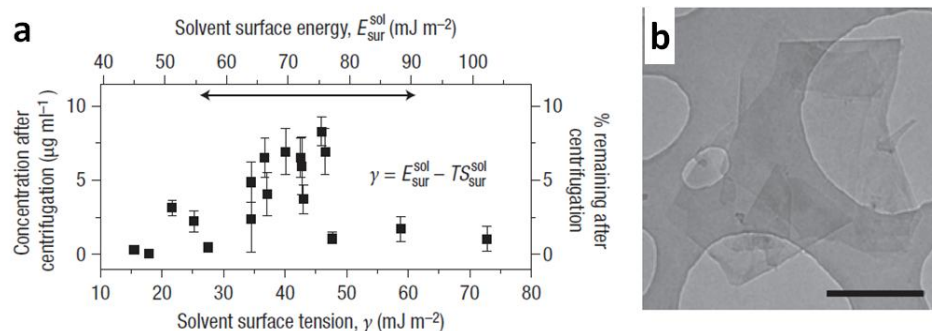


Figure 2.12. (a) Graphene concentration in various organic solvents vs. solvent surface tension plot reveals the optimum surface tension (40-50 mJ/m²) for graphene dispersion, and (b) TEM image of few-layer graphene sheets in NMP dispersion (reproduced from Hernandez *et al.*).

Bourlinos *et al.* found that the charge transfer between the graphene and a solvent with electron-withdrawing or –accepting components also leads to the exfoliation and stabilization of the sheets.¹⁶⁸ For example, the charge transfer between graphene and a group of perfluorinated aromatic molecules (through π -interactions) facilitates the sheets exfoliation and stabilization. The capability of other hydrocarbon solvents with analogous electron-withdrawing or –accepting structure (e.g. toluene, benzene, pyridine) to exfoliate and stabilize graphene has also been investigated.

Additionally, acids have been used for dissolving graphite. Chlorosulfonic acid can dissolve graphene with concentration up to 2 mg/ml without sonication.¹⁶⁹ The protonation of the graphite layers is responsible for spontaneous exfoliation and dispersion of graphene sheets, as it increase the interlayer spacing and induces repulsion between the sheets. Addition of H₂O₂ to this acid resulted in immediate exfoliation of large quantities of few-layer graphene sheets with minimum defect density.¹⁷⁰ However,

the risks associated with working with the superacids and the need for many washes to increase the pH before post-processing has restricted the practical application of the product.

(II) Aqueous dispersions

Water is widely used in industrial applications due to its low boiling point, non-toxicity, biocompatibility, and low cost. However, its surface tension of 72 mJ/m^2 is higher than that of an ideal exfoliation medium for graphene. Addition of surfactants, polymers and small organic molecules reduces its surface tension and facilitates exfoliation of graphite. Furthermore, adsorption of these dispersant molecules on the graphene surface assists the stabilization of exfoliated sheets and prevents reaggregation (Figure 2.13).

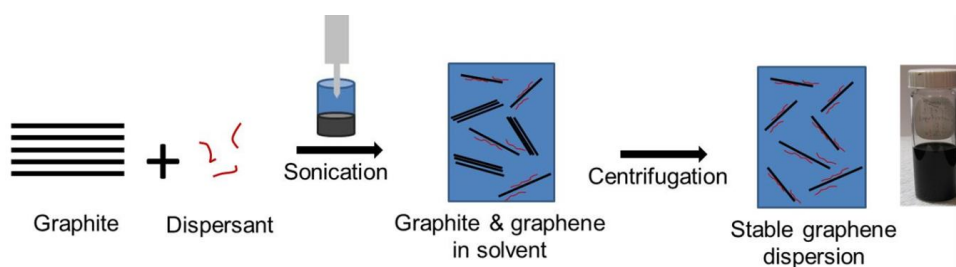


Figure 2.13. Production of stable aqueous graphene dispersions in presence of dispersants.

Surfactant molecules contain a hydrophobic tail and a hydrophilic head. The hydrophobic tail of surfactants adsorbs on graphene surface via vdW, hydrophobic or π - π interactions. In ionic surfactants, the hydrophilic head which is capable of dissociation

in presence of water molecules, positively or negatively charges the graphene surface. This surface charge (reflected in the zeta potential value) induces an electrostatic repulsion between the graphene sheets covered with surfactant molecules and stabilizes these sheets. Surfactants like sodium dodecylbenzene sulfonate (SDBS)¹⁷¹, sodium cholate (SC)^{37,172}, sodium deoxycholate (SDC)¹⁷³ have been used to disperse graphene sheets of 2-4 layers with 1 micron lateral size at a concentration of 0.1 mg/ml. Longer sonication time can improve the graphene concentration and yield. Non-ionic surfactants stabilize graphene sheets through steric repulsion induced by their long hydrophilic heads spread into the water. Guardia *et al.* and Smith *et al.* compared the graphene concentration obtained from ionic and non-ionic surfactants and reported that non-ionic surfactant can produce graphene dispersions with higher concentrations.^{174,175}

Further, polymers have been widely used to stabilize graphene in water and in organic solvents. Long polymer chains adsorbs on the graphene surface while some segments of the chain extend into the solvent and provide a shield around the graphene sheet through steric repulsion or depletion effects. Polyvinylpyrrolidone (PVP)^{38,39} and polyacrylamide (PAM)¹⁷⁶ are a few example of the polymers that assist exfoliation of few-layer graphene sheets with average one micron lateral size. The yield of polymer-assisted graphene dispersions is comparably higher than those obtained with ionic surfactants. Furthermore, the polymer-assisted graphene dispersions can be directly processed to fabricate polymer nanocomposites.

One of the main issues associated with surfactant- and polymer-assisted dispersions is the high excessive dispersant content of the final graphene product.

Removal of the excessive dispersants is tedious task which requires further processing of the dispersions and a 100 % removal of the dispersant is unachievable. Polycyclic aromatic hydrocarbon (PAH) derivatives are a promising alternative to the polymers and surfactants.^{33,177,178} These molecules have lower molecular weight than polymers and surfactants and are capable of stabilizing high quantities of graphene in the aqueous dispersions via π - π interactions with the sheets.

(III) Dispersions in Ionic liquids

Ionic liquids are semi-organic salts with hydrophobic and hydrophilic components in their molecular structure.^{138,179,180} Certain ionic liquids have been used as electrolyte in electrochemical exfoliation of graphite. Also, they have been used as solvents for direct liquid-phase exfoliation of graphite via sonication. The graphene sheets in dispersions of 1-butyl-3-methyl-imidazolium bis(trifluoromethanesulfonyl)imide ([Bmim][Tf2N]) and 1-hexyl-3-methylimidazolium hexafluorophosphate (HMIH) had less than 5 layers and were few microns in size.^{138,179} The graphene yield for one hour of sonication was quite high (~ 5 mg/ml) compared to the organic and aqueous dispersions of graphene. However, the stability of graphene in the dispersion, removal of the ionic liquids and high impurity content of the final product remain as serious challenges.

(IV) Exfoliation via shear-mixing

All the above-mentioned graphene dispersions were prepared using ultrasonication as the source of mechanical force. The average graphene concentration in these dispersions is about 1-2 mg/ml which may yield high quantities of the sheets if and

only if large volumes of the dispersions are produced. However, the sonication efficiency and graphene concentration in the dispersion decrease upon the increase of the liquid volume. Hence, the improvement of the production rate by scaling up the dispersion volume is impossible. Shear exfoliation is an alternative exfoliation technique that has been recently used for graphene exfoliation.¹⁸¹ When higher shear rates are applied in a liquid containing graphite and proper solvent and dispersant, the graphene layers delaminate from graphite. Recent reports have demonstrated that high-shear mixing can exfoliate nanosheets from the parent material with a power law relationship written as:

$$P_R \sim V^\alpha$$

where P_R is the production rate, V is the volume of the exfoliation vessel and α depends on the choice of nanosheet, solvent, and dispersant. If α is greater than or equal to 1, then scaling up to large volumes becomes feasible from a manufacturing standpoint. If α is less than 1, then scaling up results in diminishing returns, and this nanomanufacturing approach will remain confined to the lab scale. Coleman and co-workers have reported that precise control of parameters such as initial graphite concentration, liquid volume, mixing time, rotor diameter and speed can yield values of $\alpha > 1$ for several dispersant/solvent combinations.¹⁸¹ This shows excellent promise for scalable exfoliation of pristine graphene from parent graphite materials. The graphene sheets produced by this method are of high quality, have minimal defects and demonstrate excellent material properties in various applications.

2.6 Conclusion

The unique 2D structure of graphene results in extraordinary properties that can be exploited in applications such as electronics, composites, and energy conversion and storage. GO and RGO are other graphene counterparts which share similar 2D planar structure with pristine graphene. However, their properties are inferior relative to pristine graphene due to their different chemical composition, atomic, and electronic structure. Various bottom-up and top-down production techniques have been developed to produce graphene sheets (i.e., pristine graphene, GO and RGO). Most of these production techniques are restricted by a trade-off between the quality and quantity of their products. Thus, scalable production of large quantities of high-quality graphene is a challenging task. Bottom-up techniques produce high-quality pristine graphene sheets, but they are not suitable for industrial production of graphene due to their low yield and incapability for scale up. On the other hand, the liquid-phase exfoliation of graphene from graphite is a promising method because of its high yield, ease of processing and potential scalability. The tendency of graphene sheets for reaggregation in the solvent is the main issue in this method. Functionalization of graphene sheets has been used as a strategy to prevent reaggregation. GO and RGO can be produced by covalent functionalization of graphene in liquid phase, while non-covalent functionalization of graphene yields pristine graphene dispersions. The liquid-phase exfoliated pristine graphene, GO or RGO sheets can be processed further to prepare graphene-based functional materials. In Chapter III, we discuss the fabrication of various graphene-based materials using the liquid-phase exfoliated graphene sheets.

CHAPTER III

GRAPHENE-BASED FUNCTIONAL MATERIALS

3.1 Graphene-polymer nanocomposites

3.1.1 Challenges and opportunities for graphene-polymer nanocomposites

Reinforcement of polymers with filler materials enhances their bulk properties to meet the requirements of the final application. Nanomaterials are often incorporated in the polymer matrices to improve their electrical and thermal conductivity, mechanical strength and stability, electrochemical reactivity, and many other physical properties. The fillers morphology and content are the important factors that determine the structure-property relationships in the nanocomposites. The higher surface area to volume ratio, i.e. the aspect ratio, of the nanofiller enables effective filler-polymer interactions in the nanocomposites and boosts the mechanical load transfer (e.g. normal and shear forces) between the two phases. Most importantly, the high aspect ratio of the nanofiller allows for enhancement of the bulk properties by addition of minimal filler content to the polymer matrix. Therefore, the overall structure of the nanocomposite will be dictated by the polymer phase, while its properties will be defined by those of the polymer-filler interface.

Among various types of nanofillers, two-dimensional nanofillers are of great importance due to their high aspect ratios. Graphite nanoplatelets have been traditionally used as filler because their layered structures provide a larger interface and improve the polymer-filler interactions.¹⁸²⁻¹⁸⁴ The graphene sheets obtained from top-down

approaches offer high aspect ratios that are two to three orders of magnitudes higher than graphite. Also, these liquid-phase exfoliated single- to few-layer graphene sheets are ideal fillers due to their high quality and their processability in presence of solvents; this enables the usage of existing polymer processing techniques with no or minimum modifications for fabrication of graphene-polymer nanocomposites. Graphene (including pristine graphene, GO and RGO) has been added to polyolefins (e.g. PE, PP), acrylic polymers (e.g. PMMA, PAM, PNIPAM, PAN), Vinyl polymers (e.g. PVA, PS, PVDF), epoxy, polyurethane, conductive polymers (e.g. PANI, PPy, PEDOT), polycarbonate, polyamide and polyimide.^{185,186} Addition of graphene to these polymers has enhanced their mechanical strength, thermal conductivity, electrochemical activity and imparted electrical conductivity and gas barrier properties.^{8,185-187}

The improvement in polymer composites properties depends on the distribution of the fillers in the polymer matrix and the filler-polymer interfacial interactions.¹⁸⁸ Dispersion of pristine graphene in most of the polymer matrices is a challenging task due to the significant mismatch in their surface energies. This usually leads to aggregation of the sheets in the polymer matrix. Moreover, incompatibility of the pristine graphene and polymers surface energies induces a high interfacial tension that may weaken the mechanical load transfer within the nanocomposite. Also, the low chemical reactivity of pristine graphene reduces the chance for interfacial interactions through chemical bonds. On the other hand, the hydrophilic nature of GO (and to some extent RGO) and the presence of functional groups on its surface facilitates the interfacial interactions and surface energy compatibility between the two phases. However, the insulating nature of

the GO and its inferior properties relative to pristine graphene necessitates further restoration of the π -network through chemical or thermal reduction.

Additionally, the thermal and electrical conduction within an insulating polymer matrix can only be accomplished through a percolation path, i.e. an interconnected network of graphene sheets within the polymer matrix. Theoretically, such a percolation path can form upon addition of very low amount of graphene to the composite. In practice, the poor dispersion and agglomeration of graphene in polymer matrix hinder the formation of an effective percolation path at such low graphene loadings.⁸

3.1.2 Incorporation of graphene into polymer matrices

Various techniques have been used to incorporate graphene sheets into polymer matrices. Melt blending is a common technique in which the graphene in powder form is added to the polymer while high temperatures and shear forces are applied to bring the polymer into its melt phase.¹⁸⁹⁻¹⁹² The mobility of the polymer chains in the melt phase allows for proper mixing of the powder into the matrix and the strong shear forces assist to distribute the graphene sheets in the matrix.¹⁹¹ The graphene powder used in this method should be stabilized and aggregation-resistant in order to improve the dispersion quality. This method is one of the least expensive, most versatile and, from manufacturing point of view, scalable techniques for processing graphene in presence of the polymers. However, the preparation of graphene in powder form requires drying of the graphene dispersions obtained by liquid-phase exfoliation techniques. Moreover, the high viscosity of the polymers, regardless of how strong the shear forces are, restricts the

proper mixing of graphene and polymer phases.¹⁹³ Also, the incompatibility of the graphene and polymer phases may result in a phase separation and subsequent agglomeration of graphene sheets. In general, the final dispersion of the graphene in the polymer matrix obtained by melt blending technique is not ideal.¹⁹⁴

Solution blending is a simple method to prepare uniform graphene-polymer nanocomposites.^{8,195-199} In this method the graphene is dispersed and the polymer is dissolved separately in similar or two miscible solvents and then, these solutions are mixed together by agitation, stirring or sonication to homogeneously disperse graphene in the final solution. In the next step, the solvent is removed by various techniques such as evaporation and filtration.²⁰⁰ This method facilitates the processing of graphene dispersions in presence of polymers and presumably can yield higher dispersion quality in the nanocomposite. However, it is restricted by the limited number of proper solvents for graphene. Additionally, the solvent removal can be problematic as it may induce phase separation and aggregation; complete removal of the solvent from the product is also a matter of concern. Furthermore, the bulk quantities of the solvent used in this method is an obstacle to its scalability.

In situ polymerization in presence of graphene sheets is another strategy that has been explored extensively.²⁰¹⁻²⁰⁵ In this method, the graphene sheets (pristine graphene, GO or RGO) are added to polymer monomers in a common solvent and properly mixed to yield a homogenous dispersion, followed by initiation and completion of the polymerization. Various polymerization routes including radical^{204,206,207} and emulsion polymerization²⁰³ and polycondensation²⁰⁸ have been practiced depending on the

chemistry of the host monomers and the properties demanded by the final nanocomposites. This method improves the dispersion of graphene in the polymer matrix considerably and yields highly uniform nanocomposites. However, the possibility of graphene aggregation during the polymerization step in absence of external shear force, difficulties associated with the removal of remaining solvent and residual reaction initiators are the drawback of this approach.

Latex and emulsion mixing have also been used to incorporate graphene into polymer matrices; this approach is especially useful when it is impossible to achieve a uniform dispersion of graphene and polymer in the liquid phase.²⁰⁹⁻²¹¹ Using this method, the graphene sheets and polymer particle are mixed into a solvent and graphene sheets assemble at the graphene-polymer particles interface and form a segregated network. Upon removal of the liquid, graphene-coated polymer particles are obtained that can be processed by various techniques such as hot-pressing and vulcanization to produce the final nanocomposites. This method has mainly been used to fabricate electrically conductive composites with ultralow percolation threshold; the enhancement of other properties of the nanocomposite is not the main focus of this approach.^{212,213}

3.1.3 Modification of graphene-polymer interface

Some of the techniques mentioned in previous section improve the graphene dispersion in polymer matrices, but they cannot resolve the incompatibility of graphene and polymer surface energies. Thus, modification of graphene surface in order to enhance the interfacial polymer-graphene interactions is inevitable.^{214,215} The

modification may be practiced through covalent²¹⁶⁻²²⁰ or non-covalent functionalization²²¹⁻²²⁴ of the graphene sheets. While the versatile surface chemistry of GO makes it a promising candidate for covalent functionalization, the low chemical reactivity of pristine graphene only allows for non-covalent functionalization. The covalent functionalization of GO surface is possible through two different approaches called “grafting to” and “grafting from” methods.

In “grafting to” methods, the polymer chain is grafted onto the GO surface via chemical reaction with GO functional groups, mainly carboxyl and epoxide groups.²¹⁶⁻²¹⁸ Polymers containing amine groups can react with the carboxyl groups of GO, and the epoxide groups of GO can engage in ring-opening reactions and be substituted by the polymer chains. In “grafting from” method, the precursor or monomer of the final polymer is first introduced to the GO surface and reacts with its functional groups and then, through various polymerization methods, the polymer chains are directly grafted from the GO surface.^{219,220} An example of “grafting from” modification route is represented in Figure 3.1. This method combines the advantages of the graphene surface modification and in situ polymerization to enhance the compatibility of graphene and polymer matrix. Both of these grafting methods heavily rely on the density and reactivity of the GO functional groups. While the “grafting from” method provides a higher surface coverage with longer polymer chains, the “grafting to” method allows for a wider range of polymer choices and is not restricted by the polymerization methods available for specific GO surface chemistry.^{214,215}

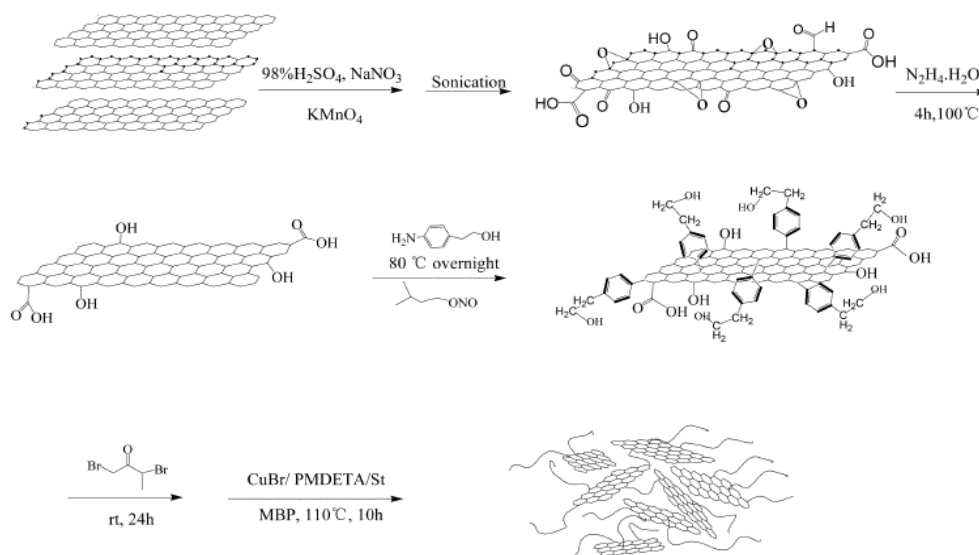


Figure 3.1. Schematic of the covalent functionalization of graphene with polystyrene using “grafting from” approach (reproduced from Fang *et al.*²¹⁹).

The non-covalent functionalization of graphene surface is feasible through π - π stacking of aromatic units of the polymers and graphene, graphene-polymer hydrogen bonding and electrostatic interactions of charged polymers and graphene surface.^{214,215} The π - π interactions can be used to modify pristine graphene, RGO and GO, but the hydrogen bonding and electrostatic modifications are restricted to RGO and GO, as they need hydroxyl groups and electrostatic charges on the graphene surface to interact with the polymer. To non-covalently functionalize the RGO or pristine graphene sheets, π - π stacking molecules such as pyrene and perylene have been grafted to various polymer chains and the final polymers were used to homogeneously disperse graphene in a

solvent (Figure 3.2).^{222,225} Also, conjugated polymers such as PEDOT are capable of π - π stacking with graphene and dispersing it in the solvent.^{223,224}

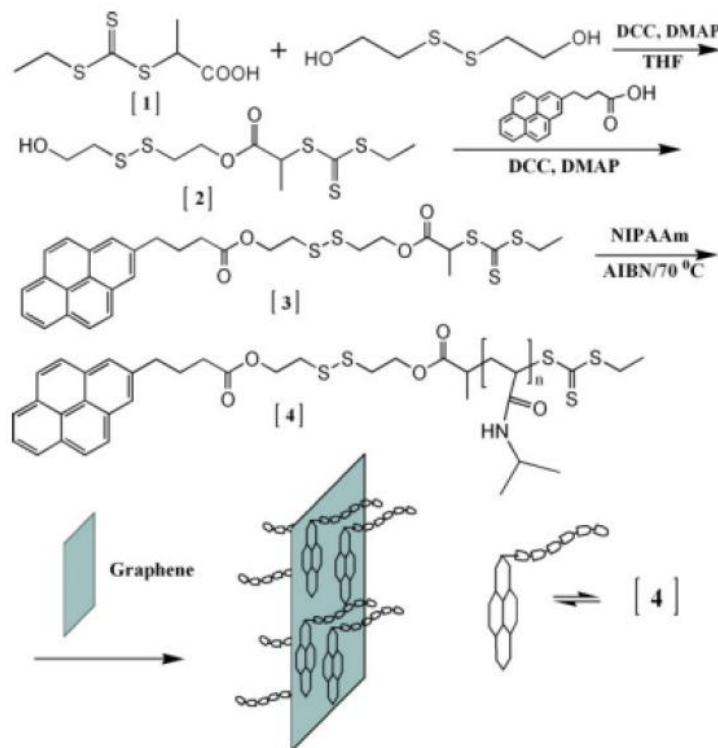


Figure 3.2. Non-covalent functionalization of graphene by grafting pyrene-terminated PANIPAAm to its surface (reproduced from Liu *et al.*²²²).

3.1.4 Fabrication of graphene-polymer nanocomposites

The graphene-polymer mixture can be processed via various fabrication techniques to produce the final nanocomposite (Figure 3.3). Conventional nanocomposite fabrication techniques such as melt processing in extruders, internal mixers and twin-roller mills, as well as masterbatching and molding approaches can be

applied on melt-blended graphene-polymer mixtures.^{191,226-229} The solvent in the solvent-blended mixtures can be removed by simple casting and evaporation or filtration techniques.^{8,197-199} The latex or emulsion-mixed samples usually require hot-pressing to form an integrated nanocomposite structure.²⁰⁹⁻²¹¹

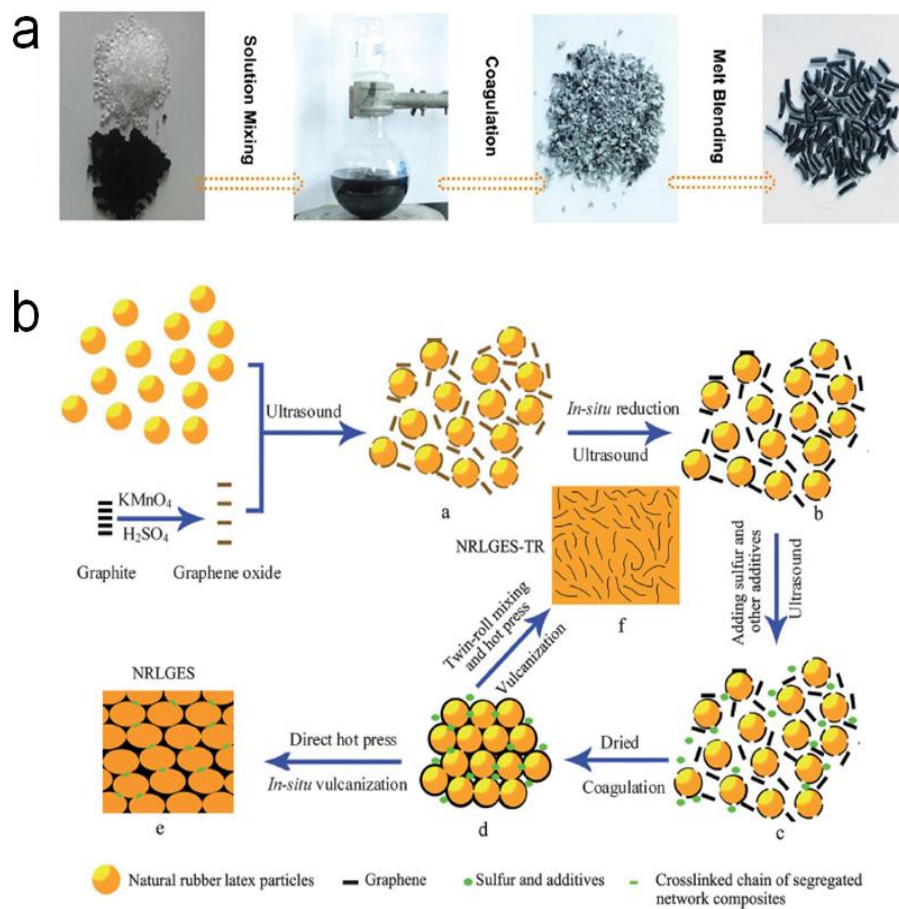


Figure 3.3. Fabrication of (a) graphene-polycarbonate nanocomposite through solution mixing and melt blending (reproduced from Shen *et al.*²²⁷), and (b) graphene-natural rubber nanocomposite through latex-mixing, melt mixing and hot-pressing (reproduced from Zhan *et al.*²¹⁰).

Electrospinning of a graphene-polymer solution is another fabrication method that produces nanocomposite fibers.^{230,231} This method produces mechanically strong fibers; however, the stability and homogeneity of graphene dispersion in the polymer solution and the lack of variety in the morphology of the final composites remains as the main concerns in this method.

A different strategy has been applied to control the arrangement of the graphene sheets within the polymer matrix. In contrast to graphene-filled nanocomposites, in which the graphene sheets are randomly distributed within the polymer matrix, 3D graphene-based aerogels have been filled with polymers to yield graphene-polymer nanocomposites with a well-structured 3D percolating path.²³² In this method, the in situ polymerization and cross-linking of the polymer chains in presence of well-dispersed graphene sheets results in graphene/polymer hydrogels.¹⁷⁶ These hydrogels can then be dried via freeze-drying and critical point drying techniques to yield a monolithic graphene/polymer aerogels. Preparation of polymer-free 3D graphene-based aerogels is also possible through hydrothermal and sol-gel techniques which will be discussed in next section.^{233,234} Backfilling of the 3D graphene-based aerogels with other polymers such as epoxy results in formation of electrically conductive graphene-polymer nanocomposites with low filler content.²³²

3.2 Graphene two-dimensional assemblies

Graphene-based 2D materials have potential applications in transparent conductive films,^{77,235-237} electronic devices and transistors,^{85,238-240} batteries and

supercapacitors,^{241,242} sensors²⁴³⁻²⁴⁵ and membranes.^{246,247} Unlike in nanocomposites, where low amounts of graphene are used to reinforce the polymer matrix, these applications demand the availability of graphene properties along the surface of a large-area graphene network. The properties of such a network are dictated by the individual graphene sheets properties, as well as the connectivity of those sheets in the network. These 2D networks can be produced by using CVD technique or by processing the graphene-containing solutions. The liquid-phase processing allows for fabrication of freestanding graphene papers and thin films of graphene sheets on a substrate.

3.2.1 Graphene-based thin films

Liquid-phase preparation of graphene thin film occurs through deposition of graphene sheets from a solution on a substrate, followed by solvent removal. This process can be performed using various fabrication methods including the conventional processing techniques such as drop-casting, as well as more recent ones like layer-by-layer (LBL) assembly (Figure 3.4). The graphene-containing solution can be chosen from various types of graphene dispersions, solution mixtures of graphene and polymers and mixtures of graphene and other nanomaterials. According to the existing literature, GO and RGO are the main sources of graphene in liquid-phase thin film preparation. Their higher solubility in the solvents simplifies their processing, while their chemical reactivity facilitates the network formation through inert-sheet and sheet-substrate interactions. However, simultaneous or subsequent reduction of these sheets is necessary to enhance the electrical, thermal and optical properties of the film. There are fewer

reports of pristine graphene 2D network in the literature; in most of these reports polymers are used as stabilizers. The choice of graphene solution, substrate and fabrication technique determines the alignment of the sheets, graphene content, thickness and uniformity of the film. Repeatability and scalability of the processing technique are other key issues in graphene thin film preparation.

In drop casting, the dispersion or the solution mixture of graphene and polymer are cast on a substrate, allowing for solvent evaporation with or without heating.^{248,249} The thickness of the film depends on the solid content of the solution. The film formation is controlled by various parameters such as graphene (and polymer, if present) concentration, temperature and the solvent evaporation from the air-liquid interface. The uniformity of the final film is usually affected by drying effects (e.g. coffee ring formation) and graphene sheets are aligned randomly within the film. Rod-coating is a variation of drop casting in which a metal bar is used to control the deposition and coating of the graphene solution on the substrate. Moreover, it is feasible to manipulate the sheets arrangement through graphene-substrate interactions; to do so, the surface of the substrate needs to be modified to attract the graphene sheets deposition.²⁵⁰

Spin-coating is another popular technique that has been used to fabricate graphene thin films. The graphene concentration (and polymer, if present), spinning speed and duration, and solution viscosity affect the thickness of the final film. The fast evaporation of the solvent, mostly resolves the drying issues associated with the drop casting method. However, the alignment of the graphene sheets in the film is dictated by

the rotational motion of the solution and cannot be altered. Mostly GO and RGO-based films have been prepared using this technique.^{75,251,252}

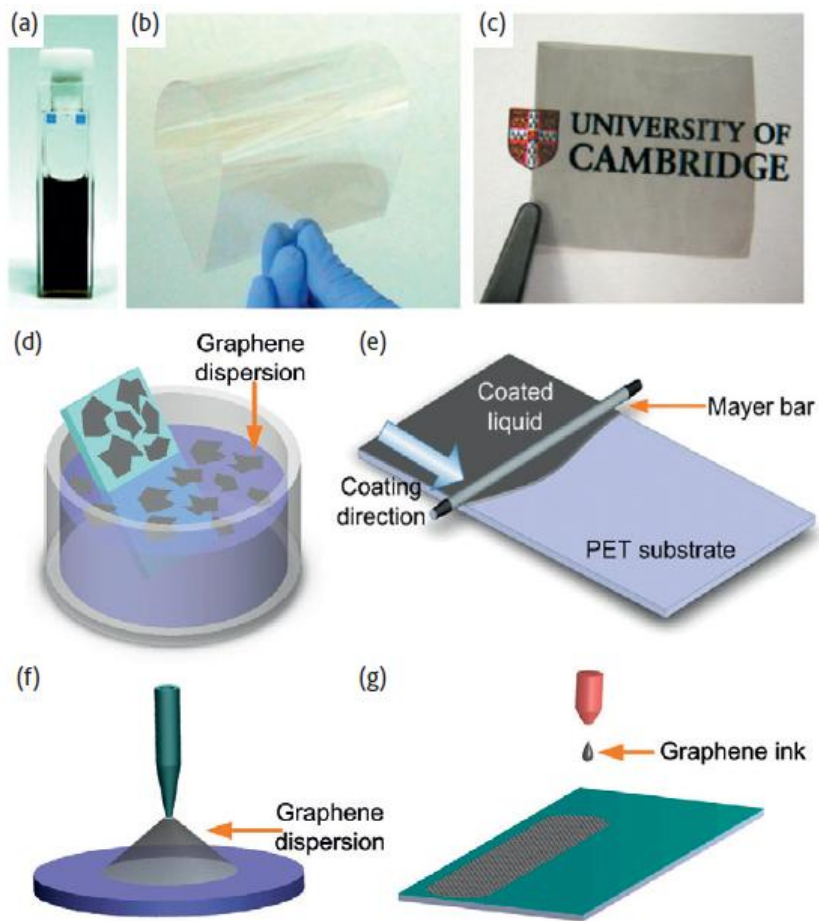


Figure 3.4. (a) Typical graphene ink/solution used in the thin film fabrication, (b) a transparent graphene conductive thin film, (c) graphene-PVA composite thin film, (d) dip-coating of a substrate in graphene dispersion is another method for thin film fabrication, (e) rod-coating of graphene solution on substrate, (f) spray-coating of graphene dispersion through air on the substrate, and (g) inkjet-printing using graphene ink (reproduced from Bonaccorso *et al.*¹²³).

Spray-coating of the graphene dispersions allows for more uniform deposition of graphene sheets on a substrate. The thickness of the film can be controlled by graphene concentration and spraying duration. Developing patterned thin films is feasible in this method by using a patterned substrate. Like with spin-coating, mostly GO and RGO-based films have been prepared using this technique.^{62,253,254}

Furthermore, electrophoretic deposition of graphene sheets from GO and RGO dispersions has been reported.^{238,255-257} In this method the negatively charged graphene sheets are deposited on a positively charged electrode. The graphene concentration in the solvent, the working voltage, and the deposition time are the parameters affecting the thickness and uniformity of the final film.

Layer-by-layer assembly of graphene sheets allows for a precise control over the alignment of the graphene sheets and the film microstructure.²⁵⁸⁻²⁶⁵ In this technique, alternating layers of materials are deposited from a graphene-containing solution and a polymer solution. The adhesion of the alternative layers is accomplished by electrostatic attraction between oppositely charged materials of each layer, hydrophobic attractions or the covalent interactions of the materials within each layer. GO has been usually used as the graphene source; GO sheets can participate in electrostatic and/or covalent interactions with the polymers in the adjacent layers. The deposition of each individual layer can be achieved via drop-casting, spin-coating, dip-coating²⁶² or spray-coating,²⁶⁶ or vacuum filtration; in this sense, the properties of each layer is controlled by the parameters mentioned earlier in discussion of these methods. However, the inter-layer interactions can be precisely controlled by adjusting the pH, temperature, deposition

time of each layer and the concentration of materials in the solutions.^{260,261} The thickness, uniformity and properties of the resultant thin film depends on the both individual layer properties and the inter-layer interactions. Recently, the LBL assembly using polymer-stabilized pristine graphene dispersion has been reported.

Inkjet-printed graphene thin films are promising candidates as electrically conductive constituents of transistors,²⁶⁷ solar cells,²⁶⁸ supercapacitors²⁴² and chemical sensors^{244,269}. Using this technique, droplets of graphene ink can be deposited on different substrates. The graphene ink needs to satisfy some requirements to yield a uniform, well-connected film of graphene flakes.²⁷⁰ First, large quantities of graphene are needed to form a continuous film upon deposition and thus, graphene dispersions with concentration much higher than those obtained by liquid-phase exfoliation methods are required.²⁷¹ Also, the graphene sheet size has to be smaller than the inkjet cartridge nozzle diameter to avoid clogging the nozzle.²⁶⁸ Moreover, the inkjet printing process requires a particular range of ink viscosity and surface tension that usually cannot be obtained through the common liquid-phase exfoliation of graphene.^{271,272} GO dispersions in water are good candidates as graphene inks since their high solubility in water assists with obtaining high concentrations of graphene.^{273,274} However, the GO sheets are not conductive, so further thermal annealing is necessary to restore electrical conductivity.²⁴² The thermal annealing conditions (i.e. high temperatures) are not always compatible with the thermally sensitive substrates. Pristine graphene inks have been developed by adding ethyl cellulose and ethyl glycol during the exfoliation process to tune the viscosity and surface tension of the ink.^{268,271,275-277} Presence of ethyl cellulose in the ink

prevents aggregation of the nanosheets caused by the drying effects. Recently, shear-exfoliated graphene dispersions have been used as graphene inks.²⁷⁸ Moreover, an alternative annealing method, intense pulsed light annealing, has been applied to remove the remaining polymer content and improve the conductivity of the films.²⁷⁹ It is worth mentioning that non-covalently functionalized graphene thin films have been prepared by vacuum filtration of surfactant-stabilized graphene dispersions.¹⁷¹

3.2.2 Freestanding graphene-based papers

Freestanding graphene films have been used to prepare battery and supercapacitor electrodes, and membranes for water purification and gas sensors. These films have been prepared by the flow-directed vacuum filtration of graphene dispersions and graphene-polymer mixture solutions. During the filtration process, the graphene sheets align and assemble on top of the filtration membrane.²⁸⁰ The tightly packed graphene film can be peeled off from the membrane to yield a paper-like freestanding film. These films were first prepared from GO dispersions; the mechanical properties of the GO paper-like films surpassed those of CNT buckypapers (Figure 3.5a and b).²⁸¹ It was argued that the interlocking of the GO sheets through hydrogen bonding between the film layers enhanced the inter-layer load transfer. The film thickness and transparency could be controlled by the dispersion concentration and total mass of the GO.⁷⁷ However, the GO freestanding film are not electrically conductive, therefore, attempts have been made to reduce them by filtering hydrazine over the film²⁸² or by flash photothermal reduction.²⁸³ The alternative was to vacuum filter the RGO

dispersion; the resultant RGO freestanding films were highly conductive and mechanically strong (Figure 3.5c and d).^{284,285} Also, graphene-polymer composite films have been produced using this method, including GO-PVA and GO-PMMA,²⁸⁶ pristine graphene-cellulose,²⁸⁷ GO-cellulose,²⁸⁸ RGO-pyrenebutyrate.²⁸⁹

3.3 Graphene three-dimensional networks

Three-dimensional networks of graphene have exceptional surface area and porosity, mechanical stability and electrical conductivity.^{290,291} Combination of all these unique properties in a bulk macroscale structure can be exploited in preparation batteries and supercapacitors electrodes, adsorbents, sensors, and catalysts.²⁹²⁻²⁹⁴ Production methods of these networks include: (1) using a pre-existing 3D network as template, followed by removal of the templates,²⁹⁵⁻²⁹⁷ and (2) assembly of the GO sheets in the liquid phase, followed by removal of liquid phase, and reduction of GO.^{233,234,298} Products of these two approaches are very different in their properties and applications.

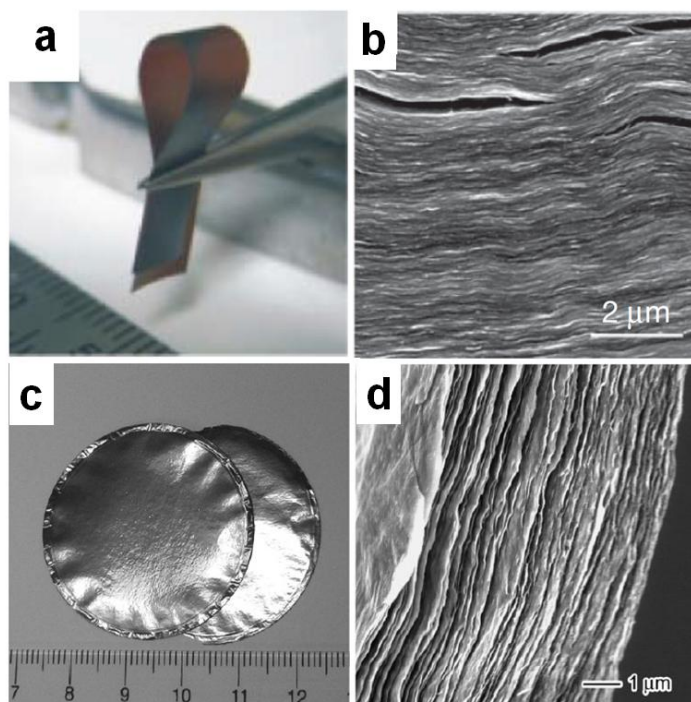


Figure 3.5. (a) Digital photo of flexible freestanding GO film, (b) SEM image of the the cross-section of GO freestanding film (reproduced from Dikin *et al.*²⁸¹), (c) digital photo of RGO freestanding films, and (d) SEM image of the cross-section of RGO freestanding film (reproduced from Chen *et al.*²⁸⁵).

Pristine graphene 3D networks have been prepared by growing graphene via CVD on metallic templates such as nickel foam²⁹⁵ and copper mesh²⁹⁹, graphitization of 3D carbonaceous structures and coating or soaking of sponges of various materials in pristine graphene dispersions.³⁰⁰ Due to the intact π -structure of pristine graphene, these 3D structures have high electrical conductivities. However, alteration of their porous structure is difficult as it is patterned by the template structure. Moreover, removal of the template is tedious and sometimes impossible. The etching techniques used for removal

of nickel foam from CVD-grown networks are costly and time consuming; also, the graphitization of sponges and carbonaceous templates demands high temperature.

On the other hand, the versatile surface chemistry of GO enables assembly of these sheets in the liquid phase to produce GO 3D networks with exceptional porous structure.^{233,234} To obtain electrical conductivity and mechanical strength, those networks need to be dried and reduced to form RGO aerogels. A homogeneous colloidal dispersion of GO sheets in the solvent is the starting medium for the assembly process. Specific combinations of the solvent polarity, GO surface chemistry (i.e. atomic composition, density, type and ionic strength of its functional groups), GO concentration, sheets size and pH of the dispersion are required to attain stable dispersions.³⁰¹ Alteration of any of those parameters may lead to destabilization of the dispersion; the assembly process initiates when the dispersion is destabilized and the GO sheets tend to aggregate. Various assembly techniques apply different stimuli such as temperature, pressure or pH of the dispersion to change the GO interactions to prompt aggregation. As the sheets approach each other, inter-sheet physical and/or chemical bonds form; under proper condition (e.g. optimum GO concentration, dispersion pH, etc), formation of these bonds leads to gelation. Subsequently, the well-integrated gel can be dried via lyophilization (i.e. freeze drying) or critical drying point (CPD) techniques in order to maintain the original porous structure and produce aerogels. Further thermal reduction of the aerogels restores the graphene π network and removes the residual functional groups from the sheets.

Hydrothermal reduction of GO sheets in an aqueous dispersion has been widely used to prepare GO hydrogels (Figure 3.6).²³³ In this method, increasing the temperature and pressure in an autoclave vessel reduces the solubility of the GO in the liquid phase.³⁰² Simultaneously, partial reduction of the GO sheets takes place as the dispersion heats up to higher temperatures.³⁰³ The sheets assembly occurs upon the phase separation of GO and water, and the alteration of GO surface chemistry. The reduced sections of the GO sheets overlap and π - π stack to form physical cross-links. Furthermore, the remaining hydroxyl groups which survived the reduction can participate in hydrogen bonding with other sheets.^{233,304,305}

Usually, temperatures higher than 150 °C are required to accomplish sufficient degree of reduction for effective localized π - π stacking.^{233,306} The GO concentration is a definitive factor that can promote gelation as opposed to aggregation. At low concentrations, the distant GO sheets are incapable of forming a continuous network; thus, a minimum saturation concentration is required for gelation.²³³ As the concentration goes above the saturation concentration, densely packed hydrogels will form. The same logic applies to the sheets size; GO sheets with larger lateral size can form the network at lower concentrations.^{304,307} The pH of the dispersion is another important parameter that can affect destabilization process and tunes the affinity of the GO sheets for assembly. The pH of solution determines the ionization status of GO functional groups, especially carboxyl groups, and the hydrophilicity of the sheets. An acidic medium reduces the ionization of carboxyl groups and facilitates the destabilization of nanosheets and even strengthens the inter-sheet hydrogen bonding

during gelation.^{308,309} Furthermore, extensive attempts have been made to perform hydrothermal-assisted co-assembly of GO sheets and various guest particles in order to accomplish multifunctional 3D networks with unique properties.³¹⁰

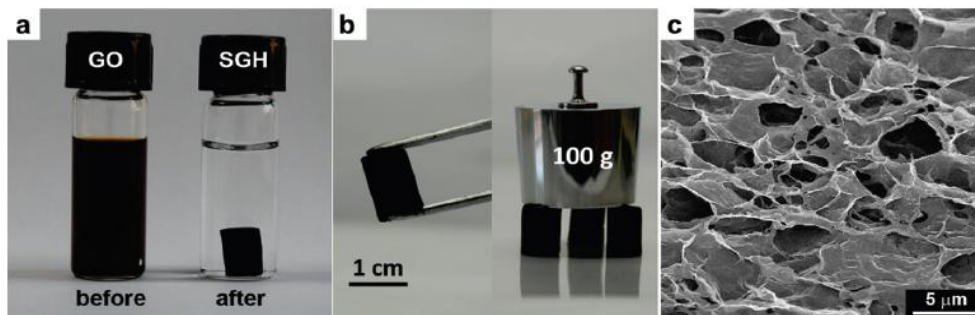


Figure 3.6. Hydrothermal synthesis of 3D graphene network, (a) digital photo of GO dispersions and GO hydrogel, (b) digital photo of the hydrothermally-reduced GO aerogels, and (c) SEM image of the microporous structure of the hydrothermally-reduced GO aerogel (reproduced from Xu *et al.*²³³).

In addition to physical cross-linking (i.e., π - π stacking and hydrogen bonding), GO sheets can be chemically cross-linked to form 3D networks. Formation of chemical bonds between the sheets promotes the network formation. These chemical bonds can be introduced to the gel structure through a second component which reacts with GO sheets and connects them together. The second component could be a polymer, metal ion or some organic molecule.^{298,304,308,311-313} The polymers mostly interact with GO sheets through bonding with their functional groups, while the metal ions promote gelation through electron donor-acceptor and ion- π interactions. The type and morphology of the second component defines the porous structure of the gels. Although the presence of

second components improves the mechanical properties of the final aerogels, but it may restricts the electrical conductivity of the product.

To address this issue, the sol-gel technique has been used to prepare highly conductive graphene aerogels by avoiding the usage of non-conductive second components. In this method, a catalyst is added to the GO dispersion to facilitate chemical bond formation between GO sheets and other components^{234,314} or to trigger direct chemical bonding of GO sheets through their epoxide and hydroxyl groups.³¹⁵ According to Worsley *et al.*, the other components used in this method (resorcinol and formaldehyde) participate in a polymeric network formation that can later be pyrolyzed at higher temperatures (Figure 3.7a).²³⁴ Direct cross-linking of GO sheets occurs through ammonia-assisted deoxygenation of functional groups, covalent bonding, GO reduction and π - π stacking of locally reduced sections of GO sheets.³¹⁵ In this case, higher temperatures (> 80 °C) are needed to activate the chemical reaction path. Like hydrothermal-assisted assembly, the temperature, GO concentration and the sheet size are important factors that affect the gel formation. The pH of reaction medium is also important; the basic condition improves ionization of the functional groups and improves their chemical reactivity. Additionally, the catalyst concentration affects the extent of chemical reactions and is definitive to the final structure of the hydrogels and dried aerogels. Room temperature drying of directly cross-linked GO sheets results in high-density aerogels and an improvement of mechanical and electrical properties by several order of magnitudes.³¹⁶

In situ reduction of GO sheets in presence of a reducing agent is another method to induce GO sheets assembly.^{306,317,318} The mechanism of gelation is similar to that of hydrothermal method; however, in this case, the chemical reduction of GO sheets induces aggregation and eliminates the need for higher temperatures. Since various reducing agents are capable of reacting with different functional groups and restore the π -conjugated network to different extents, the type and density of chemical bonds that promote the sheets assembly are different in each case. Thus, the properties of the dried aerogels vary based on the reducing agent used in the assembly process.³¹⁷ Moreover, addition of nanoparticles to the GO dispersion allows for simultaneous assembly of these particles within the 3D network of the gels.³¹²

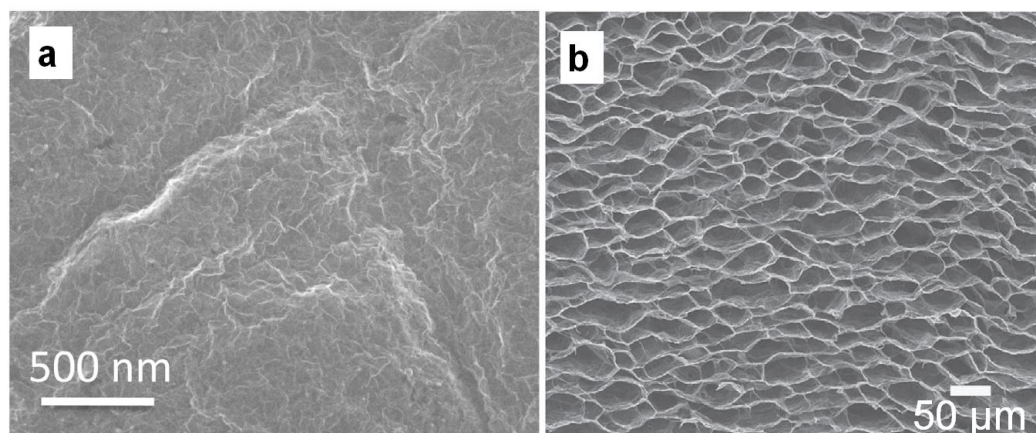


Figure 3.7. SEM images of RGO aerogels porous structure prepared by (a) sol-gel technique (reproduced from Worsley *et al.*³¹⁴), and (b) freeze-casting technique (reproduced from Qui *et al.*³¹⁹).

Freeze casting is another method to produce graphene-based porous structures with superior mechanical properties.³¹⁹ Freezing GO or partially reduced GO dispersions forms a continuous network of GO which mimics the ice crystalline structure (Figure 3.7b). During this process, as the water molecules solidify and form ice crystals, the sheets become entrapped within the ice-water crystal boundaries and form π - π stacks. Subsequent removal of the ice by freeze-drying yields a 3D GO structure which is connected by physical cross-links. Usage of partially reduced GO sheets as a starting material can enhance the π - π stacking and improves the properties.³¹⁹

3.4 Conclusion

The liquid-phase exfoliated graphene sheets are used for preparation of various graphene-based materials including nanocomposites, thin films, freestanding papers, and 3D networks. Graphene-polymer nanocomposites can be prepared by conventional polymer processing methods such as solution and melt blending. However, the significant gap in the surface energies of graphene and most of the polymers prevents the homogeneous dispersion of sheets in the matrix. Modification of graphene surface through covalent and non-covalent functionalization improves the compatibility of the sheets and the matrix and promotes the load transfer between the two phases. Furthermore, the homogeneous dispersion of graphene sheets within the matrix allows for polymer reinforcement at lower graphene loadings.

Two-dimensional assemblies of graphene are another category of graphene-based materials that are suitable for electronic devices such as transistors, sensors, and solar

cells. The thin films of graphene are deposited on various substrates via drop casting, spin coating, LBL assembly, or inkjet printing of graphene dispersions. The properties of the films are dictated by the individual sheet properties, as well as the arrangement and connectivity of the sheets within the 2D network.

Three-dimensional macrostructures of graphene are usually obtained by assembly of GO sheets in aqueous dispersions. The physical and chemical cross-linking of the GO sheets in the solvents forms a hydrogel that can be subsequently dried to yield a porous 3D network. Hydrothermal, sol-gel, and freeze-casting techniques have been used to prepare these networks. These networks have been used for preparation of battery electrodes, oil adsorbents and catalysts.

In Chapter IV, we present our work on dispersant-assisted exfoliation of pristine graphene in aqueous dispersions. In Chapter V and VI, we use the liquid-phase exfoliated pristine graphene to prepare composite films with enhanced electrical properties. In Chapter VII, we spray dry the pristine graphene dispersions to obtain crumpled graphene sheets. These crumpled particles are then used to prepare graphene 3D networks in Chapter VIII.

CHAPTER IV

GRAPHENE COLLOIDAL DISPERSIONS WITH PYRENE DERIVATIVES AS STABILIZERS*

4.1 Introduction

Production of large quantities of high-quality graphene sheets is essential for practical application of this unique material in real life. Liquid-phase exfoliation of graphene from graphite has been widely studied for its high graphene yield and quality, scalability, inexpensive precursors, ease of processing and versatility for a broad range of applications such as battery and supercapacitor electrodes,^{241,320} sensors,³²¹ polymer nanocomposites³²² and soft electronics^{273,323}. Oxidation of graphite and subsequent exfoliation of graphene oxide in water is one of the most common liquid-phase exfoliation methods.^{66,324} However, graphene oxide, with structural defects and functional groups on its surface, is electrically insulating and needs to be thermally or chemically reduced to become conductive.^{71,325} However, the complete restoration of the π -conjugated network, as in the pristine graphene structure, is impossible and RGO properties never reach those of pristine graphene.^{77,326}

Direct liquid-phase exfoliation of graphite yields pristine graphene sheets with minimal structural defects,¹⁷² but the reaggregation of these sheets in the solvent due to

* Part of the data reported in this chapter was adapted by permission from (Parviz *et al.*, "Dispersions of non-covalently functionalized graphene with minimal stabilizer", *ACS Nano*, 2012, 6, 8857-8867). Copyright 2012 American Chemical Society.

the strong inter-sheet attractive forces is a huge obstacle for obtaining stable graphene dispersions.¹⁷⁵ Using specific solvents with surface energies similar to that of graphene is a method to reduce the graphene-solvent interfacial tension and keep the graphene sheets dispersed in the solvent.^{103,133} However, many solvents including water do not have such surface energies; thus an alternative approach should be adopted to minimize the interfacial tension and/or increase the repulsive forces between graphene sheets such that they overcome the attractive forces and prevent reaggregation. Certain surfactants,^{37,137,171,174,237,327} polymers^{38,39} and aromatic molecules³²⁸ adsorb on the graphene surface and provide a repulsive shield around the graphene sheet and stabilize the exfoliated sheets in solvents with mismatching surface energies. However, presence of high quantities of adsorbed and non-adsorbed polymer and surfactants in the final dispersion affects the graphene quality by increasing the residual impurity content in the product. Thus, the search for alternative molecules that can stabilize higher graphene concentration with minimal stabilizer content is an ongoing process.

Several groups have reported the usage of different pyrene derivatives to stabilize CNTs^{329,330} and graphene^{177,178} in dispersions.^{289,331,332} However, a systematic study of the stabilization mechanism and its relationship to graphene yield and dispersion stability is missing in the existing literature. In this chapter, we investigate the effectiveness of various pyrene derivatives as graphene stabilizers, as well as the effect of different constituents of their molecular structure such as functional groups and the counterions on the graphene yield and quality. Also, we demonstrate that exceptionally

higher graphene/stabilizer ratios can be accomplished through pyrene derivatives as compared to polymers and surfactants.

The work presented in this chapter was published in 2012 as a journal article in *ACS Nano*.³³

4.2 Experimental procedures

4.2.1 Materials

Expanded graphite was provided by Asbury Carbons (CAS# 7782-42-5, Grade 3805). The pyrene derivatives including pyrene, 1-pyrenesulfonic acid sodium salt (Py-SASS), 1,3,6,8- pyrenetetrasulfonic acid tetra sodium salt (Py-(SO₃)₄), 1-pyrenesulfonic acid hydrate (Py-SAH), 1-aminopyrene (Py-NH₂), 1-pyrenemethylamine hydrochloride (Py-M-NH₂), 1-pyrenebutanol, 1-pyrenecarboxylic acid (PCA) and 1-pyrenebutyric acid (PBA) were purchased from Sigma-Aldrich. Sodium dodecylbenzene sulfonate (SDBS) was purchased from MP Biomedicals. Polyvinylpyrrolidone (PVP) (M_w ~10000) was purchased from Sigma-Aldrich. Epoxy resin and hardener were purchased from FibreGlast Developments Corporation. All the chemicals were used as received.

4.2.2 Preparation of graphene dispersions

In a typical preparation, a specific amount of stabilizer (pyrene derivatives, PVP or SDBS) was dissolved in 20 ml of deionized water (DI). In case of PCA and PBA, the pH of solution was increased to 10 by addition of ammonium hydroxide in order to completely dissolve them in DI water. Expanded graphite (EG) was added to the

stabilizer solution and tip sonicated for one hour using a Misonix sonicator (XL 2000) at output wattage of 7W at room temperature. During the sonication the temperature was kept in at room temperature using a water bath as a heat sink. The dispersion was then centrifuged (Centrifuge 225, Fischer Scientific) at 5000 rpm for 4 hours to remove larger graphitic aggregates and the supernatant was collected as the final dispersion. This stable dispersion was used for further characterizations and composite production. The initial concentrations of stabilizers were varied over a range of 0.5-7mg/ml. The ratio of the initial concentration of EG to initial concentration of stabilizer was 10, 20 and 30 in order to study the effect of concentration of EG on the graphene yield. The initial concentration of SDBS and PVP was 6 and 10 mg/ml, respectively.

4.2.3 Preparation of graphene/epoxy composite

Py-SASS-stabilized graphene dispersion with 3 mg/ml of Py-SASS and 0.8 mg/ml graphene was freeze-dried overnight. To prepare 0.5 wt% graphene/epoxy composite 0.1 g of freeze-dried powder was added gradually to 3.15 g of epoxy resin and vigorously stirred for half an hour. Then the mixture was sonicated for 30 min. 0.85 g of hardener agent was added to the mixture and stirred. Resulting homogeneous mixture was degassed in vacuum oven at 50 oC to get rid of bubbles. Finally the sample was doctor-bladed on a dog-bone shaped substrate and cured in the oven at 77 oC for 6 hours. For comparison, 0.5 wt% graphene/epoxy composite was prepared by same procedure using PVP-stabilized graphene. The final concentration value of graphene in PVP-assisted dispersion was 1 mg/ml.

4.2.4 Characterization of graphene dispersions

To calculate the post-centrifugation concentration of graphene, the UV-vis spectroscopy was performed on a Shimadzu UV-vis spectrophotometer 2550 at a wavelength of 660 nm on the dispersions. A stabilizer solution with a concentration similar to that of graphene dispersion was used as the blank to eliminate the effects of the stabilizer on the absorbance. The graphene concentration was determined using Beer's law. According to Beer's law, $A = \alpha * C * l$, in which A is the absorbance at the given wavelength, α is the molar extinction coefficient in the solution, l is the path length of the light and C is the concentration. In order to calculate the extinction coefficient, a regular vacuum filtration setup was utilized to measure the concentration of graphene in the dispersion. Polytetrafluoroethylene (PTFE) membrane with a pore size of 0.02 μm was used as the filter. The mass of the PTFE membrane, before and after filtration was measured and used to determine the concentration of graphene. The absorbance of the same dispersion (with now known concentration) was measured at 660 and used to calculate the extinction coefficient in the stabilizer solution. The same filtered samples were used to measure Raman spectra on a Renishaw Raman microscope using a 633 nm He-Ne laser.

High Resolution Transmission Electron Microscopy (HRTEM) samples were prepared by deposition of a single drop of the dispersion on a 400-mesh carbon-coated copper grid (Electron Microscopy Sciences, CF400-Cu), followed by air drying for a few minutes. A voltage of 75 kV was used to image the samples on Hitachi H8100.

Thermogravimetric analysis (TGA) was carried out in TGA i 1000, Instrument Specialist Inc. The temperature was raised from 0 °C to 1000 °C at the rate of 10 °C/min.

Zeta potential measurements were conducted on a Zetatrac analyzer from Microtrac Inc. Two laser beams at 780 nm were irradiated to measure the electrophoretic mobility of particles using the principles of dynamic light scattering. The Zetatrac analyzer calculates the value of zeta potential from electrophoretic mobility using the Smoluchowski equation: $\xi = \mu\eta / \epsilon$, where ξ is the zeta potential, μ is the mobility, η is the viscosity of solution and ϵ is the dielectric constant of the solvent. Also, stability of the dispersions against pH changes was examined by the zeta potential measurements at various pH values of the dispersions. For these experiments, drop-wise addition of hydrochloric acid (HCl) and sodium hydroxide (NaOH) to the dispersions in an autotitrator from Microtrac Inc was used to alter the dispersion pH. All measurements were carried at room temperature.

The average particle size was measured using Dynamic Light Scattering (DLS) technique within the Zetatrac particle size analyzer unit from Microtrac Inc. Samples concentration, if necessary, were diluted to at 0.05 -0.1 mg/ml for these measurements.

4.2.5 Dispersion stability tests

Graphene dispersions were frozen in a freezer at -15 °C and then freeze-dried (Vitrif Benchtop Freeze Dryer) overnight to yield graphene powder samples. The freeze-dried samples were redispersed in water and sonicated for 5 min. Redispersed samples

were centrifuged and the concentration of graphene in supernatant was measured to evaluate the redispersibility of the graphene. Visible stability of the dispersion at higher temperatures was tested by heating and centrifugation of the dispersions. Samples were heated up gradually and after each 10 °C raise in the temperature they were centrifuged for 30 min to check the possibility of visible sedimentation at higher temperatures. Above 70 °C, samples were centrifuged after each 5 °C raise in the temperature.

Desorption of Py-SASS from graphene surface in presence of ethanol was studied by adding ethanol to Py-SASS-assisted dispersions to get dispersions with 10 to 90 vol% of ethanol. All samples were centrifuged simultaneously for 1 hr and then the concentration of graphene in supernatant was measured to study desorption of Py-SASS from graphene in presence of ethanol. Samples containing graphene in the supernatant were centrifuged for another 1 hr to test the time dependence of the desorption process.

4.2.6 Characterization of graphene/epoxy composites

Scanning Electron Microscopy (SEM): Samples were prepared by mounting the samples on double-faced carbon tape and sputter coating with gold at 10 mA current for 1 min. An accelerating voltage of 5 kV was used to image the specimens on a Hitachi S4300 SE/N.

Mechanical tests: Tensile tests were performed in a Test ResourcesTM universal testing machine (made in USA). Young's modulus and tensile strength were averaged from three tested specimens. Monotonic tensile testing was conducted on the specimens by moving the linear actuator of the machine; the upper grip was moved up with the

actuator over a fixed displacement of 10 mm in 1000 sec and the lower grip was fixed. The machine was operated on displacement feedback mode. The resulting load data was plotted as a function of the displacement and the initial part of the curve was fitted with a linear trend line. Based on a high fitting coefficient (i.e., $R^2 > 95\%$), the elastic modulus and the yield strength were determined from this linear regime.³²⁸

Electrical conductivity measurement: Electrical resistivity of the composites was measured by standard four point probe method. The four point probe head (Signatone, SP4-40045TBY) was mounted on a resistivity measurement stand (Signatone, Model 302). Two outer probes were connected to high impedance current source (Keithley 2400) to supply current through the sample and inner probes were coupled with a digital voltmeter (Keithley 2000) to measure the voltage drop across the two probes.³²⁸

4.3 Results and discussion

4.3.1 Quality of graphene sheets

Various pyrene derivatives with various functional groups were used to stabilize graphene in aqueous solutions. The molecular structure of these pyrene derivatives is demonstrated in Figure 4.1. Among these derivatives, pyrene, P-NH₂ and PB were insoluble in water, but all other derivatives were dissolved in water either by pH change or by heating the solution.

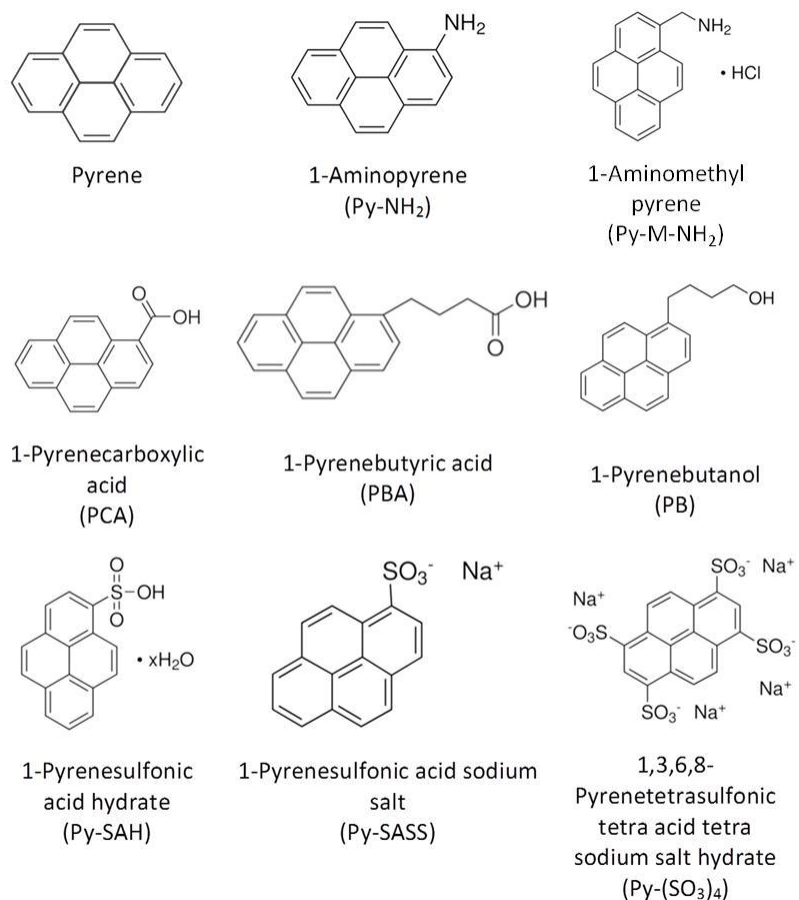


Figure 4.1. The molecular structure of various pyrene derivatives used in this study as graphene stabilizers.

To evaluate the quality of graphene dispersed by pyrene derivatives, Py-SASS-stabilized samples were characterized by HRTEM (Figure 4.2). Counting the number of layers at the edge of the graphene sheet, which is a common technique for assessment of the number of graphene layers,^{38,169,171} indicated that PY-SASS-stabilized graphene sheets are consisted of 2-4 graphene layers. Also, the lateral dimensions of the sheets

varied between 2 to 3 μm . The lateral size and number of layers of the sheets are consistent with the values reported in the literature for directly-exfoliated graphene sheets in the liquid phase after centrifugation.³⁸

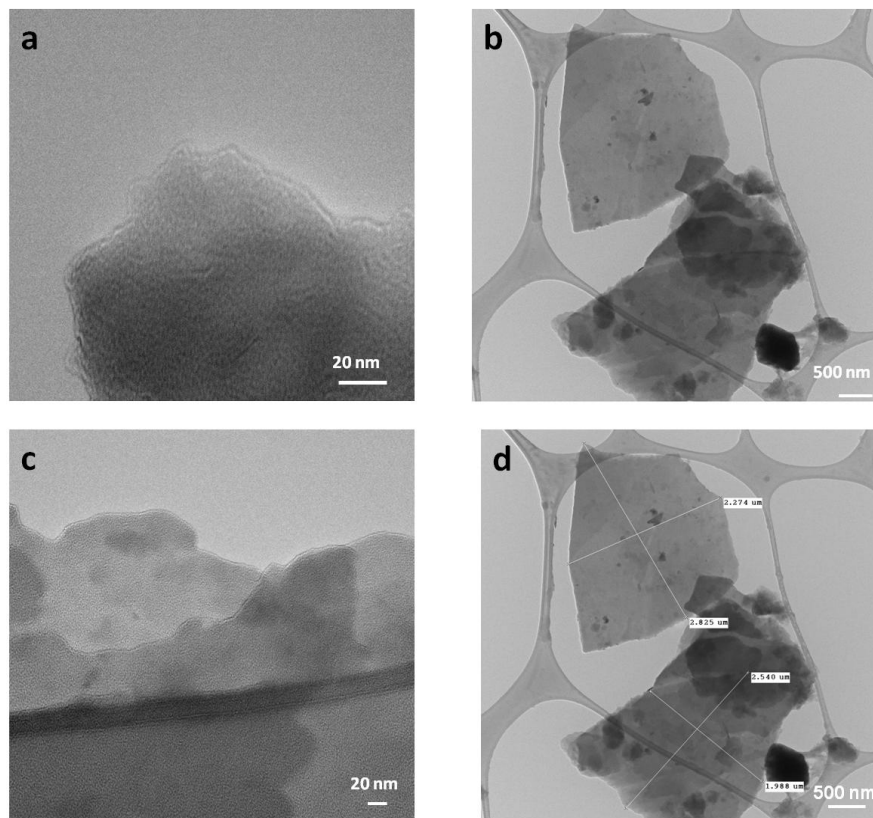


Figure 4.2. HRTEM images of the graphene sheets in Py-SASS-stabilized aqueous dispersion. Counting the number of the layers on the edge of the sheets reveals the few-layer nature of stabilized graphene. The sheet size varies between 2 to 3 μm .

The degree of exfoliation and the structural defects of the PY-SASS-stabilized graphene sheets were evaluated using RAMAN spectroscopy and comparison against parent expanded graphite spectra (Figure 4.3). Raman spectra of both materials

demonstrate the three characteristic peaks of graphitic materials at 1330, 1580, and 2680 cm^{-1} , corresponding to the D, G and 2D bands, respectively. The G band represents the presence of sp^2 -hybridized carbon bonds in both graphene and expanded graphite samples. The 2D band reflects the number of layers in the graphene and graphite sheets.⁸⁸ The downward shift of graphene 2D band compared to the parent graphite 2D peak verifies the few-layer nature of the Py-SASS-stabilized graphene sheets. The D band is representative of lattice defects and edge effects. Compared to parent graphite, the D band of graphene sample demonstrated increased intensity; this could be attributed to the increase in the number of graphene edges exposed in exfoliated sheets with lower later size.^{88,169}

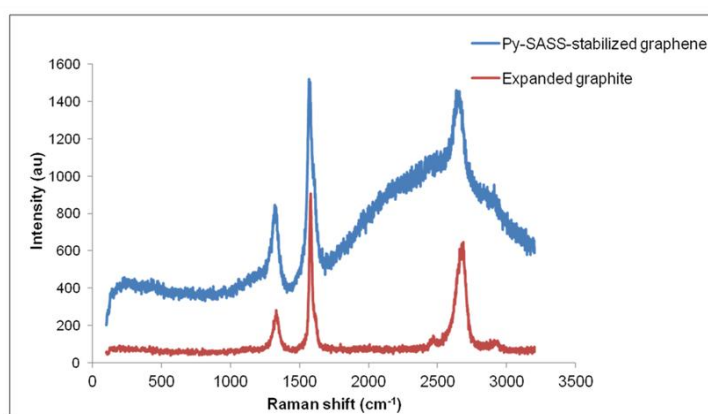


Figure 4.3. Raman spectra of expanded graphite and Py-SASS-stabilized graphene. Downward shift of the 2D band at 2675 cm^{-1} confirms the few-layer nature of the stabilized graphene. Presence of Py-SASS on the graphene surface appears in the broad shoulder bound to the 2D band.

4.3.2 Effectiveness of pyrene derivatives as graphene stabilizers

Pyrene is a prominent polycyclic aromatic hydrocarbon (PAH) with a molecular structure similar to graphene. The existence of sp^2 -hybridized carbon network in pyrene facilitates the electron sharing with graphene through π - π interactions.^{333,334} Pyrene derivatives consist of a pyrene basal plane which is covalently functionalized by any of the carboxyl, sulfonyl, hydroxyl and amine groups. In the water, these molecules adsorb on graphene surface through π - π interactions to minimize the total surface energy of the dispersion. Meanwhile, the polar functional groups provide stability in water, as well as an electrostatic repulsive shield around the graphene sheets (Figure 4.4).

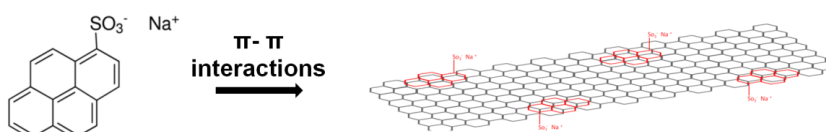


Figure 4.4. Schematic of mechanism of pyrene derivatives adsorption on graphene surface.

The effectiveness of pyrene derivatives as graphene stabilizers was evaluated by measuring the post-centrifugation concentration of graphene sheets in the dispersions. Figure 4.5 demonstrates the final graphene concentrations in the dispersions, stabilized by various concentrations of different pyrene derivatives.

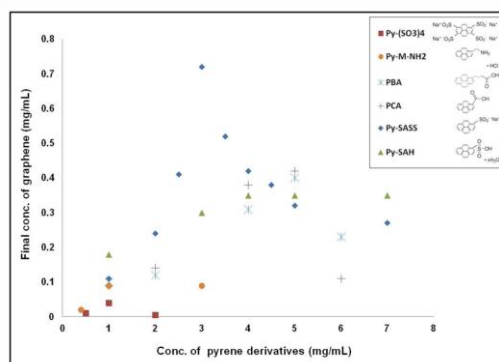


Figure 4.5. Final concentration of graphene stabilized by different pyrene derivatives concentrations. The concentration of parent expanded graphite in all the dispersions was 20 mg/ml.

Since different graphene concentrations were obtained using different pyrene derivatives, and based on the fact that pyrene derivatives are only different in their functional groups, we argue that the effectiveness of these molecules as stabilizers is determined by the type of the functional group attached to the pyrene basal plane. For a range of initial stabilizer concentrations, Py-SASS and Py-SAH with one sulfonyl group yielded higher graphene concentrations than the PCA and PBA which each have one carboxyl group. Moreover, the Py-M-NH₂ with amine functional group was the least effective stabilizer among all the pyrene derivatives, yielded the lowest graphene concentration (0.089 mg/ml). Therefore, a trend of functional groups effectiveness exists, summarized as sulfonyl > carboxyl > amine (Table 4.1). This trend may be explained by the mechanism behind the adsorption of pyrene derivatives on graphene surface. The pyrene derivatives adsorb on graphene by sharing π electrons (i.e. π - π interactions); the electron acceptance/donation between the two surfaces occurs due to

the variation in the electron density on their aromatic planes. The electron density on pyrene changes due to the temporary polarization that occurs in presence of the polar functional groups. The electron depletion/accumulation on pyrene surface is controlled by the electronegativity of the functional groups. The sulfonyl group in Py-SASS and Py-SAH has the highest electronegativity between the above-mentioned functional groups. This electron-withdrawing group reduces the electron density on the pyrene basal plane and facilitates the electron acceptance from the π -network of graphene surface. Hence, Py-SASS and Py-SAH have higher affinity to adsorb on the graphene surface and can stabilize higher number of exfoliated graphene sheets during the sonication process. The electronegativity of carboxyl group is lower than sulfonyl, thus, it has a lower tendency withdraw electrons from graphene and adsorb on its surface compared to sulfonyl group. The amine group has the least electronegativity among all the functional groups and is a weak electron-donor group. Hence, it has lower tendency for adsorption on graphene surface compared the other functional groups and yield the minimum stabilized graphene concentration.

Stabilizer	Functional group	Stabilizer conc. (mg/mL)	EG conc. (mg/mL)	Final graphene conc. (mg/mL)
1-pyrenesulfonic acid sodium Salt	Sulfonyl	2	20	0.24
1-pyrenecarboxylic acid	Carboxyl	2	20	0.14
1-aminomethylpyrene	Amine	2	20	0.089

Table 4.1. Effect of functional groups on the graphene yield. The effectiveness of the functional groups changes in the order of sulfonyl > carboxyl > amine.

As the pyrene derivatives adsorb on graphene, their polar functional groups dissociate in the water and form an outer layer of counterions around the stabilized graphene sheets. According to DLVO theory, the total neutralization of the ions in the solution occurs at a distance from the surface, leaving a layer of counterions with a total opposite charge around the graphene.³³⁵ This layer acts as an electrostatic shield which imposes repulsive forces between the stabilized graphene sheets and prevents aggregation. A comparison between Py-SASS and Py-SAH-assisted dispersions allowed evaluating the effect of this ionic shield on the effectiveness of pyrene derivatives for graphene stabilization. These two pyrene derivatives are similar in structure with exception of their counterions. The PY-SASS with sodium as the counterion yields higher graphene concentrations (up to its solubility limit) than Py-SAH. This may be attributed to the higher ionic strength and size of sodium compared to hydrogen ions (in Py-SAH). An electrostatic shield of sodium ions may provide stronger repulsive forces than a shield of hydrogen ions and thus, enables stabilization of higher number of graphene sheets by preventing the reaggregation.

The number and position of functional groups attached to the pyrene is another important factor that affects the adsorption behavior and effectiveness of pyrene derivatives as graphene stabilizers. To our surprise, the Py-(SO₃)₄ with four sulfonyl groups yielded lower graphene concentration in the dispersion relative to Py-SASS (Figure 4.6). Also, this molecule could not disperse graphene at stabilizer concentration higher than 1 mg/ml. It is possible that the symmetric arrangement of four sulfonyl groups around pyrene reduces the probability of temporary polarization on aromatic

plane and reduces the electron-depletion on pyrene surface which is the adsorption driving force. Also, the presence of four functional groups creates a steric hindrance that prevents adsorption of this molecule on graphene surface. These effects intensify at higher concentrations of stabilizer as the repulsion forces between the particles increase the electron density on the pyrene plane.

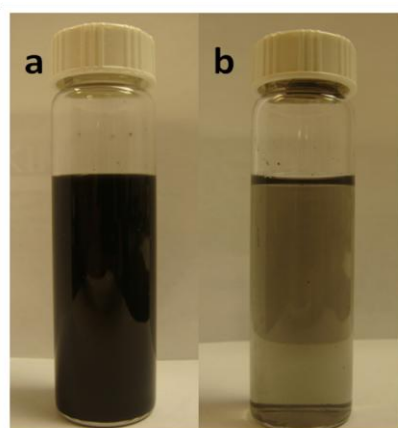


Figure 4.6. The number and position of functional groups affects the graphene concentration in the dispersions. a) Py-SASS assisted dispersion with final graphene concentration of 0.11 mg/ml and b) Py-(SO₃)₄ assisted dispersion with final graphene concentration of 0.04 mg/ml. The same concentration of stabilizer (1 mg/ml) was used in both samples.

The distance of functional groups from the pyrene is also an important parameter. Comparison of PCA- and PBA-stabilized dispersions reveals that with an increase in the stabilizer concentration PBA became more effective than PCA. At low stabilizer concentrations, the shorter distance of electronegative group from the pyrene facilitates the electron-withdrawal from the aromatic plane and improves the adsorption of PCA in

which the carboxyl group is closer to pyrene. However, as the stabilizer concentration increases, the repulsive forces between the sheets become stronger and lead to an increased electron density on the pyrene plane. In this situation, a larger distance from the pyrene reduces the charge transfer to aromatic plane and maintains the affinity of PBA for adsorption on graphene surface.

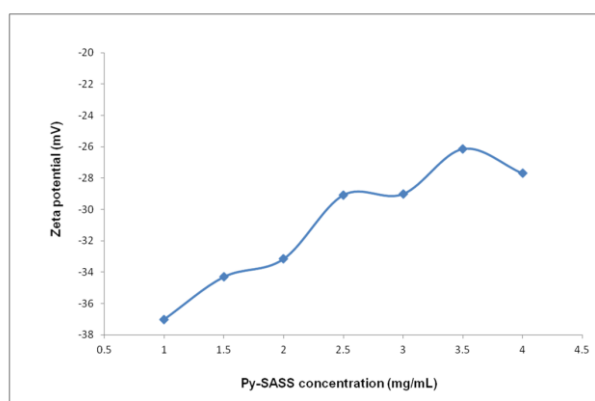


Figure 4.7. Zeta potential changes with stabilizer concentration in Py-SASS-stabilized dispersions. The absolute value of the zeta potential decreased gradually with an increase in the Py-SASS concentration.

For all the pyrene derivatives (except Py-SAH and Py-M-NH₂) the graphene concentration in the dispersions went through a maximum as the stabilizer concentration increased. To study the reason of such behavior, we measured the zeta potential of a Py-SASS-stabilized dispersion at various stabilizer concentrations (Figure 4.7). As the pyrene derivatives adsorb on the graphene surface in water, the dissociated functional groups impose a net charge on the graphene sheets. The average value of this surface

charge is represented by the zeta potential value of the graphene dispersions. For Py-SASS-stabilized dispersions, the reduction of the zeta potential absolute value upon addition of more stabilizers indicates a decrease in dissociation of the functional group at higher stabilizer concentrations. Despite of the availability of more pyrene derivatives for adsorption onto the graphene surface, the electrostatic repulsive forces provided by them is not sufficient to prevent reaggregation of graphene sheets.³³⁶ Thus, the overall graphene concentration decreases upon increase in stabilizer concentration. The graphene concentration in Py-SAH and Py-M-NH₂-assisted dispersion initially increased and then remained constant. Reduced solubility of these two pyrene derivatives in water at higher concentrations is the main reason for plateau in the graphene concentration. Above the saturation concentration of these pyrene derivatives, the excess stabilizer could not contribute to graphene stabilization and the graphene concentration remained constant beyond the stabilizer solubility limit.

TGA was performed to estimate the surface coverage of graphene by Py-SASS. Py-SASS carbonized completely at 750 °C. The remaining mass of graphene at this temperature after deduction of Py-SASS fraction was about 11.25 %. The surface coverage of Py-SASS on graphene was calculated to be $\sim 9.85 \times 10^{-10}$ mol/cm², based on the theoretical surface area of graphene (2630 m²/g) and remaining mass of Py-SAA which was 88.75%. This is one order of magnitude higher than the previously reported surface coverage by covalently-bonded polymers on the graphene surface.²²²

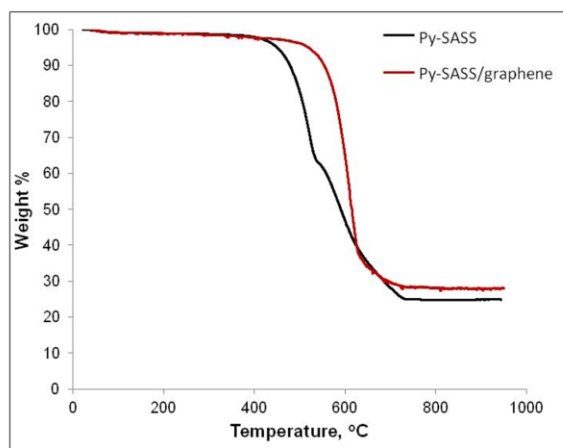


Figure 4.8. Thermogravimetric analysis of Py-SASS and freeze-dried Py-SASS/graphene powder.

4.3.3 Graphene yield and processability

The most important characteristic of pyrene derivatives-assisted dispersions is the high graphene to stabilizer ratio. The graphene concentration obtained using Py-SASS at its optimal concentration was ~ 0.8 mg/ml; this concentration reached values as high as 1.2 mg/ml depending on the sonicator efficiency. The higher graphene concentrations reported in the literature were usually achieved by excessive sonication time (up to 400 hrs) and lower centrifugation force (500-1500 rpm) and duration (2-90 min).³³⁷ Table 4.2 indicates the comparison of graphene ratio for dispersions prepared at the same experimental condition using Py-SASS, PVP and SDBS.^{36,39} The higher graphene/stabilizer ratio in Py-SASS-assisted dispersions enhances the graphene quality by reducing the amount of excessive stabilizer and facilitates the application of this

product in nanocomposites and electrode where the presence of residual impurities is a challenging issue.

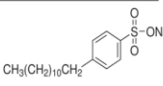
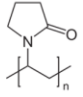
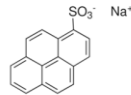
Stabilizer	Conc. of stabilizer (mg/mL)	Conc. of EG (mg/mL)	Final conc. of graphene (mg/mL)	Graphene conc. /Stabilizer conc.	Molecular structure
SDBS	6	50	0.22 ± 0.03	0.036	
PVP	10	50	1 ± 0.1	0.1	
Py-SASS	3	50	1 ± 0.05	0.33	

Table 4.2. Effectiveness of surfactants, polymers and pyrene derivatives as graphene stabilizers compared by their graphene yield and graphene/stabilizer ratio.

In an attempt to accomplish higher graphene yields, the initial graphite concentration was altered. Figure 4.9 illustrated the graphene concentration obtained using different expanded graphite concentration. For all the pyrene derivatives, the increase in EG concentration led to an increase in the final graphene concentration. However, large quantities of graphite may hinder an effective exfoliation during the sonication process. Furthermore, the increase in graphene yield upon addition of more EG depends on the stabilizer; Py-SASS- assisted sample showed the highest rate of increase in graphene yield.

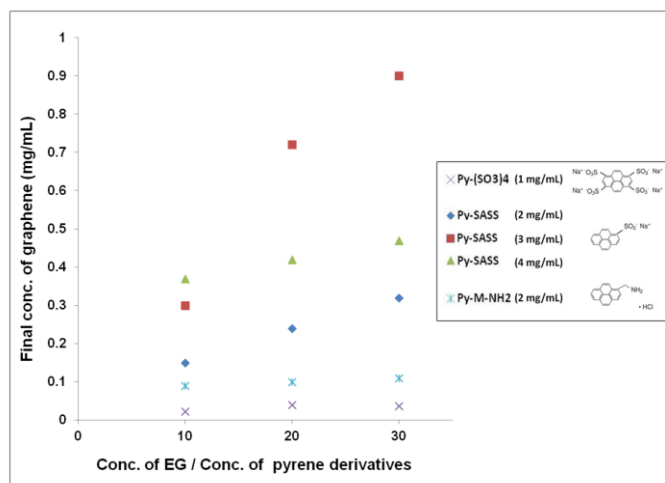


Figure 4.9. Graphene concentration increases with addition of initial expanded graphite concentration.

Also, we attempted to disperse graphene into organic solvents including methanol, ethanol and acetone using pyrene derivatives. However, an immediate sedimentation of graphite after sonication indicated the incapability of pyrene derivatives for stabilization of exfoliated graphene in pure organic solvent. This might be attributed to the lack of a huge difference in polarities of pyrene derivatives and these solvents; under these circumstances the minimization of total surface energy of the dispersion does not occur through the adsorption path. Even if the pyrene derivatives adsorb on graphene surface, the weak dissociation of the functional groups in organic solvents cannot provide the strong repulsive shield around the graphene sheets. Thus, the aggregation of exfoliated graphene sheets is inevitable.

In addition, we investigated the stability of graphene dispersion in mixtures of water and ethanol. Graphene concentration after addition of different amounts of ethanol to the dispersions and centrifugation is indicated in Figure 4.10. The graphene concentration decreased upon addition of more ethanol to the dispersion. With more than 60 vol% of ethanol in the dispersion, complete aggregation of graphene sheets and sedimentation occurred after one hour of centrifugation. Addition of ethanol to the dispersion changes the polarity of the solution and affinity of Py-SASS to remain adsorbed on the graphene surface. In presence of more ethanol molecules, desorption of Py-SASS from graphene surface reduces the net charge of the surface and weakens the repulsive shield around the sheets which leads to destabilization of graphene. Further centrifugation of samples containing 50 and 60 vol% of ethanol for one more hour led to aggregation and sedimentation of the graphene. This observation confirms the fact that desorption of Py-SASS from graphene surface after addition of ethanol is a transition between two equilibrium states that happens in a timely manner. The overnight centrifugation of samples with 10-40 vol% of ethanol did not change the graphene concentration; this means that desorption of Py-SASS in presence of up to 40 vol% of ethanol is negligible.

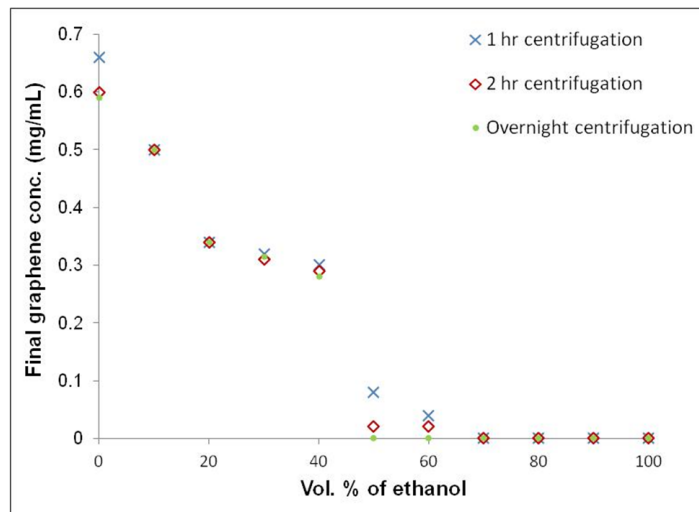


Figure 4.10. The post-centrifugation graphene concentration in mixtures of ethanol/water. Ethanol was added to an aqueous dispersion of graphene to prepare dispersions with 10-90 vol.% of ethanol.

In order to obtain aggregation-resistant graphene powder, the aqueous dispersions were freeze-dried after centrifugation. The stability of the resultant graphene powders against aggregation was tested by redispersion into the water and subsequent centrifugation. The Py-SASS/ and Py-SAH/graphene powders were easily redispersible without any further sonication (Figure 4.11), but partial sedimentation occurred in all other samples.



Figure 4.11. Redispersion of freeze-dried Py-SASS/graphene powder in water at original dispersion concentration.

4.3.4 Stability of graphene dispersions

In terms of long-term stability, all the dispersions were stable several months with exception of Py-SAH-assisted sample which was slightly aggregated after 2 months. The colloidal stability of all the dispersions was evaluated by zeta potential measurement over a wide range of pH. The results are represented in Figure 4.12. The samples stabilized with sulfonyl-containing pyrene derivatives were highly stable over a wide range of pH compared to the other dispersions. Both Py-SASS- and Py-(SO₃)₄-assisted samples had zeta potential values higher than ± 30 at their original pH which is indicative of their colloidal stability. The Py-SAH-assisted sample had a low zeta potential value at its original pH of 2 which explains its aggregation over time. However, the increase in the pH of this sample made it stable at a pH range of 6-8.5. The aggregation of the graphene sheets in these samples were traced with the increase in the average particle size measured by the dynamic light scattering (Table 4.3).

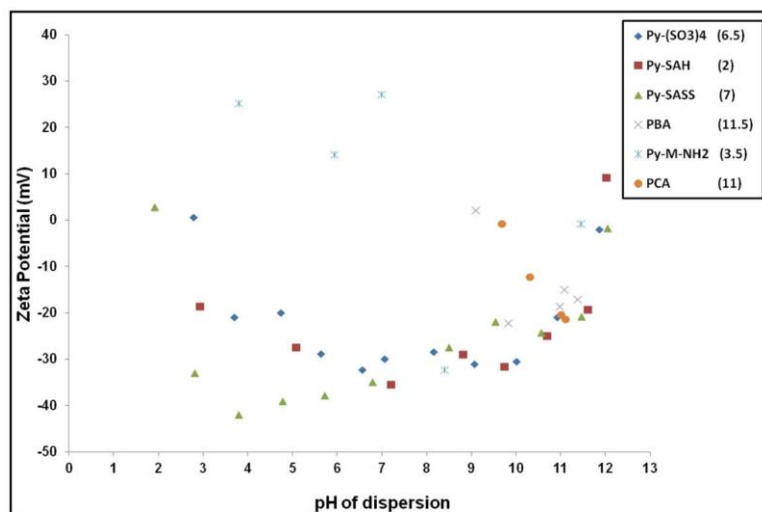


Figure 4.12. zeta potential of graphene dispersion prepared with pyrene derivatives at different pH values. The original pH of the dispersions before any change by acid or base addition is mentioned in the parentheses in front of each pyrene derivative.

Py-SASS/graphene dispersion		Py-SAH/graphene dispersion		Py-(SO ₃) ₄ /graphene dispersion	
pH	Average particle size (nm)	pH	Average particle size (nm)	pH	Average particle size (nm)
2.81	110	2.93	590	3.7	264
3.8	89	3.85	157	4.73	211
4.77	114	5.08	145	5.63	183
5.71	123	7.20	133	6.56	162
6.79	131	8.81	149	7.05	128
8.5	138	9.73	142	8.15	133
9.53	142	10.69	141	9.06	132
10.56	132	11.60	180	10	147
11.46	132	12.01	336	10.92	169

Table 4.3. Average particle size in sulfonyl-containing graphene dispersions at various pH values measured by DLS technique.

Despite of the lower zeta potential values measured for the PCA, PBA and P-M-NH₂-assisted samples, these dispersions were stable over months. The stability of the PCA and PBA-assisted dispersions was restricted to highly basic media due to the presence of carboxyl groups and they destabilized with slight decrease in the pH. However the destabilized PCA and PBA-samples were recovered to the original well-dispersed state upon addition of a base (Figure 4.13). This observation confirms that the destabilization of these samples is a reversible flocculation process that occurs solely because of the lower solubility of PCA and PBA in water at lower pH values. PCA and PBA remain adsorbed on graphene surface during the destabilization and prevent reaggregation of graphene sheets; upon recovery of the original pH these sheets redisperse back into the water.

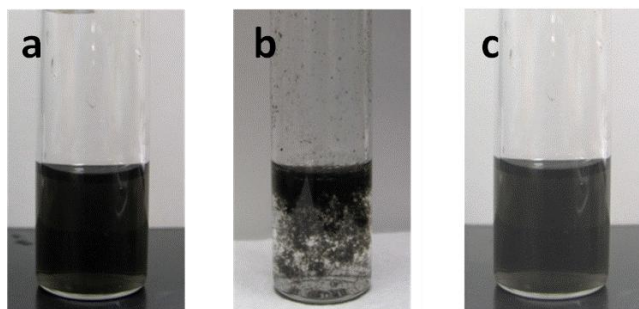


Figure 4.13. Flocculation and redispersion of PCA-stabilized graphene dispersion upon pH changes: a) The original dispersion at pH= 11, b) the destabilized dispersion after addition of acid at pH= 3 and c) the recovered dispersion after increasing the pH to 10.5 by addition of base. (Note that the concentration is lowered simply by dilution effects of the acid and base.)

The stability of dispersions at higher temperature is illustrated in Figure 4.14. The dispersions with sulfonyl groups showed thermal stability at higher temperatures compared to the other samples. In fact, the Py-SASS-assisted dispersion was stable up to 100 °C; the stability at higher temperatures makes it a promising candidate for further processing for nanocomposite applications.

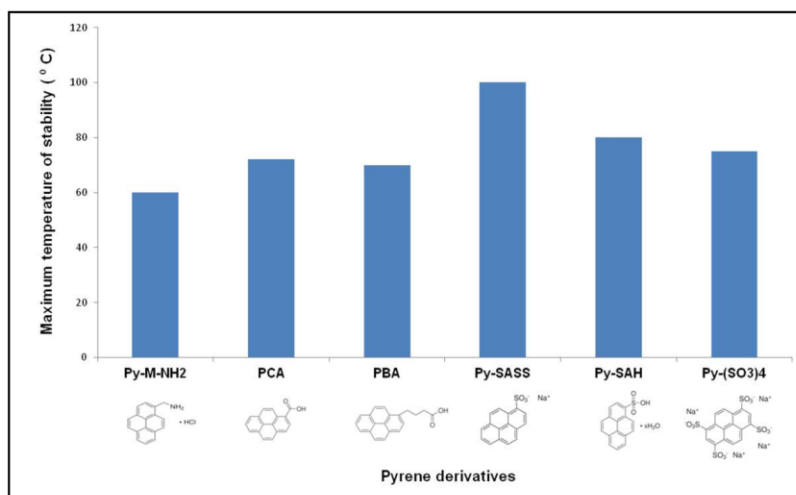


Figure 4.14. Visible stability of graphene dispersions against temperature changes.

4.3.5 Graphene-polymer nanocomposites

For the first time, we investigated the application of graphene dispersion stabilized with pyrene derivatives in polymer nanocomposites. To prepare graphene/epoxy composite thin film, the Py-SASS-stabilized graphene dispersions were freeze-dried and the resultant graphene powder was mixed into the epoxy matrix, followed by degassing and doctor-blading of the mixture (Figure 4.15). The SEM images the epoxy before and after graphene addition are depicted in Figure 4.16.



Figure 4.15. 0.5 wt % graphene/epoxy composites prepared by a) Doctor-blading and b) casting in a Teflon mold.

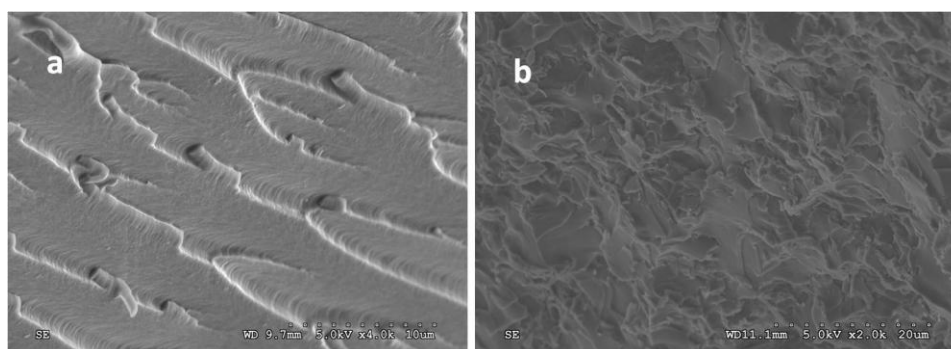


Figure 4.16. SEM images of a) epoxy and b) Py-SASS stabilized graphene/epoxy composite.

The mechanical and electrical properties of doctor-bladed thin films of Py-SASS- and PVP- stabilized graphene/epoxy are represented in Table 4.4. The electrical conductivity of both samples is in the same range and both graphene samples enhanced the electrical conductivity of the insulating epoxy matrix. The Py-SASS-stabilized sample had a higher Young's modulus than the PVP-stabilized sample; however, the lower yield strength of the Py-SASS containing sample may be attributed to the poor

dispersion of the Py-SASS/graphene powder in the epoxy matrix. While the Py-SASS/graphene powder slightly agglomerated in epoxy matrix even after 40 min of sonication, the PVP/graphene sample homogeneously disperses into epoxy matrix.

Stabilizer	Electrical Conductivity (S/m)	Yield strength (MPa)	Young Modulus (GPa)
Py-SASS	1.95×10^{-6}	43.2	1.9
PVP	3.06×10^{-6}	44.1	1.65

Table 4.4. Mechanical and electrical properties of 0.5 wt% PVP- and Py-SASS-stabilized graphene/epoxy composites.

4.4 Conclusion

In summary, we investigated the applicability of pyrene derivatives as graphene stabilizer in aqueous dispersions. We showed that using Py-SASS, graphene concentrations as high as 1 mg/ml were obtained. Also the graphene to stabilizer ratio achieved by pyrene derivative is much higher than those obtained using polymers and surfactants as stabilizers. Also, the effect of the molecular structure of pyrene derivatives on the graphene yield was studied. We demonstrated that the electronegativity of the functional groups is an important factor that affects the adsorption of these species on the graphene surface. The ionic strength and size of the counterions of the functional groups determines the strength of the repulsive shield around the graphene sheets and

affects the final graphene concentration. The number and position of the functional groups, as well as their distance from the pyrene basal plane are the other parameters that control the adsorption of pyrene derivatives, graphene stabilization and final concentration. The long-term colloidal stability of the solution were examined by centrifugation and zeta potential measurements. We evaluated the processability of the dispersions by studying the effects of solvent exchange and stability against lyophilization. Also, the stability of dispersions against pH and temperature changes was investigated. Finally, we prepared graphene/epoxy composite thin film using the Py-SASS-stabilized graphene dispersions. The knowledge of stabilization mechanism and the effect of controlling parameters allows for design of novel graphene stabilizers with desirable molecular structures that match with various exfoliation and dispersion media. In Chapter V, we use pyrene-graphene π - π interactions to design a novel polymeric dispersant for pristine graphene.

CHAPTER V

DESIGNER PYRENE-FUNCTIONAL STABILIZER FOR PRISTINE GRAPHENE/POLYSILOXANE CONDUCTIVE FILMS AND NETWORKS*

5.1 Introduction

Incorporation of graphene sheets into polymer matrices allows the unique properties of these sheets to be exploited not only in transparent thin films, but also in bulk materials like polymers. In nanocomposites, graphene's electrical and thermal conductivity and mechanical rigidity are able to enhance the material properties of the polymeric matrix.^{185,186,214,215} Liquid-phase exfoliated graphene sheets are promising fillers for nanocomposites due to their high quality, processability and the large quantities in which they can be produced. Solution mixing and melt blending are the common methods used to disperse the graphene sheets into the polymer matrix.^{186,189,190,194-196,214} However, the poor graphene dispersion obtained by these methods prevents the enhancement of nanocomposite properties at low loadings of graphene. The poor dispersion and aggregation of sheets is more pronounced when pristine graphene is used instead of GO or RGO; the surface chemistry of GO and RGO makes them more polymer-philic.

*Part of the data reported in this chapter was reproduced by permission of Royal Society of Chemistry from (Parviz *et al.*, "Designer stabilizer for preparation of pristine graphene/polysiloxane films and networks", *Nanoscale*, 2014, 6, 11722-11731).

As mentioned in Chapter III, alternative dispersing methods such as in situ polymerization,^{201-203,205} modification of graphene surface through covalent,^{216-218,220} and non-covalent functionalization.^{221,222,225,338} have been practiced to improve the polymer-graphene interfacial interactions. Yet, these methods heavily rely on the surface chemistry and reactivity of GO sheets. The few exceptions were those cases in which conjugated copolymers and conductive polymers were attached to pristine graphene surface via π - π interactions.^{223,224} The non-covalent functionalization of pristine graphene with polymers has been rarely reported.³³⁹

The usage of GO in nanocomposites is problematic since it is electrically insulating and needs further reduction to become conductive; however, the common chemical or thermal reduction methods are not always applicable in presence of polymers. Usage of RGO in nanocomposites has its own complications; RGO shows poor dispersibility in most of the solvents relative to GO, while its properties cannot reach those of pristine graphene.^{326,340}

In the last chapter, we demonstrated that exfoliation and stabilization of pristine graphene in water is feasible using pyrene derivatives. The pyrene basal plane can adsorb on graphene surface through π - π interactions and the functional groups provide an electrostatic repulsive shield around the sheets to prevent reaggregation. However, addition of those stabilized graphene sheets to the epoxy matrix was not sufficient to enhance its electrical conductivity drastically. We argued that poor dispersion of graphene sheets within the epoxy due to their incompatibility was responsible for the lack of a considerable increase in electrical conductivity of the nanocomposite.

Furthermore, the presence of excessive pyrene derivatives in the matrix induces extra interfacial tension which can prevent proper electron transfer within the nanocomposite.

In this chapter, we take advantage of the pyrene-graphene interactions to design a polymer-based stabilizer for graphene. We tailor the polymer structure by grafting pyrene groups to its backbone to induce π - π interactions between the polymer and graphene. Such a designer polymer acts as both graphene stabilizer and polymer matrix in the nanocomposite. Using this polymer, the exfoliation of graphene sheets in the solvent and mixing them into the polymer matrix are performed in one single step in presence of an appropriate solvent. The polymer-stabilized graphene dispersions are simply cast to form graphene/polymer composite films and networks. In those composites, the presence of excessive incompatible stabilizer molecules is not anymore an issue.

This work was done in collaboration with Dr. Ronald Hedden at Texas Tech University, Department of Chemical Engineering. The polymer synthesis and characterizations were partially performed by his Ph.D. student, Ziniu Yu. This work was published in 2014 as a journal article in *Nanoscale*.³⁴¹

5.2 Background of the graphene/silicone nanocomposites

Polydimethylsiloxane (PDMS) is an organosiloxane polymer having a low glass transition temperature and good thermal stability, which is used in a wide range of applications such as elastomers, electronic materials, microfluidics, medical devices, and piezoresistive devices.³⁴² Due to the attractive possibilities of enhancing mechanical or

electrical properties of silicones by addition of carbon nanomaterials, numerous studies have reported incorporation of graphite nanoplatelets, GO and RGO into PDMS. Kujawski *et al.* mixed exfoliated graphite into the PDMS and observed a percolation threshold at 3 wt. % loading of the filler, along with enhanced mechanical properties of the composite.³⁴³ Chen *et al.* studied the piezoresistive behavior of PDMS composites filled with graphite nanosheets by wet-mixing.³⁴⁴ Raza *et al.* blended PDMS with graphite nanoplatelets through mechanical mixing and studied thermally conductive behavior at interfaces.³⁴⁵ Ozbas *et al.* mixed exfoliated, oxidized graphite sheets into PDMS, which led to a low percolation threshold at 0.8 wt. % loading of the filler and also a tenfold decrease in gas permeability through the composite.³⁴⁶ Xu *et al.* shear-mixed RGO into PDMS to enhance the mechanical properties.³⁴⁷ However, the aggregation of nanosheets made it difficult to obtain a homogenous dispersion of the fillers in the polymer. To overcome this issue, several research groups tried methods other than conventional mixing of the filler into the polymer matrix. Guimont *et al.* grafted PDMS onto graphite oxide sheets via a hydrosilylation reaction and varied the grafting density to enhance the filler dispersion quality in the PDMS.³⁴⁸ Gao *et al.* covalently attached the GO to PDMS, and they observed enhancement in mechanical properties.³⁴⁹ Hou *et al.* functionalized GO to make its surface energy more compatible with PDMS.³⁵⁰ Also, some groups have infused pre-made graphene or CNT aerogels (or other conductive monoliths) with PDMS, creating rigid composites.³⁵¹

In all prior studies, expanded graphite, GO or RGO were used as conventional nanofillers, with varying degrees of success in dispersion. One possibility which has not

been explored is to incorporate pristine graphene into linear PDMS or its copolymers in order to produce a conductive, liquid-phase nanocomposite that is well above its glass transition temperature at ambient temperature. In the absence of solvent, such a material does not have any vapor pressure, which is potentially favorable for conductive fluid applications. In order to disperse pristine graphene in a solvent-free polymer, graphene sheets should interact strongly with the surrounding polymer matrix.

Here we introduce a new strategy for combining pristine graphene with a siloxane-based matrix using a designer stabilizer that utilizes graphene-pyrene π - π interactions (Figure 5.1). Pyrene side groups are grafted to a PDMS backbone through hydrosilylation reaction. Pristine graphene-rich films with electrical conductivity up to 200 S/m were prepared by casting the copolymer-stabilized graphene dispersions and leaching out the excess, unbound polymer on a porous substrate. The graphene-containing PDMS-pyrene copolymers can also be crosslinked readily by simply changing the stoichiometry of the hydrosilylation reaction, producing the first example of a silicone elastomer containing pristine graphene. The final pristine graphene/polymer composite is a two-component system which does not have functional groups covalently bonded to the graphene, leaving the conjugation of the graphene rings intact.

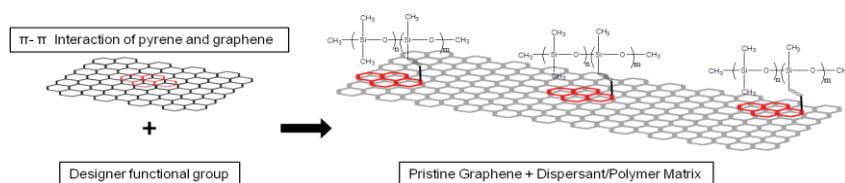


Figure 5.1. Designing pyrene-based polymeric stabilizer for pristine graphene.

5.3 Experimental procedures

5.3.1 Materials

Poly(dimethylsiloxane)-*co*-(methylhydrosiloxane) copolymer (HMS-064, 5-7 mole % PMHS) was purchased from Gelest Inc (USA). Cis-dichlorobis(diethyl sulfide) Pt (II) catalyst was purchased from Strem Chemicals (USA). 1-ethynylpyrene, chloroform (HPLC grade), toluene (ACS grade) and methanol (ACS grade) were purchased from Sigma-Aldrich (USA). Expanded graphite was provided by Asbury Carbons (CAS# 7782-42-5, Grade 3806, USA).

5.3.2 Synthesis of the pyrene-containing copolymers

Synthesis of poly(dimethylsiloxane)-co-(methyl(vinylpyrenyl)siloxane) linear copolymers (PMPyS): 5.0 g of HMS-064 copolymer was dissolved in 52.8 g of chloroform. 30 mol % excess (1.2 g, 5.3 mmol) of 1-ethynylpyrene was added to the solution, which was homogenized by stirring and heated to 44 °C. 847 µl of a toluene solution of cis-dichlorobis(diethyl sulfide) Pt (II) (2.66×10^{-3} g/g toluene) was added to initiate the hydrosilylation reaction. This grafting reaction was allowed to proceed at 44 °C for 3 d in solution. The reaction product was purified and separated into fractions of comparatively narrow molar mass distribution by fractional precipitation from chloroform (a good solvent) by incremental addition of methanol (a poor solvent). Initial polymer concentration was approximately 10 g/L in chloroform. The residual liquid phase was discarded.

Synthesis of poly(dimethylsiloxane)-co-(methyl(vinylpyrenyl)siloxane) networks (PMPyS-N): A crosslinked network of PMPyS was obtained by reacting poly(dimethylsiloxane)-co-(methylhydrosiloxane) with an amount of 1-ethynylpyrene that was insufficient to convert all of the silane groups of the copolymer to vinylpyrene groups. An initial mole ratio of silane:alkyne groups of 1.7:1 was chosen. 1.84 g of HMS-064 copolymer was dissolved in 6.2 g of chloroform. 0.20 g (0.88 mmol) of 1-ethynylpyrene was added to the solution, which was homogenized by stirring and subsequently heated to 44 °C. 110 µl of a solution (2.66×10^{-3} g/g toluene) of cis-dichlorobis(diethyl sulfide) Pt (II) was added to initiate the hydrosilylation reaction between the alkyne group of the 1-ethynylpyrene and the silane groups of the polymer backbone. The grafting reaction was allowed to proceed at 44 °C for 3 d without stirring. The reaction product was poured into an open PTFE container and chloroform was allowed to evaporate at 22 °C for 4 h until a viscous, bronze-colored film was obtained. The temperature was increased to 110 °C and the film was allowed to cure for 7 d in air. No precautions were taken to prevent ambient moisture from entering the film, and the relative humidity was approximately 40-50 % at the ambient temperature of 22 °C. The resulting network was swelled to equilibrium in excess chloroform at 22 °C for 3 d, during which time the chloroform was changed twice. The extractable mass fraction of the network was determined after de-swelling the network by gradual addition of methanol, vacuum-drying the material, and recording its mass.

5.3.3 Preparation of graphene dispersions

Preparation of Graphene Dispersions using PMPyS linear copolymers (PMPyS-G): In a typical preparation, a specific amount of a fractionated PMPyS polymer was dissolved in chloroform to obtain 1.0 mg/ml of pyrene in the final solution. Expanded graphite (EG) was subsequently added to the solution (30 mg/ml) and was tip sonicated (Misonix sonicator, XL 2000) for 1 h. During the sonication, an ice bath was used to maintain the sample at room temperature to avoid any chloroform evaporation and to maximize the efficiency of the exfoliation process. All dispersions were centrifuged (Centrifuge 225, Fischer Scientific) at 5000 rpm for 4 h in order to remove graphitic aggregates. The supernatant of the centrifuged samples was collected and used for further processing and characterization. Also, the original unfractionated polymer was used to disperse graphene through a similar procedure.

5.3.4 Preparation of graphene/copolymer composite films and networks

Synthesis of PMPyS network with Included Graphene (PMPyS-NG): A crosslinked network containing pristine graphene flakes was prepared by a procedure similar to PMPyS-*N* networks. After 3 d reaction between HMS-064 and 1-ethynylpyrene in chloroform, the resulting polymer solution (with solids concentration of 20 mg/ml) was sonicated in the presence of expanded graphite (30 mg/ml). The resulting suspension was centrifuged to remove excess graphite, leaving a black solution of polymer-stabilized graphene in the supernatant. The concentration of graphene was measured using the absorbance of the dispersion at 660 nm. This solution was deposited

into the PTFE container and cured in air using the same temperature and humidity profile used for PMPyS-N.

5.3.5 Characterization

FT-IR (Fourier Transform Infrared Spectroscopy): The expected product structure of linear PMPyS was confirmed by FT-IR analysis of the purified fractions using a Thermo Nicolet Nexus 470 spectrometer. In addition, the crosslinking reaction was monitored by FT-IR spectroscopy. A thin film of the reaction mixture was deposited onto a KBr disk and cured with the same temperature program used to prepare bulk samples, while spectra were recorded periodically.

GPC (Gel Permeation Chromatography): The PMPyS fractions obtained were characterized by GPC using tetrahydrofuran as mobile phase and four Phenomenex Phenogel columns ($5 \mu\text{m}-10^6 \text{ \AA}$, $5 \mu\text{m}-10^5 \text{ \AA}$, $5 \mu\text{m}-10^4 \text{ \AA}$, $5 \mu\text{m}-10^3 \text{ \AA}$) in series covering a molar mass range of 1 kg mol^{-1} to $10,000 \text{ kg mol}^{-1}$, which were calibrated by poly(methyl methacrylate) (PMMA) standards. All molar masses reported are relative to PMMA. Elution of the polymer was detected by a Varian 380-LC mass-evaporative detector, and elution of the pyrene groups was detected by a KNAUER V2.8 ultraviolet-visible detector at a wavelength of 348 nm.

UV-Vis Spectroscopy: UV-Vis spectroscopy was performed on a Shimadzu 2550 spectrophotometer on fractionated PMPyS solutions in chloroform to measure the pyrene content of each fraction. All fractions of PMPyS were dissolved in chloroform with a polymer concentration of 1 mg/ml. Samples were scanned from wavelength 200

nm to 800 nm with pure chloroform as a reference. Also, the absorbance was measured on all PMPyS-G samples at 660 nm to measure the concentration of graphene in dispersions. The absorbance of the PMPyS copolymer was negligible at this wavelength. The extinction coefficient for graphene in presence of the polymers in chloroform was calculated through the vacuum filtration method.

HR-TEM (High Resolution Transmission Electron Microscopy): The dispersions of PMPyS-G and the dispersion prepared with unfractionated polymer in chloroform were deposited on lacey carbon TEM grids and dried in the air for 1 min. A voltage of 75 kV on a Hitachi H8100 was used to image the samples.

SEM (Scanning Electron Microscopy): An accelerating voltage of 2 kV was used to image the samples on a Hitachi S4300 SE/N. The PMPyS-G sample was cast on a filtration membrane (PTFE, 0.2 μm , Omnipore Membrane Filters) for imaging. Samples were mounted on double face carbon tape.

Conductivity measurements: The electrical resistance of the samples was measured using the four-point probe method. The four-point probe head (Signatone, SP4-40045TBY) was mounted on a resistivity measurement stand (Signatone, Model 302). The current was supplied by a high impedance current source (Keithley 2400) through the outer two probes. A voltmeter (Keithley 2000) was used to measure the voltage across the inner two probes.

DSC (Differential Scanning Calorimetry): The thermal behavior of the polymers before and after graphene loading was characterized by DSC (TA Instruments, Model Q-20-1848). Approximately 5 mg of each sample was sealed in an aluminum pan and

heating traces were recorded under a nitrogen atmosphere. The heating rate for all the samples was $10\text{ }^{\circ}\text{C min}^{-1}$ and samples were heated from $-80\text{ }^{\circ}\text{C}$ to $90\text{ }^{\circ}\text{C}$.

5.4 Results and discussion

5.4.1 Design of pyrene-containing copolymer

To synthesize a pyrene-containing polysiloxane stabilizer, pyrene groups of 1-ethynylpyrene were grafted to the backbone of a silicon-based copolymer through hydrosilylation reaction. Figure 5.2 shows the proposed mechanism of reaction between the alkyne group of the 1-ethynylpyrene and the silane groups of the polymer backbone. The Si-H groups of PHMS covalently bond to the ethynyl groups through hydrosilylation, forming a substituted alkene. Further reaction of the alkene with an additional Si-H is unlikely due to both steric hindrance and due to conjugation with the adjacent pyrene ring. The percentage of Si-H groups bonding to pyrenes through this reaction depends on the initial mole ratio of ethynyl and Si-H groups present in the reaction medium. If the ratio of SiH:ethynyl is higher than 1.0, then excess Si-H groups remain intact after the alkynes are exhausted. These remaining Si-H groups self-crosslink later and form networks. However, if this ratio is lower than one, then most or all of the Si-H groups undergo the hydrosilylation reaction and the product is a linear copolymer. We studied 1.7:1.0 and 1.0:1.3 as SiH:alkyne ratios to illustrate the dramatic differences in the product resulting from reaction stoichiometry.

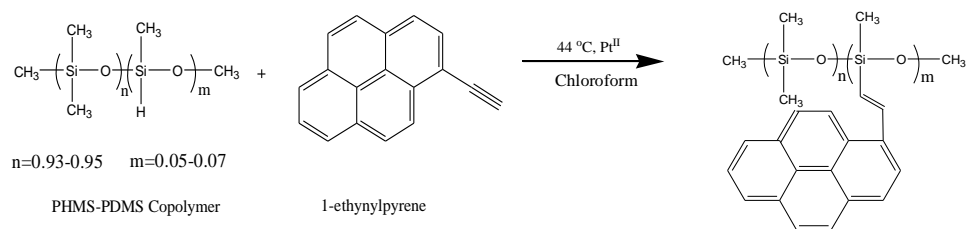


Figure 5.2. Synthesis of PMPyS copolymer via grafting 1-ethynylpyrene to PDMS-PHMS copolymer backbone through a Pt-catalyzed hydrosilylation reaction.

5.4.2 Analysis of linear copolymers (PMPyS)

The reaction with the SiH:ethynyl ratio of 1.0:1.3 produces a linear copolymer having a broad chain length distribution. Therefore, we separated the sample into seven fractions of narrower molar mass distribution, with M_w ranging from 49 kg mol^{-1} to 262 kg mol^{-1} , by fractional precipitation. The goal was to create well-defined polymeric stabilizers that were free of low molar mass species, in order to evaluate their effectiveness as graphene dispersants. The fractionation procedure not only narrows the molar mass distribution, but also removes the majority of low molar mass by-products and oligomers. GPC results (Figure 5.3) show the fractionated samples with polydispersity index (PDI, M_w/M_n) much less than 2.0 and containing a minimum amount of oligomeric impurities. Average molar mass characteristics of the fractions are summarized in Table 5.1.

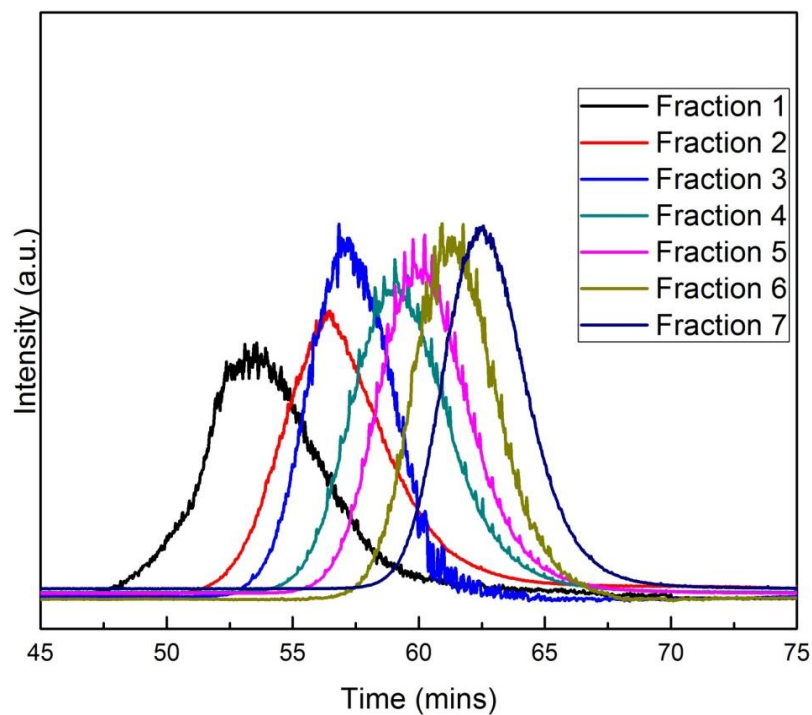


Figure 5.3. Elution profiles of different PMPyS fractions from GPC (performed by Ziniu Yu).

	Fraction 1	Fraction 2	Fraction 3	Fraction 4	Fraction 5	Fraction 6	Fraction 7
M_w (kg/mol)	262	143	135	92	77	57	49
M_n (kg/mol)	170	82	124	78	66	56	43
M_w/M_n	1.55	1.74	1.09	1.18	1.17	1.02	1.13

Table 5.1. Molar masses of the PMPyS fractions obtained from GPC analysis (performed by Ziniu Yu).

The expected structure of the PMPyS copolymer was confirmed by FT-IR analysis of the purified fractions (Figure 5.4). Absence of the alkyne band at 3294 cm^{-1} in the PMPyS copolymers indicated a lack of free 1-ethynylpyrene, and appearance of

both a C=C stretch band at 1596 cm^{-1} and a second band at 1508 cm^{-1} is indicative of a C=C:Pt complex formed after grafting of pyrene groups to the polymer chains.^{352,353} Attachment of the pyrene groups to the polymer backbone was also confirmed by GPC analysis with multiple detections. Simultaneous elution of pyrene groups and polymer chains confirmed that grafting of pyrene groups to the backbone was successful (Figure 5.5). A minimal amount of free pyrene groups elutes with the residual impurity peak around $t = 80\text{-}95\text{ min}$, indicating that a majority of the original pyrene groups were successfully grafted to the polymer backbone.

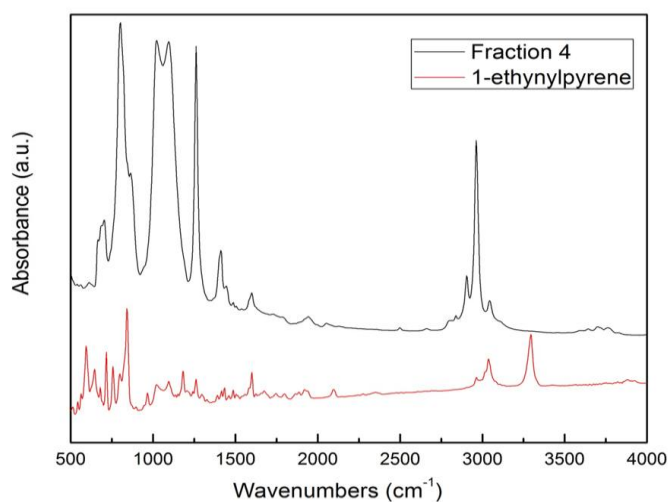


Figure 5.4. FT-IR spectra of fraction 4 of the PMPyS sample (performed by Ziniu Yu).

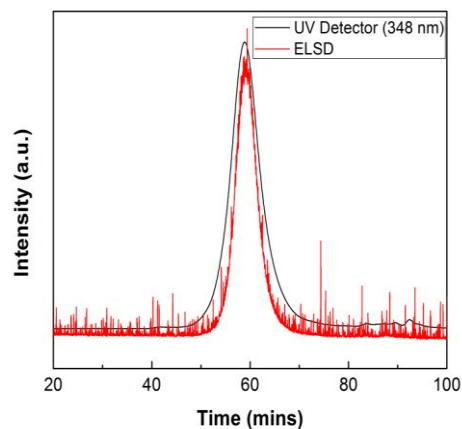


Figure 5.5. GPC analysis of a fraction 4 of the PMPyS sample confirms the attachment of vinylpyrene groups to the polymer backbone (performed by Ziniu Yu).

The pyrene content of each PMPyS fraction was estimated by comparing its UV absorbance spectrum to that of 1-ethynylpyrene (Figure 5.6, Table 5.2). 1-ethynylpyrene exhibits two absorbance bands near 350 and 330 nm, as do the PMPyS fractions; these bands are absent in the PDMS-PMHS copolymer as obtained from the supplier. The pyrene content in each PMPyS fraction was therefore estimated from these bands by comparison to a 1-ethynylpyrene solution of known concentration. The results show that the pyrene content of the PMPyS fractions is independent of the M_w within the limits of uncertainty of the experiment. There is no discernable trend in the pyrene content of the PMPyS chains with increasing molar mass.

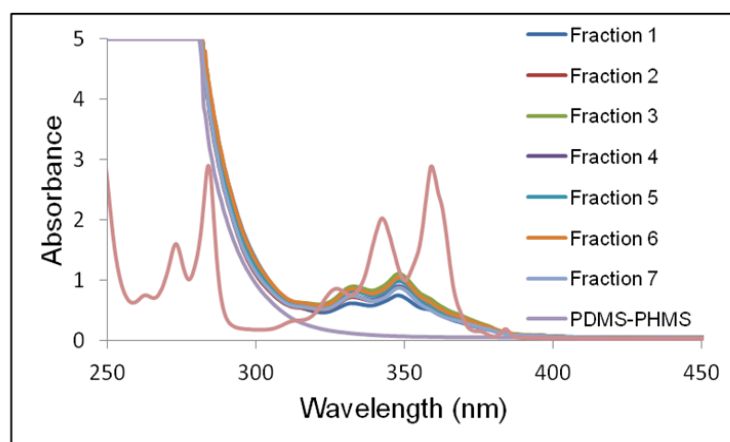


Figure 5.6. UV-vis spectra of the copolymer precursors and all of the PMPyS fractions.

	Fraction 1	Fraction 2	Fraction 3	Fraction 4	Fraction 5	Fraction 6	Fraction 7
Pyrene content (wt%)	8.43	9.57	16.85	8.86	12.91	13.89	10.58

Table 5.2. Pyrene content of different PMPyS fractions (based on the area under UV-vis spectra of each fraction).

5.4.3 Graphene/copolymer (PMPyS-G) dispersions

The basic procedure for preparing dispersions of stabilized pristine graphene involves exfoliation of the graphene using tip sonication in a given solvent with the stabilizer pre-dissolved in the solvent; this step is followed by centrifugation to remove non-exfoliated graphitic material. The stable colloidal graphene remains in the supernatant with a concentration measured by UV-vis absorbance at 660 nm. We first

checked whether 1-ethynylpyrene itself can act as a stabilizer in chloroform, but the resulting concentration of dispersed graphene was zero. This observation is consistent with our prior work;³³ regardless of π - π interactions between the graphene and pyrene, this particular functional group on the pyrene cannot provide enough electrostatic or steric repulsion to prevent aggregation of graphene sheets. In contrast, we successfully dispersed the graphene via the fractionated PMPyS samples in chloroform. Adsorption of the PMPyS to the surface of the graphene sheets not only hinders aggregation of the sheets, but provides a mechanism for the sheets to remain suspended in solution indefinitely due to the favorable free energy of mixing between the macromolecular stabilizers and the solvent.

The average extinction coefficient (at 660 nm) for graphene in presence of the polymer in chloroform was $2200 \text{ L g}^{-1}\text{m}^{-1}$, which was measured by the typical procedure of vacuum filtration. The graphene concentration after centrifugation was between 0.1-0.7 mg/ml for various fractions (Figure 5.7). In prior work on pristine graphene dispersions, the graphene concentration showed a clear trend with stabilizer concentration.^{33,39} The dependence of graphene concentration on stabilizer concentration is somewhat complex in the current case since the fractions vary in both molar mass and pyrene content. For simplicity, pyrene concentration was held constant for each fraction in the graphene dispersion experiments. With pyrene concentration held constant, the other quantities that vary from one fraction to another are the total polymer concentration and the molar mass. No trend in graphene concentration is seen at constant pyrene content. All PMPyS fractions are clearly capable of dispersing graphene in

chloroform solution, regardless of molar mass. Thus, it appears that the overall concentration of the pyrene groups, rather than chain length, may be the key factor that governs the maximum achievable concentration of dispersed graphene.

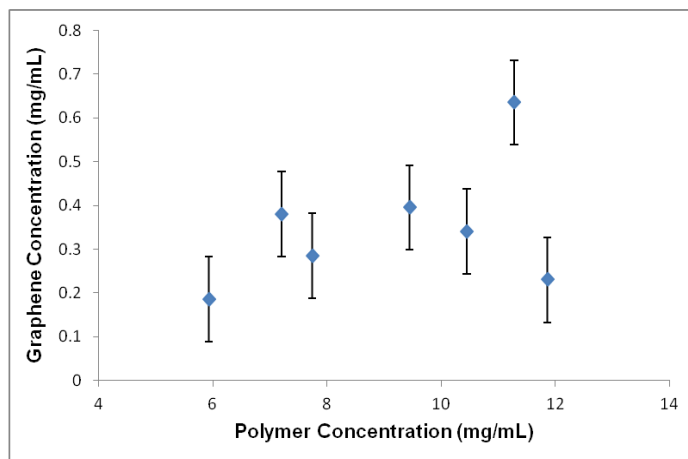


Figure 5.7. Graphene concentration variation vs. PMPyS fractions concentration; the pyrene content in the dispersions of all fractions was held constant at 1 mg/mL.

HRTEM images (Figure 5.8) show representative graphene sheets deposited from the dispersions onto a grid. The typical sheet sizes are 1 μm . The edge count for several samples shows that sheets typically consist of 3-4 layers. This edge count is typical for tip-sonicated pristine graphene dispersions enabled by a stabilizer.^{38,169}

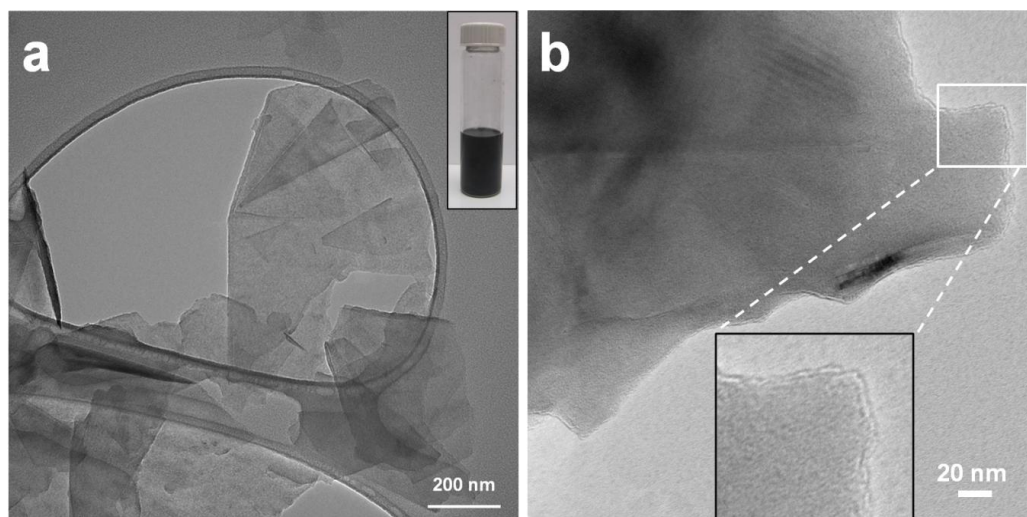


Figure 5.8. HRTEM images of (a) graphene sheets stabilized by unfractionated PMPyS copolymer, the inset shows the fraction 4 graphene dispersion and (b) a graphene sheet in dispersion prepared by fraction 4 of the PMPyS copolymer, the inset shows the edge of the same graphene sheets and verifies the few-layer nature of stabilized graphene sheets.

5.4.4 Graphene/copolymer (PMPyS-G) films

To evaluate the properties of the graphene/copolymer system in the absence of the solvent, a sample with an initial concentration of 1.7 vol. % graphene was cast onto a non-porous polypropylene substrate to form a film. The sample was kept at room temperature for a day to ensure that the chloroform was completely removed. The electrical conductivity of this film was 2.6×10^{-5} S/m, and no increase in conductivity was observed within a few weeks afterward. We hypothesized that removal of the unbound polymer chains which are not adsorbed on the graphene may enhance the electrical conductivity of the sample. In order to substantiate this hypothesis, a simple technique was applied to remove the free polymer chains from the sample. The same

dispersion was cast onto the PTFE membrane with 0.2 μm pore size to yield a film with initial 1.7 vol. % graphene content (Figure 5.9). This film was not crosslinked or glassy, so the free PMPyS chains were absorbed into the pores of the membrane, leaving a concentrated film of graphene and bound PMPyS on the surface. The lateral dimensions of the graphene sheet are large enough to prevent sheets from entering the pores. SEM images show no large graphene aggregates and the film morphology has a uniform appearance (Fig. 5.9).

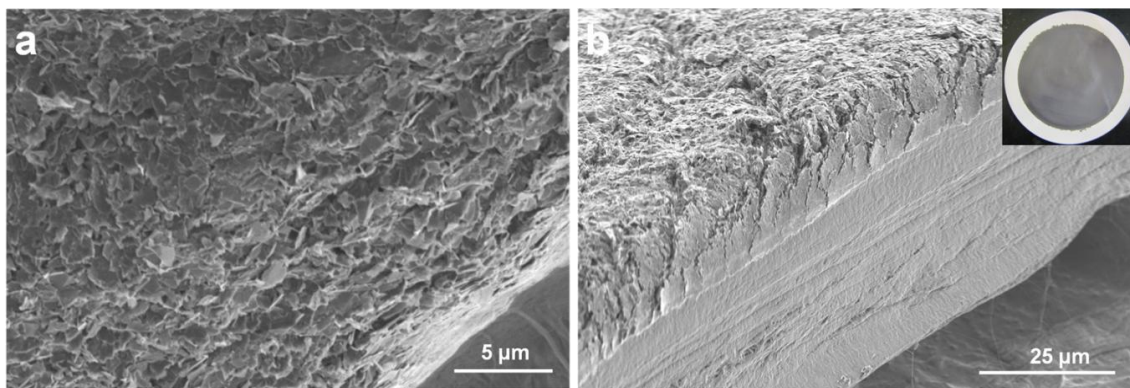


Figure 5.9. SEM images of (a) the top surface of the graphene/PDMS film (fraction 4) cast on the membrane and (b) cross section of the film on the membrane (inset shows digital image of the cast film). The average thickness of the sample is $\sim 10 \mu\text{m}$. This film has an electrical conductivity of 220 S/m.

The electrical conductivity of the sample on the membrane was $\sim 4 \text{ S/m}$ after being kept at ambient temperature for 2 d. The drastic increase in the electrical conductivity of the sample verifies the removal of unbound polymer chains, increasing the graphene concentration. Furthermore, the electrical conductivity of the same sample

was measured after 3 months, at which point the conductivity had increased to 220 S/m. Such a considerable increase can be attributed to gradual leaching of unbound PMPyS chains into the membrane, leaving a concentrated film of polymer-stabilized graphene on the surface. As the PMPyS linear copolymers are well above their T_g at room temperature and can be considered to be a melt, leaching of unbound chains from the film into the pores is likely. The capillary effect induced by the porous structure of the membrane drives the migration of the free polymer chains into the membrane, while the graphene-bound chains remain on top of the membrane. The conductivity value of 220 S/m is significantly higher than what has been reported for polymeric films in the pristine graphene nanocomposite literature. Furthermore, removal of unbound polymer using a porous substrate can be considered as a useful post-processing technique to increase graphene content and composite conductivity that may be useful in the broader field of polymer nanocomposite processing.

The thermal behavior of the PMPyS and PMPyS-G was also investigated using DSC (Figure 5.10). The T_g of the PMPyS is lower than $-95\text{ }^{\circ}\text{C}$ and could not be observed in our setup. As shown in the figure, an endotherm due to crystallization was observed at about $-50\text{ }^{\circ}\text{C}$ for the fraction of higher molar mass (fraction 2). The appearance of a polymer crystallization peak likely indicates that the sequence distribution in the PMPyS copolymers has some blocky character. The crystallization is probably dominated by a population of chains having long, uninterrupted runs of PDMS repeat units. The bulky pyrene groups are unlikely to participate in crystallization, especially if they are adsorbed to the surface of graphene sheets. For fractions of higher M_w , the addition of

graphene does not change the crystallization temperature, further suggesting that pyrene groups do not participate in crystallization. For PMPyS copolymers of lower M_w , crystallization was weak or not observed at all, probably due to the influence of numerous chain ends.

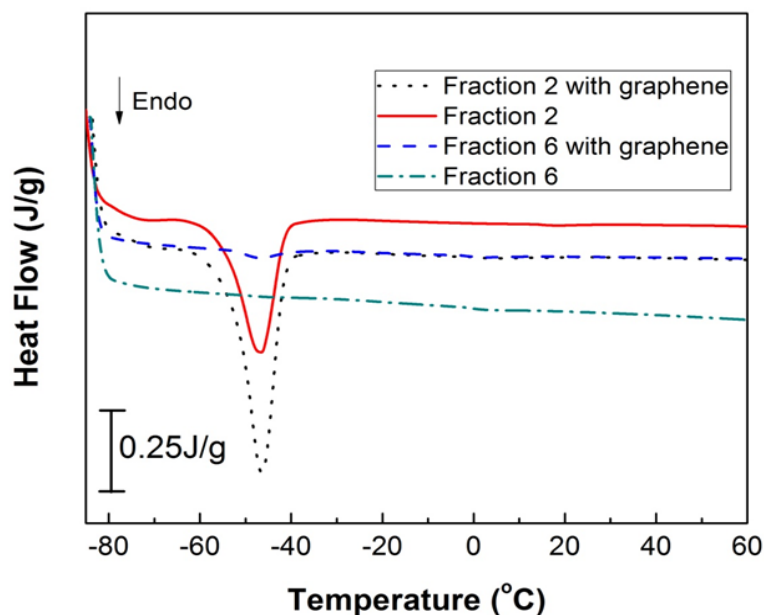


Figure 5.10. DSC heating traces for fractions 2 and 6 of PMPyS and PMPyS-G samples (performed by Ziniu Yu).

5.4.5 Networks of self-crosslinking copolymer (PMPyS-N)

The fractionated PMPyS samples did not crosslink at high temperatures due to replacement of nearly all SiH groups with pendant pyrene groups. In contrast, the polymer with SiH:ethynyl ratio of 1.7:1.0 was able to undergo a slow self-crosslinking reaction due to the presence of excess SiH groups. The proposed route of crosslinking

reaction is demonstrated in Figure 5.11a. This polymer was cured in chloroform solution for 3 d as before, and a film of this polymer was then cast from chloroform solution and heated to 110 °C in air at 40-50 % relative humidity for an additional 4 d (Figure 5.11b).

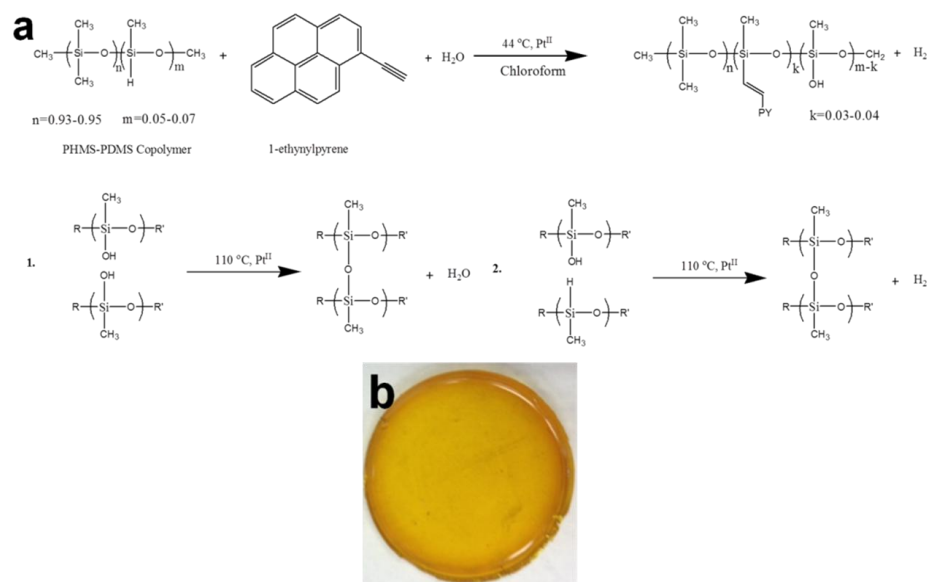


Figure 5.11. (a) proposed mechanism of crosslinking of PMPyS-N copolymer, and (b) digital image of the crosslinked film of PMPyS-N.

The reaction progress was observed by FT-IR (Figure 5.12). After 3 d in chloroform, absence of bands characteristic of alkynes and the presence of C=C (1596 cm^{-1}) bands confirmed that the grafting of 1-ethynylpyrene to the polymer backbone (Figure 5.11a, top row) was essentially complete. The band at approximately 2160 cm^{-1} is associated with Si-H groups, which are consumed during the grafting reaction, but are still present in significant excess after 60 h. After 7 d at 110 °C, the sample had become

a firm, rubber-like network. In the presence of the Pt catalyst, excess Si-H groups are able to react with adventitious moisture (Figure 5.11a, bottom row). Disappearance of the band at 2160 cm^{-1} and appearance of a weak, broad band at approximately 3200 to 3500 cm^{-1} confirms that silanol (SiOH) groups play a role in the crosslinking. Condensation of silanol groups $110\text{ }^{\circ}\text{C}$ produces Si-O-Si linkages, which are not easily detected spectroscopically due to the presence of a large number of such bonds in the starting material. No new bands are detected except the C=C:Pt band at 1508 cm^{-1} . Pt catalyst residues associate with a portion of the C=C bonds generated during the grafting reaction. This association does not play a role in the crosslinking, as this band was also present in the spectra of the linear PMPyS copolymers, which did not crosslink when heated to $110\text{ }^{\circ}\text{C}$.

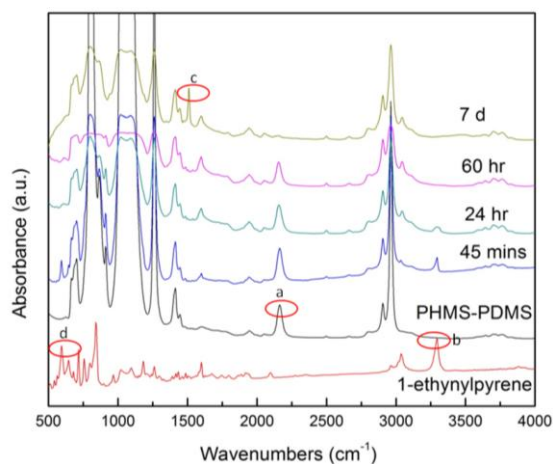


Figure 5.12. FT-IR spectra of the crosslinking copolymer precursors and the PMPyS-N products at various reaction times. (a) SiH peak, these peaks were present during the reaction and disappeared only after 7 days, (b) alkyne band peak, absence of this peak at 3294 cm^{-1} in the PMPyS copolymers indicated a lack of free 1-ethynylpyrene in the product, (c) a second band at 1508 cm^{-1} is indicative of a C=C: Pt complex formed after grafting of pyrene groups to the polymer chains and (d) $-\text{C}\equiv\text{C}-\text{H}$ peak which disappeared after the reaction.

5.4.6 Graphene/copolymer crosslinked networks (PMPyS-NG)

The network-forming copolymer (PMPyS-N) was used as a stabilizer for graphene as described previously. The polymer concentration was 20 mg/mL and the resulting stable graphene concentration after centrifugation was 0.3 mg/mL as measured by absorbance. The chloroform in these dispersions was evaporated at room temperature to yield a film with 0.6 vol. % graphene. The neat copolymer was heated to 110 °C in humid air, as with the PMPyS-N sample, and underwent a crosslinking reaction. After 14 d, the PMPyS-NG sample was removed from the heat and characterized. The PMPyS-NG sample is shown in the inset of Figure 5.13a. The PMPyS-N sample appeared to reach the gel point more quickly than the graphene-loaded sample, which may be due to the ability of nanofillers to hinder the mobility of the reactive species (e.g. water) during crosslinking. SEM images (Figure 5.13) show a smooth, uniform surface with some areas of roughness on top and cross-section of PMPyS-NG crosslinked network.

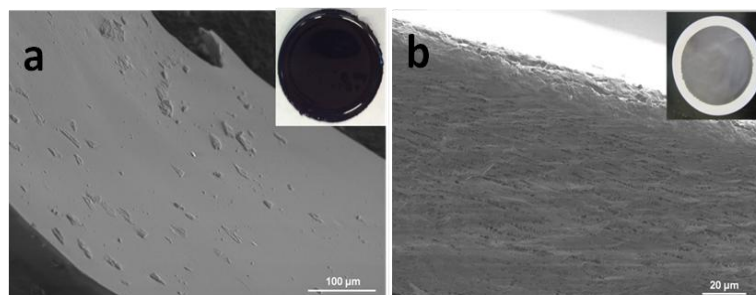


Figure 5.13. SEM images of (a) top surface of the crosslinked graphene containing PMPyS-NG film (digital image of the sample is shown in the inset), and (b) cross-section of the graphene containing dispersion of the same sample cast on the PTFE membrane (digital image of the sample is shown in the inset).

The graphene-loaded sample (PMPyS-NG) had a conductivity of 4.28×10^{-6} S/m. We used the membrane deposition technique as before to remove some of the unbound polymer chains via leaching to enhance the electrical conductivity of the crosslinked composite. A 0.6 vol. % PMPyS-NG film was cast onto the PTFE membrane (as shown in Figure 5.13b). The conductivity of this sample immediately after chloroform removal was $\sim 10^{-3}$ S/m. Improvement of the electrical conductivity in this case was not as drastic as in the case of the linear PMPyS-G sample. The most likely explanation is that fewer unbound polymer chains leached into the membrane due to the onset of crosslinking, so the increase in the graphene concentration was not as pronounced in the crosslinked film as in the melt. In addition, the precursor solution for PMPyS-NG contained fewer pyrene units per chain, so the initial amount of graphene stabilized was lower. Also, the conductivity of the crosslinked composite on the membrane did not change after several months, which verifies that completion of crosslinking inhibits further leaching of the unbound polymer chains.

To illustrate that the sample was fully crosslinked, the sample was swelled in chloroform (Figure 5.14). The sample did not dissolve, and after deswelling in methanol (a poor solvent for PDMS), the mass decreased from 0.60 g to 0.51 g. The removed mass corresponds to uncrosslinked polymer and any other low molar mass species present. The conductivity of the sample after swelling and deswelling was approximately the same. The conductivity of this sample is typical for pristine graphene/polymer composites reported in the literature, although some RGO/polymer composites have reported substantially higher values.^{8,354-356}

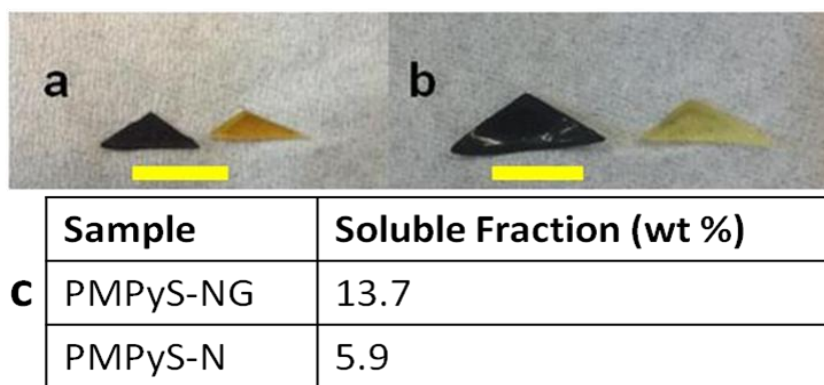


Figure 5.14. (a) PDMS gel with (0.6 vol. %) and without graphene before swelling; (b) PDMS gel with and without graphene after swelling in chloroform. Scale bars are ~ 1 cm; (c) Soluble fraction of gel as measured from swelling study (performed by Ziniu Yu).

5.5 Conclusion

A conductive, silicone-stabilized graphene film was synthesized for the first time using a copolymeric designer stabilizer as the polymer matrix. A pyrene group was grafted to a PDMS backbone via hydrosilylation reaction with a SiH:ethynyl ratio of 1.0:1.3. The resulting polymer was able to stabilize pristine graphene in chloroform through π - π interactions between the pyrene groups and graphene sheets. When cast onto a filtration membrane, the graphene/polysiloxane film had an electrical conductivity as high as 220 S/m. Such a drastic increase in the conductivity was attributed to the removal of unbound polymer which led to higher graphene concentration. Changing the SiH:ethynyl ratio in the hydrosilylation reaction to 1.7:1.0 leaves some unreacted SiH groups in the polymer chain which self-crosslink at higher temperatures in the presence of adventitious water. The crosslinked graphene/PDMS composite containing 0.6 vol. %

graphene had an electrical conductivity of 4.28×10^{-6} S/m, which is typical for pristine graphene/polymer composites reported in the literature. When the same sample was cast onto the porous membrane, the conductivity increased to $\sim 10^{-3}$ S/m due to the removal of unbound polymer. This work holds promise for the synthesis of polymers with graphene-binding pendant groups as a new framework for graphene/polymer nanocomposite design. In Chapter VI, we use a similar approach to design pyrene-functional PMMA and PS copolymers as novel dispersants for pristine graphene.

CHAPTER VI

JANUS FILMS OF PRISTINE GRAPHENE STABILIZED BY PYRENE-FUNCTIONAL COPOLYMERS

6.1 Introduction

Polystyrene (PS) and poly(methylmethacrylate) (PMMA) are two of the most common non-crystallizable, thermoplastic resins. Nanocomposites of GO, RGO or pristine graphene with PS^{8,357-408}, PMMA^{205,381,383,409-454}, and their blends with each other^{356,455,456} or with other polymers^{380,457-459} are among the most well-studied graphene nanocomposite systems. The number of studies underscores the importance of understanding and controlling the properties of PS and PMMA nanocomposites. In some cases, the surface of GO or RGO were modified through covalent and non-covalent functionalization to improve the dispersion and graphene interfaces in these polymer matrices. However, the modification of pristine graphene surface through non-covalent functionalization in presence of these polymers has been rarely reported. In the most recent attempts, pyrene-functional PMMA-based block copolymers⁴³⁸ and pyrene end-functional telechelic PS polymers³⁹⁶ have been employed as non-covalent stabilizers of graphene oxide and pristine graphene, respectively.

Inspired by our work on pyrene-functional silicone stabilizers (discussed in the previous chapter), we present a new approach for preparing novel thin films of PS or PMMA with one graphene-enriched surface. Random copolymers of 1-pyrenemethylmethacrylate with styrene or methyl methacrylate are prepared by simple,

bulk, free-radical polymerizations. After dispersing graphene nanosheets in solutions of these polymeric stabilizers, cast films are prepared, and their electrical properties are characterized for the first time. Applying a leaching approach in conjunction with vacuum filtration increases the overall concentration of graphene in the films, while promoting accumulation of graphene at the surface in contact with the filter. The resulting asymmetric films are the first examples of graphene-containing thin films having widely dissimilar electrical conductivities on the top and bottom surfaces. Here, we describe the preparation, properties, and possible applications of these "Janus graphene films," which have one electrically conductive surface and one electrically insulating surface.

This work was done in collaboration with Dr. Ronald Hedden group at Texas Tech University, Department of Chemical Engineering. The polymer synthesis and some of the characterizations were performed by the Ph.D. student in this group, Ziniu Yu.⁴⁶⁰

6.2 Experimental procedures

6.2.1 Materials

Styrene (CAS# 100-42-5, 99 %) was purchased from Acros. Methyl methacrylate (CAS# 80-62-6, 99 %) was purchased from Alfa Aesar. 1-pyrenemethyl methacrylate (99 %), 2,2'-azobis(2-methylpropionitrile) (98 %), chloroform (HPLC grade), tetrahydrofuran (ACS grade) and methanol (ACS grade) were purchased from Sigma-Aldrich. Expanded graphite (Grade 3806) was provided by Asbury Carbons. All the chemicals were used as received.

6.2.2 Synthesis of pyrene-containing copolymers

Polymer synthesis and characterization are adapted from the Ph.D. thesis of Ziniu Yu.⁴⁶⁰

Synthesis of Poly(methyl methacrylate - co- 1-pyrenemethyl methacrylate) Random Copolymers (PMPMA): Various mass fractions of 1-pyrenemethyl methacrylate (0.01, 0.05, 0.10 and 0.15) were dissolved in methyl methacrylate (MMA) monomer to yield a mixture of total mass 5.0 g. To initiate bulk free radical polymerization, 0.05 g of 2,2'-azobis(2-methylpropionitrile) (azobisisobutyronitrile, AIBN) was dissolved in the monomer mixture, which was placed in a pre-heated dry-bath at 80 °C for 12 h in a sealed PTFE container. After cooling to room temperature, the reaction product was a transparent, light yellow, glassy solid. Each polymer was purified by dissolving the material in tetrahydrofuran (THF) at a concentration of 100 mg mL⁻¹, followed by precipitation from THF by slow addition of excess methanol (typical methanol:THF volume ratio of 2:1) with vigorous stirring. Copolymers synthesized with 1-pyrenemethyl methacrylate mass fractions of 0.01, 0.05, 0.10, and 0.15 were named PMPMA-1, PMPMA-5, PMPMA-10 and PMPMA-15, respectively.

Synthesis of Poly(styrene - co- 1-pyrenemethyl methacrylate) Random Copolymers (PSPMA): Procedures followed were similar to synthesis of PMPMA copolymers, except styrene monomer was substituted for methyl methacrylate. PSPMA copolymers with 1-pyrenemethyl methacrylate mass fractions of 0.01, 0.05, 0.10, and 0.15 were named PSPMA-1, PSPMA-5, PSPMA-10 and PSPMA-15, respectively.

6.2.3 Preparation of graphene dispersions

In order to prepare graphene dispersions, 200 mg mL⁻¹ of copolymer-1, 40 mg/mL of copolymer-5, 20 mg/mL of copolymer-10 and 13.33 mg mL⁻¹ of copolymer-15 were dissolved in chloroform. These specific concentrations of the copolymers were chosen to yield ~ 1.3 mg mL⁻¹ of pyrenemethylmethacrylate groups in the solution. Subsequently, 30 mg mL⁻¹ of expanded graphite was added to the solution and the mixture was tip-sonicated (Misonix sonicator, XL 2000) for 1 h. To avoid solvent evaporation, an ice bath was used during the sonication. To separate the exfoliated nanosheets from the graphitic aggregates, the resultant dispersions were centrifuged (Centrifuge 225, Fischer Scientific) for 4 h at 5000 rpm. The supernatant of the centrifuged dispersions was collected and used for characterization experiments and nanocomposite preparation.

6.2.4 Preparation of G/PMPMA and G/PSPMA Janus films

To prepare the Janus films, 10 mL of the graphene dispersions stabilized by PMPMA-10, PSPMA-10, PMPMA-15, and PSPMA-15 were vacuum filtered through a porous filtration membrane (PTFE, 0.2 μm, 47 mm in diameter, Omnipore Membrane Filters). After the removal of the solvent, the resultant graphene/polymer films were peeled off from the membrane and dried at room temperature for 24 hrs for complete removal of the solvent. For electrical conductivity comparison, graphene/polymer films were prepared by drop casting the same dispersions on kapton substrate.

6.2.5 Characterization

UV-Vis Spectroscopy: a Shimadzu 2550 spectrophotometer was used for UV-vis spectrometry of 1-pyrenemethyl methacrylate, PMPMA-15 and PSPMA15 copolymers. The samples were dissolved in chloroform (0.01 mg/mL) and pure chloroform was used as the blank for the measurements. The pyrene peak at 348 nm was used to confirm the presence of pyrene group in the backbone of copolymers.

GPC (Gel Permeation Chromatography): The copolymers were characterized by GPC to calculate their molecular weight and PDI. Phenomenex Phenogel columns (5 μm to 106 Å, 5 μm to 105 Å, 5 μm to 104 Å, 5 μm to 103 Å) in series were used for polymer exclusion characterization. A molar mass range of 1 kg/mol to 10000 kg/mol was covered by these columns and THF was used as the mobile phase. The calibration curve for PSPMA and PMPMA copolymers were obtained using PS and PMMA standards, respectively. Elution of PMPMA and PSPMA copolymers was recorded by a KNAUER Smartline 2300 Refractive Index detector. In addition, elution of pyrene groups was recorded by a Knauer V2.8 ultraviolet-visible detector at 348 nm which is the wavelength of UV absorption peak of the pyrene group.

HRTEM (High Resolution Transmission Electron Microscopy): The graphene dispersions were deposited on 200 mesh carbon-coated copper grids (Electron Microscopy Sciences, CF200-Cu) and dried at room temperature for 1 min. A voltage of 200 kV and a Gatan camera on FEI Tecani G2 F20 HRTEM were used for imaging the samples.

SEM (Scanning Electron Microscopy): graphene/copolymer nanocomposites were cut to pieces and mounted on a double face carbon tape. An accelerating voltage of 2 kV was used to image the top surface and cross-section of the samples with a JEOL JSM-7500F instrument.

TGA (Thermogravimetric Analysis): TGA was performed in a TA Instruments Q50 TGA to determine the graphene content of the dispersions and nanocomposites. Dispersions were drop casted on Kapton polyimide substrate and the solvent was evaporated completely before the TGA experiments were conducted. 15 mg of each sample was heated up from room temperature to 1000 °C at a rate of 10 °C /min in a nitrogen atmosphere.

Conductivity measurements: The electrical resistance of the nanocomposites was measured using the four-point probe method. The four-point probe head (Signatone, SP4-40045TBY) was mounted on a resistivity measurement stand (Signatone, Model 302). The spacing between the probe tips was 1.5875 mm. The current was passed to the sample through the outer probes using a Keithley 6221 AC and DC current source. A Keithley 2000 multimeter was used to measure the voltage across the sample. The sheet resistance and electrical conductivity of the samples were calculated using the measured values of the voltage.

6.3 Results and discussion

6.3.1 Analysis of pyrene-functional copolymers

Our goal was to design pyrene-containing PMMA and PS polymer chains which can stabilize graphene through π - π interactions. Figure 6.1 indicates the synthesis route applied to prepare such polymers. Free radical polymerization of styrene and methyl methacrylate (MMA) in presence of pyrene precursor yielded the random copolymers of PSPMA and PMPMA, respectively. Varying the amount of pyrene precursor can change the mole fraction of the pyrenemethyl methacrylate in the polymer chains. Copolymers synthesized with 1-pyrenemethyl methacrylate mass fractions of 0.01, 0.05, 0.10, and 0.15 were named copolymer-1, copolymer-5, copolymer-10 and copolymer-15, respectively. Observation of the pyrene characteristic peak at 348 nm in the absorbance spectra of pyrenemethyl methacrylate and the copolymers verified the presence of pyrene in the copolymers molecular structure (Figure 6.2). This specific peak does not appear in the absorbance spectra of bulk PMMA and PS.⁴⁶¹

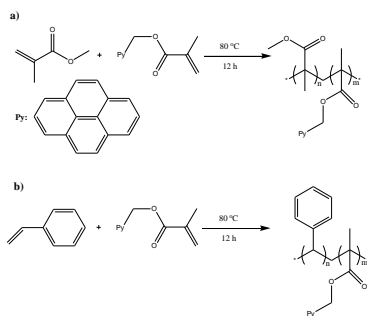


Figure 6.1. Proposed synthesis route of (a) PMPMA, and (b) PSPMA random copolymers. n and m represent the mole fractions of MMA/Styrene and pyrenemethyl methacrylate in the copolymer chain, respectively.

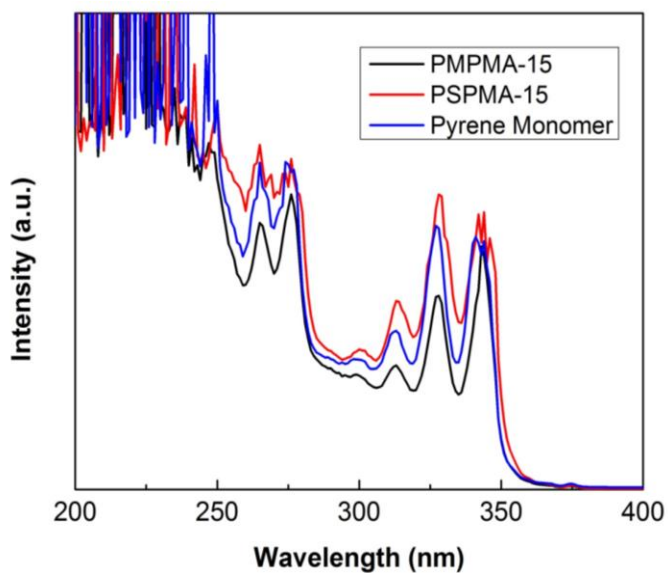


Figure 6.2. Absorbance spectra of pyrenemethyl methacrylate and the synthesized copolymers. The pyrene characteristic peak appears for all three samples at 348 nm (performed by Ziniu Yu).

To investigate the molecular structure of the copolymers, GPC analysis was performed using a UV-Vis detector and a Refractive Index (RI) detector. Setting the wavelength of the UV-Vis detector allowed for tracing the pyrene groups, while the RI detector was used to detect the elution of the whole copolymer chains. The simultaneous elution of the pyrene groups and the whole copolymer chains, shown in Figure 6.3 and 6.4, confirms the copolymerization of the 1- pyrenemethyl methacrylate with styrene and MMA.

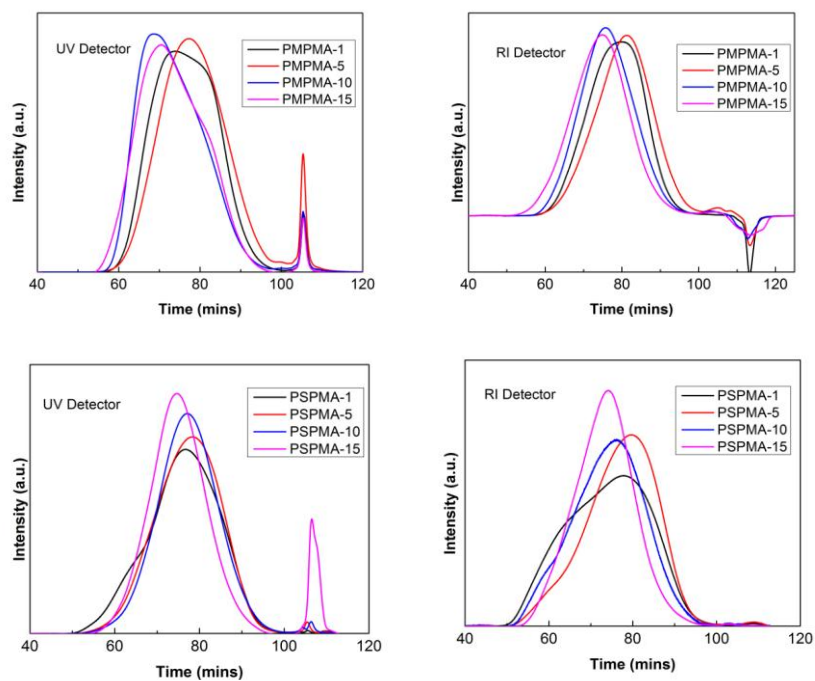


Figure 6.3. Elution profiles of copolymers obtained from the GPC analysis (performed by Ziniu Yu).

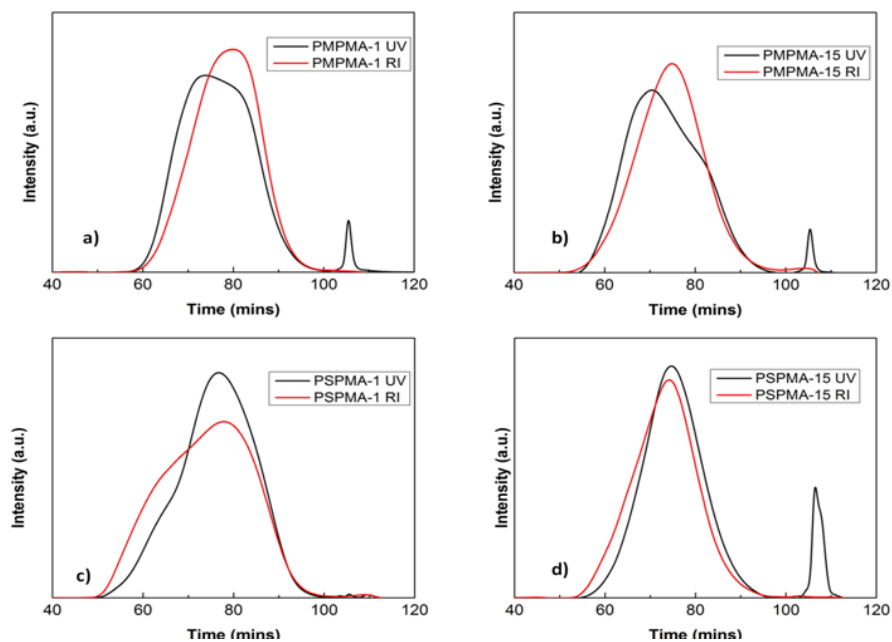


Figure 6.4. Comparison of the copolymers elution profiles traced by the UV-vis and RI detectors (performed by Ziniu Yu).

The molecular weight and PDI of the copolymers were calculated from the GPC results and are represented in Table 6.1. The PDI of PMPMA copolymers increased with addition of more pyrene content, while the PDI of PSPMA copolymers showed an opposite trend. This observation indicates that the presence of pyrene precursor affects the polymerization of styrene and MMA differently. It may be explained by the fact that large pyrene groups impose a significant steric hindrance during polymerization of MMA monomers, leading to a broad distribution of polymer chains length. On the other hand, the similarity of the pyrene structure and styrene may enhance the polymerization of this monomer in presence of pyrene precursor. Additionally, the molar masses of PMPMA copolymers obtained from UV-vis detector are higher than those obtained with RI detector; this shows the preference of pyrene groups for attachment to the longer PMPMA chains with higher molecular weight. On the other hand, the molar mass of PSPMA copolymers calculated from RI detector data were higher than those obtained from UV-vis detector. Therefore, the pyrene groups were attached to shorter PSPMA chains with lower molecular weight.

Sample	M_n (UV Detector)	PDI	M_n (RI Detector)	PDI
PMPMA-1	2.3×10^4	3.0	2.9×10^4	3.1
PMPMA-5	1.6×10^4	3.4	2.0×10^4	3.7
PMPMA-10	3.0×10^4	3.1	4.0×10^4	3.7
PMPMA-15	3.7×10^4	3.7	4.0×10^4	4.1
PSPMA-1	1.7×10^4	8.8	1.6×10^4	5.6
PSPMA-5	1.5×10^4	5.2	1.6×10^4	3.9
PSPMA-10	2.0×10^4	6.3	1.6×10^4	3.5
PSPMA-15	2.7×10^4	3.9	2.3×10^4	3.1

Table 6.1. Number average molecular weight (M_n) and polydispersity index (PDI) of the copolymers obtained from the GPC results, using the UV-vis and RI detectors (prepared by Ziniu Yu).

6.3.2 Graphene/copolymer dispersion and films

The as-synthesized copolymers were used as dispersants to stabilize colloidal pristine graphene. The concentrations of copolymers were chosen such that the pyrene content remains constant (1.3 mg/ml) in all the dispersions. The exfoliation of graphene sheets was carried by tip sonication in the chloroform solution of all the copolymers. The residual graphitic materials were removed by a centrifugation step after exfoliation and the supernatants were collected. Stable graphene dispersions were obtained through the use of all the copolymers, except for PSPMA-1. Figure 6.5 depicts HRTEM images of graphene nanosheets in graphene/PSPMA-15 (the inset of Figure 6.5) and graphene PMPMA-15 dispersions. The lateral size of graphene nanosheets is $\sim 1 \mu\text{m}$. Because of

polymer coverage on the graphene surface, it was difficult to perform the normal edge count of the graphene sheets. Folding of the graphene sheets may be due to the entrapment of the sheets within high concentration of polymer chains during drying step for TEM sample preparation.

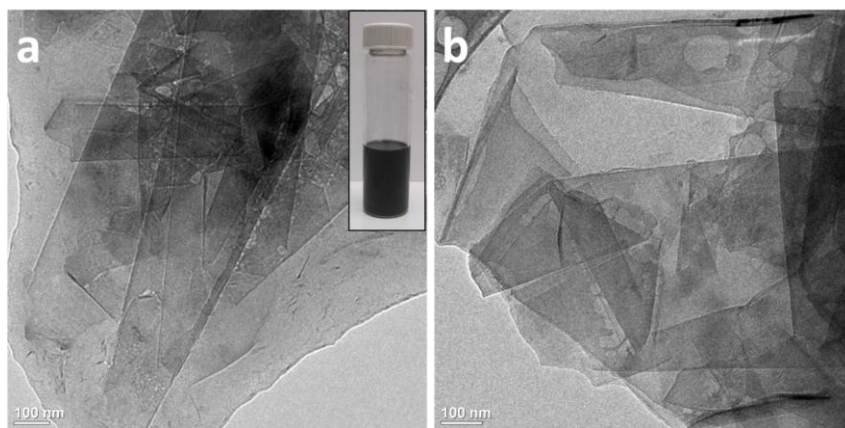


Figure 6.5. HRTEM images of graphene sheets cast from dispersions of (a) graphene/PSPMA-15, and (b) graphene/PMPMA-15.

Graphene/polymer films were prepared by vacuum filtration of the dispersion as illustrated in Figure 6.6. In the dispersions, a certain fraction of the copolymer chains adsorb on the surface due to π - π interactions between pyrenes and graphene; these chains sterically prevent aggregation of the dispersed nanosheets. The other polymer chains remain unbound in the dispersion. Upon vacuum filtration of the dispersion on a porous membrane, the unbound polymer chains leach through the membrane pores. The leaching of unbound polymer chains causes a graphene-rich layer to form adjacent to the

membrane. As this graphene-rich layer becomes thicker throughout the filtration process, it prevents further diffusion of the polymer chains toward the membrane pores, effectively limiting the leaching phenomenon. Consequently, the upper layers of the final film (in which leaching does not occur) maintain a polymer concentration similar to the original dispersion. This distinction between the upper and lower portion results in the Janus-like structure.

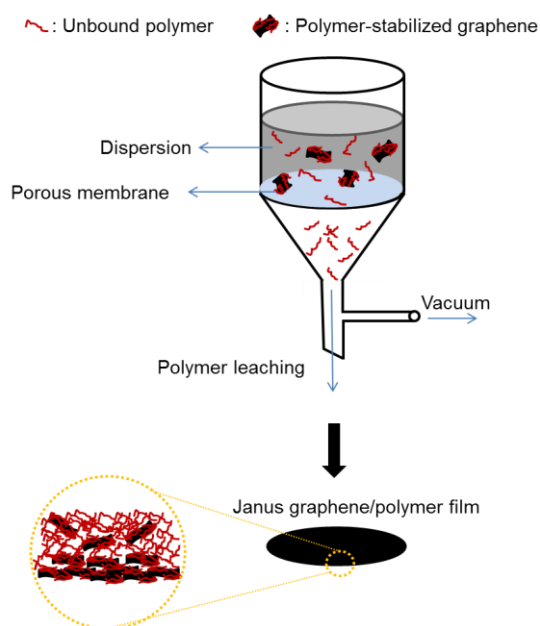


Figure 6.6. Schematic of Janus graphene/copolymer film preparation by vacuum filtration.

Figure 6.7a shows the cross-section SEM image of Janus graphene/PSPMA-10 film. The dual character of the Janus film and the transition from the polymer-rich side (on top of the film) to the graphene-rich side (at the bottom of the film) are depicted in

this image. In the polymer-rich side (Figure 6.7b), fewer graphene sheets with random orientation are embedded in the polymer matrix. In contrast, the graphene sheets in the graphene-rich side (Figure 6.7c) are highly aligned and are not covered with the polymer layer; this confirms the polymer leaching in this section of the film. The alignment of the graphene sheets may be attributed to the larger hydrostatic forces exerted at the bottom of the film during the filtration. The same structure was observed in Janus graphene/PMPMA-10 film cross-section (Figure 6.7d-f); however, the transition from polymer-rich side to the graphene-rich area was not as sharp as in the graphene/PSPMA-10 film. Additionally, the graphene sheets stacking in the graphene-rich area are less compact compared to graphene/PSPMA-10 film.

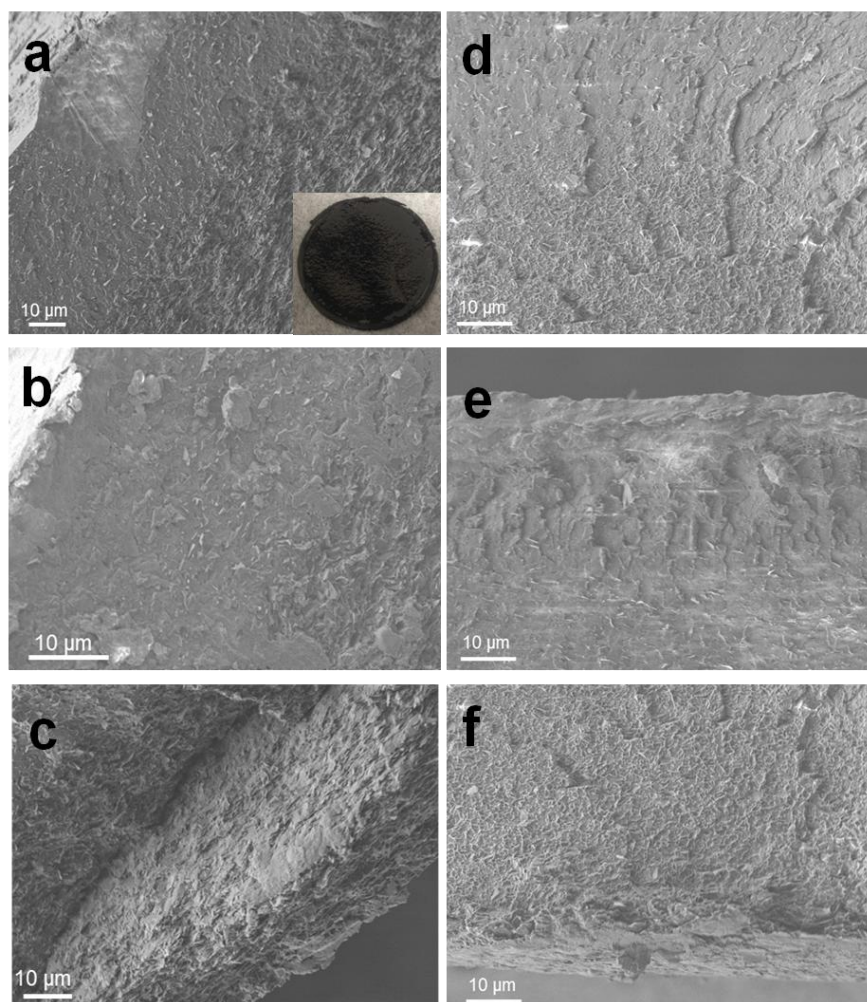


Figure 6.7. SEM images of the cross-section of (a and d) Janus graphene/PSPMA-10 and graphene/PMPMA-10 films, respectively (the inset shows the digital photo of the graphene/PSPMA-10 film), (b and f) polymer-rich sections of the Janus graphene/PSPMA-10 and graphene/PMPMA-10 films, respectively, and (c and e) graphene-rich sections of the Janus graphene/PSPMA-10 and graphene/PMPMA-10 films, respectively.

This leaching hypothesis suggests that there is an increase in the graphene/polymer ratio from the original dispersion to the final Janus film. To assess the original graphene content of the dispersions, the dispersions were cast on the Kapton substrate to form films. TGA was then carried out on both the cast-films (representing

the dispersion) and the Janus films. The complete thermal degradation of the copolymers themselves occurs by ~ 450 °C, (Figure 6.8). Any remaining mass above this temperature represents the graphene content of the samples.

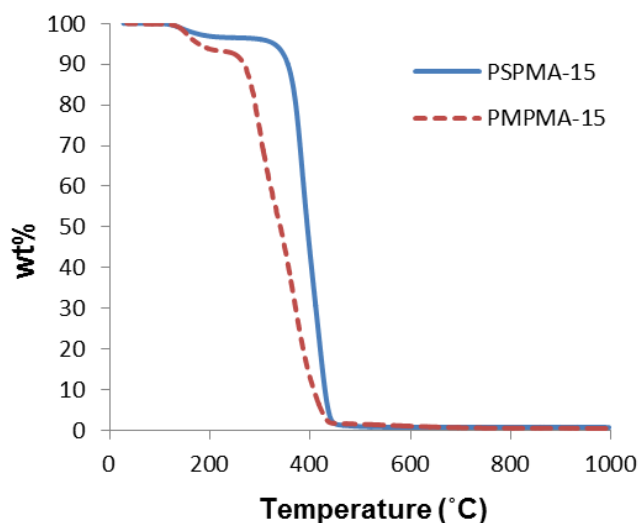


Figure 6.8. Thermogravimetric analysis of PSPMA-15 and PMPMA-15 copolymers.

Figure 6.9 depicts the TGA results for the cast and Janus films prepared by PSPMA copolymers. All the samples demonstrate similar degradation behavior to the PSPMA copolymers, which confirms that graphene-copolymer interactions did not affect the thermal degradation pattern of the PSPMA. Both cast films had the same graphene content (~ 7.5 wt %). Since the same pyrene content was used in preparation of all the dispersions, the similarity of graphene content in the cast films (and dispersions) proves the fact that stabilization occurs through the π - π interactions of pyrene and

graphene. Both Janus films have higher graphene content (~ 20 wt %) which confirms considerable leaching of the unbound polymer chains during the vacuum filtration.

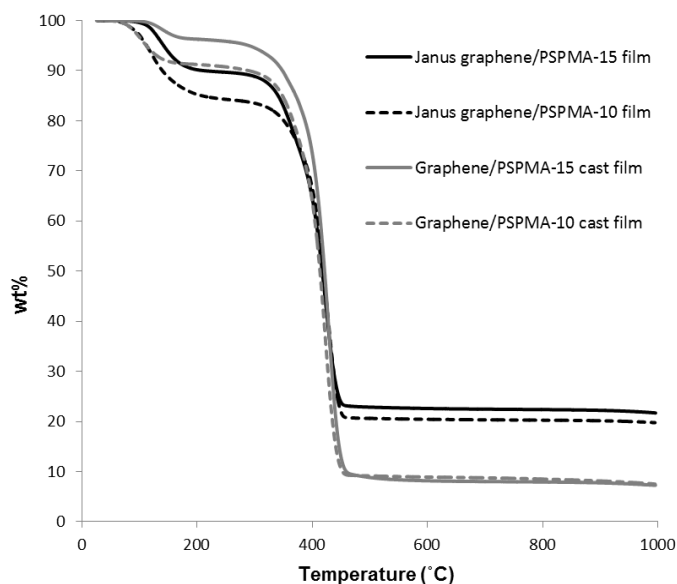


Figure 6.9. Thermogravimetric analysis of Janus and cast films of graphene/PSPMA-10 and graphene/PSPMA-15.

Similarly, Figure 6.10 shows the TGA results for the graphene films prepared using the methacrylate-based copolymer, PMPMA. All the cast and Janus films featured an extra degradation step compared to the PMPMA copolymer. Unlike the PSPMA case above, the graphene-PMPMA interactions do affect the thermal degradation of the polymer. Both cast films contained 5 wt % graphene which again confirms the π - π stacking stabilization mechanism for graphene in presence of PMPMA copolymers. However, their lower graphene content compared to the graphene/PSPMA cast films

means that PSPMA copolymers are better stabilizers. The slight increase in the graphene content of Janus graphene/PMPMA-10 film (6.51 wt %) reveals the limited polymer leaching in this sample. Though, the polymer leaching in the graphene/PMPMA-15 film is less restricted and the graphene content rose to 11.15 wt % in this sample. However, a comparison between the PSPMA and PMPMA samples indicates increased polymer leaching in graphene/PSPMA films. This observation is consistent with the SEM images which displayed a larger graphene-rich section in the Janus graphene/PSPMA film, compared to the graphene/PMPMA film. It may be attributed to the fact that in PSPMA copolymer, the pyrene groups and thus, the graphene sheets are mostly attached to the shorter polymer chains; allowing the longer and heavier unbound polymer chains leach through the membrane during vacuum filtration.

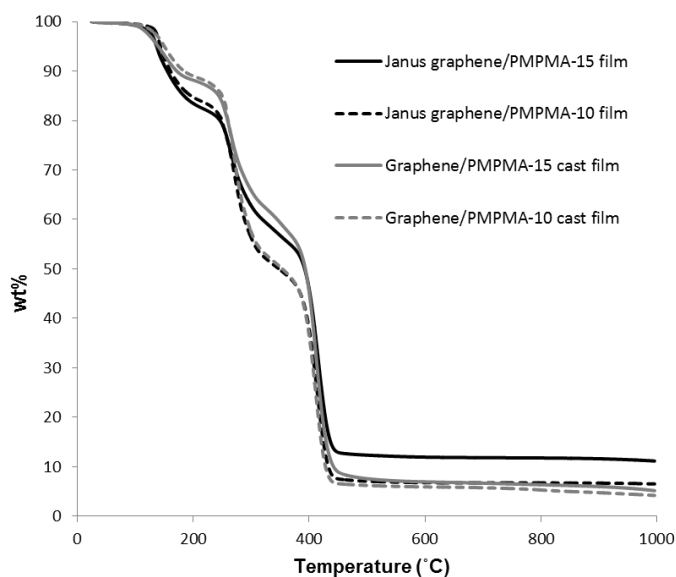


Figure 6.10. Thermogravimetric analysis of Janus and cast films of graphene/PMPMA-10 and graphene/PMPMA-15.

The electrical conductivity of the cast and Janus films were also measured (Table 6.2). Despite the high graphene content in the cast films, their conductivity was below the measureable threshold. The phase separation of unbound polymers and polymer-stabilized graphene sheets may be a possible explanation for this observation. All the Janus films were conductive on the graphene-rich side and non-conductive on the polymer-rich side. This is the first report of the pristine graphene-polymer films with the electrical properties changing from one side to other one. The conductivity values for all the Janus film were in the same order of magnitude and among the highest values reported for graphene/PMMA and graphene/PS nanocomposites in the literature^{356,379,423,462-465}

	Graphene/PSPMA-10	Graphene/PSPMA-15	Graphene/PMPMA-10	Graphene/PMPMA-15
Graphene content of cast film (wt%)	7.50	7.28	4.19	5.16
Graphene content of vacuum filtered film (wt%)	19.77	21.71	6.51	11.15
Electrical conductivity of cast film (S/m)	Not conductive	Not conductive	Not conductive	Not conductive
Electrical conductivity of vacuum filtered film (S/m)	162.35 (± 18.40)	194.83 (± 67.96)	60.14 (± 5.37)	83.18 (± 4.69)

Table 6.2. Electrical conductivity and graphene content of the Janus and cast films of graphene/PSPMA and graphene/PMPMA samples.

6.4 Conclusions

In this work, pyrene-functional copolymers of PS and PMMA were synthesized through a facile, one step radical polymerization route. The molecular structure of the

copolymers was characterized by UV-vis spectroscopy and GPC. The attachment of pyrene to the polymer backbone was confirmed; different polymerization behavior of the monomers in presence of pyrene precursor was revealed. The copolymers were used to exfoliate and stabilize pristine graphene in chloroform. The Janus films of graphene/copolymers were prepared by vacuum filtration of these dispersions. These Janus graphene films have an electrically-conductive side with conductivities as high as ~ 140 S/m, and another polymer-rich electrically-insulating side. These Janus graphene composite films may have potential application in sensors and specialized coatings.

CHAPTER VII

CRUMPLING AND UNFOLDING OF SPRAY-DRIED PRISTINE GRAPHENE AND GRAPHENE OXIDE NANOSHEETS*

7.1 Introduction

The ability to controllably alter nanosheet morphology from a 2D planar structure to a 3D “crumpled” structure is an exciting new avenue for engineering high-surface area materials.^{466,467} Crumpled graphene sheets are less prone to reaggregation since their morphology hinders the inter-sheet π - π stacking. Thus, crumpling can be used as method for producing aggregation-resistant graphene powder that can be easily redispersed in the liquids. Crumpling of 2D nanosheets into 3D particles occurs under compressive forces. Recent work shows that aerosolization of nanosheets aqueous dispersions can accomplish this goal due to droplet confinement forces; as aerosolized droplets evaporate, compressive forces associated with evaporation alter dispersed nanosheets into a “crumpled paper” morphology.

Thus far, such techniques have been limited to water-soluble, hydrophilic graphene oxide. No studies have investigated crumpling of pristine, unfunctionalized graphene. Huang *et al.* used an atomizer/furnace combination to process dispersed GO into crumpled GO nanoparticles; they also investigated the response of such crumpled particles to external compression and wetting and reported that the 3D morphology

*Part of the data reported in this chapter was reproduced with permission from (Parviz *et al.*, “ Tailored crumpling and unfolding of spray-dried pristine graphene and graphene oxide sheets”, *Small*, 2015, 11, 2661-2668).

remained unchanged.⁴⁶⁸ Similarly, Zangmeister *et al.* used an aerosolization technique to create crumpled graphene oxide; they investigated the change in fractal dimension of the nanosheets and the appearance of defects in the structure of the nanosheets as a result of crumpling.^{469,470} A more recent paper reported correlations between the confinement force, rate of evaporation, and the final particle size.⁴⁷¹ Such crumpled GO nanosheets are useful in high surface area electrode material for batteries and ultracapacitor applications.^{472,473} Separately, hollow nanospheres produced by assembly of the nanosheets during the drying process were tested as oil absorbents in water.⁴⁷⁴ Additionally, metal nanoparticles such as Ni and Fe were encapsulated within the crumpled nanosheets to produce graphene-based nanohybrids.⁴⁷⁵⁻⁴⁷⁹

However, despite the intense interest in this area, much remains unknown about the nature of the morphology transition and the mechanism of crumpling in nanosheets. Several theoretical studies have simulated folding and wrinkling of nanosheets under compressive forces and tried to explain these phenomena in the context of nanosheet elasticity and surface chemistry.⁴⁸⁰⁻⁴⁸⁴ Experiments that provide a clear picture of the mechanism and dynamics of nanosheet deformation are critical.

It is also noteworthy that despite the novelty of 3D crumpled graphene, the aerosolization and drying process used to make them is actually a mature engineering field. In fact, in contrast to specialized atomizer/furnace setups,^{468,469} we found that this process could be duplicated using a conventional industrial spray dryer. Spray dryers have been used extensively for aerosolization and drying of colloidal dispersions to produce a variety of powdered products, particularly in the pharmaceutical

industry.^{485,486} The processing parameters used in spray drying, such as temperature, pressure and droplet size and their effect on the product morphology, has been extensively investigated for a number of colloidal systems and can be used to tune product structure.^{487,488}

In this chapter, we use this scalable industrial technique to crumple pristine graphene nanosheets and study the differences in crumpling mechanisms as a function of surface chemistry (graphene vs. GO) and spray drying parameters. We do so using an in-situ sample collection technique to examine the crumpling process using electron microscopy. This is the first time in the literature that evolution of 2D graphene nanosheets under compressive forces has been directly observed. On this basis, we can propose distinct mechanisms for the two nanosheet types as a function of surface chemistry. We use dimensionless analysis of the spray drying process to show how morphology differences may be tuned by spray drying process parameters (pressure, temperature, droplet size). Additionally, we examine the reversibility of the crumpled state of both GO and pristine graphene by observing redispersion and unfolding behavior of the crumpled product. We believe that these insightful observations shed light on the nature of nanosheet crumpling and bridge the theoretical predictions to real experimental systems. Such information may allow control over folding and unfolding of the graphene nanosheets and may extend to other nanosheet types for multifunctional materials engineering. The work presented in this chapter was published in 2015 as a journal article in *Small*.⁴⁸⁹

7.2 Experimental procedures

7.2.1 Materials

Expanded graphite was provided by Asbury Carbons (CAS# 7782-42-5, Grade 3806). 1-pyrenesulfonic acid sodium salt (Py-SASS), polyvinylpyrrolidone (PVP) with $M_w \sim 10000$ and polyacrylamide (PAM) with nominal molar mass of $5 * 10^6$ g/mol (nonionic, water solubale) were purchased from Sigma-Aldrich. Sodium dodecyl benzene sulfonate (SDBS) (157889) was purchased from MPBiochemicals. Single layer graphene oxide (GO) was purchased from Cheap Tubes Inc. All the solvents including chloroform, ethanol and acetone were purchased from Sigma Aldrich. All the chemicals were used as received.

7.2.2 Preparation of graphene dispersions

In a typical preparation, specific amount of stabilizers including Py-SASS (2 mg/ml), PVP (10 mg/ml), PAM (10 mg/ml) or SDBS (6 mg/ml) was dissolved in the deionized water (DI). EG (50 mg/ml) was added to the solution and tip sonicated for one hour by a Misonix sonicator (XL 2000) at output wattage of 7W. A water bath was used to maintain the room temperature during the sonication. The dispersion was then centrifuged (Centrifuge 225, Fischer Scientific) at 5000 rpm for 4 hours to remove larger aggregates and the supernatant was collected. This stable dispersion was used for spray drying and further characterizations.

In order to prepare GO dispersions, GO powder was added to the DI water with specific concentration and tip sonicated for 5-10 minutes. The dispersion was used for spray drying and further characterizations.

7.2.3 Spray drying of the dispersions

Graphene and GO dispersions were processed in a spray dryer (Buchi 290 mini spray dryer) to yield crumpled nanosheets. In this process, micron sized droplets of dispersion were produced by the atomizer of spray dryer. The droplets were carried away and dried by hot air to produce powder particles. The dry powders were settled by a cyclone separator and the air was discharged from the separator along with small particles. The atomizer pressure was 60 psi and the hot air temperature was 220 °C. Temperature and pressure were changed in various experiments in order to assess the effect of these parameters on the final morphology of the product. In all experiments, 10% of the dispersion flow rate and 100% of the aspirator rate was used for spraying the dispersions.

7.2.4 Characterization

UV-vis spectroscopy was used to measure the concentration of graphene nanosheets in the dispersions. The absorbance was measured using a Shimadzu UV-vis spectrophotometer 2550 at a wavelength of 660 nm on the liquid samples against the stabilizer solution to eliminate the effects of the stabilizer solution. The concentration

was determined using Beer's law. Vacuum filtration was used to calculate the extinction coefficient of stabilizer solution in water.

SEM (Scanning Electron Microscopy). Imaging of the powder samples was carried on a Hitachi S4300 SE/N. All the samples were mounted on double face carbon tape and an accelerating voltage of 2 kV was used to image.

High Resolution Transmission Electron Microscopy (HRTEM). A voltage of 75 kV was used to image the samples on Hitachi H8100. Samples were placed on 400 mesh carbon-coated copper grids (Electron Microscopy Sciences, CF400-Cu). To observe the change of morphology of the nanosheets during the drying process, grids were fixed inside the spray dryer column and samples were directly collected on them. Collection of the samples was done stages with 10 cm distance from each other. In order to image the redispersed crumpled nanosheets in the solvent, liquid sample was deposited on the grid and dried in the air for 1 min. Also, to assess the immediate response of the crumpled nanosheets against hydration, samples were placed on the grids and micron sized droplet of the solvent was deposited on top of them and was dried in the air for 1 min.

Freeze drying. Graphene and GO dispersions were frozen in a freezer at -15 °C and further dried in a freeze dryer (Vitriscience Benchtop Freeze Dryer) overnight to yield dry powdered samples. The final powder was used for imaging.

7.3 Results and discussion

7.3.1 Crumpling of the nanosheets

Aqueous dispersions of pristine graphene and GO were prepared with similar nanosheet concentrations. TEM images in Figure 7.1a show pristine graphene nanosheets which were deposited and dried on the TEM grid from the original Py-SASS-assisted dispersion. Pristine graphene nanosheets typically consisted of 2-3 layers with a typical lateral size of 1-1.5 μm ; this is consistent with our work on pristine graphene dispersions discussed in Chapter III.^{33,39,328} Images of GO nanosheets revealed single layers with an average size of 3-4 μm as represented in Figure 7.1b. In contrast to pristine graphene nanosheets, these sheets showed ripples and wrinkles on a small scale rather than large-scale folds; again, these images are consistent with prior work.^{490,491} These ripples and wrinkles may be attributed to the capillary forces associated with the evaporation of water on the surface of GO during sample preparation for TEM, which is highly hydrophilic compared to pristine graphene.⁴⁹²

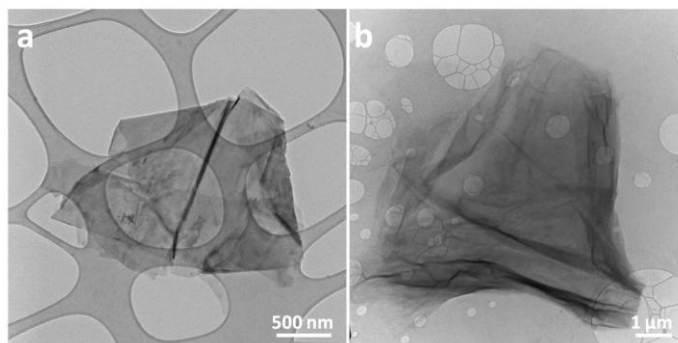


Figure 7.1. TEM images of nanosheets of (a) pristine graphene and (b) GO cast from the aqueous dispersions.

Both dispersions were spray dried at an atomizer pressure of 60 psi and temperature of 220°C. The initial droplet diameter varied in the range of 1-15 μm and 90% of the droplets were smaller than 10 μm at this operating condition of the spray dryer (this data was provided by the manufacturer). The concentration of graphene and GO nanosheets in the dispersions was 0.1 mg/ml. Figure 7.2 shows SEM and TEM images of the spray-dried pristine graphene particles with sizes in the range of 0.5-1.5 μm . Particle size polydispersity is due to both the original nanosheet size polydispersity and droplet size variation. The drying process turned the 2D pristine graphene nanosheets to 3D compact multi-faced crumpled particles with dimples on the surface. This is the first report of 3D crumpled pristine graphene nanosheets. In prior reports, simultaneous aerosolization and in situ heating of GO yielded crumpled nanosheets of reduced graphene oxide (rGO). In those cases, presence of functional groups and defects on the GO surface during the crumpling process conduct the nanosheet deformation through a different mechanism than defect-free pristine graphene deformation pattern which we have studied in this work.

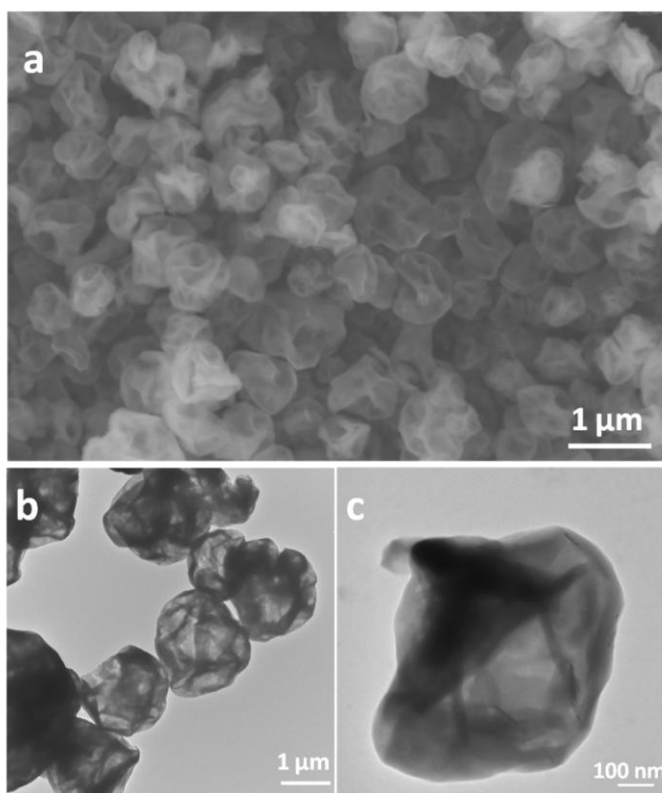


Figure 7.2. (a) SEM and (b and c) HRTEM images of crumpled nanosheets of pristine graphene. Dispersions of nanosheets were spray dried at atomizer pressure of 60 Psi and drying temperature of 220 °C. The concentration of nanosheets in dispersion was 0.1 mg/mL.

GO nanosheets in Figure 7.3 display a different morphology. These sheets were also converted to 3D compact particles, but instead of dimples, their surface show ridges and ripples. These particles have a more highly compacted appearance than the pristine graphene particles and showed a size range of 0.5-1 μm. The difference in the morphology of these two products may be attributed to differences in surface chemistry, wettability, and elasticity of the nanosheets. Earlier reports of crumpled GO displayed a wrinkled surface morphology similar to our results here;^{468,469} however, our results

display a more compacted, sphere-like shape as opposed to the deflated, crumpled morphology reported in the prior literature. This difference in the morphology may be attributed to usage of an industrial spray dryer in our experiments which provides different initial droplet size and drying rate compared to the atomizer/furnace setups. Both of these parameters may affect the stacking state of nanosheets within the droplet and deformation of nanosheets; hence, the final products of the crumpling process have different morphologies.

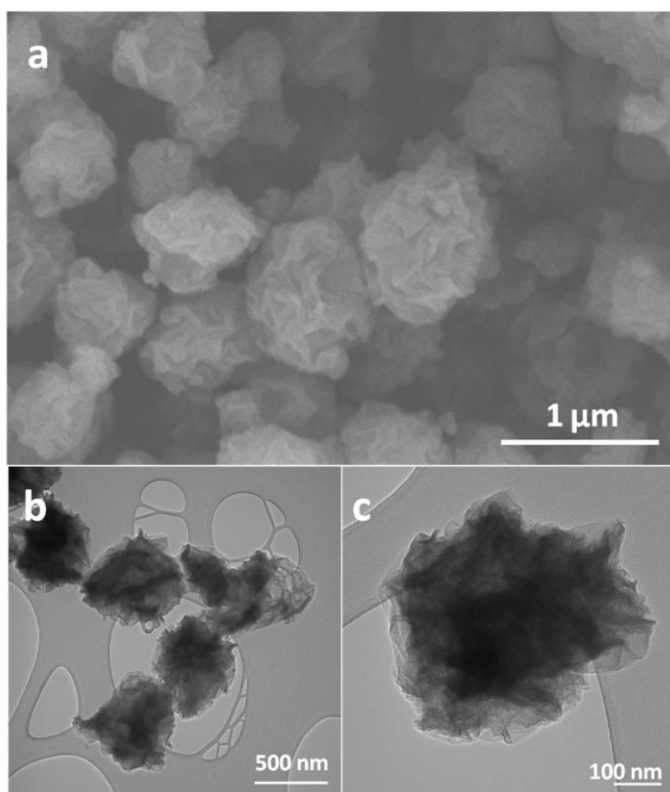


Figure 7.3. (a) SEM and (b and c) HRTEM images of crumpled nanosheets of GO. Dispersions of nanosheets were spray dried at atomizer pressure of 60 Psi and drying temperature of 220 °C. The concentration of nanosheets in dispersion was 0.1 mg/mL.

7.3.2 Mechanism of nanosheets crumpling

To further investigate the crumpling process, we collected samples at various points inside the spray drying setup using suspended TEM grids. This sample capture technique is novel and allows the first-ever direct study of the gradual transition of the morphology of nanosheets during the spray drying process. Samples were collected directly on TEM grids fixed at stages 10 cm apart within the gas chamber as shown in Figure 7.4. Figure 7.4a shows several pristine graphene nanosheets collected at 10 cm away from the atomizer tip. At this stage, the nanosheets were still flat; specifically, they were not folded or crumpled. Upon the evaporation of the water and shrinkage of the droplet, pristine graphene nanosheets started to deform (Figure 7.4b). At this stage, the deformation mainly occurred as folding and bending at the edges (Figure 7.5). As the particles moved through the chamber, most of the water evaporated from the surface, and a higher degree of deformation occurred due to higher capillary forces. Figure 7.4c shows that the nanosheets were finally compacted into a 3D morphology with dimples on the surface. We did not observe any particles that consisted of only dispersant (Py-SASS) molecules. We also spray dried a batch of dispersant (Py-SASS) with the same concentration and could not collect any product at the outlet of the spray dryer; this verifies that the stabilizer molecules did not form crumpled aggregates during the process and may be eliminated with the carrier gas. This also suggests that bulk dispersant in droplets, unassociated with graphene, may be eliminated by this process. We have investigated this topic in details somewhere else.⁴⁹³

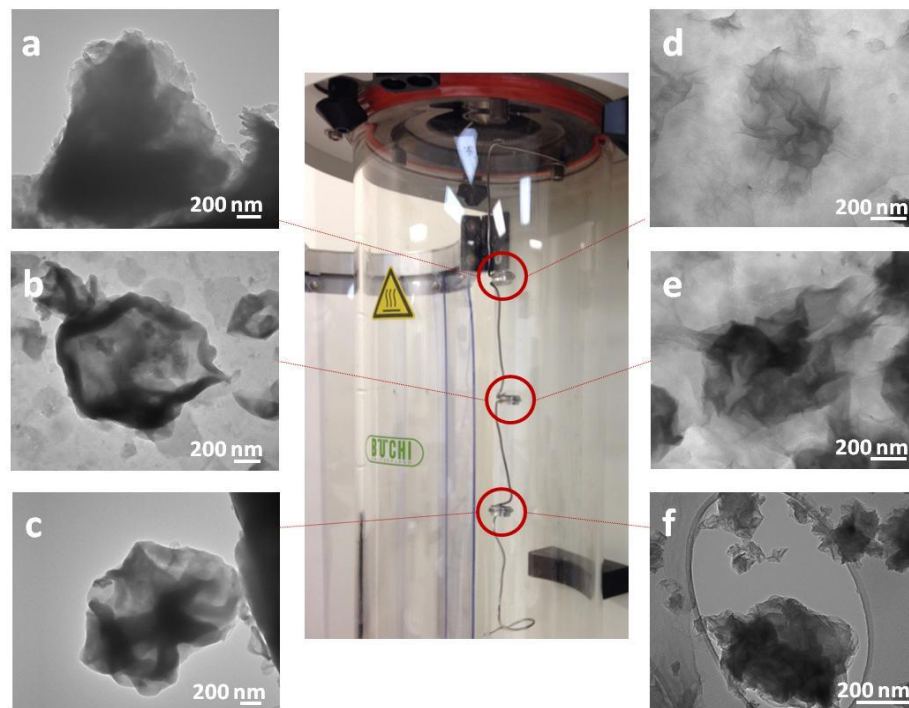


Figure 7.4. TEM images of the evolution of nanosheets during drying within the spray dryer, (a,b,c) pristine graphene and (d,e,f) GO nanosheets. Samples were collected on TEM grids which were fixed at different stages within the spray dryer. Stages were 10 cm apart from each other.

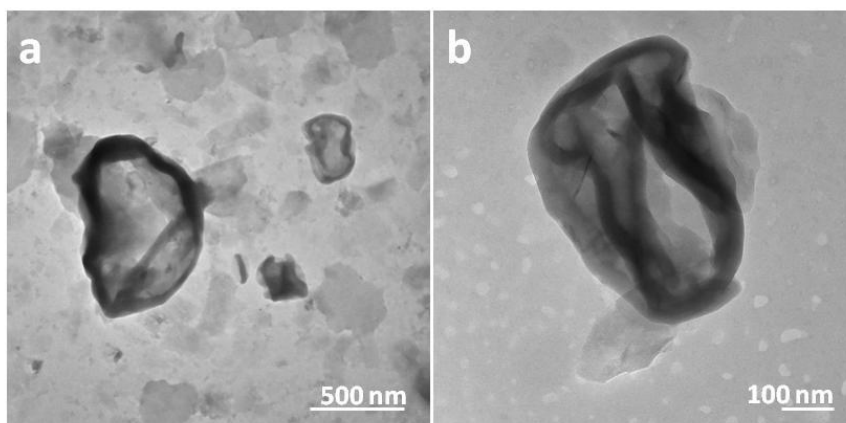


Figure 7.5. HRTEM images of the edge folding phenomenon in pristine graphene nanosheets. Samples were collected directly on TEM grids at the second stage within the spray dryer.

GO nanosheets showed a different trend during the drying process. At the first stage (Figure 7.4d), GO nanosheets were wrinkled across their surface, and their morphology was similar to the sample that was dried at room temperature in Figure 7.1. As the water evaporated from the surface, the nanosheets began to buckle and deform (Figure 7.4e). Deformation of GO nanosheets occurred through the formation and compaction of more pronounced ripples and vertices on the surface, with low values for the local radii of curvature. Figure 7.4f shows that the final GO particles are finally compacted into a tight, highly wrinkled morphology.

Based on Figures 7.1-5, we may posit a mechanism for crumpling of pristine graphene and GO nanosheets. Figure 7.6a-d schematically shows the proposed mechanism of formation of 3D crumpled particles from dispersed pristine graphene nanosheets. As the droplet emerges from the atomizer (Figure 7.6a) and begins to evaporate, the hydrophilic Py-SASS molecules diffuse toward the center of the droplet from the concentrated interface, while the hydrophobic graphene nanosheets with lower mobility remain at the interface (Figure 7.6b). Evaporation of the water from the surface of the droplet causes the surface tension to exert capillary forces on the nanosheets. When the capillary forces dominate the electrostatic forces, the nanosheets will form a continuous shell at the interface (Figure 7.6c). Finally, evaporation of water from inside this shell induces further shell deformation and the deformation begins.

This process can be explained by elastic deformation theory.⁴⁹⁴ The mechanism of buckling depends on the shell elastic modulus, thickness and wettability.^{495,496} An elastic shell may bend or locally stretch under capillary pressure. For pristine graphene

nanosheets, which have a higher elastic modulus than GO, bending is the main mechanism of deformation. The first step in deformation was folding of the nanosheets at the edge of the pristine graphene shell (Figure 7.6d); folding at the edges requires less energy than bending of the nanosheets in the middle. This observation of folding was consistent with previous simulation results.⁴⁹⁷ In the next step, additional bending of the nanosheets appeared in the form of dimples on the surface. If the shell is not uniform and enclosed, capillary forces due to evaporation are not homogeneously distributed on the shell such that localized dimples appeared (Figure 7.6e). Further evaporation of water resulted in more dimples on the surface and enclosing of the shell (Figure 7.6f). Presence of large amount of free dispersant molecules in the bulk dispersion may affect the shell formation on the droplet surface; however, the exceptionally high graphene to Py-SASS ratio in our dispersions (~ 0.34) and higher diffusivity of Py-SASS molecules compared to graphene nanosheets impedes the formation of a separate dispersant shell on the droplet surface.

For the crumpled GO particles, the mechanism differs substantially. GO nanosheets also emerge from the atomizer within the droplet (Figure 7.6g), accumulate at the surface of the droplet (Figure 7.6h) and are subjected to capillary forces on the surface (Figure 7.6i). The presence of the hydrophilic functional groups on the surface of GO enhances its wettability and causes increased capillary forces compared to pristine graphene sheets. Also, GO nanosheets have a lower elastic modulus than pristine graphene nanosheets which is caused by higher concentration of atomic-level defects and single-layer nature of GO.³²⁵ Additionally, single-layer GO nanosheets form thinner

shell with lower bending stiffness compared to few-layer pristine graphene. Under the enhanced capillary pressure they may undergo local deformation, and small wrinkles appear on the surface (Figure 7.6j).^{483,484} Therefore, the initial step of the deformation for GO shell is not folding; instead, the initial step is the formation of ripples and vertices as observed in TEM images (Figure 7.1). Additional wrinkling and enclosure of the shell occurs during evaporation of the water (Figure 7.6k). As the drying process continues, more ripples appear on the surface, and the wrinkled surface is compressed (Figure 7.6l). The difference in deformation behavior of pristine graphene and GO that we observed is consistent with the results of a recent molecular simulation study which predicted a highly wrinkled morphology for the GO and more smooth, folded, buckled morphology for the pristine graphene nanosheets.⁴⁹⁷

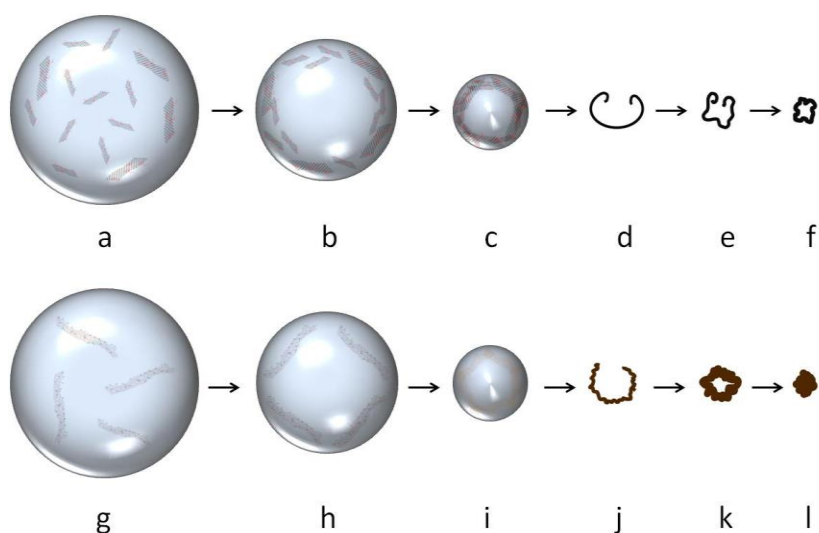


Figure 7.6. Proposed mechanism of crumpling for pristine graphene and graphene oxide nanosheets.

7.3.3 Tuning crumpled particles morphology

Various processing parameters in spray drying affect the deformation of the shell. These parameters (temperature, pressure, droplet size) and their effect on product morphology have been extensively reviewed for general spray drying elsewhere.⁴⁸⁵ It is well established that the rate of drying relative to diffusion rate is the main parameter which controls the deformation process; this ratio can be assessed by the Peclet number, defined as $R^2/(D t_{\text{dry}})$. Here R is the radius of the droplets, D is the diffusivity coefficient of the dispersed sheets, and t_{dry} is the drying time. $Pe \gg 1$ represents a fast drying regime in which shell deformation occurs at large R and results in formation of a crumpled shell with a hollow core. When $Pe < 1$, the drying is considered to be slow; in this case the shell forms at lower R and shrinks to form highly crumpled and compact particles. With these two regimes in mind, we examined how morphology varies with these processing parameters. To calculate the Peclet number, the diffusion coefficient of the pristine graphene nanosheets was calculated from Stokes-Einstein equation, $D = k_B T / 6\pi\eta R_h$, where k_B is the Boltzmann constant, T is the temperature, η is the viscosity of the solvent and R_h is the hydrodynamic radius of the nanosheets in this case. Hydrodynamic radius of pristine graphene nanosheets (~ 150 nm) was measured by dynamic light scattering technique. At 220°C , $\eta = 0.282 \times 10^{-3}$. The diffusion coefficient of the pristine graphene nanosheets turned out to be $8.53 \times 10^{-12} \text{ m}^2/\text{s}$. For all the experiments, the aspiration rate was kept at $35 \text{ m}^3/\text{h}$. The diameter of the drying chamber was 20 cm and its length was 60 cm. Therefore, the residence time of the droplets inside the drying chamber (t_{dry}) was calculated as ~ 1.5 s. Figure 7.7 shows the

variation of morphology and particle size with the increase in atomizer pressure. At $P = 20$ psi, the average droplet size was close to $50 \mu\text{m}$ and droplets formed at $Pe = 48.8$. At this pressure, the shell formation occurred on larger droplets because of rapid water evaporation; therefore, the final product contained crumpled, hollow particles with relatively low density. Variation of the atomizer pressure to 60 psi changed the average droplet size to less than $10 \mu\text{m}$ and Pe to 1.95; smaller droplets with narrower size distribution were atomized at higher pressure. Thus, at lower Pe regime, a slower evaporation rate led to formation of the shell on the surface of smaller droplets. Hence, a compact crumpled morphology and a smaller, more homogeneous particle size distribution were obtained for both pristine graphene and GO nanosheets.

The temperature of the carrier air was also changed to study its effect on the crumpling of the nanosheets (Figure 7.8). The rise of temperature caused t_{dry} to decrease and D to increase simultaneously. However, within the range of $90\text{-}220 \text{ }^{\circ}\text{C}$ drying was rapid and the change in the drying rate was not drastic enough to change the morphology of the particles. The increase in the temperature only decreased the size polydispersity of the final product.

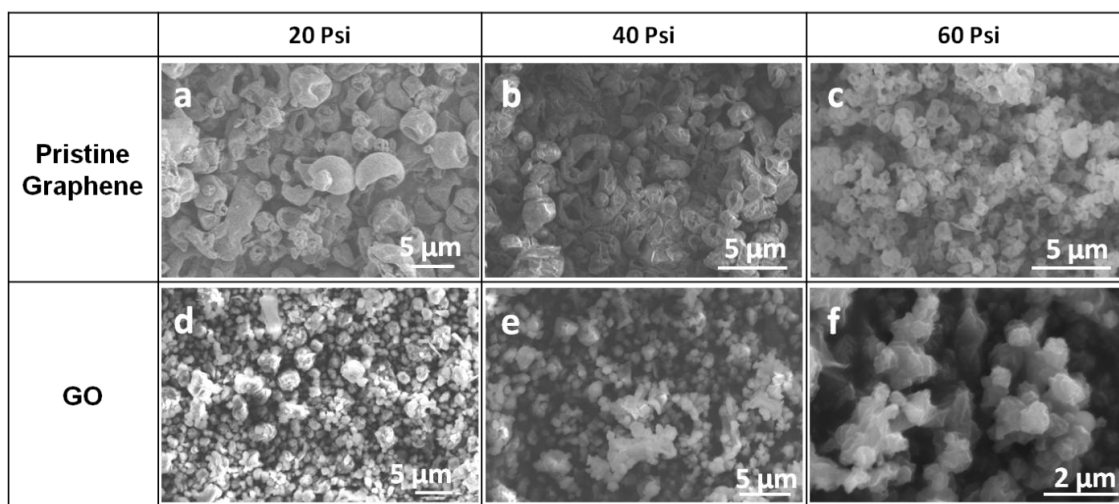


Figure 7.7. Effect of initial droplet size (varied by changing the atomizer pressure) on final morphology of the crumpled (a,b,c) pristine graphene and (d,e,f) GO nanosheets. Samples were dried at 120 °C and concentration of nanosheets in the dispersion was 0.1 mg/mL.

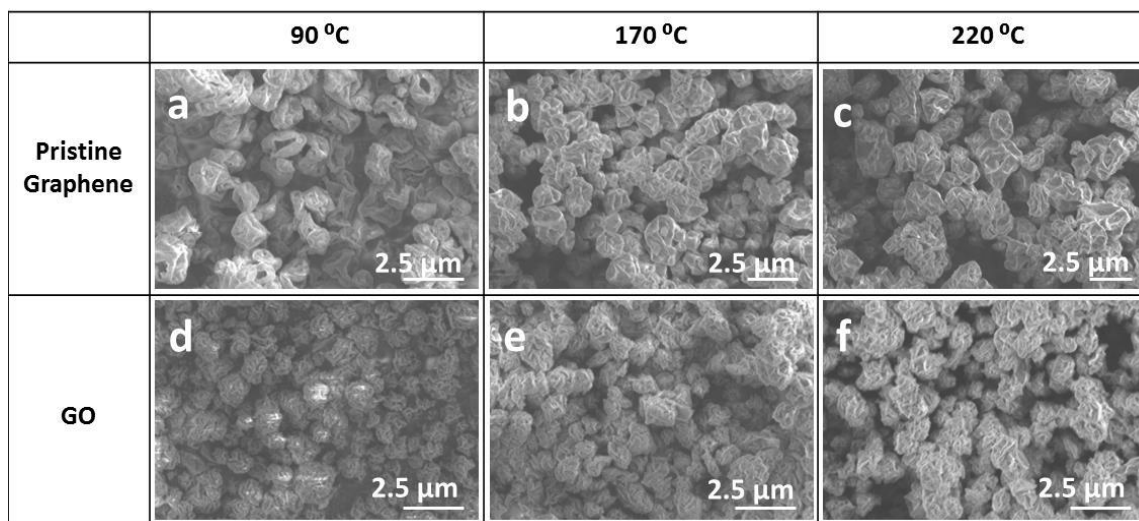


Figure 7.8. Effect of drying temperature on final morphology of crumpled (a,b,c) pristine graphene and (d,e,f) GO nanosheets. All the samples were sprayed at atomizer pressure of 40 psi and the concentration of the nanosheets in the dispersion was 0.1 mg/ml.

We also investigated the effect of nanosheet concentration on the final morphology and size of the particles. Figure 7.9 shows the final morphology of the sample prepared with different concentrations. The increase in concentration results in formation of larger particles which are less crumpled and are more similar to spherical particles. The thickness of the shell is the parameter that defines the energy required for the bending; if the number of the nanosheets increases within a single droplet, then a thicker shell will form at the interface. Such a shell needs a larger capillary force for deformation; it does not deform easily and will shrink to form a smooth semi-spherical morphology, rather than highly crumpled particles.

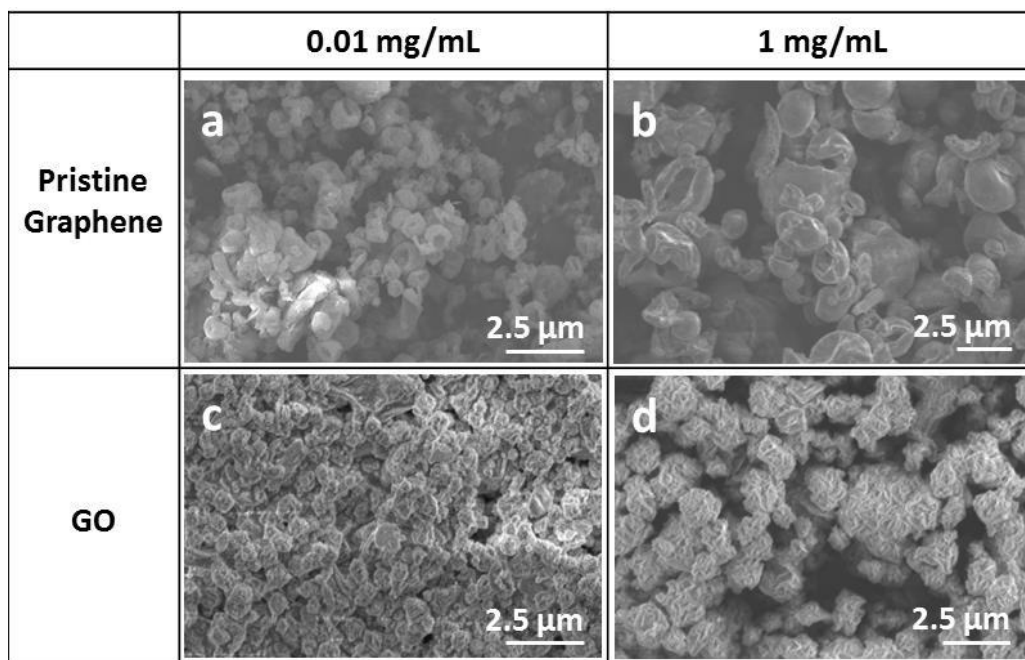


Figure 7.9. Effect of nanosheets concentration on the final morphology of (a,b) pristine graphene and (c,d) GO nanosheets. All the samples were sprayed at an atomizer pressure of 40 psi and dried at 170 °C.

7.3.4 Effect of dispersant and drying method

We also include a comparison of freeze drying and spray drying effects on dry, crumpled graphene and GO powder morphology (Figure 7.10). In order to study the effect of the drying method on the final morphology of the nanosheets, we freeze dried pristine graphene and GO dispersions. Figure 7.10 shows the SEM images of the freeze dried powder. Agglomerated nanosheets of pristine graphene did not bend or fold after during freeze drying. Although the lateral size of the freeze-dried nanosheets is comparable to those seen in the dispersion (Figure 7.1), the increased thickness shows multiple layers stacked together. Similarly, large aggregates of the GO nanosheets formed during the freeze drying process. All of these large aggregated nanosheets had a wrinkled appearance with lots of ripples on the surface, but they were not bent or buckled. These images demonstrate that it is the capillary forces unique to spray drying that are responsible for the compression forces.

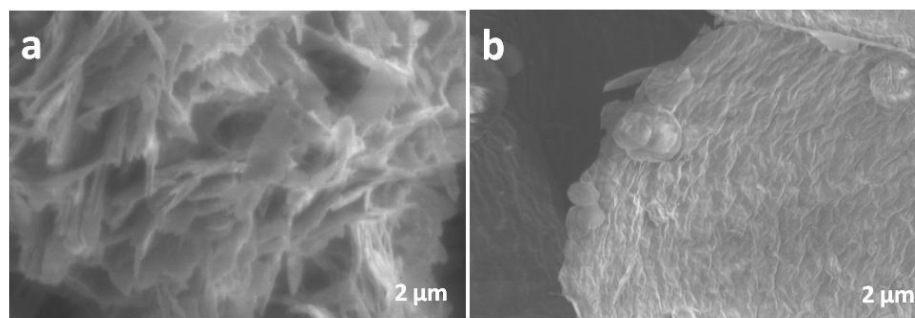


Figure 7.10. Morphology of the freeze-dried (a) pristine graphene and (b) GO nanosheets.

We also investigated the effect of the dispersant on the final morphology of crumpled pristine graphene nanosheets. We dispersed pristine graphene nanosheets in solutions of PVP, PAM and SDBS. The ratio of stabilizer to graphene in PVP, PAM and SDBS- stabilized samples was 10, 100 and 30, respectively. The PVP-stabilized crumpled particles had similar morphology to Py-SASS stabilized sample with less dimples on the surface (Figure 7.11). This can be attributed to presence of long polymer chains on the surface of graphene which may reduce the capillary forces exerted on the surface. In the case of PAM and SDBS- stabilized sample, the concentration of free stabilizer was so high in the dispersion that the stabilizer is the main component and simply covered the nanosheets on the surface of the droplet; thus, we could not observe the deformation of the nanosheets in these samples.

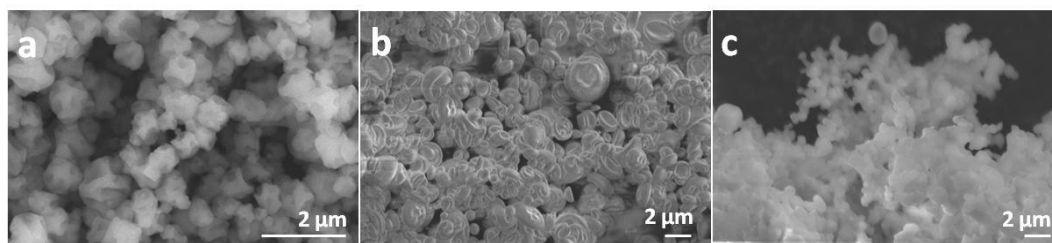


Figure 7.11. Effect of the dispersant on crumpling of pristine graphene nanosheets. Pristine graphene nanosheets stabilized by (a) PVP, (b) PAM and (c) SDBS were sprayed at atomizer pressure of 60 psi and dried at 220°C.

7.3.5 Unfolding of crumpled nanosheets

To investigate the stability of the crumpled morphology against hydration, crumpled particles were placed on a TEM grid and a single droplet of water was cast on top of the sample. Imaging of the sample was carried out immediately after evaporation. Figure 7.12a shows that the crumpled pristine graphene nanosheets immediately unfold after contacting the water droplet. Additionally, the crumpled pristine graphene nanosheets were redispersed in water with the original concentration and centrifuged. We also carried out TEM on these redispersed nanosheets (Figure 7.12b) and again we observed that the pristine graphene nanosheets completely unfolded in the presence of the water and became flat. However, the change in morphology did not affect the stability of these particles within the dispersion since they were stable against centrifugation (Figure 7.12b, inset). As demonstrated earlier, the presence of stabilizer molecules on the surface of the sheets prevents the inter-sheet interactions; this indicates that stabilizer molecules non-covalently bound to the pristine graphene surface remain intact through the spray drying process. Thus, the crumpling morphology is reversible and elastic. As soon as the water is added onto these particles, the crumpled particles unfold to release the elastic energy which was stored in the dimples and minimize the surface energy.

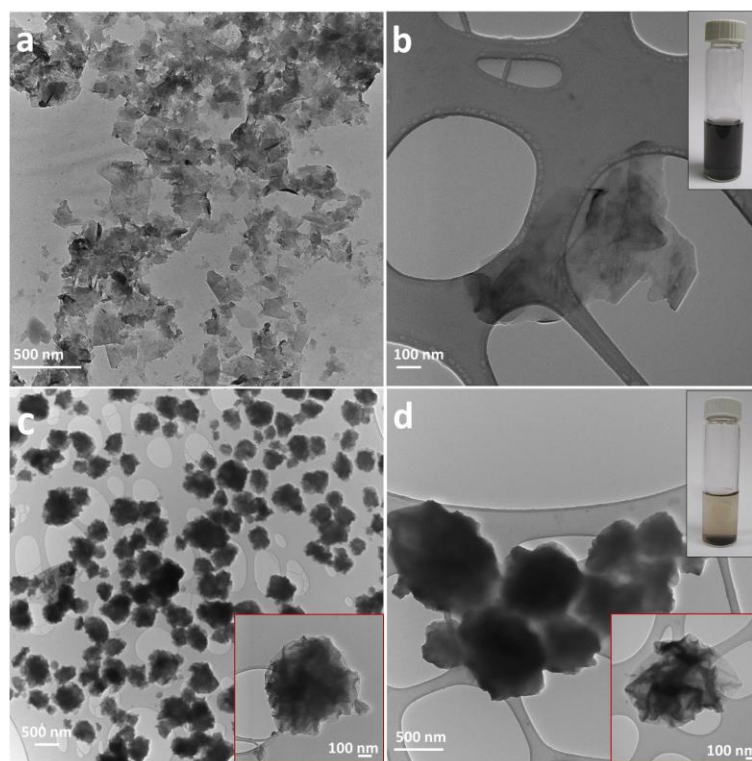


Figure 7.12. TEM images of: a) Crumpled pristine graphene unfolding after hydration on TEM grid; b) Crumpled pristine graphene unfolding after redispersion in water; c) Crumpled GO remains crumpled after hydration on TEM grid; d) Crumpled GO remains crumpled and does not redisperse in water.

The same experiment was carried out with the GO crumpled particles. Figure 7.12c shows that the GO particles preserve the crumpled morphology after contacting water on the TEM grid. Moreover, they remain crumpled even after redispersion in water and centrifugation (Figure 7.12d). The origin of this preserved crumpled morphology is unknown. It is possible that covalent ether bonds form between GO nanosheets during the spray drying process (220 °C); prior work indicates that partial reduction of GO in air can occur as low as 175 °C.⁴⁹⁸ Additionally, we annealed

crumpled GO nanosheets at 600 °C; TEM images of this annealed powder can be seen in Figures 7.13a and 7.13b. Interestingly, these particles preserved a less compact crumpled morphology compared with those seen in Figure 7.3. Again, these annealed crumpled GO nanosheets maintained the same morphology even after hydration on the TEM grid (Figures 7.13c and 7.13d).

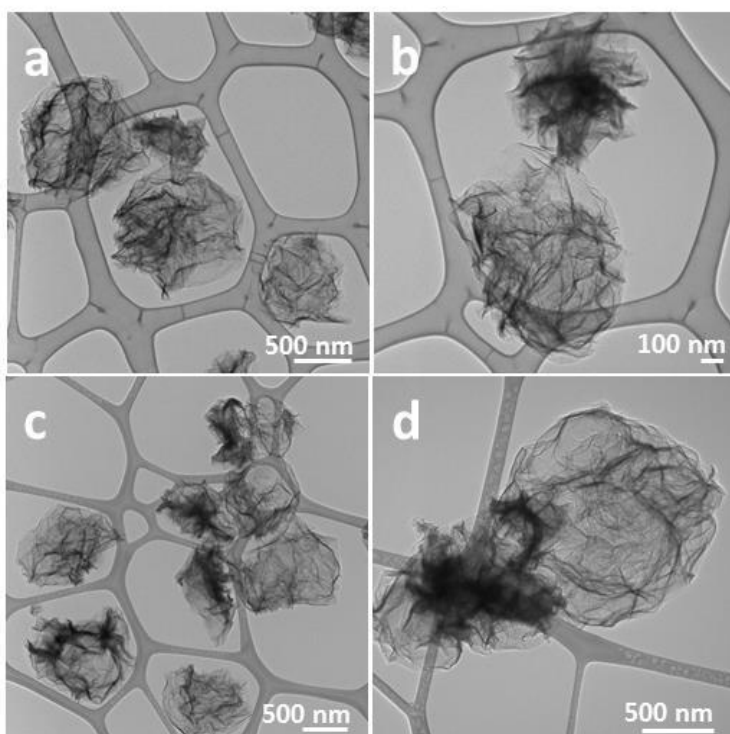


Figure 7.13. TEM images of (a,b) annealed crumpled GO nanosheets and (c,d) annealed crumpled GO nanosheets after rehydration on the TEM grid. Annealing of the crumpled nanosheets was carried under nitrogen atmosphere and at 600 °C.

Minimization of the surface energy is the main driving force for unfolding of the pristine graphene nanosheets and strongly depends on the interactions between the

nanosheets, stabilizer molecules and the solvent. Therefore, the pristine graphene crumpled particles were redispersed in other solvents in order to study the effect of solvent on the unfolding behavior of these nanosheets. Figure 7.14 depicts TEM images of the pristine graphene nanosheets after being redispersed and centrifuged in various solvents. The nanosheets partially precipitated in presence of acetone and ethanol, and some nanosheets remained in the supernatant. In presence of the chloroform all the nanosheets remained in the supernatant. The supernatant was used for imaging of the samples. The graphene nanosheets unfold easily in presence of ethanol and acetone. The dispersant molecule (Py-SASS) is soluble in both ethanol and acetone; minimization of surface energy requires the dissolution of the dispersant and rearrangement of the graphene nanosheets which results in the unfolding of the crumpled particles. When chloroform was used as the solvent, the crumpled pristine graphene sheets did not unfold at all and remained crumpled. In this case, both stabilizer molecules and graphene sheets have low affinity to dissolve and disperse in chloroform. Thus, the crumpled morphology provides the lowest surface energy in this system and further minimization of surface energy does not occur. This is the first demonstration that crumpled pristine graphene nanosheets can preserve their morphology and yet be redispersed in presence of a solvent. We conclude that it is possible to preserve the crumpled morphology of pristine graphene nanosheets by controlling the relative surface energy of the solvent, stabilizer and nanosheets. This concept brings up the possibility of further processing of crumpled pristine graphene in liquid phase and use in films, composites, and electronics.

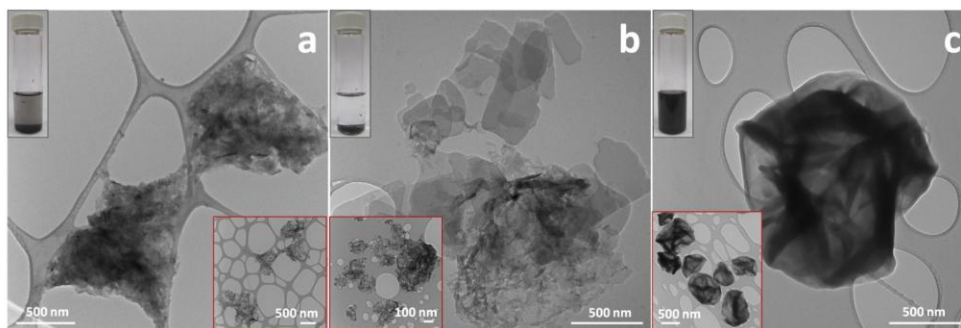


Figure 7.14. We attempted to redisperse crumpled pristine graphene in (a) ethanol, (b) acetone, and (c) chloroform. Aggregation was observed for ethanol and acetone but redispersion (but not unfolding) occurred in chloroform.

7.4 Conclusions

Pristine graphene nanosheets can be processed to 3D crumpled powders using a spray drying technique. This drying technique is rapid and scalable, allowing nanosheets to be altered to a 3D morphology at a faster rate than they can be exfoliated and dispersed. Monitoring the deformation of nanosheets at consecutive stages within the spray dryer provides the first experimental insight of the gradual dimensional transition of pristine graphene nanosheets. Our observations verify the theoretical predictions that the crumpling mechanism depends on the elasticity and surface chemistry of the nanosheets; while the pristine graphene nanosheets crumple to form dimpled particles, crumpled GO nanosheets feature a highly wrinkled morphology. The final particle size and morphology can be easily tuned by changing the dimensionless ratio of evaporation rate to diffusion rate, mediated by controllable spray drying parameters such as temperature, pressure, and concentration of the original dispersion. Furthermore, we investigated the reversibility of the crumpling by capturing the immediate morphology

changes of the nanosheets. We demonstrated that crumpling of pristine graphene nanosheets is reversed upon rehydration. Surprisingly, this unfolding mechanism is solvent-dependent; by choosing the appropriate solvent (chloroform vs. water) stable dispersions of either the crumpled or unfolded nanosheets may be obtained. On the other hand, GO nanosheets remain crumpled even after annealing and rehydration. These findings may allow for tailored folding and unfolding of nanosheets. Since the GO crumpled particles preserve their morphology upon rehydration, in Chapter VIII we use them to prepare 3D graphene macrostructure with high surface area and electrical conductivity.

CHAPTER VIII

MORPHOLOGY AND CROSSLINK CONTROL IN GRAPHENE

THREE-DIMENSIONAL NETWORKS

8.1 Introduction

Preparation of graphene 3D networks allows for individual nanosheets properties to be utilized in bulk macroscopic materials while retaining high specific surface area.⁴⁹⁹ These 3D networks may be prepared by crosslinking of the 2D nanosheets. These structures are prized for a range of interesting properties, including high specific surface area, electrical conductivity, and potential for binder-free electrochemical energy storage with mechanical integrity.^{500,501}

In previous chapters, we focused on graphene nanosheets stabilization, surface modification, and processing in order to improve their applicability in various applications. However, for the scalable processing of nanosheets into 3D structures, a host of additional issues become critical. For instance, the bulk electrical and mechanical responses are dictated largely by the nature of the nanosheet crosslinks rather than the individual nanosheet properties.⁵⁰² Similarly, the bulk electrochemical or catalytic properties of these materials are limited by issues such as pore size and available surface area,⁵⁰³ which stem not only from precursor nanosheet dimensions but also from the processing technique.

As discussed in Chapter III, various techniques have been employed to create graphene-based gels and foams. Pristine graphene 3D networks have been prepared by template-directed assembly of the nanosheets.^{295,299,300} Alternatively, simple freeze-casting of GO (or RGO) dispersions may form crosslinked porous structures that mimic the ice crystals morphology.³¹⁹ In these cases, the pore distribution and surface area are determined chiefly by the morphology of the template itself.⁵⁰⁴ Moreover, the removal of the template may be costly and difficult, involving etching solutions or high temperature.^{310,312}

On the other hand, the versatile surface chemistry of GO enables its assembly into 3D networks with a range of porous structures.⁵⁰⁵ This is frequently accomplished through simultaneous partial reduction of GO and crosslinking in aqueous solution to produce a monolithic, robust hydrogel.^{233,234,304} As mentioned in Chapter III, two main methods are commonly used to accomplish the gelation step. The first is the hydrothermal reduction of GO nanosheets.^{233,302,303} Overlapping of the reduced sections of the GO nanosheets and their consequent π - π stacking triggers the physical crosslinking of the nanosheets.^{233,304,305} Another approach to the GO network formation is the creation of chemical crosslinks in addition to π - π stacking through the use of additional reactive components.^{298,304,308,311-313}

In contrast to these approaches, a one step sol-gel technique can be used to synthesize GO gel with direct covalent bonds between the nanosheets. This process avoids the usage of non-conductive additives. In this process, a catalyst (typically ammonia) is added to a GO dispersion and held at high temperatures (90 °C).^{234,506} The

high temperature facilitates the formation of inter-sheet covalent bonds through both catalytic reactions of the functional groups and also induces partial chemical reduction on the GO surface.^{507,508} This suggests that both physical (π - π stacking) and chemical (covalent) bonding between GO nanosheets are occurring. Either freeze-drying or critical point drying (CPD) is then used to convert the hydrogel into a porous, interconnected aerogel structure.^{506,509} CPD is useful for removing water without a first order phase transition; this allows the gel to avoid capillary-induced densification or loss of mechanical integrity during drying. This is typically done after a solvent exchange to CO₂.²³² Further thermal reduction can remove many of the remaining functional groups to yield a conductive RGO 3D network.³¹⁶

Little is known about graphene-graphene crosslinks created during the sol-gel process and how they connect to the precursor graphene structure or catalyst content. Our goal in this chapter is to establish synthesis-structure-properties relationships for graphene gelation reactions. The structure of the gel is assessed by the degree of crosslinking, the pore size distribution, and the arrangement of the nanosheets within the network. The experimental parameters that affect the structure are the concentration of GO and the ratio of GO to catalyst (ammonia). We aim to probe the effects of these parameters in detail. We focus on the sol-gel method because other gelation methods are less versatile and tend to yield materials that are either brittle or dense.⁵¹⁰⁻⁵¹²

Another factor that has not been examined is the possibility of using crumpled graphene oxide (CGO).⁴⁶⁸ The use of spherical graphene structures such as CGO rather than native GO would allow for an additional handle in the creation of GO-based gels

with tunable density and compressibility. In previous chapter, we demonstrated that crumpled graphene oxide (CGO) particles can be easily created using spray drying.⁵¹³ Interestingly, redispersion of the aggregation-resistant CGO particles into water preserved the spherical, crumple morphology. Thus, these particles can be process via sol-gel technique in an aqueous environment. Here, we study the gelation of CGO and the properties of the produced 3D network of CGO. We create gels with varying ratios of CGO/GO content in the precursors to assess the porous morphology of the final products, as well as their electrical conductivity and surface area.

8.2 Experimental procedures

8.2.1 Materials and methods

Materials: Single layer graphene oxide (GO) was purchased from Cheap Tubes Inc. Ammonia (anhydrous, >99.99%) was purchased from Sigma-Aldrich. All the chemicals were used as received.

Preparation of crumpled GO (CGO): In order to prepare CGO dispersions, GO powder was added to the DI water with at 1 mg/ml concentration and tip sonicated for 5-10 minutes. The dispersions were diluted to yield 0.1 mg/ml concentration. The GO dispersions were then processed in a spray dryer (Buchi 290 mini spray dryer) to yield crumpled nanosheets according to procedure reported in Chapter VII. Two different batches of CGO particles were prepared by spraying at 120 and 150 °C. In all experiments, 10% of the dispersion flow rate, 40 psi of nozzle air pressure, and 100% of the aspirator rate were used for spraying the dispersions.

Preparation of GO, CGO and CGO/GO hydrogels: To prepare 100% GO hydrogels, GO nanosheets were dispersed in DI water (with concentrations of 10 and 20 mg/ml) by 2 hrs of bath sonication. Various amount of ammonia (1.8 and 3.6 ml) were added to the dispersions, the mixtures were sealed in glass vials, and placed in an oven at 90 °C. The reaction was carried out for 72 hrs for the hydrogels to form.

To prepare 100% CGO hydrogels, CGO particles were added to DI water with 10 mg/ml concentration and bath sonicated for 1hr to obtain homogeneous CGO dispersions. 3.6 ml of ammonia was added to the dispersions; the mixtures were sealed in glass vials, and placed in an oven at 90 °C. The reaction was carried out for 72 hrs for the hydrogels to form.

To prepare CGO/GO hydrogels, 10 mg/ml of GO and 10 mg/ml of were dispersed in DI water separately using similar procedure of GO and CGO dispersions. The two dispersions were then mixed to yield solutions with 25, 50 and 75% of CGO total solid mass. The gelatin process was similar to that used for 100% CGO gels.

Critical point drying (CPD) of hydrogels: Before drying, the hydrogels were solvent-exchanged in ethanol bath for 3 days to remove the excess DI water and residual ammonia. The CPD of the hydrogels was carried out in a Samdri-PVT-3D critical point dryer after solvent exchange with the liquid CO₂ in the dryer chamber.

8.2.2 Characterization

SEM (Scanning Electron Microscopy): graphene/copolymer nanocomposites were cut to pieces and mounted on a double face carbon tape. An accelerating voltage of

2 kV was used to image the top surface and cross-section of the samples with a JEOL JSM-7500F instrument.

TGA (Thermogravimetric Analysis): TGA was performed in a TA Instruments Q50 TGA to determine the mass loss of the aerogels. 20-30 mg of each sample was heated up from room temperature to 1000 °C at a rate of 1 °C /min in a nitrogen atmosphere.

Conductivity measurements: The electrical resistance of the dried aerogels was measured using the four-point probe method. The four-point probe head (Signatone, SP4-40045TBY) was mounted on a resistivity measurement stand (Signatone, Model 302). The spacing between the probe tips was 1.5875 mm. The current was passed to the sample through the outer probes using a Keithley 6221 AC and DC current source. A Keithley 2000 multimeter was used to measure the voltage across the sample. The sheet resistance and electrical conductivity of the samples were calculated using the measured values of the voltage.

BET surface area measurements: the surface area of the dried aerogels was calculated through BET method from the nitrogen adsorption/desorption isotherms. All the samples were degassed for 24 hrs to remove the moisture from their surface. The adsorption of nitrogen was performed at a relative pressure range of 0.05-0.3.

8.3 Results and discussion

8.3.1 GO-catalyst interactions and bridging structures

The GO hydrogels were synthesized by sol-gel technique using ammonia as the catalyst. The hydrogels were subsequently dried using CPD technique to preserve their porous structure (Figure 8.1). It has been suggested that both covalent crosslinking and π - π stacking of the GO sheets are responsible for the gel formation in this synthesis route.³¹⁴ However, the interplay between the two crosslinking mechanisms is not well-understood, with very little direct observation of covalent bonding in the prior literature. We suggest that the synthesis parameters affect the extent of the two mechanisms; to evaluate these effects we varied the GO concentration and catalyst/GO ratio during the synthesis and observed the morphological changes in the porous structure of aerogels.

To understand the effect of GO concentration, we prepared samples with 1 and 2 wt% GO sheets, while keeping the amount of ammonia constant at 3.6 ml. The SEM images of these samples (Figure 8.2a and b) suggest that lower GO concentration result in a more densely packed structure, where the sheet-like morphology is not prominent anymore. On the other hand, the higher concentration of GO yields a less compact structure of highly wrinkled GO sheets. Additionally, more “bridging” structures were observed at lower nanosheets concentration. These “bridges” are ubiquitous in our preliminary images, but there has been little discussion on this front in the prior literature.^{234,304,305,514}

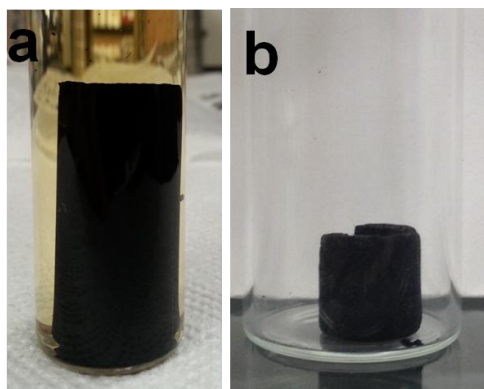


Figure 8.1. Images of (a) as-synthesized GO hydrogel, and (b) GO aerogel dried using CPD.

Furthermore, the catalyst/GO ratio was altered by decreasing the amount of ammonia from 3.6 ml to 1.8 at constant 1 wt% GO content. The SEM images demonstrate that a higher catalyst/GO ratio displays extensive bridging structures (Figure 8.2c), whereas lower catalyst/GO ratio shows relatively little inter-sheet bridging (Figure 8.2d). It is possible that the presence of more catalyst molecules facilitates the reaction of GO functional groups and forms more inter-sheet covalent bonds. Thus, more bridging structures can be observed at higher catalyst/GO ratio. It is unknown whether the increase in these bridging structures would actually contribute to load-bearing crosslinks.

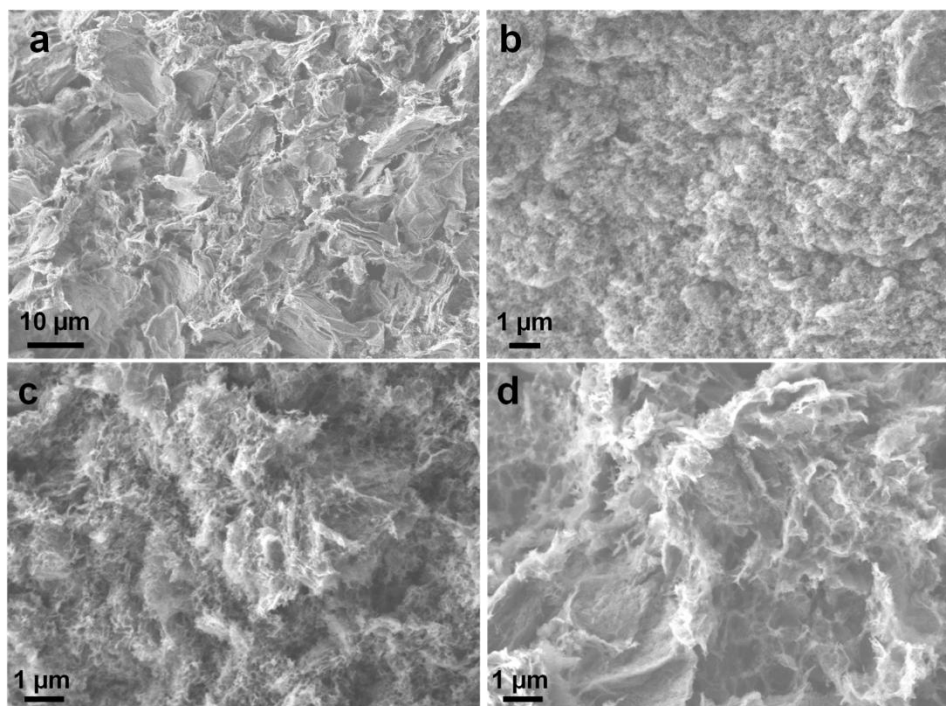


Figure 8.2. SEM images of GO aerogels prepared with (a and b) 2 and 1 wt % of GO content, respectively, (3.6 ml of ammonia was used), and (c and d) 1 wt% GO content using 3.6 and 1.8 ml of ammonia, respectively.

Based on these observations, we hypothesize that the gelation of GO sheets occurs through two main routes (Figure 8.3). One involves the localized partial reduction of graphene oxide to reduced graphene oxide (RGO) during gelation, resulting in localized attractive π - π interactions between those reduced portions of the nanosheets (depicted in gray).⁵¹⁵ The second is the catalyst-assisted formation of covalent bonds, including large “bridging” structures between nanosheets (depicted in red). With addition of the catalyst/GO ratio, the density of catalyst-assisted covalent bonds in the aerogels increases. It is feasible that these bridges are low-density carbonaceous structures that initially form locally at the nanosheet surface; these structures may be the

product of the much-debated “oxidative debris” associated with the synthesis of the parent GO nanosheets.^{78,516,517} (Oxidative debris is a by-product of common synthesis GO methods, and it has been argued that oxidative debris acts in a surfactant-like manner to allow for GO dispersion in water.⁷⁸)

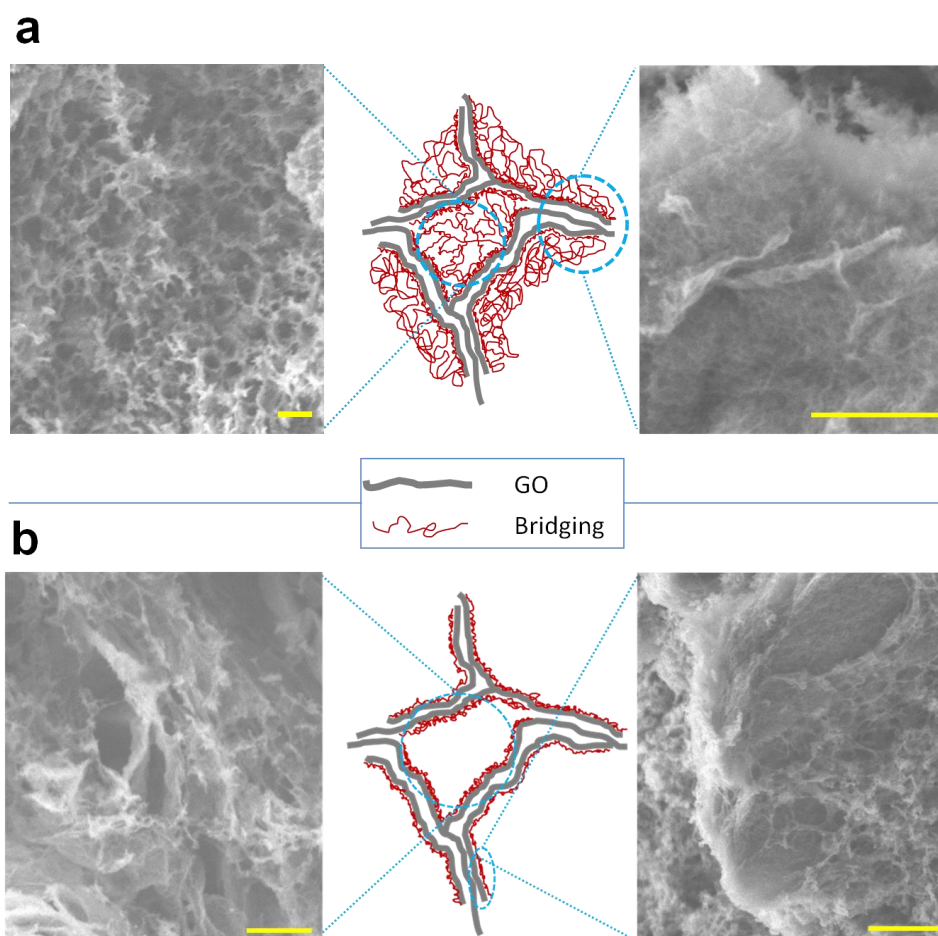


Figure 8.3. Proposed mechanism for gel crosslinking and bridge formation. (a) high catalyst/GO ratio (0.024), (b) low catalyst/GO ratio (0.012), (scalebars ~ 1 μm in SEM images).

8.3.2 GO morphology effects

Prior studies have indicated that the nanosheet size does affect the structure, with larger nanosheets interacting at lower concentrations.^{518,519} We explored the gelation process at an extreme aspect ratio of 1 in spherical, crumpled graphene. Initially, the CGO particles sprayed at 150 °C were used to synthesize the CGO hydrogels. These particles formed a very brittle hydrogel. The crumpled morphology of the particles and the low density of the bridging structures can be observed in the SEM images of its corresponding aerogel (Figure 8.4a and b). The crumpled particles are prone to π - π stacking due to their highly wrinkled surface, thus, the physical crosslinking through the π - π stacking is not the primary mechanism of gelation using these particles. On the other hand the chemical crosslinking requires sufficient functional groups on the sheets surface to participate in the covalent bond formation. The spray drying of the GO sheets at 150 °C may partially remove the functional groups; hence, the chemical crosslinking is also hindered in this sample. In order to promote the covalent bond formation between the CGO particles, we reduced the spraying temperature to 120 °C. These CGO particles formed a well-integrated hydrogel with high density of the bridging structures (Figure 8.4c and d). Observation of more bridging structure confirms that they indeed represent the chemical crosslinks. Additionally, the CGO aerogels demonstrate a more homogenous porosity and higher packing density compared to the GO aerogels. This may be because CGO particles tend to interact at shorter distances such that higher (denser) packing is required for the same particle-particle interactions and bond formation during gelation.

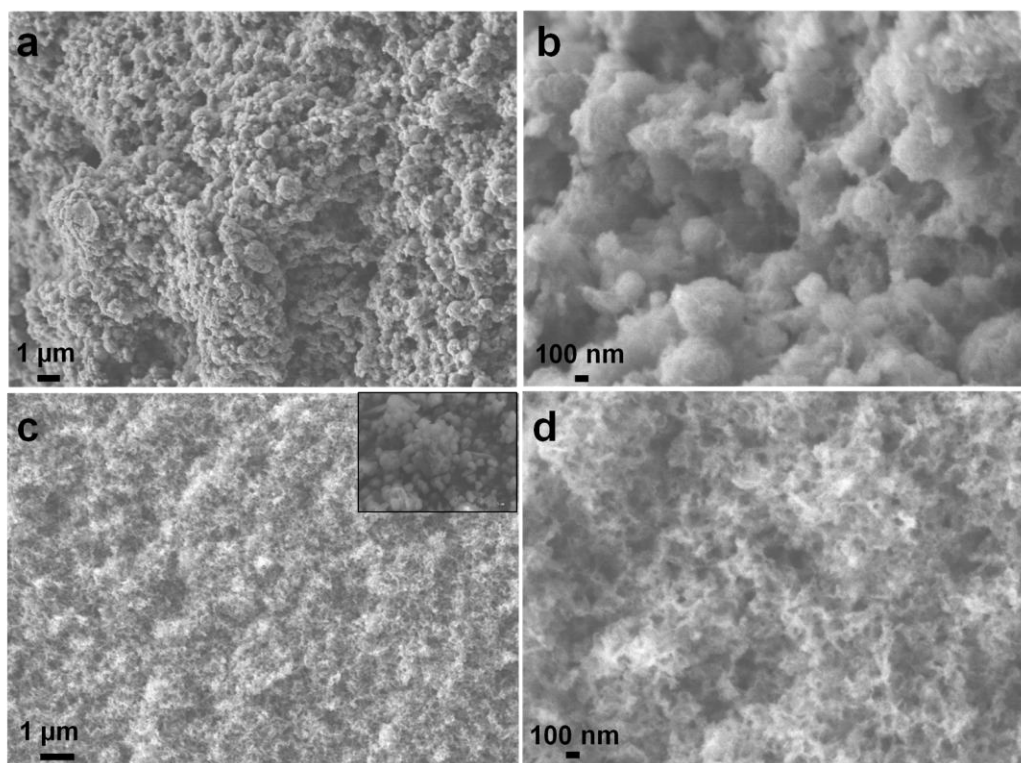


Figure 8.4. SEM images of CGO aerogels prepared using (a and b) CGO particles sprayed at 150 °C, and (c and d) CGO particles sprayed at 120 °C (the inset shows the CGO particles morphology sprayed at 120 °C).

To better understand the precursor morphology effect, we also synthesized hydrogels with varying ratios of CGO/GO. At lower CGO/GO ratios, the porous structure roughly resembles that of GO aerogels. As the CGO/GO ratio increases, the structure becomes more like CGO aerogels. The gradual alteration of the aerogels morphology is indicated in Figure 8.5. This trend of morphological changes with the CGO/GO ratio confirms that the precursor morphology affects the crosslinking mechanism and density.

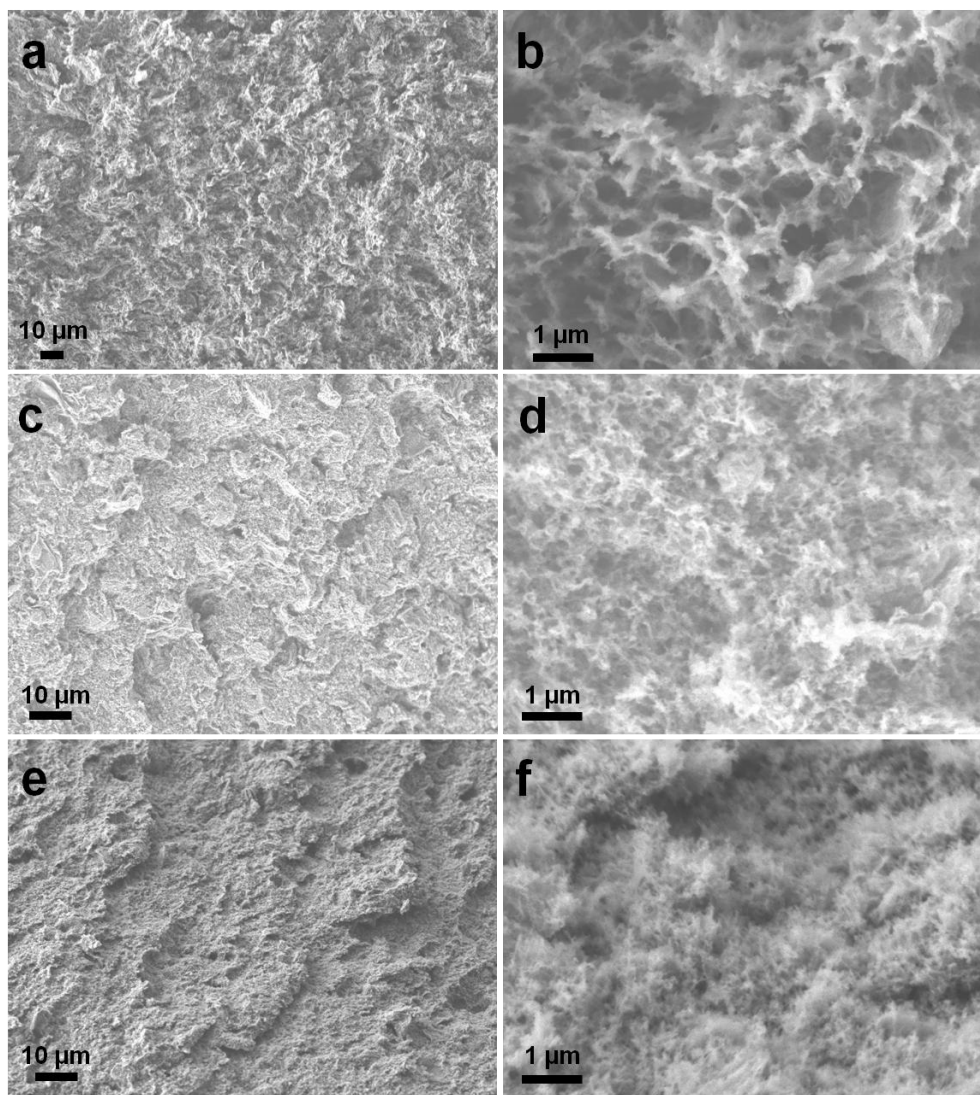


Figure 8.5. SEM images of aerogels prepared using CGO/GO ratios of (a and b) 0.3 (c and d) 1, and (e and f) 3. All the CGO particles were sprayed at 120 °C.

The electrical conductivities of GO, CGO and CGO/GO aerogels are indicated in Table 8.1. All the aerogels are electrically conductive and their conductivity values are in the same order of magnitude (~ 0.1 S/m). Interestingly, the electrical conductivity in

these GO-based aerogels is achieved without further chemical or thermal reduction that normally is needed to restore the π - network of the graphene. This observation confirms the partial reduction of GO and CGO sheets during the gelation process. Moreover, assuming that electrical conduction happens through the interconnected network of reduced sections of the GO sheets, we may infer that the extent of π - π stacking (i.e., physical crosslinking) is the same in all the equally conductive aerogels.

	100% GO 2 wt%	100% GO 1 wt%	75% GO 1 wt%	50% GO 1 wt%	25% GO 1 wt%	100% CGO 1 wt%
Conductivity (S/m)	0.46	0.06	0.08	0.2	0.13	0.16
BET Surface area (m ² /g)	970	1648	1175	1291	998	1566

Table 8.1. The electrical conductivities and BET surface areas of the aerogels. All these gels were prepared using 3.6 ml of ammonia as the catalyst. All the CGO particles were sprayed at 120 °C.

The BET surface areas of the aerogels are also represented in Table 8.1. Both GO and CGO aerogels prepared with 1wt% of total nanosheets content displayed higher surface areas than the combination CGO/GO aerogels. This might be attributed to the anomalous morphology of GO and CGO nanosheets which leads to their non-uniform arrangement within the 3D network and reduction of accessible surface area. Moreover, both 1 wt% GO and CGO aerogels have higher surface area than the 2 wt% GO aerogel. It implies that the presence of more bridging structures in aerogels prepared with higher catalyst/GO ratio increases the available surface area of the samples.

The thermogravimetric analysis of the GO and CGO aerogels demonstrates a rapid mass loss in all the samples up to 1000 °C (Figure 8.6). However, higher mass loss was observed in 1 wt% GO and CGO gels compared to the 2 wt% GO gel. The extra mass loss of 1 wt% GO and CGO aerogels may be attributed to the reduction of bridging structures which are the major constituents of these samples.

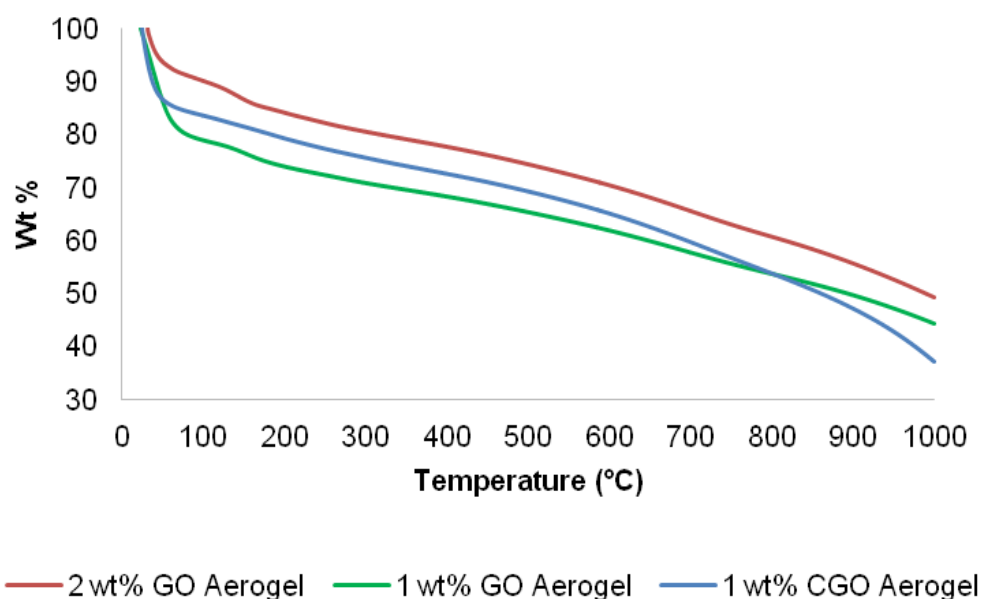


Figure 8.6. Thermogravimetric characterization of GO and CGO aerogels.

8.4 Conclusion

Gelation of GO nanosheets is a simple method to prepare graphene 3D networks. The sol-gel technique facilitates the chemical and physical crosslinking of the GO nanosheets in presence of the catalyst molecules. The final morphology and properties of

the 3D network depends on the type and density of the crosslinks. We varied various parameters such as GO concentration, catalyst/GO ratio and the nanosheets morphology to gain a better understanding of the gelation and crosslinking mechanism in GO hydrogels. Bridging structures were observed in samples prepared with higher catalyst/GO ratio. These structures may be the product of inter-sheet covalent bonding and thus, represents the chemical crosslinks in the GO aerogel. It is possible to alter the nanosheets morphology to crumpled particle and prepared CGO aerogel. These aerogels display extensive bridging between the nanosheets; it may be implied that the gelation of CGO particles occur mainly through chemical crosslinking since these particles are prone to π - π stacking. All the aerogels were electrically conductive without needing further reduction. Moreover, exceptionally high surface area was observed in aerogels with more bridging crosslinks. Further spectroscopic characterizations are required to reveal the chemical composition of the bridging structure. We also expect a drastic increase in the electrical conductivity of the aerogels after additional thermal annealing.

CHAPTER IX

CONCLUSION AND FUTURE WORK

9.1 Summary of thesis

In this thesis, the dispersant-assisted exfoliation of pristine graphene in the liquid phase is studied. Also, graphene-philic copolymers are synthesized and used as dispersants to enhance the graphene-polymer compatibility in the nanocomposites. Additionally, the crumpling of graphene sheets is explored as a strategy for production of aggregation-resistant graphene powder. The crumpled graphene sheets are used to prepare highly porous and conductive graphene 3D networks. The experimental results discussed in Chapters IV-VIII can be summarized as follows.

9.1.1 Direct liquid-phase exfoliation of pristine graphene by pyrene derivatives

We demonstrated that pyrene derivatives are promising dispersants for graphene in aqueous dispersions. Single- to few-layer graphene sheets were stabilized by these molecules, yielding exceptionally higher graphene/dispersant ratio compared to polymers and surfactants. The effectiveness of pyrene derivatives is determined by the type, number and electronegativity of functional groups and counterion. It also depends on the distance between functional group and pyrene basal plane, and the pH of the dispersion. The stability of dispersions against centrifugation lyophilization was confirmed. The dispersions were also stable over a broad range of pH and temperature.

These dispersions show promise for applications such as nanocomposites, organic solar cells, conductive films, and inkjet-printed electronic devices.

9.1.2 Pyrene-based designer dispersant for graphene/polysiloxane composites

A designer polysiloxane-based dispersant for graphene was synthesized and applied to prepare a highly conductive polymer film. This stabilizer was simultaneously used as the polymer matrix. To synthesize the stabilizer, 1-ethynylpyrene was grafted to the backbone of a poly(dimethylsiloxane)-*co*-(methylhydrosiloxane) random copolymer by Pt-catalyzed hydrosilylation reaction with a SiH: ethynyl ratio of 1.0:1.3. Dispersion of graphene in chloroform was prepared through the π - π interactions between the graphene sheets and the pyrene groups of the resulting copolymer. A graphene/polymer film was cast from this dispersion. SEM and TEM images confirmed the homogeneous distribution of the graphene sheets in the film. The conductivity of this film with 4 wt% loading of graphene was measured to be 220 S/m. This is the first case of a melt-processable, conductive graphene/polymer film reported in the literature. Later the ratio of SiH:ethynyl was changed to 1.7:1.0, which led to self-crosslinking of the polymer at 110 °C and resulted in a direct production of a conductive graphene/silicone elastomeric composite. The crosslinking reaction was observed by FT-IR spectroscopy and the network formation was confirmed by swelling and extraction of the product.

9.1.3 Pyrene-functional PMMA & PS copolymers for Janus graphene films

Similar strategy was applied to tailor the PS and PMMA polymer into a graphene-philic copolymer. Pyrene-functional copolymers were synthesized by radical polymerization in presence of 1-pyrenemethyl methacrylate. Graphene dispersions in chloroform were obtained using these copolymers. The Janus graphene-based composite films were prepared via vacuum filtration of the dispersions. These Janus films have an electrically-conductive side with conductivities as high as ~ 140 S/m, and another polymer-rich electrically-insulating side. The SEM images of the films cross-section confirms that the leaching of unbound polymer chains into the porous filtration membrane forms a graphene-rich section at the bottom of the film. The higher concentration of graphene at this section of the film is responsible for its high electrical conductivity.

9.1.4 Crumpling and unfolding of pristine graphene and graphene oxide sheets

A scalable spray drying technique was used to crumple pristine graphene sheets for the first time. Aqueous graphene and graphene oxide dispersions were atomized and dried in a spray dryer. During this process, 2D graphene sheets crumpled and transformed into 3D particles. Transition of the sheets morphology during the drying process was investigated by collecting samples at various heights of the spray dryer. Pristine graphene sheets deformed as the droplet shrinkage induced capillary forces at the interface and transformed into multi-faced crumpled particles with several dimples. Graphene oxide sheets were spray dried using the same procedure; however, their highly

wrinkled final morphology was different than the crumpled pristine graphene sheets. Differences in the elasticity and surface chemistry of pristine graphene and GO sheets are the main reason for the difference in the final morphology. Spray drying parameters such as atomizer pressure, drying temperature and concentration of sheets in the dispersions were varied in order to observe their effect on the final morphology of crumpled particles. Crumpled particles were redispersed into various solvents to assess their unfolding behavior. GO particles remained crumpled in the water; however, pristine graphene sheets immediately unfolded in the water due to the high affinity of pyrene derivatives for water. However, the pristine graphene particles preserved their crumpled morphology upon redispersion in chloroform. Thus, it was concluded that unfolding of the pristine graphene sheets depends on the solvent choice.

9.1.5 Graphene conductive 3D networks with high surface area

Graphene oxide hydrogels were synthesized using a simple one step sol-gel technique. Using this method, the gelation of graphene oxide nanosheets occurred in an aqueous dispersion in presence of ammonia molecules as catalyst at 90 °C. The hydrogels were then dried in a critical point dryer to yield highly porous aerogels. The structures of these aerogels were observed using SEM microscopy to evaluate the physical and chemical crosslinking of the nanosheets. Stacking of the nanosheets and the inter-sheets bridging were the dominant features of the aerogels structure. The stacking of nanosheets was attributed to the overlapping and subsequent π - π stacking of the reduced sections of the nanosheets. On the other hand, the bridging structures were

attributed to the covalent bond formation between the functional groups of the nanosheets. We varied several parameters including nanosheets concentration, catalyst/GO ratio and the nanosheets morphology to understand how they affect the crosslinking mechanism. We observed that the higher catalyst/GO ratio intensifies the covalent bond formation and increases the density of bridging structures in the final aerogel. Crumpled graphene oxide particles were used in preparation of hydrogel to assess the effect of nanosheets morphology on the aerogel crosslinks and properties. These CGO hydrogels displayed extensive inter-sheet bridging which is due to their aggregation- (and π - π stacking-) resistant morphology. All the aerogels were electrically conductive (~ 0.1 S/m) without needing further reduction. This confirmed that partial reduction of nanosheets occurs during the gelation. Samples with higher inter-sheet bridging (including CGO aerogels) demonstrated an exceptionally high surface area (1500-1600 m²/g).

9.2 Conclusions

The purpose of our research is to increase the graphene yield of liquid-phase exfoliation method, as well as improving the pristine graphene compatibility and dispersion within the polymer nanocomposites. Additionally, by crumpling and assembling the graphene sheets into macrostructures, we attempt to harness the graphene properties in bulk graphene-based materials. From the results of our experiments we can conclude that:

- (1) The proper choice of dispersant molecules can considerably improve the graphene yield of direct liquid-phase exfoliation method. Moreover, the presence of dispersant guarantees the redispersibility of pristine graphene freeze-dried powder in the original solvent. However, the graphene yield of this method remains restricted by other factors such as low efficiency of the sonication technique and the need for separation of graphene from graphitic materials in the final dispersions.
- (2) It is important to come up with simple synthetic methods for preparation of polymeric dispersants that are graphene-philic and can be directly used as host matrix. This allows for better interactions at graphene-polymer interface and achieving high electrical properties. The control over the molecular structure of such dispersants (i.e., location and density of pyrene groups in the polymer chain) can assist to exfoliate and stabilize more graphene sheets.
- (3) Crumpling of graphene oxide is proved to be effective for production of aggregation-resistant particles that can be processed later in the liquid phase; but the crumpling of the pristine graphene is limited by the unfolding of these sheets upon rewetting. Thus, it is easier to use crumpled graphene oxide particle for preparation of high surface area materials. The gelation and crosslinking of the crumpled graphene oxide particles is a facile method to prepare pure graphene-based structures with superior electrical conductivity and high surface area.

9.3 Future research directions

In Chapter IV we discussed that graphene yield can be increased through stabilization of more nanosheets in the dispersion. However, the graphene yield is constrained with the total volume of the dispersion that can be prepared by sonication technique. It is possible to improve the graphene yield and scalability of liquid-phase exfoliation method by substituting the sonication technique with shear mixing. Shear-mixing in presence of proper solvent and dispersant can produce large volumes of graphene dispersion. Moreover, exfoliation of nanosheets from parent materials invariably results in a mixture of exfoliated and unexfoliated material that need to be separated to yield stable dispersions. Common lab-scale techniques for separation typically involve centrifugation and are not scalable. It is feasible to design a separation unit that can handle large volumes of the exfoliated and unexfoliated sheets mixture through multiple cycles of settling and washing of sediment.

The graphene/polysiloxane composites can be used in preparation of piezoresistive coatings and microchips for biomedical devices. The graphene/PMMA and PS composites may have potential application in conductive coatings. The ability to customize the molecular structure of the synthesized copolymer allows for a better control over the polymer-graphene interface. Alternative synthetic route may be explored to prepare these customized polymeric graphene dispersant.

There are plenty of questions about crumpled graphene that have to be answered. Currently, we are trying to obtain a deeper understanding of these particles at the molecular level. The atomic and electronic structures of graphene in the crumpled state

are not well known and need to be studied. The mechanical properties of these particles at the molecular level have to be investigated. Also, it is important to correlate the molecular level changes with the bulk properties in the crumpled state.

The conductive 3D networks of graphene that we prepared using GO and CGO may be used directly in Li-ion battery electrodes. The highly porous structure of these materials provides a more accessible path for ion diffusion. The high surface area of these structures facilitates the adsorption of these ions on the graphene sheets. Tailoring of the structure for higher mechanical stability is possible through variation of crosslinks density.

Finally, it is worth to mention that all the production and processing techniques that we used for graphene can be (and in some cases have been) extended to many other 2D nanosheets including boron nitride, molybdenum sulfide, tungsten sulfide, and many other transition metal dichalcogenide nanosheets.

REFERENCES

- (1) Novoselov, K. S.; Geim, A. K.; Morozov, S. V.; Jiang, D.; Zhang, Y.; Dubonos, S. V.; Grigorieva, I. V.; Firsov, A. A. Electric field effect in atomically thin carbon films. *Science* **2004**, *306*, 666-669.
- (2) Geim, A. K.; Novoselov, K. S. The rise of graphene. *Nature Materials* **2007**, *6*, 183-191.
- (3) Venables, J. A.; Spiller, G. D. T.; Hanbucken, M. NUCLEATION AND GROWTH OF THIN-FILMS. *Reports on Progress in Physics* **1984**, *47*, 399-459.
- (4) Evans, J. W.; Thiel, P. A.; Bartelt, M. C. Morphological evolution during epitaxial thin film growth: Formation of 2D islands and 3D mounds. *Surface Science Reports* **2006**, *61*, 1-128.
- (5) Krishnan, A.; Dujardin, E.; Treacy, M. M. J.; Hugdahl, J.; Lynam, S.; Ebbesen, T. W. Graphitic cones and the nucleation of curved carbon surfaces. *Nature* **1997**, *388*, 451-454.
- (6) Land, T. A.; Michely, T.; Behm, R. J.; Hemminger, J. C.; Comsa, G. STM INVESTIGATION OF SINGLE LAYER GRAPHITE STRUCTURES PRODUCED ON PT(111) BY HYDROCARBON DECOMPOSITION. *Surface Science* **1992**, *264*, 261-270.
- (7) Novoselov, K. S.; Geim, A. K.; Morozov, S. V.; Jiang, D.; Katsnelson, M. I.; Grigorieva, I. V.; Dubonos, S. V.; Firsov, A. A. Two-dimensional gas of massless Dirac fermions in graphene. *Nature* **2005**, *438*, 197-200.
- (8) Stankovich, S.; Dikin, D. A.; Dommett, G. H. B.; Kohlhaas, K. M.; Zimney, E. J.; Stach, E. A.; Piner, R. D.; Nguyen, S. T.; Ruoff, R. S. Graphene-based composite materials. *Nature* **2006**, *442*, 282-286.
- (9) Meyer, J. C.; Geim, A. K.; Katsnelson, M. I.; Novoselov, K. S.; Booth, T. J.; Roth, S. The structure of suspended graphene sheets. *Nature* **2007**, *446*, 60-63.
- (10) Slonczewski, J. C.; Weiss, P. R. BAND STRUCTURE OF GRAPHITE. *Physical Review* **1958**, *109*, 272-279.
- (11) Fasolino, A.; Los, J. H.; Katsnelson, M. I. Intrinsic ripples in graphene. *Nature Materials* **2007**, *6*, 858-861.
- (12) Stolyarova, E.; Rim, K. T.; Ryu, S. M.; Maultzsch, J.; Kim, P.; Brus, L. E.; Heinz, T. F.; Hybertsen, M. S.; Flynn, G. W. High-resolution scanning tunneling

microscopy imaging of mesoscopic graphene sheets on an insulating surface. *Proceedings of the National Academy of Sciences of the United States of America* **2007**, *104*, 9209-9212.

(13) Partoens, B.; Peeters, F. M. From graphene to graphite: Electronic structure around the K point. *Physical Review B* **2006**, *74*.

(14) Dato, A.; Lee, Z.; Jeon, K.-J.; Erni, R.; Radmilovic, V.; Richardson, T. J.; Frenklach, M. Clean and highly ordered graphene synthesized in the gas phase. *Chemical Communications* **2009**, 6095-6097.

(15) Zhang, Y. B.; Tan, Y. W.; Stormer, H. L.; Kim, P. Experimental observation of the quantum Hall effect and Berry's phase in graphene. *Nature* **2005**, *438*, 201-204.

(16) Du, X.; Skachko, I.; Barker, A.; Andrei, E. Y. Approaching ballistic transport in suspended graphene. *Nature Nanotechnology* **2008**, *3*, 491-495.

(17) Hwang, E. H.; Adam, S.; Das Sarma, S. Carrier transport in two-dimensional graphene layers. *Physical Review Letters* **2007**, *98*.

(18) Bolotin, K. I.; Sikes, K. J.; Jiang, Z.; Klima, M.; Fudenberg, G.; Hone, J.; Kim, P.; Stormer, H. L. Ultrahigh electron mobility in suspended graphene. *Solid State Communications* **2008**, *146*, 351-355.

(19) Morozov, S. V.; Novoselov, K. S.; Schedin, F.; Jiang, D.; Firsov, A. A.; Geim, A. K. Two-dimensional electron and hole gases at the surface of graphite. *Physical Review B* **2005**, *72*.

(20) Ryu, S.; Han, M. Y.; Maultzsch, J.; Heinz, T. F.; Kim, P.; Steigerwald, M. L.; Brus, L. E. Reversible Basal Plane Hydrogenation of Graphene. *Nano Letters* **2008**, *8*, 4597-4602.

(21) Rodriguez-Perez, L.; Angeles Herranz, M.; Martin, N. The chemistry of pristine graphene. *Chemical Communications* **2013**, *49*, 3721-3735.

(22) Meyer, J. C.; Kisielowski, C.; Erni, R.; Rossell, M. D.; Crommie, M. F.; Zettl, A. Direct Imaging of Lattice Atoms and Topological Defects in Graphene Membranes. *Nano Letters* **2008**, *8*, 3582-3586.

(23) Hashimoto, A.; Suenaga, K.; Gloter, A.; Urita, K.; Iijima, S. Direct evidence for atomic defects in graphene layers. *Nature* **2004**, *430*, 870-873.

- (24) Gao, X.; Wang, Y.; Liu, X.; Chan, T. L.; Irle, S.; Zhao, Y.; Zhang, S. B. Regioselectivity control of graphene functionalization by ripples. *Physical Chemistry Chemical Physics* **2011**, *13*, 19449-19453.
- (25) Nakada, K.; Fujita, M.; Dresselhaus, G.; Dresselhaus, M. S. Edge state in graphene ribbons: Nanometer size effect and edge shape dependence. *Physical Review B* **1996**, *54*, 17954-17961.
- (26) Subrahmanyam, K. S.; Kumar, P.; Maitra, U.; Govindaraj, A.; Hembram, K. P. S. S.; Waghmare, U. V.; Rao, C. N. R. Chemical storage of hydrogen in few-layer graphene. *Proceedings of the National Academy of Sciences of the United States of America* **2011**, *108*, 2674-2677.
- (27) Schaefer, R. A.; Englert, J. M.; Wehrfritz, P.; Bauer, W.; Hauke, F.; Seyller, T.; Hirsch, A. On the Way to Graphane Pronounced Fluorescence of Polyhydrogenated Graphene. *Angewandte Chemie-International Edition* **2013**, *52*, 754-757.
- (28) Zboril, R.; Karlicky, F.; Bourlinos, A. B.; Steriotis, T. A.; Stubos, A. K.; Georgakilas, V.; Safarova, K.; Jancik, D.; Trapalis, C.; Otyepka, M. Graphene Fluoride: A Stable Stoichiometric Graphene Derivative and its Chemical Conversion to Graphene. *Small* **2010**, *6*, 2885-2891.
- (29) Nair, R. R.; Ren, W.; Jalil, R.; Riaz, I.; Kravets, V. G.; Britnell, L.; Blake, P.; Schedin, F.; Mayorov, A. S.; Yuan, S.; Katsnelson, M. I.; Cheng, H.-M.; Strupinski, W.; Bulusheva, L. G.; Okotrub, A. V.; Grigorieva, I. V.; Grigorenko, A. N.; Novoselov, K. S.; Geim, A. K. Fluorographene: A Two-Dimensional Counterpart of Teflon. *Small* **2010**, *6*, 2877-2884.
- (30) Georgakilas, V.; Otyepka, M.; Bourlinos, A. B.; Chandra, V.; Kim, N.; Kemp, K. C.; Hobza, P.; Zboril, R.; Kim, K. S. Functionalization of Graphene: Covalent and Non-Covalent Approaches, Derivatives and Applications. *Chemical Reviews* **2012**, *112*, 6156-6214.
- (31) Sinitskii, A.; Dimiev, A.; Corley, D. A.; Fursina, A. A.; Kosynkin, D. V.; Tour, J. M. Kinetics of Diazonium Functionalization of Chemically Converted Graphene Nanoribbons. *ACS Nano* **2010**, *4*, 1949-1954.
- (32) Georgakilas, V.; Bourlinos, A. B.; Zboril, R.; Steriotis, T. A.; Dallas, P.; Stubos, A. K.; Trapalis, C. Organic functionalisation of graphenes. *Chemical Communications* **2010**, *46*, 1766-1768.
- (33) Parviz, D.; Das, S.; Ahmed, H. S. T.; Irin, F.; Bhattacharia, S.; Green, M. J. Dispersions of Non-Covalently Functionalized Graphene with Minimal Stabilizer. *ACS Nano* **2012**, *6*, 8857-8867.

- (34) Malig, J.; Stephenson, A. W. I.; Wagner, P.; Wallace, G. G.; Officer, D. L.; Guldi, D. M. Direct exfoliation of graphite with a porphyrin - creating functionalizable nanographene hybrids. *Chemical Communications* **2012**, *48*, 8745-8747.
- (35) Backes, C.; Hauke, F.; Hirsch, A. The Potential of Perylene Bisimide Derivatives for the Solubilization of Carbon Nanotubes and Graphene. *Advanced Materials* **2011**, *23*, 2588-2601.
- (36) Das, S.; Wajid, A. S.; Shelburne, J. L.; Liao, Y.-C.; Green, M. J. Localized In situ Polymerization on Graphene Surfaces for Stabilized Graphene Dispersions. *Acs Applied Materials & Interfaces* **2011**, *3*.
- (37) Green, A. A.; Hersam, M. C. Solution Phase Production of Graphene with Controlled Thickness via Density Differentiation. *Nano Letters* **2009**, *9*, 4031-4036.
- (38) Bourlinos, A. B.; Georgakilas, V.; Zboril, R.; Steriotis, T. A.; Stubos, A. K.; Trapalis, C. Aqueous-phase exfoliation of graphite in the presence of polyvinylpyrrolidone for the production of water-soluble graphenes. *Solid State Communications* **2009**, *149*, 2172-2176.
- (39) Wajid, A. S.; Das, S.; Irin, F.; Ahmed, H. S. T.; Shelburne, J. L.; Parviz, D.; Fullerton, R. J.; Jankowski, A. F.; Hedden, R. C.; Green, M. J. Polymer-stabilized graphene dispersions at high concentrations in organic solvents for composite production. *Carbon* **2012**, *50*, 526-534.
- (40) Voggu, R.; Das, B.; Rout, C. S.; Rao, C. N. R. Effects of charge transfer interaction of graphene with electron donor and acceptor molecules examined using Raman spectroscopy and cognate techniques. *Journal of Physics-Condensed Matter* **2008**, *20*.
- (41) Suenaga, K.; Koshino, M. Atom-by-atom spectroscopy at graphene edge. *Nature* **2010**, *468*, 1088-1090.
- (42) Van Lier, G.; Van Alsenoy, C.; Van Doren, V.; Geerlings, P. Ab initio study of the elastic properties of single-walled carbon nanotubes and graphene. *Chemical Physics Letters* **2000**, *326*, 181-185.
- (43) Lee, C.; Wei, X.; Kysar, J. W.; Hone, J. Measurement of the elastic properties and intrinsic strength of monolayer graphene. *Science* **2008**, *321*, 385-388.
- (44) Frank, I. W.; Tanenbaum, D. M.; Van der Zande, A. M.; McEuen, P. L. Mechanical properties of suspended graphene sheets. *Journal of Vacuum Science & Technology B* **2007**, *25*, 2558-2561.

- (45) Poot, M.; van der Zant, H. S. J. Nanomechanical properties of few-layer graphene membranes. *Applied Physics Letters* **2008**, *92*.
- (46) Yu, C. H.; Shi, L.; Yao, Z.; Li, D. Y.; Majumdar, A. Thermal conductance and thermopower of an individual single-wall carbon nanotube. *Nano Letters* **2005**, *5*, 1842-1846.
- (47) Balandin, A. A.; Ghosh, S.; Bao, W.; Calizo, I.; Teweldebrhan, D.; Miao, F.; Lau, C. N. Superior thermal conductivity of single-layer graphene. *Nano Letters* **2008**, *8*, 902-907.
- (48) Cai, W. W.; Moore, A. L.; Zhu, Y. W.; Li, X. S.; Chen, S. S.; Shi, L.; Ruoff, R. S. Thermal Transport in Suspended and Supported Monolayer Graphene Grown by Chemical Vapor Deposition. *Nano Letters* **2010**, *10*, 1645-1651.
- (49) Seol, J. H.; Jo, I.; Moore, A. L.; Lindsay, L.; Aitken, Z. H.; Pettes, M. T.; Li, X. S.; Yao, Z.; Huang, R.; Broido, D.; Mingo, N.; Ruoff, R. S.; Shi, L. Two-Dimensional Phonon Transport in Supported Graphene. *Science* **2010**, *328*, 213-216.
- (50) Nika, D. L.; Ghosh, S.; Pokatilov, E. P.; Balandin, A. A. Lattice thermal conductivity of graphene flakes: Comparison with bulk graphite. *Applied Physics Letters* **2009**, *94*.
- (51) Koh, Y. K.; Bae, M.-H.; Cahill, D. G.; Pop, E. Heat Conduction across Monolayer and Few-Layer Graphenes. *Nano Letters* **2010**, *10*, 4363-4368.
- (52) Nair, R. R.; Blake, P.; Grigorenko, A. N.; Novoselov, K. S.; Booth, T. J.; Stauber, T.; Peres, N. M. R.; Geim, A. K. Fine structure constant defines visual transparency of graphene. *Science* **2008**, *320*, 1308-1308.
- (53) Singh, V.; Joung, D.; Zhai, L.; Das, S.; Khondaker, S. I.; Seal, S. Graphene based materials: Past, present and future. *Progress in Materials Science* **2011**, *56*, 1178-1271.
- (54) Kravets, V. G.; Grigorenko, A. N.; Nair, R. R.; Blake, P.; Anissimova, S.; Novoselov, K. S.; Geim, A. K. Spectroscopic ellipsometry of graphene and an exciton-shifted van Hove peak in absorption. *Physical Review B* **2010**, *81*, 155413.
- (55) Rana, F.; George, P. A.; Strait, J. H.; Dawlaty, J.; Shivaraman, S.; Chandrashekhara, M.; Spencer, M. G. Carrier recombination and generation rates for intravalley and intervalley phonon scattering in graphene. *Physical Review B* **2009**, *79*, 115447.

- (56) Peigney, A.; Laurent, C.; Flahaut, E.; Bacsa, R. R.; Rousset, A. Specific surface area of carbon nanotubes and bundles of carbon nanotubes. *Carbon* **2001**, *39*, 507-514.
- (57) Bonaccorso, F.; Colombo, L.; Yu, G.; Stoller, M.; Tozzini, V.; Ferrari, A. C.; Ruoff, R. S.; Pellegrini, V. Graphene, related two-dimensional crystals, and hybrid systems for energy conversion and storage. *Science* **2015**, *347*.
- (58) Park, S.; Ruoff, R. S. Chemical methods for the production of graphenes. *Nature Nanotechnology* **2009**, *4*, 217-224.
- (59) Yoo, B. M.; Shin, H. J.; Yoon, H. W.; Park, H. B. Graphene and Graphene Oxide and Their Uses in Barrier Polymers. *Journal of Applied Polymer Science* **2014**, *131*.
- (60) Han, W.; Kawakami, R. K.; Gmitra, M.; Fabian, J. Graphene spintronics. *Nature Nanotechnology* **2014**, *9*, 794-807.
- (61) Schniepp, H. C.; Li, J.-L.; McAllister, M. J.; Sai, H.; Herrera-Alonso, M.; Adamson, D. H.; Prud'homme, R. K.; Car, R.; Saville, D. A.; Aksay, I. A. Functionalized Single Graphene Sheets Derived from Splitting Graphite Oxide. *The Journal of Physical Chemistry B* **2006**, *110*, 8535-8539.
- (62) Gilje, S.; Han, S.; Wang, M.; Wang, K. L.; Kaner, R. B. A Chemical Route to Graphene for Device Applications. *Nano Letters* **2007**, *7*, 3394-3398.
- (63) Ruoff, R. Graphene: Calling all chemists. *Nat Nano* **2008**, *3*, 10-11.
- (64) Dreyer, D. R.; Park, S.; Bielawski, C. W.; Ruoff, R. S. The chemistry of graphene oxide. *Chemical Society Reviews* **2010**, *39*, 228-240.
- (65) Hummers, W. S.; Offeman, R. E. PREPARATION OF GRAPHITIC OXIDE. *Journal of the American Chemical Society* **1958**, *80*, 1339-1339.
- (66) Stankovich, S.; Dikin, D. A.; Piner, R. D.; Kohlhaas, K. A.; Kleinhammes, A.; Jia, Y.; Wu, Y.; Nguyen, S. T.; Ruoff, R. S. Synthesis of graphene-based nanosheets via chemical reduction of exfoliated graphite oxide. *Carbon* **2007**, *45*, 1558-1565.
- (67) Paredes, J. I.; Villar-Rodil, S.; Martinez-Alonso, A.; Tascon, J. M. D. Graphene oxide dispersions in organic solvents. *Langmuir* **2008**, *24*, 10560-10564.
- (68) He, H. Y.; Klinowski, J.; Forster, M.; Lerf, A. A new structural model for graphite oxide. *Chemical Physics Letters* **1998**, *287*, 53-56.

- (69) Buchsteiner, A.; Lerf, A.; Pieper, J. Water dynamics in graphite oxide investigated with neutron scattering. *Journal of Physical Chemistry B* **2006**, *110*, 22328-22338.
- (70) Szabó, T.; Berkesi, O.; Forgó, P.; Josepovits, K.; Sanakis, Y.; Petridis, D.; Dékány, I. Evolution of Surface Functional Groups in a Series of Progressively Oxidized Graphite Oxides. *Chemistry of Materials* **2006**, *18*, 2740-2749.
- (71) Dreyer, D. R.; Park, S.; Bielawski, C. W.; Ruoff, R. S. The chemistry of graphene oxide. *Chemical Society Reviews* **2010**, *39*.
- (72) Erickson, K.; Erni, R.; Lee, Z.; Alem, N.; Gannett, W.; Zettl, A. Determination of the Local Chemical Structure of Graphene Oxide and Reduced Graphene Oxide. *Advanced Materials* **2010**, *22*, 4467-4472.
- (73) Kim, F.; Cote, L. J.; Huang, J. Graphene Oxide: Surface Activity and Two-Dimensional Assembly. *Advanced Materials* **2010**, *22*, 1954-1958.
- (74) Stankovich, S.; Piner, R. D.; Chen, X.; Wu, N.; Nguyen, S. T.; Ruoff, R. S. Stable aqueous dispersions of graphitic nanoplatelets via the reduction of exfoliated graphite oxide in the presence of poly(sodium 4-styrenesulfonate). *Journal of Materials Chemistry* **2006**, *16*, 155-158.
- (75) Becerril, H. A.; Mao, J.; Liu, Z.; Stoltenberg, R. M.; Bao, Z.; Chen, Y. Evaluation of Solution-Processed Reduced Graphene Oxide Films as Transparent Conductors. *ACS Nano* **2008**, *2*, 463-470.
- (76) Eda, G.; Chhowalla, M. Chemically Derived Graphene Oxide: Towards Large-Area Thin-Film Electronics and Optoelectronics. *Advanced Materials* **2010**, *22*, 2392-2415.
- (77) Eda, G.; Fanchini, G.; Chhowalla, M. Large-area ultrathin films of reduced graphene oxide as a transparent and flexible electronic material. *Nature Nanotechnology* **2008**, *3*, 270-274.
- (78) Rourke, J. P.; Pandey, P. A.; Moore, J. J.; Bates, M.; Kinloch, I. A.; Young, R. J.; Wilson, N. R. The Real Graphene Oxide Revealed: Stripping the Oxidative Debris from the Graphene-like Sheets. *Angew. Chem.-Int. Edit.* **2011**, *50*, 3173-3177.
- (79) Yang, H.; Shan, C.; Li, F.; Han, D.; Zhang, Q.; Niu, L. Covalent functionalization of polydisperse chemically-converted graphene sheets with amine-terminated ionic liquid. *Chemical Communications* **2009**, 3880-3882.

- (80) Niyogi, S.; Bekyarova, E.; Itkis, M. E.; McWilliams, J. L.; Hamon, M. A.; Haddon, R. C. Solution Properties of Graphite and Graphene. *Journal of the American Chemical Society* **2006**, *128*, 7720-7721.
- (81) Yang, X.; Zhang, X.; Liu, Z.; Ma, Y.; Huang, Y.; Chen, Y. High-Efficiency Loading and Controlled Release of Doxorubicin Hydrochloride on Graphene Oxide. *Journal of Physical Chemistry C* **2008**, *112*, 17554-17558.
- (82) Suk, J. W.; Piner, R. D.; An, J.; Ruoff, R. S. Mechanical Properties of Mono layer Graphene Oxide. *Acs Nano* **2010**, *4*, 6557-6564.
- (83) Gómez-Navarro, C.; Meyer, J. C.; Sundaram, R. S.; Chuvilin, A.; Kurasch, S.; Burghard, M.; Kern, K.; Kaiser, U. Atomic Structure of Reduced Graphene Oxide. *Nano Letters* **2010**, *10*, 1144-1148.
- (84) Chen, J.-H.; Cullen, W. G.; Jang, C.; Fuhrer, M. S.; Williams, E. D. Defect Scattering in Graphene. *Physical Review Letters* **2009**, *102*, 236805.
- (85) Robinson, J. T.; Zalalutdinov, M.; Baldwin, J. W.; Snow, E. S.; Wei, Z.; Sheehan, P.; Houston, B. H. Wafer-scale Reduced Graphene Oxide Films for Nanomechanical Devices. *Nano Letters* **2008**, *8*, 3441-3445.
- (86) Edwards, R. S.; Coleman, K. S. Graphene synthesis: relationship to applications. *Nanoscale* **2013**, *5*, 38-51.
- (87) Huang, X.; Yin, Z.; Wu, S.; Qi, X.; He, Q.; Zhang, Q.; Yan, Q.; Boey, F.; Zhang, H. Graphene-Based Materials: Synthesis, Characterization, Properties, and Applications. *Small* **2011**, *7*, 1876-1902.
- (88) Ferrari, A. C.; Meyer, J. C.; Scardaci, V.; Casiraghi, C.; Lazzeri, M.; Mauri, F.; Piscanec, S.; Jiang, D.; Novoselov, K. S.; Roth, S.; Geim, A. K. Raman spectrum of graphene and graphene layers. *Physical Review Letters* **2006**, *97*.
- (89) Ferrari, A. C. Raman spectroscopy of graphene and graphite: Disorder, electron-phonon coupling, doping and nonadiabatic effects. *Solid State Communications* **2007**, *143*, 47-57.
- (90) Cancado, L. G.; Jorio, A.; Martins Ferreira, E. H.; Stavale, F.; Achete, C. A.; Capaz, R. B.; Moutinho, M. V. O.; Lombardo, A.; Kulmala, T. S.; Ferrari, A. C. Quantifying Defects in Graphene via Raman Spectroscopy at Different Excitation Energies. *Nano Letters* **2011**, *11*, 3190-3196.
- (91) Gass, M. H.; Bangert, U.; Bleloch, A. L.; Wang, P.; Nair, R. R.; Geim, A. K. Free-standing graphene at atomic resolution. *Nat Nano* **2008**, *3*, 676-681.

- (92) Bonaccorso, F.; Sun, Z.; Hasan, T.; Ferrari, A. C. Graphene photonics and optoelectronics. *Nat Photon* **2010**, *4*, 611-622.
- (93) Novoselov, K. S.; Falko, V. I.; Colombo, L.; Gellert, P. R.; Schwab, M. G.; Kim, K. A roadmap for graphene. *Nature* **2012**, *490*, 192-200.
- (94) Raccichini, R.; Varzi, A.; Passerini, S.; Scrosati, B. The role of graphene for electrochemical energy storage. *Nat Mater* **2015**, *14*, 271-279.
- (95) Lu, C.-H.; Yang, H.-H.; Zhu, C.-L.; Chen, X.; Chen, G.-N. A Graphene Platform for Sensing Biomolecules. *Angewandte Chemie-International Edition* **2009**, *48*, 4785-4787.
- (96) Kim, K. S.; Zhao, Y.; Jang, H.; Lee, S. Y.; Kim, J. M.; Kim, K. S.; Ahn, J.-H.; Kim, P.; Choi, J.-Y.; Hong, B. H. Large-scale pattern growth of graphene films for stretchable transparent electrodes. *Nature* **2009**, *457*, 706-710.
- (97) Kobayashi, T.; Bando, M.; Kimura, N.; Shimizu, K.; Kadono, K.; Umezu, N.; Miyahara, K.; Hayazaki, S.; Nagai, S.; Mizuguchi, Y.; Murakami, Y.; Hobara, D. Production of a 100-m-long high-quality graphene transparent conductive film by roll-to-roll chemical vapor deposition and transfer process. *Applied Physics Letters* **2013**, *102*.
- (98) Bae, S.; Kim, H.; Lee, Y.; Xu, X.; Park, J.-S.; Zheng, Y.; Balakrishnan, J.; Lei, T.; Ri Kim, H.; Song, Y. I.; Kim, Y.-J.; Kim, K. S.; Ozyilmaz, B.; Ahn, J.-H.; Hong, B. H.; Iijima, S. Roll-to-roll production of 30-inch graphene films for transparent electrodes. *Nat Nano* **2010**, *5*, 574-578.
- (99) Wintterlin, J.; Bocquet, M. L. Graphene on metal surfaces. *Surface Science* **2009**, *603*, 1841-1852.
- (100) Liu, N.; Fu, L.; Dai, B.; Yan, K.; Liu, X.; Zhao, R.; Zhang, Y.; Liu, Z. Universal Segregation Growth Approach to Wafer-Size Graphene from Non-Noble Metals. *Nano Letters* **2011**, *11*, 297-303.
- (101) Sutter, P. Epitaxial graphene: How silicon leaves the scene. *Nat Mater* **2009**, *8*, 171-172.
- (102) Hannon, J. B.; Tromp, R. M. Pit formation during graphene synthesis on SiC(0001): *\textit{In situ}* electron microscopy. *Physical Review B* **2008**, *77*, 241404.
- (103) Hernandez, Y.; Nicolosi, V.; Lotya, M.; Blighe, F. M.; Sun, Z.; De, S.; McGovern, I. T.; Holland, B.; Byrne, M.; Gun'ko, Y. K.; Boland, J. J.; Niraj, P.; Duesberg, G.; Krishnamurthy, S.; Goodhue, R.; Hutchison, J.; Scardaci, V.; Ferrari, A.

C.; Coleman, J. N. High-yield production of graphene by liquid-phase exfoliation of graphite. *Nature Nanotechnology* **2008**, *3*, 563-568.

(104) Coleman, J. N. Liquid Exfoliation of Defect-Free Graphene. *Accounts of Chemical Research* **2013**, *46*, 14-22.

(105) Sivudu, K. S.; Mahajan, Y. R. **Challenges and opportunities for the mass production of high quality graphene: an analysis of worldwide patents.** *Nanotech Insights* **2012**, *3*, 6-19.

(106) Ren, W.; Cheng, H.-M. The global growth of graphene. *Nat Nano* **2014**, *9*, 726-730.

(107) Berger, C.; Song, Z.; Li, X.; Wu, X.; Brown, N.; Naud, C.; Mayou, D.; Li, T.; Hass, J.; Marchenkov, A. N.; Conrad, E. H.; First, P. N.; de Heer, W. A. Electronic confinement and coherence in patterned epitaxial graphene. *Science* **2006**, *312*, 1191-1196.

(108) Li, X.; Cai, W.; An, J.; Kim, S.; Nah, J.; Yang, D.; Piner, R.; Velamakanni, A.; Jung, I.; Tutuc, E.; Banerjee, S. K.; Colombo, L.; Ruoff, R. S. Large-Area Synthesis of High-Quality and Uniform Graphene Films on Copper Foils. *Science* **2009**, *324*, 1312-1314.

(109) Chen, L.; Hernandez, Y.; Feng, X.; Muellen, K. From Nanographene and Graphene Nanoribbons to Graphene Sheets: Chemical Synthesis. *Angewandte Chemie-International Edition* **2012**, *51*, 7640-7654.

(110) Choucair, M.; Thordarson, P.; Stride, J. A. Gram-scale production of graphene based on solvothermal synthesis and sonication. *Nat Nano* **2009**, *4*, 30-33.

(111) Simpson, C. D.; Brand, J. D.; Berresheim, A. J.; Przybilla, L.; Rader, H. J.; Mullen, K. Synthesis of a giant 222 carbon graphite sheet. *Chemistry-a European Journal* **2002**, *8*, 1424-1429.

(112) Dato, A.; Radmilovic, V.; Lee, Z.; Phillips, J.; Frenklach, M. Substrate-Free Gas-Phase Synthesis of Graphene Sheets. *Nano Letters* **2008**, *8*, 2012-2016.

(113) Wei, D.; Liu, Y.; Wang, Y.; Zhang, H.; Huang, L.; Yu, G. Synthesis of N-Doped Graphene by Chemical Vapor Deposition and Its Electrical Properties. *Nano Letters* **2009**, *9*, 1752-1758.

(114) Reddy, A. L. M.; Srivastava, A.; Gowda, S. R.; Gullapalli, H.; Dubey, M.; Ajayan, P. M. Synthesis Of Nitrogen-Doped Graphene Films For Lithium Battery Application. *ACS Nano* **2010**, *4*, 6337-6342.

- (115) Caldwell, J. D.; Anderson, T. J.; Culbertson, J. C.; Jernigan, G. G.; Hobart, K. D.; Kub, F. J.; Tadjer, M. J.; Tedesco, J. L.; Hite, J. K.; Mastro, M. A.; Myers-Ward, R. L.; Eddy, C. R.; Campbell, P. M.; Gaskill, D. K. Technique for the Dry Transfer of Epitaxial Graphene onto Arbitrary Substrates. *ACS Nano* **2010**, *4*, 1108-1114.
- (116) Unarunotai, S.; Murata, Y.; Chialvo, C. E.; Kim, H.-s.; MacLaren, S.; Mason, N.; Petrov, I.; Rogers, J. A. Transfer of graphene layers grown on SiC wafers to other substrates and their integration into field effect transistors. *Applied Physics Letters* **2009**, *95*.
- (117) Lee, Y.; Bae, S.; Jang, H.; Jang, S.; Zhu, S.-E.; Sim, S. H.; Song, Y. I.; Hong, B. H.; Ahn, J.-H. Wafer-Scale Synthesis and Transfer of Graphene Films. *Nano Letters* **2010**, *10*, 490-493.
- (118) Lippert, G.; Dabrowski, J.; Lemme, M.; Marcus, C.; Seifarth, O.; Lupina, G. Direct graphene growth on insulator. *Physica Status Solidi B-Basic Solid State Physics* **2011**, *248*, 2619-2622.
- (119) Kosynkin, D. V.; Higginbotham, A. L.; Sinitskii, A.; Lomeda, J. R.; Dimiev, A.; Price, B. K.; Tour, J. M. Longitudinal unzipping of carbon nanotubes to form graphene nanoribbons. *Nature* **2009**, *458*, 872-876.
- (120) Valentini, L. Formation of unzipped carbon nanotubes by CF₄ plasma treatment. *Diamond and Related Materials* **2011**, *20*, 445-448.
- (121) Jiao, L.; Zhang, L.; Wang, X.; Diankov, G.; Dai, H. Narrow graphene nanoribbons from carbon nanotubes. *Nature* **2009**, *458*, 877-880.
- (122) Wu, J.; Pisula, W.; Müllen, K. Graphenes as Potential Material for Electronics. *Chemical Reviews* **2007**, *107*, 718-747.
- (123) Bonaccorso, F.; Lombardo, A.; Hasan, T.; Sun, Z.; Colombo, L.; Ferrari, A. C. Production and processing of graphene and 2d crystals. *Materials Today* **2012**, *15*, 564-589.
- (124) Fu, W.; Kiggans, J.; Overbury, S. H.; Schwartz, V.; Liang, C. Low-temperature exfoliation of multilayer-graphene material from FeCl₃ and CH₃NO₂ co-intercalated graphite compound. *Chemical Communications* **2011**, *47*, 5265-5267.
- (125) Liu, Z.; Liu, Q.; Huang, Y.; Ma, Y.; Yin, S.; Zhang, X.; Sun, W.; Chen, Y. Organic Photovoltaic Devices Based on a Novel Acceptor Material: Graphene. *Advanced Materials* **2008**, *20*, 3924-+.

(126) Posudievsky, O. Y.; Khazieieva, O. A.; Cherepanov, V. V.; Koshechko, V. G.; Pokhodenko, V. D. High yield of graphene by dispersant-free liquid exfoliation of mechanochemically delaminated graphite. *Journal of Nanoparticle Research* **2013**, *15*, 1-9.

(127) Lv, Y.; Yu, L.; Jiang, C.; Chen, S.; Nie, Z. Synthesis of graphene nanosheet powder with layer number control via a soluble salt-assisted route. *RSC Advances* **2014**, *4*, 13350-13354.

(128) Leon, V.; Quintana, M.; Herrero, M. A.; Fierro, J. L. G.; Hoz, A. d. I.; Prato, M.; Vazquez, E. Few-layer graphenes from ball-milling of graphite with melamine. *Chemical Communications* **2011**, *47*, 10936-10938.

(129) Jeon, I.-Y.; Choi, H.-J.; Jung, S.-M.; Seo, J.-M.; Kim, M.-J.; Dai, L.; Baek, J.-B. Large-Scale Production of Edge-Selectively Functionalized Graphene Nanoplatelets via Ball Milling and Their Use as Metal-Free Electrocatalysts for Oxygen Reduction Reaction. *Journal of the American Chemical Society* **2013**, *135*, 1386-1393.

(130) Yi, M.; Shen, Z. A review on mechanical exfoliation for the scalable production of graphene. *Journal of Materials Chemistry A* **2015**, *3*, 11700-11715.

(131) Zhao, W.; Wu, F.; Wu, H.; Chen, G. Preparation of Colloidal Dispersions of Graphene Sheets in Organic Solvents by Using Ball Milling. *Journal of Nanomaterials* **2010**.

(132) Morales, G. M.; Schifani, P.; Ellis, G.; Ballesteros, C.; Martinez, G.; Barbero, C.; Salvagione, H. J. High-quality few layer graphene produced by electrochemical intercalation and microwave-assisted expansion of graphite. *Carbon* **2011**, *49*, 2809-2816.

(133) Israelachvili, J. N.: *Intermolecular and surface forces*. revised 3rd edition ed.; Academic press.

(134) Johnson, D. W.; Dobson, B. P.; Coleman, K. S. A manufacturing perspective on graphene dispersions. *Current Opinion in Colloid & Interface Science* **2015**, *20*, 367-382.

(135) Khan, U.; O'Neill, A.; Lotya, M.; De, S.; Coleman, J. N. High-Concentration Solvent Exfoliation of Graphene. *Small* **2010**, *6*.

(136) Khan, U.; Porwal, H.; O'Neill, A.; Nawaz, K.; May, P.; Coleman, J. N. Solvent-Exfoliated Graphene at Extremely High Concentration. *Langmuir* **2011**, *27*, 9077-9082.

- (137) Lotya, M.; King, P. J.; Khan, U.; De, S.; Coleman, J. N. High-Concentration, Surfactant-Stabilized Graphene Dispersions. *Acs Nano* **2010**, *4*.
- (138) Nuvoli, D.; Valentini, L.; Alzari, V.; Scognamillo, S.; Bon, S. B.; Piccinini, M.; Illescas, J.; Mariani, A. High concentration few-layer graphene sheets obtained by liquid phase exfoliation of graphite in ionic liquid. *Journal of Materials Chemistry* **2011**, *21*, 3428-3431.
- (139) Liu, W. W.; Wang, J. N.; Wang, X. X. Charging of unfunctionalized graphene in organic solvents. *Nanoscale* **2012**, *4*, 425-428.
- (140) Konkena, B.; Vasudevan, S. Understanding Aqueous Dispersibility of Graphene Oxide and Reduced Graphene Oxide through pKa Measurements. *The Journal of Physical Chemistry Letters* **2012**, *3*, 867-872.
- (141) Hunter, R.: **Zeta potential in colloid science: principles and applications**. Academic Press, 1981.
- (142) Bourlinos, A. B.; Gournis, D.; Petridis, D.; Szabo, T.; Szeri, A.; Dekany, I. Graphite oxide: Chemical reduction to graphite and surface modification with primary aliphatic amines and amino acids. *Langmuir* **2003**, *19*, 6050-6055.
- (143) Park, S.; Hu, Y.; Hwang, J. O.; Lee, E.-S.; Casabianca, L. B.; Cai, W.; Potts, J. R.; Ha, H.-W.; Chen, S.; Oh, J.; Kim, S. O.; Kim, Y.-H.; Ishii, Y.; Ruoff, R. S. Chemical structures of hydrazine-treated graphene oxide and generation of aromatic nitrogen doping. *Nat Commun* **2012**, *3*, 638.
- (144) Youn, S. C.; Geng, J.; Son, B. S.; Yang, S. B.; Kim, D. W.; Cho, H. M.; Jung, H.-T. Effect of the Exposure Time of Hydrazine Vapor on the Reduction of Graphene Oxide Films. *Journal of Nanoscience and Nanotechnology* **2011**, *11*, 5959-5964.
- (145) McAllister, M. J.; Li, J.-L.; Adamson, D. H.; Schniepp, H. C.; Abdala, A. A.; Liu, J.; Herrera-Alonso, M.; Milius, D. L.; Car, R.; Prud'homme, R. K.; Aksay, I. A. Single Sheet Functionalized Graphene by Oxidation and Thermal Expansion of Graphite. *Chemistry of Materials* **2007**, *19*, 4396-4404.
- (146) Zhou, M.; Wang, Y.; Zhai, Y.; Zhai, J.; Ren, W.; Wang, F.; Dong, S. Controlled Synthesis of Large-Area and Patterned Electrochemically Reduced Graphene Oxide Films. *Chemistry-a European Journal* **2009**, *15*, 6116-6120.
- (147) Lee, C.-G.; Park, S.; Ruoff, R. S.; Dodabalapur, A. Integration of reduced graphene oxide into organic field-effect transistors as conducting electrodes and as a metal modification layer. *Applied Physics Letters* **2009**, *95*.

(148) Shin, H.-J.; Kim, K. K.; Benayad, A.; Yoon, S.-M.; Park, H. K.; Jung, I.-S.; Jin, M. H.; Jeong, H.-K.; Kim, J. M.; Choi, J.-Y.; Lee, Y. H. Efficient Reduction of Graphite Oxide by Sodium Borohydride and Its Effect on Electrical Conductance. *Advanced Functional Materials* **2009**, *19*, 1987-1992.

(149) Wang, S.; Chia, P.-J.; Chua, L.-L.; Zhao, L.-H.; Png, R.-Q.; Sivaramakrishnan, S.; Zhou, M.; Goh, R. G. S.; Friend, R. H.; Wee, A. T. S.; Ho, P. K. H. Band-like transport in surface-functionalized highly solution-processable graphene nanosheets. *Advanced Materials* **2008**, *20*, 3440-+.

(150) Wu, Z.-S.; Ren, W.; Gao, L.; Liu, B.; Jiang, C.; Cheng, H.-M. Synthesis of high-quality graphene with a pre-determined number of layers. *Carbon* **2009**, *47*, 493-499.

(151) Schniepp, H. C.; Li, J. L.; McAllister, M. J.; Sai, H.; Herrera-Alonso, M.; Adamson, D. H.; Prud'homme, R. K.; Car, R.; Saville, D. A.; Aksay, I. A. Functionalized single graphene sheets derived from splitting graphite oxide. *Journal of Physical Chemistry B* **2006**, *110*, 8535-8539.

(152) Abdelkader, A. M.; Cooper, A. J.; Dryfe, R. A. W.; Kinloch, I. A. How to get between the sheets: a review of recent works on the electrochemical exfoliation of graphene materials from bulk graphite. *Nanoscale* **2015**, *7*, 6944-6956.

(153) Low, C. T. J.; Walsh, F. C.; Chakrabarti, M. H.; Hashim, M. A.; Hussain, M. A. Electrochemical approaches to the production of graphene flakes and their potential applications. *Carbon* **2013**, *54*, 1-21.

(154) Alanyalioglu, M.; Jose Segura, J.; Oro-Sole, J.; Casan-Pastor, N. The synthesis of graphene sheets with controlled thickness and order using surfactant-assisted electrochemical processes. *Carbon* **2012**, *50*, 142-152.

(155) Wang, J.; Manga, K. K.; Bao, Q.; Loh, K. P. High-Yield Synthesis of Few-Layer Graphene Flakes through Electrochemical Expansion of Graphite in Propylene Carbonate Electrolyte. *Journal of the American Chemical Society* **2011**, *133*, 8888-8891.

(156) Parvez, K.; Wu, Z.-S.; Li, R.; Liu, X.; Graf, R.; Feng, X.; Muellen, K. Exfoliation of Graphite into Graphene in Aqueous Solutions of Inorganic Salts. *Journal of the American Chemical Society* **2014**, *136*, 6083-6091.

(157) Su, C.-Y.; Lu, A.-Y.; Xu, Y.; Chen, F.-R.; Khlobystov, A. N.; Li, L.-J. High-Quality Thin Graphene Films from Fast Electrochemical Exfoliation. *ACS Nano* **2011**, *5*, 2332-2339.

- (158) Parvez, K.; Li, R. J.; Puniredd, S. R.; Hernandez, Y.; Hinkel, F.; Wang, S. H.; Feng, X. L.; Mullen, K. Electrochemically Exfoliated Graphene as Solution-Processable, Highly Conductive Electrodes for Organic Electronics. *Acs Nano* **2013**, *7*, 3598-3606.
- (159) Li, P.; Bae, S. H.; Zan, Q. Y.; Kim, N. H.; Lee, J. H. One-step process for the exfoliation and surface modification of graphene by electrochemical method. *Multi-Functional Materials and Structures Iii, Pts 1 and 2* **2010**, *123-125*, 743-746.
- (160) Zhou, M.; Tang, J.; Cheng, Q.; Xu, G. J.; Cui, P.; Qin, L. C. Few-layer graphene obtained by electrochemical exfoliation of graphite cathode. *Chemical Physics Letters* **2013**, *572*, 61-65.
- (161) Yang, Y. C.; Lu, F.; Zhou, Z.; Song, W. X.; Chen, Q. Y.; Ji, X. B. Electrochemically cathodic exfoliation of graphene sheets in room temperature ionic liquids N-butyl, methylpyrrolidinium bis(trifluoromethylsulfonyl)imide and their electrochemical properties. *Electrochimica Acta* **2013**, *113*, 9-16.
- (162) Hernandez, Y.; Lotya, M.; Rickard, D.; Bergin, S. D.; Coleman, J. N. Measurement of Multicomponent Solubility Parameters for Graphene Facilitates Solvent Discovery. *Langmuir* **2010**, *26*, 3208-3213.
- (163) Geng, J.; Kong, B.-S.; Yang, S. B.; Jung, H.-T. Preparation of graphene relying on porphyrin exfoliation of graphite. *Chemical Communications* **2010**, *46*, 5091-5093.
- (164) Du, W.; Jiang, X.; Zhu, L. From graphite to graphene: direct liquid-phase exfoliation of graphite to produce single- and few-layered pristine graphene. *Journal of Materials Chemistry A* **2013**, *1*, 10592-10606.
- (165) O'Neill, A.; Khan, U.; Nirmalraj, P. N.; Boland, J.; Coleman, J. N. Graphene Dispersion and Exfoliation in Low Boiling Point Solvents. *Journal of Physical Chemistry C* **2011**, *115*, 5422-5428.
- (166) Eun-Young Choi and Won San Choi and Young Boo Lee and Yong-Young, N. Production of graphene by exfoliation of graphite in a volatile organic solvent. *Nanotechnology* **2011**, *22*, 365601.
- (167) Zhang, X.; Coleman, A. C.; Katsonis, N.; Browne, W. R.; van Wees, B. J.; Feringa, B. L. Dispersion of graphene in ethanol using a simple solvent exchange method. *Chemical Communications* **2010**, *46*, 7539-7541.
- (168) Bourlinos, A. B.; Georgakilas, V.; Zboril, R.; Steriotis, T. A.; Stubos, A. K. Liquid-Phase Exfoliation of Graphite Towards Solubilized Graphenes. *Small* **2009**, *5*, 1841-1845.

(169) Behabtu, N.; Lomeda, J. R.; Green, M. J.; Higginbotham, A. L.; Sinitskii, A.; Kosynkin, D. V.; Tsentlovich, D.; Parra-Vasquez, A. N. G.; Schmidt, J.; Kesselman, E.; Cohen, Y.; Talmon, Y.; Tour, J. M.; Pasquali, M. Spontaneous high-concentration dispersions and liquid crystals of graphene. *Nature Nanotechnology* **2010**, *5*.

(170) Lu, W.; Liu, S.; Qin, X.; Wang, L.; Tian, J.; Luo, Y.; Asiri, A. M.; Al-Youbi, A. O.; Sun, X. High-yield, large-scale production of few-layer graphene flakes within seconds: using chlorosulfonic acid and H₂O₂ as exfoliating agents. *Journal of Materials Chemistry* **2012**, *22*, 8775-8777.

(171) Lotya, M.; Hernandez, Y.; King, P. J.; Smith, R. J.; Nicolosi, V.; Karlsson, L. S.; Blighe, F. M.; De, S.; Wang, Z.; McGovern, I. T.; Duesberg, G. S.; Coleman, J. N. Liquid Phase Production of Graphene by Exfoliation of Graphite in Surfactant/Water Solutions. *Journal of the American Chemical Society* **2009**, *131*, 3611-3620.

(172) Lotya, M.; King, P. J.; Khan, U.; De, S.; Coleman, J. N. High-Concentration, Surfactant-Stabilized Graphene Dispersions. *Acs Nano* **2010**, *4*, 3155-3162.

(173) Hasan, T.; Torrisi, F.; Sun, Z.; Popa, D.; Nicolosi, V.; Privitera, G.; Bonaccorso, F.; Ferrari, A. C. Solution-phase exfoliation of graphite for ultrafast photonics. *Physica Status Solidi B-Basic Solid State Physics* **2010**, *247*, 2953-2957.

(174) Guardia, L.; Fernandez-Merino, M. J.; Paredes, J. I.; Solis-Fernandez, P.; Villar-Rodil, S.; Martinez-Alonso, A.; Tascon, J. M. D. High-throughput production of pristine graphene in an aqueous dispersion assisted by non-ionic surfactants. *Carbon* **2011**, *49*, 1653-1662.

(175) Smith, R. J.; Lotya, M.; Coleman, J. N. The importance of repulsive potential barriers for the dispersion of graphene using surfactants. *New Journal of Physics* **2010**, *12*.

(176) Das, S.; Irin, F.; Ma, L.; Bhattacharia, S. K.; Hedden, R. C.; Green, M. J. Rheology and Morphology of Pristine Graphene/Polyacrylamide Gels. *Acs Applied Materials & Interfaces* **2013**, *5*, 8633-8640.

(177) An, X.; Simmons, T. J.; Shah, R.; Wolfe, C.; Lewis, K. M.; Washington, M.; Nayak, S. K.; Talapatra, S.; Kar, S. Stable Aqueous Dispersions of Noncovalently Functionalized Graphene from Graphite and their Multifunctional High-Performance Applications. *Nano Letters* **2010**, *10*, 4295-4301.

(178) Zhang, M.; Parajuli, R. R.; Mastrogiovanni, D.; Dai, B.; Lo, P.; Cheung, W.; Brukh, R.; Chiu, P. L.; Zhou, T.; Liu, Z.; Garfunkel, E.; He, H. Production of

Graphene Sheets by Direct Dispersion with Aromatic Healing Agents. *Small* **2010**, *6*, 1100-1107.

(179) Wang, X. Q.; Fulvio, P. F.; Baker, G. A.; Veith, G. M.; Unocic, R. R.; Mahurin, S. M.; Chi, M. F.; Dai, S. Direct exfoliation of natural graphite into micrometre size few layers graphene sheets using ionic liquids. *Chemical Communications* **2010**, *46*, 4487-4489.

(180) Bari, R.; Tamas, G.; Irin, F.; Aquino, A. J. A.; Green, M. J.; Quitevis, E. L. Direct exfoliation of graphene in ionic liquids with aromatic groups. *Colloids and Surfaces a-Physicochemical and Engineering Aspects* **2014**, *463*, 63-69.

(181) Paton, K. R.; Varrla, E.; Backes, C.; Smith, R. J.; Khan, U.; O'Neill, A.; Boland, C.; Lotya, M.; Istrate, O. M.; King, P.; Higgins, T.; Barwich, S.; May, P.; Puczkarski, P.; Ahmed, I.; Moebius, M.; Pettersson, H.; Long, E.; Coelho, J.; O'Brien, S. E.; McGuire, E. K.; Sanchez, B. M.; Duesberg, G. S.; McEvoy, N.; Pennycook, T. J.; Downing, C.; Crossley, A.; Nicolosi, V.; Coleman, J. N. Scalable production of large quantities of defect-free few-layer graphene by shear exfoliation in liquids. *Nature Materials* **2014**, *13*, 624-630.

(182) Zheng, W.; Lu, X. H.; Wong, S. C. Electrical and mechanical properties of expanded graphite-reinforced high-density polyethylene. *Journal of Applied Polymer Science* **2004**, *91*, 2781-2788.

(183) Zheng, W.; Wong, S.-C. Electrical conductivity and dielectric properties of PMMA/expanded graphite composites. *Composites Science and Technology* **2003**, *63*, 225-235.

(184) Shen, J. W.; Huang, W. Y.; Zuo, S. W.; Hou, J. Polyethylene/grafted polyethylene/graphite nanocomposites: Preparation, structure, and electrical properties. *Journal of Applied Polymer Science* **2005**, *97*, 51-59.

(185) Kim, H.; Abdala, A. A.; Macosko, C. W. Graphene/Polymer Nanocomposites. *Macromolecules* **2010**, *43*, 6515-6530.

(186) Chee, W. K.; Lim, H. N.; Huang, N. M.; Harrison, I. Nanocomposites of graphene/polymers: a review. *RSC Advances* **2015**, *5*, 68014-68051.

(187) Xu, Q.; Xu, H.; Chen, J.; Lv, Y.; Dong, C.; Sreeprasad, T. S. Graphene and graphene oxide: advanced membranes for gas separation and water purification. *Inorganic Chemistry Frontiers* **2015**, *2*, 417-424.

(188) Thostenson, E. T.; Li, C.; Chou, T.-W. Nanocomposites in context. *Composites Science and Technology* **2005**, *65*, 491-516.

- (189) Mahmoud, W. E. Morphology and physical properties of poly(ethylene oxide) loaded graphene nanocomposites prepared by two different techniques. *European Polymer Journal* **2011**, *47*, 1534-1540.
- (190) Bian, J.; Lin, H. L.; He, F. X.; Wei, X. W.; Chang, I. T.; Sancaktar, E. Fabrication of microwave exfoliated graphite oxide reinforced thermoplastic polyurethane nanocomposites: Effects of filler on morphology, mechanical, thermal and conductive properties. *Composites Part A: Applied Science and Manufacturing* **2013**, *47*, 72-82.
- (191) Shen, B.; Zhai, W.; Chen, C.; Lu, D.; Wang, J.; Zheng, W. Melt Blending In situ Enhances the Interaction between Polystyrene and Graphene through pi-pi Stacking. *Acs Applied Materials & Interfaces* **2011**, *3*, 3103-3109.
- (192) Pang, H.; Chen, C.; Zhang, Y.-C.; Ren, P.-G.; Yan, D.-X.; Li, Z.-M. The effect of electric field, annealing temperature and filler loading on the percolation threshold of polystyrene containing carbon nanotubes and graphene nanosheets. *Carbon* **2011**, *49*, 1980-1988.
- (193) Kalaitzidou, K.; Fukushima, H.; Drzal, L. T. A new compounding method for exfoliated graphite-polypropylene nanocomposites with enhanced flexural properties and lower percolation threshold. *Composites Science and Technology* **2007**, *67*, 2045-2051.
- (194) Sherif Araby and Izzuddin Zaman and Qingshi Meng and Nobuyuki Kawashima and Andrew Michelmores and Hsu-Chiang Kuan and Peter Majewski and Jun Ma and Liqun, Z. Melt compounding with graphene to develop functional, high-performance elastomers. *Nanotechnology* **2013**, *24*, 165601.
- (195) RamanathanT; Abdala, A. A.; StankovichS; Dikin, D. A.; Herrera Alonso, M.; Piner, R. D.; Adamson, D. H.; Schniepp, H. C.; ChenX; Ruoff, R. S.; Nguyen, S. T.; Aksay, I. A.; Prud'Homme, R. K.; Brinson, L. C. Functionalized graphene sheets for polymer nanocomposites. *Nat Nano* **2008**, *3*, 327-331.
- (196) Villar-Rodil, S.; Paredes, J. I.; Martinez-Alonso, A.; Tascon, J. M. D. Preparation of graphene dispersions and graphene-polymer composites in organic media. *Journal of Materials Chemistry* **2009**, *19*, 3591-3593.
- (197) Li, X.; Xiao, Y.; Bergeret, A.; Longerey, M.; Che, J. Preparation of Poly(lactide)/Graphene Composites From Liquid-Phase Exfoliated Graphite Sheets. *Polymer Composites* **2014**, *35*, 396-403.
- (198) Wu, D.; Cheng, Y.; Feng, S.; Yao, Z.; Zhang, M. Crystallization Behavior of Poly(lactide)/Graphene Composites. *Industrial & Engineering Chemistry Research* **2013**, *52*, 6731-6739.

- (199) Qi, X.-Y.; Yan, D.; Jiang, Z.; Cao, Y.-K.; Yu, Z.-Z.; Yavari, F.; Koratkar, N. Enhanced Electrical Conductivity in Polystyrene Nanocomposites at Ultra-Low Graphene Content. *ACS Applied Materials & Interfaces* **2011**, *3*, 3130-3133.
- (200) Li, R.; Liu, C.; Ma, J. Studies on the properties of graphene oxide-reinforced starch biocomposites. *Carbohydrate Polymers* **2011**, *84*, 631-637.
- (201) Wang, X.; Hu, Y.; Song, L.; Yang, H.; Xing, W.; Lu, H. In situ polymerization of graphene nanosheets and polyurethane with enhanced mechanical and thermal properties. *Journal of Materials Chemistry* **2011**, *21*, 4222-4227.
- (202) Kuila, T.; Bose, S.; Khanra, P.; Kim, N. H.; Rhee, K. Y.; Lee, J. H. Characterization and properties of in situ emulsion polymerized poly(methyl methacrylate)/graphene nanocomposites. *Composites Part A: Applied Science and Manufacturing* **2011**, *42*, 1856-1861.
- (203) Patole, A. S.; Patole, S. P.; Kang, H.; Yoo, J.-B.; Kim, T.-H.; Ahn, J.-H. A facile approach to the fabrication of graphene/polystyrene nanocomposite by in situ microemulsion polymerization. *Journal of Colloid and Interface Science* **2010**, *350*, 530-537.
- (204) Wu, F.; Lu, Y.; Shao, G.; Zeng, F.; Wu, Q. Preparation of polyacrylonitrile/graphene oxide by in situ polymerization. *Polymer International* **2012**, *61*, 1394-1399.
- (205) Potts, J. R.; Lee, S. H.; Alam, T. M.; An, J.; Stoller, M. D.; Piner, R. D.; Ruoff, R. S. Thermomechanical properties of chemically modified graphene/poly(methyl methacrylate) composites made by in situ polymerization. *Carbon* **2011**, *49*, 2615-2623.
- (206) Bose, S.; Kuila, T.; Uddin, M. E.; Kim, N. H.; Lau, A. K. T.; Lee, J. H. In-situ synthesis and characterization of electrically conductive polypyrrole/graphene nanocomposites. *Polymer* **2010**, *51*, 5921-5928.
- (207) Choi, K. S.; Liu, F.; Choi, J. S.; Seo, T. S. Fabrication of Free-Standing Multilayered Graphene and Poly(3,4-ethylenedioxythiophene) Composite Films with Enhanced Conductive and Mechanical Properties. *Langmuir* **2010**, *26*, 12902-12908.
- (208) Paszkiewicz, S.; Szymczyk, A.; Špitalský, Z.; Mosnáček, J.; Kwiatkowski, K.; Rosłaniec, Z. Structure and properties of nanocomposites based on PTT-block-PTMO copolymer and graphene oxide prepared by in situ polymerization. *European Polymer Journal* **2014**, *50*, 69-77.
- (209) Tian, M.; Zhang, J.; Zhang, L.; Liu, S.; Zan, X.; Nishi, T.; Ning, N. Graphene encapsulated rubber latex composites with high dielectric constant, low

dielectric loss and low percolation threshold. *Journal of Colloid and Interface Science* **2014**, *430*, 249-256.

(210) Zhan, Y.; Lavorgna, M.; Buonocore, G.; Xia, H. Enhancing electrical conductivity of rubber composites by constructing interconnected network of self-assembled graphene with latex mixing. *Journal of Materials Chemistry* **2012**, *22*, 10464-10468.

(211) Li, M.; Gao, C.; Hu, H.; Zhao, Z. Electrical conductivity of thermally reduced graphene oxide/polymer composites with a segregated structure. *Carbon* **2013**, *65*, 371-373.

(212) Du, J.; Zhao, L.; Zeng, Y.; Zhang, L.; Li, F.; Liu, P.; Liu, C. Comparison of electrical properties between multi-walled carbon nanotube and graphene nanosheet/high density polyethylene composites with a segregated network structure. *Carbon* **2011**, *49*, 1094-1100.

(213) Pang, H.; Chen, T.; Zhang, G.; Zeng, B.; Li, Z.-M. An electrically conducting polymer/graphene composite with a very low percolation threshold. *Materials Letters* **2010**, *64*, 2226-2229.

(214) Zhang, M.; Li, Y.; Su, Z.; Wei, G. Recent advances in the synthesis and applications of graphene-polymer nanocomposites. *Polymer Chemistry* **2015**, *6*, 6107-6124.

(215) Layek, R. K.; Nandi, A. K. A review on synthesis and properties of polymer functionalized graphene. *Polymer* **2013**, *54*, 5087-5103.

(216) Zhang, Y.; Mark, J. E.; Zhu, Y.; Ruoff, R. S.; Schaefer, D. W. Mechanical properties of polybutadiene reinforced with octadecylamine modified graphene oxide. *Polymer* **2014**, *55*, 5389-5395.

(217) Cano, M.; Khan, U.; Sainsbury, T.; O'Neill, A.; Wang, Z.; McGovern, I. T.; Maser, W. K.; Benito, A. M.; Coleman, J. N. Improving the mechanical properties of graphene oxide based materials by covalent attachment of polymer chains. *Carbon* **2013**, *52*, 363-371.

(218) Zarrin, H.; Fu, J.; Jiang, G.; Yoo, S.; Lenos, J.; Fowler, M.; Chen, Z. Quaternized Graphene Oxide Nanocomposites as Fast Hydroxide Conductors. *ACS Nano* **2015**, *9*, 2028-2037.

(219) Fang, M.; Wang, K.; Lu, H.; Yang, Y.; Nutt, S. Covalent polymer functionalization of graphene nanosheets and mechanical properties of composites. *Journal of Materials Chemistry* **2009**, *19*, 7098-7105.

(220) Beckert, F.; Friedrich, C.; Thomann, R.; Mülhaupt, R. Sulfur-Functionalized Graphenes as Macro-Chain-Transfer and RAFT Agents for Producing Graphene Polymer Brushes and Polystyrene Nanocomposites. *Macromolecules* **2012**, *45*, 7083-7090.

(221) Liang, J.; Huang, Y.; Zhang, L.; Wang, Y.; Ma, Y.; Guo, T.; Chen, Y. Molecular-Level Dispersion of Graphene into Poly(vinyl alcohol) and Effective Reinforcement of their Nanocomposites. *Advanced Functional Materials* **2009**, *19*, 2297-2302.

(222) Liu, J.; Yang, W.; Tao, L.; Li, D.; Boyer, C.; Davis, T. P. Thermosensitive Graphene Nanocomposites Formed Using Pyrene-Terminal Polymers Made by RAFT Polymerization. *Journal of Polymer Science Part a-Polymer Chemistry* **2010**, *48*, 425-433.

(223) Jo, K.; Lee, T.; Choi, H. J.; Park, J. H.; Lee, D. J.; Lee, D. W.; Kim, B.-S. Stable Aqueous Dispersion of Reduced Graphene Nanosheets via Non-Covalent Functionalization with Conducting Polymers and Application in Transparent Electrodes. *Langmuir* **2011**, *27*, 2014-2018.

(224) Qi, X.; Pu, K.-Y.; Li, H.; Zhou, X.; Wu, S.; Fan, Q.-L.; Liu, B.; Boey, F.; Huang, W.; Zhang, H. Amphiphilic Graphene Composites. *Angewandte Chemie-International Edition* **2010**, *49*, 9426-9429.

(225) Xu, L. Q.; Wang, L.; Zhang, B.; Lim, C. H.; Chen, Y.; Neoh, K.-G.; Kang, E.-T.; Fu, G. D. Functionalization of reduced graphene oxide nanosheets via stacking interactions with the fluorescent and water-soluble perylene bisimide-containing polymers. *Polymer* **2011**, *52*, 2376-2383.

(226) Yuan, B.; Bao, C.; Song, L.; Hong, N.; Liew, K. M.; Hu, Y. Preparation of functionalized graphene oxide/polypropylene nanocomposite with significantly improved thermal stability and studies on the crystallization behavior and mechanical properties. *Chemical Engineering Journal* **2014**, *237*, 411-420.

(227) Shen, B.; Zhai, W.; Tao, M.; Lu, D.; Zheng, W. Enhanced interfacial interaction between polycarbonate and thermally reduced graphene induced by melt blending. *Composites Science and Technology* **2013**, *86*, 109-116.

(228) Istrate, O. M.; Paton, K. R.; Khan, U.; O'Neill, A.; Bell, A. P.; Coleman, J. N. Reinforcement in melt-processed polymer-graphene composites at extremely low graphene loading level. *Carbon* **2014**, *78*, 243-249.

(229) Bao, C.; Song, L.; Wilkie, C. A.; Yuan, B.; Guo, Y.; Hu, Y.; Gong, X. Graphite oxide, graphene, and metal-loaded graphene for fire safety applications of polystyrene. *Journal of Materials Chemistry* **2012**, *22*, 16399-16406.

- (230) Das, S.; Wajid, A. S.; Bhattacharia, S. K.; Wilting, M. D.; Rivero, I. V.; Green, M. J. Electrospinning of polymer nanofibers loaded with noncovalently functionalized graphene. *Journal of Applied Polymer Science* **2013**, *128*, 4040-4046.
- (231) Bao, Q. L.; Zhang, H.; Yang, J. X.; Wang, S.; Tong, D. Y.; Jose, R.; Ramakrishna, S.; Lim, C. T.; Loh, K. P. Graphene-Polymer Nanofiber Membrane for Ultrafast Photonics. *Advanced Functional Materials* **2010**, *20*, 782-791.
- (232) Irin, F.; Das, S.; Atore, F. O.; Green, M. J. Ultralow Percolation Threshold in Aerogel and Cryogel Templated Composites. *Langmuir* **2013**, *29*, 11449-11456.
- (233) Xu, Y.; Sheng, K.; Li, C.; Shi, G. Self-Assembled Graphene Hydrogel via a One-Step Hydrothermal Process. *Acs Nano* **2010**, *4*, 4324-4330.
- (234) Worsley, M. A.; Pauzauskie, P. J.; Olson, T. Y.; Biener, J.; Satcher, J. H., Jr.; Baumann, T. F. Synthesis of Graphene Aerogel with High Electrical Conductivity. *Journal of the American Chemical Society* **2010**, *132*, 14067-14069.
- (235) Wang, X.; Zhi, L.; Müllen, K. Transparent, Conductive Graphene Electrodes for Dye-Sensitized Solar Cells. *Nano Letters* **2008**, *8*, 323-327.
- (236) Zheng, Q.; Li, Z.; Yang, J.; Kim, J.-K. Graphene oxide-based transparent conductive films. *Progress in Materials Science* **2014**, *64*, 200-247.
- (237) De, S.; King, P. J.; Lotya, M.; O'Neill, A.; Doherty, E. M.; Hernandez, Y.; Duesberg, G. S.; Coleman, J. N. Flexible, Transparent, Conducting Films of Randomly Stacked Graphene from Surfactant-Stabilized, Oxide-Free Graphene Dispersions. *Small* **2010**, *6*, 458-464.
- (238) Wu, Z.-S.; Pei, S.; Ren, W.; Tang, D.; Gao, L.; Liu, B.; Li, F.; Liu, C.; Cheng, H.-M. Field Emission of Single-Layer Graphene Films Prepared by Electrophoretic Deposition. *Advanced Materials* **2009**, *21*, 1756-+.
- (239) Hwang, H.; Joo, P.; Kang, M. S.; Ahn, G.; Han, J. T.; Kim, B.-S.; Cho, J. H. Highly Tunable Charge Transport in Layer-by-Layer Assembled Graphene Transistors. *ACS Nano* **2012**, *6*, 2432-2440.
- (240) Chang, H.; Sun, Z.; Yuan, Q.; Ding, F.; Tao, X.; Yan, F.; Zheng, Z. Thin Film Field-Effect Phototransistors from Bandgap-Tunable, Solution-Processed, Few-Layer Reduced Graphene Oxide Films. *Advanced Materials* **2010**, *22*, 4872-+.
- (241) Liang, M.; Zhi, L. Graphene-based electrode materials for rechargeable lithium batteries. *Journal of Materials Chemistry* **2009**, *19*, 5871-5878.

- (242) Le, L. T.; Ervin, M. H.; Qiu, H. W.; Fuchs, B. E.; Lee, W. Y. Graphene supercapacitor electrodes fabricated by inkjet printing and thermal reduction of graphene oxide. *Electrochemistry Communications* **2011**, *13*, 355-358.
- (243) He, Q.; Sudibya, H. G.; Yin, Z.; Wu, S.; Li, H.; Boey, F.; Huang, W.; Chen, P.; Zhang, H. Centimeter-Long and Large-Scale Micropatterns of Reduced Graphene Oxide Films: Fabrication and Sensing Applications. *ACS Nano* **2010**, *4*, 3201-3208.
- (244) Dua, V.; Surwade, S. P.; Ammu, S.; Agnihotra, S. R.; Jain, S.; Roberts, K. E.; Park, S.; Ruoff, R. S.; Manohar, S. K. All-Organic Vapor Sensor Using Inkjet-Printed Reduced Graphene Oxide. *Angewandte Chemie-International Edition* **2010**, *49*, 2154-2157.
- (245) Yin, Z.; He, Q.; Huang, X.; Zhang, J.; Wu, S.; Chen, P.; Lu, G.; Zhang, Q.; Yan, Q.; Zhang, H. Real-time DNA detection using Pt nanoparticle-decorated reduced graphene oxide field-effect transistors. *Nanoscale* **2012**, *4*, 293-297.
- (246) Yang, X.; Qiu, L.; Cheng, C.; Wu, Y.; Ma, Z.-F.; Li, D. Ordered Gelation of Chemically Converted Graphene for Next-Generation Electroconductive Hydrogel Films. *Angewandte Chemie-International Edition* **2011**, *50*, 7325-7328.
- (247) Qiu, L.; Zhang, X.; Yang, W.; Wang, Y.; Simon, G. P.; Li, D. Controllable corrugation of chemically converted graphene sheets in water and potential application for nanofiltration. *Chemical Communications* **2011**, *47*, 5810-5812.
- (248) Bae, S.-Y.; Jeon, I.-Y.; Yang, J.; Park, N.; Shin, H. S.; Park, S.; Ruoff, R. S.; Dai, L.; Baek, J.-B. Large-Area Graphene Films by Simple Solution Casting of Edge-Selectively Functionalized Graphite. *ACS Nano* **2011**, *5*, 4974-4980.
- (249) Zhang, X.; Wang, Y.; Watanabe, S.; Uddin, M. H.; Li, D. Evaporation-induced flattening and self-assembly of chemically converted graphene on a solid surface. *Soft Matter* **2011**, *7*, 8745-8748.
- (250) Wu, C.; Cheng, Q.; Sun, S.; Han, B. Templated patterning of graphene oxide using self-assembled monolayers. *Carbon* **2012**, *50*, 1083-1089.
- (251) Chang, H.; Wang, G.; Yang, A.; Tao, X.; Liu, X.; Shen, Y.; Zheng, Z. A Transparent, Flexible, Low-Temperature, and Solution-Processible Graphene Composite Electrode. *Advanced Functional Materials* **2010**, *20*, 2893-2902.
- (252) Li, S.-S.; Tu, K.-H.; Lin, C.-C.; Chen, C.-W.; Chhowalla, M. Solution-Processible Graphene Oxide as an Efficient Hole Transport Layer in Polymer Solar Cells. *ACS Nano* **2010**, *4*, 3169-3174.

(253) Layek, R. K.; Das, A. K.; Park, M. U.; Kim, N. H.; Lee, J. H. Layer-structured graphene oxide/polyvinyl alcohol nanocomposites: dramatic enhancement of hydrogen gas barrier properties. *Journal of Materials Chemistry A* **2014**, *2*, 12158-12161.

(254) Min, K.; Han, T. H.; Kim, J.; Jung, J.; Jung, C.; Hong, S. M.; Koo, C. M. A facile route to fabricate stable reduced graphene oxide dispersions in various media and their transparent conductive thin films. *Journal of Colloid and Interface Science* **2012**, *383*, 36-42.

(255) Wang, M.; Oh, J.; Ghosh, T.; Hong, S.; Nam, G.; Hwang, T.; Nam, J.-D. An interleaved porous laminate composed of reduced graphene oxide sheets and carbon black spacers by in situ electrophoretic deposition. *RSC Advances* **2014**, *4*, 3284-3292.

(256) Singh, B. P.; Nayak, S.; Nanda, K. K.; Jena, B. K.; Bhattacharjee, S.; Besra, L. The production of a corrosion resistant graphene reinforced composite coating on copper by electrophoretic deposition. *Carbon* **2013**, *61*, 47-56.

(257) An, S. J.; Zhu, Y.; Lee, S. H.; Stoller, M. D.; Emilsson, T.; Park, S.; Velamakanni, A.; An, J.; Ruoff, R. S. Thin Film Fabrication and Simultaneous Anodic Reduction of Deposited Graphene Oxide Platelets by Electrophoretic Deposition. *The Journal of Physical Chemistry Letters* **2010**, *1*, 1259-1263.

(258) Zhu, J.; Zhang, H.; Kotov, N. A. Thermodynamic and Structural Insights into Nanocomposites Engineering by Comparing Two Materials Assembly Techniques for Graphene. *ACS Nano* **2013**, *7*, 4818-4829.

(259) Alazemi, M.; Dutta, I.; Wang, F.; Blunk, R. H.; Angelopoulos, A. P. Adsorption kinetics and nanostructure development during layer by layer assembly of graphene nanoplatelets and amorphous carbon nanospheres. *Carbon* **2010**, *48*, 4063-4073.

(260) Chen, J.-T.; Fu, Y.-J.; An, Q.-F.; Lo, S.-C.; Huang, S.-H.; Hung, W.-S.; Hu, C.-C.; Lee, K.-R.; Lai, J.-Y. Tuning nanostructure of graphene oxide/polyelectrolyte LbL assemblies by controlling pH of GO suspension to fabricate transparent and super gas barrier films. *Nanoscale* **2013**, *5*, 9081-9088.

(261) Yu, L.; Lim, Y.-S.; Han, J. H.; Kim, K.; Kim, J. Y.; Choi, S.-Y.; Shin, K. A graphene oxide oxygen barrier film deposited via a self-assembly coating method. *Synthetic Metals* **2012**, *162*, 710-714.

(262) Yang, Y.-H.; Bolling, L.; Priolo, M. A.; Grunlan, J. C. Super Gas Barrier and Selectivity of Graphene Oxide-Polymer Multilayer Thin Films. *Advanced Materials* **2013**, *25*, 503-508.

- (263) Ji, Q.; Honma, I.; Paek, S.-M.; Akada, M.; Hill, J. P.; Vinu, A.; Ariga, K. Layer-by-Layer Films of Graphene and Ionic Liquids for Highly Selective Gas Sensing. *Angewandte Chemie-International Edition* **2010**, *49*, 9737-9739.
- (264) Kulkarni, D. D.; Choi, I.; Singamaneni, S. S.; Tsukruk, V. V. Graphene Oxide–Polyelectrolyte Nanomembranes. *ACS Nano* **2010**, *4*, 4667-4676.
- (265) Zeng, G.; Xing, Y.; Gao, J.; Wang, Z.; Zhang, X. Unconventional Layer-by-Layer Assembly of Graphene Multilayer Films for Enzyme-Based Glucose and Maltose Biosensing. *Langmuir* **2010**, *26*, 15022-15026.
- (266) Jeon, J.-W.; Kwon, S. R.; Lutkenhaus, J. L. Polyaniline nanofiber/electrochemically reduced graphene oxide layer-by-layer electrodes for electrochemical energy storage. *Journal of Materials Chemistry A* **2015**, *3*, 3757-3767.
- (267) Akihiko, Tanioka, Y. Y. a. H. W. a. J.-i. I. a. S. I. a. Y. K. a. K. T. a. H. M. a. M. A. a. T. M. a. M. M. a. Inkjet Printing of Graphene Nanoribbons for Organic Field-Effect Transistors. *Applied Physics Express* **2011**, *4*, 115101.
- (268) Torrisi, F.; Hasan, T.; Wu, W. P.; Sun, Z. P.; Lombardo, A.; Kulmala, T. S.; Hsieh, G. W.; Jung, S. J.; Bonaccorso, F.; Paul, P. J.; Chu, D. P.; Ferrari, A. C. Inkjet-Printed Graphene Electronics. *Acs Nano* **2012**, *6*, 2992-3006.
- (269) Sriprachuabwong, C.; Karuwan, C.; Wisitsorrat, A.; Phokharatkul, D.; Lomas, T.; Sritongkham, P.; Tuantranont, A. Inkjet-printed graphene-PEDOT:PSS modified screen printed carbon electrode for biochemical sensing. *Journal of Materials Chemistry* **2012**, *22*, 5478-5485.
- (270) Jang, D.; Kim, D.; Moon, J. Influence of Fluid Physical Properties on Ink-Jet Printability. *Langmuir* **2009**, *25*, 2629-2635.
- (271) Li, J. T.; Ye, F.; Vaziri, S.; Muhammed, M.; Lemme, M. C.; Ostling, M. Efficient Inkjet Printing of Graphene. *Advanced Materials* **2013**, *25*, 3985-3992.
- (272) Capasso, A.; Castillo, A. E. D.; Sun, H.; Ansaldo, A.; Pellegrini, V.; Bonaccorso, F. Ink-jet printing of graphene for flexible electronics: An environmentally-friendly approach. *Solid State Communications* **2015**, *224*, 53-63.
- (273) Huang, L.; Huang, Y.; Liang, J.; Wan, X.; Chen, Y. Graphene-based conducting inks for direct inkjet printing of flexible conductive patterns and their applications in electric circuits and chemical sensors. *Nano Research* **2011**, *4*, 675-684.
- (274) Shin, K.-Y.; Hong, J.-Y.; Jang, J. Flexible and transparent graphene films as acoustic actuator electrodes using inkjet printing. *Chemical Communications* **2011**, *47*, 8527-8529.

(275) Secor, E. B.; Hersam, M. C. Emerging Carbon and Post-Carbon Nanomaterial Inks for Printed Electronics. *The Journal of Physical Chemistry Letters* **2015**, *6*, 620-626.

(276) Gao, Y.; Shi, W.; Wang, W.; Leng, Y.; Zhao, Y. Inkjet Printing Patterns of Highly Conductive Pristine Graphene on Flexible Substrates. *Industrial & Engineering Chemistry Research* **2014**, *53*, 16777-16784.

(277) Secor, E. B.; Prabhumirashi, P. L.; Puntambekar, K.; Geier, M. L.; Hersam, M. C. Inkjet Printing of High Conductivity, Flexible Graphene Patterns. *The Journal of Physical Chemistry Letters* **2013**, *4*, 1347-1351.

(278) Majee, S.; Song, M.; Zhang, S.-L.; Zhang, Z.-B. Scalable inkjet printing of shear-exfoliated graphene transparent conductive films. *Carbon* **2016**, *102*, 51-57.

(279) Secor, E. B.; Ahn, B. Y.; Gao, T. Z.; Lewis, J. A.; Hersam, M. C. Rapid and Versatile Photonic Annealing of Graphene Inks for Flexible Printed Electronics. *Advanced Materials* **2015**, *27*, 6683-+.

(280) Putz, K. W.; Compton, O. C.; Segar, C.; An, Z.; Nguyen, S. T.; Brinson, L. C. Evolution of Order During Vacuum-Assisted Self-Assembly of Graphene Oxide Paper and Associated Polymer Nanocomposites. *ACS Nano* **2011**, *5*, 6601-6609.

(281) Dikin, D. A.; Stankovich, S.; Zimney, E. J.; Piner, R. D.; Dommett, G. H. B.; Evmenenko, G.; Nguyen, S. T.; Ruoff, R. S. Preparation and characterization of graphene oxide paper. *Nature* **2007**, *448*, 457-460.

(282) Compton, O. C.; Dikin, D. A.; Putz, K. W.; Brinson, L. C.; Nguyen, S. T. Electrically Conductive "Alkylated" Graphene Paper via Chemical Reduction of Amine-Functionalized Graphene Oxide Paper. *Advanced Materials* **2010**, *22*, 892-+.

(283) Cote, L. J.; Cruz-Silva, R.; Huang, J. Flash Reduction and Patterning of Graphite Oxide and Its Polymer Composite. *Journal of the American Chemical Society* **2009**, *131*, 11027-11032.

(284) Li, D.; Mueller, M. B.; Gilje, S.; Kaner, R. B.; Wallace, G. G. Processable aqueous dispersions of graphene nanosheets. *Nature Nanotechnology* **2008**, *3*, 101-105.

(285) Chen, H.; Mueller, M. B.; Gilmore, K. J.; Wallace, G. G.; Li, D. Mechanically strong, electrically conductive, and biocompatible graphene paper. *Advanced Materials* **2008**, *20*, 3557-+.

- (286) Putz, K. W.; Compton, O. C.; Palmeri, M. J.; Nguyen, S. T.; Brinson, L. C. High-Nanofiller-Content Graphene Oxide-Polymer Nanocomposites via Vacuum-Assisted Self-Assembly. *Advanced Functional Materials* **2010**, *20*, 3322-3329.
- (287) Malho, J.-M.; Laaksonen, P.; Walther, A.; Ikkala, O.; Linder, M. B. Facile Method for Stiff, Tough, and Strong Nanocomposites by Direct Exfoliation of Multilayered Graphene into Native Nanocellulose Matrix. *Biomacromolecules* **2012**, *13*, 1093-1099.
- (288) Valentini, L.; Cardinali, M.; Fortunati, E.; Torre, L.; Kenny, J. M. A novel method to prepare conductive nanocrystalline cellulose/graphene oxide composite films. *Materials Letters* **2013**, *105*, 4-7.
- (289) Xu, Y.; Bai, H.; Lu, G.; Li, C.; Shi, G. Flexible graphene films via the filtration of water-soluble noncovalent functionalized graphene sheets. *Journal of the American Chemical Society* **2008**, *130*, 5856-+.
- (290) Zhou, G.; Ye, Z.; Shi, W.; Liu, J.; Xi, F. Applications of Three Dimensional Graphene and Its Composite Materials. *Progress in Chemistry* **2014**, *26*, 950-960.
- (291) Yin, S.; Niu, Z.; Chen, X. Assembly of Graphene Sheets into 3D Macroscopic Structures. *Small* **2012**, *8*, 2458-2463.
- (292) Yavari, F.; Chen, Z.; Thomas, A. V.; Ren, W.; Cheng, H.-M.; Koratkar, N. High Sensitivity Gas Detection Using a Macroscopic Three-Dimensional Graphene Foam Network. *Scientific Reports* **2011**, *1*.
- (293) Peng, L.; Zheng, Y.; Li, J.; Jin, Y.; Gao, C. Monolithic Neat Graphene Oxide Aerogel for Efficient Catalysis of S \rightarrow O Acetyl Migration. *Acs Catalysis* **2015**, *5*, 3387-3392.
- (294) Wu, X.; Zhou, J.; Xing, W.; Wang, G.; Cui, H.; Zhuo, S.; Xue, Q.; Yan, Z.; Qiao, S. Z. High-rate capacitive performance of graphene aerogel with a superhigh C/O molar ratio. *Journal of Materials Chemistry* **2012**, *22*, 23186-23193.
- (295) Chen, Z.; Ren, W.; Gao, L.; Liu, B.; Pei, S.; Cheng, H.-M. Three-dimensional flexible and conductive interconnected graphene networks grown by chemical vapour deposition. *Nature Materials* **2011**, *10*, 424-428.
- (296) Zeng, Z.; Huang, X.; Yin, Z.; Li, H.; Chen, Y.; Li, H.; Zhang, Q.; Ma, J.; Boey, F.; Zhang, H. Fabrication of Graphene Nanomesh by Using an Anodic Aluminum Oxide Membrane as a Template. *Advanced Materials* **2012**, *24*, 4138-4142.

- (297) Ji, H.; Zhang, L.; Pettes, M. T.; Li, H.; Chen, S.; Shi, L.; Piner, R.; Ruoff, R. S. Ultrathin Graphite Foam: A Three-Dimensional Conductive Network for Battery Electrodes. *Nano Letters* **2012**, *12*, 2446-2451.
- (298) Wang, J.; Ellsworth, M. W. Graphene Aerogels. *Graphene and Emerging Materials for Post-Cmos Applications* **2009**, *19*, 241-247.
- (299) Ma, Y.; Chen, Y. Three-dimensional graphene networks: synthesis, properties and applications. *National Science Review* **2015**, *2*, 40-53.
- (300) Yang, Z.-Y.; Jin, L.-J.; Lu, G.-Q.; Xiao, Q.-Q.; Zhang, Y.-X.; Jing, L.; Zhang, X.-X.; Yan, Y.-M.; Sun, K.-N. Sponge-Templated Preparation of High Surface Area Graphene with Ultrahigh Capacitive Deionization Performance. *Advanced Functional Materials* **2014**, *24*, 3917-3925.
- (301) Cheng, C.; Li, D. Solvated Graphenes: An Emerging Class of Functional Soft Materials. *Advanced Materials* **2013**, *25*, 13-30.
- (302) Mungse, H. P.; Sharma, O. P.; Sugimura, H.; Khatri, O. P. Hydrothermal deoxygenation of graphene oxide in sub- and supercritical water. *Rsc Advances* **2014**, *4*, 22589-22595.
- (303) Choudhary, S.; Mungse, H. P.; Khatri, O. P. Hydrothermal Deoxygenation of Graphene Oxide: Chemical and Structural Evolution. *Chemistry-an Asian Journal* **2013**, *8*, 2070-2078.
- (304) Bai, H.; Li, C.; Wang, X.; Shi, G. On the Gelation of Graphene Oxide. *Journal of Physical Chemistry C* **2011**, *115*, 5545-5551.
- (305) Goldstein, A. P.; Mickelson, W.; Machness, A.; Lee, G.; Worsley, M. A.; Woo, L.; Zettl, A. Simultaneous Sheet Cross-Linking and Deoxygenation in the Graphene Oxide Sol-Gel Transition. *Journal of Physical Chemistry C* **2014**, *118*, 28855-28860.
- (306) Lv, W.; Tao, Y.; Ni, W.; Zhou, Z.; Su, F.-Y.; Chen, X.-C.; Jin, F.-M.; Yang, Q.-H. One-pot self-assembly of three-dimensional graphene macroassemblies with porous core and layered shell. *Journal of Materials Chemistry* **2011**, *21*, 12352-12357.
- (307) Li, C.; Shi, G. Functional Gels Based on Chemically Modified Graphenes. *Advanced Materials* **2014**, *26*, 3992-4012.
- (308) Bai, H.; Li, C.; Wang, X.; Shi, G. A pH-sensitive graphene oxide composite hydrogel. *Chemical Communications* **2010**, *46*, 2376-2378.

(309) Qin, S.-Y.; Liu, X.-J.; Zhuo, R.-X.; Zhang, X.-Z. Microstructure-Controllable Graphene Oxide Hydrogel Film Based on a pH-Responsive Graphene Oxide Hydrogel. *Macromolecular Chemistry and Physics* **2012**, *213*, 2044-2051.

(310) Niu, Z.; Liu, L.; Zhang, L.; Shao, Q.; Zhou, W.; Chen, X.; Xie, S. A Universal Strategy to Prepare Functional Porous Graphene Hybrid Architectures. *Advanced Materials* **2014**, *26*, 3681-3687.

(311) Wan, W.; Li, L.; Zhao, Z.; Hu, H.; Hao, X.; Winkler, D. A.; Xi, L.; Hughes, T. C.; Qiu, J. Ultrafast Fabrication of Covalently Cross-linked Multifunctional Graphene Oxide Monoliths. *Advanced Functional Materials* **2014**, *24*, 4915-4921.

(312) Cong, H.-P.; Ren, X.-C.; Wang, P.; Yu, S.-H. Macroscopic Multifunctional Graphene-Based Hydrogels and Aerogels by a Metal Ion Induced Self-Assembly Process. *Acs Nano* **2012**, *6*, 2693-2703.

(313) Srinivasan, S.; Je, S. H.; Back, S.; Barin, G.; Buyukcakir, O.; Guliyev, R.; Jung, Y.; Coskun, A. Ordered Supramolecular Gels Based on Graphene Oxide and Tetracationic Cyclophanes. *Advanced Materials* **2014**, *26*, 2725-2729.

(314) Worsley, M. A.; Olson, T. Y.; Lee, J. R. I.; Willey, T. M.; Nielsen, M. H.; Roberts, S. K.; Pauzauskie, P. J.; Biener, J.; Satcher, J. H., Jr.; Baumann, T. F. High Surface Area, sp²-Cross-Linked Three-Dimensional Graphene Monoliths. *Journal of Physical Chemistry Letters* **2011**, *2*, 921-925.

(315) Worsley, M. A.; Kucheyev, S. O.; Mason, H. E.; Merrill, M. D.; Mayer, B. P.; Lewicki, J.; Valdez, C. A.; Suss, M. E.; Stadermann, M.; Pauzauskie, P. J.; Satcher, J. H., Jr.; Biener, J.; Baumann, T. F. Mechanically robust 3D graphene macroassembly with high surface area. *Chemical Communications* **2012**, *48*, 8428-8430.

(316) Worsley, M. A.; Charnvanichborikarn, S.; Montalvo, E.; Shin, S. J.; Tylski, E. D.; Lewicki, J. P.; Nelson, A. J.; Satcher, J. H., Jr.; Biener, J.; Baumann, T. F.; Kucheyev, S. O. Toward Macroscale, Isotropic Carbons with Graphene-Sheet-Like Electrical and Mechanical Properties. *Advanced Functional Materials* **2014**, *24*, 4259-4264.

(317) Chen, W.; Yan, L. In situ self-assembly of mild chemical reduction graphene for three-dimensional architectures. *Nanoscale* **2011**, *3*, 3132-3137.

(318) Chen, M.; Zhang, C.; Li, X.; Zhang, L.; Ma, Y.; Zhang, L.; Xu, X.; Xia, F.; Wang, W.; Gao, J. A one-step method for reduction and self-assembling of graphene oxide into reduced graphene oxide aerogels. *Journal of Materials Chemistry A* **2013**, *1*, 2869-2877.

- (319) Qiu, L.; Liu, J. Z.; Chang, S. L. Y.; Wu, Y.; Li, D. Biomimetic superelastic graphene-based cellular monoliths. *Nature Communications* **2012**, *3*.
- (320) Huang, Y.; Liang, J.; Chen, Y. An Overview of the Applications of Graphene-Based Materials in Supercapacitors. *Small* **2012**, *8*, 1805-1834.
- (321) Liu, Y.; Dong, X.; Chen, P. Biological and chemical sensors based on graphene materials. *Chemical Society Reviews* **2012**, *41*, 2283-2307.
- (322) Huang, X.; Qi, X.; Boey, F.; Zhang, H. Graphene-based composites. *Chemical Society Reviews* **2012**, *41*, 666-686.
- (323) Schwierz, F. Graphene transistors. *Nat Nano* **2010**, *5*, 487-496.
- (324) Park, S.; An, J.; Jung, I.; Piner, R. D.; An, S. J.; Li, X.; Velamakanni, A.; Ruoff, R. S. Colloidal Suspensions of Highly Reduced Graphene Oxide in a Wide Variety of Organic Solvents. *Nano Letters* **2009**, *9*, 1593-1597.
- (325) Zhu, Y.; Murali, S.; Cai, W.; Li, X.; Suk, J. W.; Potts, J. R.; Ruoff, R. S. Graphene and Graphene Oxide: Synthesis, Properties, and Applications. *Advanced Materials* **2010**, *22*, 3906-3924.
- (326) Tung, V. C.; Allen, M. J.; Yang, Y.; Kaner, R. B. High-throughput solution processing of large-scale graphene. *Nature Nanotechnology* **2009**, *4*, 25-29.
- (327) Vadukumpully, S.; Paul, J.; Valiyaveetil, S. Cationic surfactant mediated exfoliation of graphite into graphene flakes. *Carbon* **2009**, *47*, 3288-3294.
- (328) Das, S.; Kin, F.; Ahmed, H. S. T.; Cortinas, A. B.; Wajid, A. S.; Parviz, D.; Jankowski, A. F.; Kato, M.; Green, M. J. Non-covalent functionalization of pristine few-layer graphene using triphenylene derivatives for conductive poly (vinyl alcohol) composites. *Polymer* **2012**, *53*, 2485-2494.
- (329) Etika, K. C.; Jochum, F. D.; Cox, M. A.; Schattling, P.; Theato, P.; Grunlan, J. C. Tailoring Properties of Carbon Nanotube Dispersions and Nanocomposites Using Temperature-Responsive Copolymers of Pyrene-Modified Poly(N-cyclopropylacrylamide). *Macromolecules* **2010**, *43*, 9447-9453.
- (330) Fujigaya, T.; Nakashima, N. Methodology for homogeneous dispersion of single-walled carbon nanotubes by physical modification. *Polymer Journal* **2008**, *40*, 577-589.
- (331) Su, Q.; Pang, S.; Alijani, V.; Li, C.; Feng, X.; Muellen, K. Composites of Graphene with Large Aromatic Molecules. *Advanced Materials* **2009**, *21*, 3191-+.

(332) Jang, J.-H.; Rangappa, D.; Kwon, Y.-U.; Honma, I. Direct preparation of 1-PSA modified graphene nanosheets by supercritical fluidic exfoliation and its electrochemical properties. *Journal of Materials Chemistry* **2011**, *21*, 3462-3466.

(333) Bjoerk, J.; Hanke, F.; Palma, C.-A.; Samori, P.; Cecchini, M.; Persson, M. Adsorption of Aromatic and Anti-Aromatic Systems on Graphene through pi-pi Stacking. *Journal of Physical Chemistry Letters* **2010**, *1*, 3407-3412.

(334) Ershova, O. V.; Lillestolen, T. C.; Bichoutskaia, E. Study of polycyclic aromatic hydrocarbons adsorbed on graphene using density functional theory with empirical dispersion correction. *Physical Chemistry Chemical Physics* **2010**, *12*, 6483-6491.

(335) Hunter, R. J.: *Zeta potential in colloid science : principles and applications*; 2 ed.; Academic Press, 1981.

(336) Vigolo, B.; Penicaud, A.; Coulon, C.; Sauder, C.; Pailier, R.; Journet, C.; Bernier, P.; Poulin, P. Macroscopic fibers and ribbons of oriented carbon nanotubes. *Science* **2000**, *290*.

(337) Sun, Z.; Masa, J.; Liu, Z.; Schuhmann, W.; Muhler, M. Highly Concentrated Aqueous Dispersions of Graphene Exfoliated by Sodium Taurodeoxycholate: Dispersion Behavior and Potential Application as a Catalyst Support for the Oxygen-Reduction Reaction. *Chemistry-a European Journal* **2012**, *18*.

(338) Teng, C.-C.; Ma, C.-C. M.; Lu, C.-H.; Yang, S.-Y.; Lee, S.-H.; Hsiao, M.-C.; Yen, M.-Y.; Chiou, K.-C.; Lee, T.-M. Thermal conductivity and structure of non-covalent functionalized graphene/epoxy composites. *Carbon* **2011**, *49*, 5107-5116.

(339) Wang, H.; Chen, Z.; Xin, L.; Cui, J.; Zhao, S.; Yan, Y. Synthesis of pyrene-capped polystyrene by free radical polymerization and its application in direct exfoliation of graphite into graphene nanosheets. *Journal of Polymer Science Part a-Polymer Chemistry* **2015**, *53*, 2175-2185.

(340) Li, D.; Muller, M. B.; Gilje, S.; Kaner, R. B.; Wallace, G. G. Processable aqueous dispersions of graphene nanosheets. *Nat Nano* **2008**, *3*, 101-105.

(341) Parviz, D.; Yu, Z.; Hedden, R. C.; Green, M. J. Designer stabilizer for preparation of pristine graphene/polysiloxane films and networks. *Nanoscale* **2014**, *6*, 11722-11731.

(342) Luo, C.; Zuo, X.; Wang, L.; Wang, E.; Song, S.; Wang, J.; Wang, J.; Fan, C.; Cao, Y. Flexible Carbon Nanotube-Polymer Composite Films with High Conductivity and Superhydrophobicity Made by Solution Process. *Nano Letters* **2008**, *8*, 4454-4458.

- (343) Kujawski, M.; Pearse, J. D.; Smela, E. Elastomers filled with exfoliated graphite as compliant electrodes. *Carbon* **2010**, *48*, 2409-2417.
- (344) Chen, L.; Chen, G.; Lu, L. Piezoresistive behavior study on finger-sensing silicone rubber/graphite nanosheet nanocomposites. *Advanced Functional Materials* **2007**, *17*, 898-904.
- (345) Raza, M. A.; Westwood, A.; Brown, A.; Hondow, N.; Stirling, C. Characterisation of graphite nanoplatelets and the physical properties of graphite nanoplatelet/silicone composites for thermal interface applications. *Carbon* **2011**, *49*, 4269-4279.
- (346) Ozbas, B.; O'Neill, C. D.; Register, R. A.; Aksay, I. A.; Prud'homme, R. K.; Adamson, D. H. Multifunctional elastomer nanocomposites with functionalized graphene single sheets. *Journal of Polymer Science Part B-Polymer Physics* **2012**, *50*, 910-916.
- (347) Xu, P.; Loomis, J.; Bradshaw, R. D.; Panchapakesan, B. Load transfer and mechanical properties of chemically reduced graphene reinforcements in polymer composites. *Nanotechnology* **2012**, *23*.
- (348) Guimont, A.; Beyou, E.; Alcouffe, P.; Martin, G.; Sonntag, P.; Cassagnau, P. Synthesis and characterization of PDMS-grafted graphite oxide sheets. *Polymer* **2013**, *54*, 4830-4837.
- (349) Gao, J.; Shen, K.; Bao, F.; Yin, J.; Wang, D.; Ma, R.; Yan, C.; Chen, T.; Wang, G.; Liu, X.; Zhang, X.; Zhang, D. Preparation and Characterization of a Graphene Oxide Film Modified by the Covalent Attachment of Polysiloxane. *Polymer-Plastics Technology and Engineering* **2013**, *52*, 553-557.
- (350) Hou, Y.; Wang, D.; Zhang, X.-M.; Zhao, H.; Zha, J.-W.; Dang, Z.-M. Positive piezoresistive behavior of electrically conductive alkyl-functionalized graphene/polydimethylsilicone nanocomposites. *Journal of Materials Chemistry C* **2013**, *1*, 515-521.
- (351) Chen, M.; Tao, T.; Zhang, L.; Gao, W.; Li, C. Highly conductive and stretchable polymer composites based on graphene/MWCNT network. *Chemical Communications* **2013**, *49*, 1612-1614.
- (352) Powell, D. B.; Sheppard, N. Nuclear magnetic resonance and infrared spectroscopic evidence for the structure of some metal-olefin complexes. *Journal of the Chemical Society* **1960**, 2519-2521.
- (353) Wertz, D.W.; Bouian, D. F.; Hazouri, M. J. . *Spectrochimica Acta* **1973**, *29* A, 1439-1449.

- (354) Zaman, I.; Kuan, H.-C.; Meng, Q.; Michelmore, A.; Kawashima, N.; Pitt, T.; Zhang, L.; Gouda, S.; Luong, L.; Ma, J. A Facile Approach to Chemically Modified Graphene and its Polymer Nanocomposites. *Advanced Functional Materials* **2012**, *22*, 2735-2743.
- (355) Martin-Gallego, M.; Hernandez, M.; Lorenzo, V.; Verdejo, R.; Lopez-Manchado, M. A.; Sangermano, M. Cationic photocured epoxy nanocomposites filled with different carbon fillers. *Polymer* **2012**, *53*, 1831-1838.
- (356) Mao, C.; Zhu, Y.; Jiang, W. Design of Electrical Conductive Composites: Tuning the Morphology to Improve the Electrical Properties of Graphene Filled Immiscible Polymer Blends. *ACS Applied Materials & Interfaces* **2012**, *4*, 5281-5286.
- (357) Alekseev, A.; Chen, D. L.; Tkalya, E. E.; Ghislandi, M. G.; Syurik, Y.; Ageev, O.; Loos, J.; de With, G. Local Organization of Graphene Network Inside Graphene/Polymer Composites. *Advanced Functional Materials* **2012**, *22*, 1311-1318.
- (358) Alsharaeh, E. H.; Othman, A. A.; Aldosari, M. A. Microwave Irradiation Effect on the Dispersion and Thermal Stability of RGO Nanosheets within a Polystyrene Matrix. *Materials* **2014**, *7*, 5212-5224.
- (359) Bao, C. L.; Song, L.; Wilkie, C. A.; Yuan, B. H.; Guo, Y. Q.; Hu, Y.; Gong, X. L. Graphite oxide, graphene, and metal-loaded graphene for fire safety applications of polystyrene. *Journal of Materials Chemistry* **2012**, *22*, 16399-16406.
- (360) Basu, S.; Singhi, M.; Satapathy, B. K.; Fahim, M. Dielectric, Electrical, and Rheological Characterization of Graphene-Filled Polystyrene Nanocomposites. *Polymer Composites* **2013**, *34*, 2082-2093.
- (361) Chen, X. Y.; Shi, Y. L.; Yang, D.; Hu, J. H.; Yang, P. Y. Preparation of Polystyrene Functionalized Graphene by Atom Transfer Nitroxide Radical Coupling Reaction. *Acta Chimica Sinica* **2012**, *70*, 817-821.
- (362) Compton, O. C.; Kim, S.; Pierre, C.; Torkelson, J. M.; Nguyen, S. T. Crumpled Graphene Nanosheets as Highly Effective Barrier Property Enhancers. *Advanced Materials* **2010**, *22*, 4759-+.
- (363) Fan, W.; Zhang, C.; Tjiu, W. W.; Liu, T. X. Fabrication of electrically conductive graphene/polystyrene composites via a combination of latex and layer-by-layer assembly approaches. *Journal of Materials Research* **2013**, *28*, 611-619.
- (364) Fang, M.; Wang, K. G.; Lu, H. B.; Yang, Y. L.; Nutt, S. Single-layer graphene nanosheets with controlled grafting of polymer chains. *Journal of Materials Chemistry* **2010**, *20*, 1982-1992.

(365) Gu, R. P.; Xu, W. Z.; Charpentier, P. A. Synthesis of graphene-polystyrene nanocomposites via RAFT polymerization. *Polymer* **2014**, *55*, 5322-5331.

(366) Han, Y. Q.; Wu, Y.; Shen, M. X.; Huang, X. L.; Zhu, J. J.; Zhang, X. G. Preparation and properties of polystyrene nanocomposites with graphite oxide and graphene as flame retardants. *Journal of Materials Science* **2013**, *48*, 4214-4222.

(367) Heeder, N.; Yussuf, A.; Guo, F.; Chakraborty, I.; Godfrin, M. P.; Hurt, R.; Tripathi, A.; Bose, A.; Shukla, A. Highly conductive graphene-based segregated composites prepared by particle templating. *Journal of Materials Science* **2014**, *49*, 2567-2570.

(368) Hu, H. T.; Wang, X. B.; Wang, J. C.; Wan, L.; Liu, F. M.; Zheng, H.; Chen, R.; Xu, C. H. Preparation and properties of graphene nanosheets-polystyrene nanocomposites via in situ emulsion polymerization. *Chemical Physics Letters* **2010**, *484*, 247-253.

(369) Kattimuttathu, S. I.; Krishnappan, C.; Vellorathekkaepadil, V.; Nutenki, R.; Mandapati, V. R.; Cernik, M. Synthesis, characterization and optical properties of graphene oxide-polystyrene nanocomposites. *Polymers for Advanced Technologies* **2015**, *26*, 214-222.

(370) Kim, S. D.; Zhang, W. L.; Choi, H. J. Pickering emulsion-fabricated polystyrene-graphene oxide microspheres and their electrorheology. *Journal of Materials Chemistry C* **2014**, *2*, 7541-7546.

(371) Lee, J.; Yun, Y. S.; Kim, D. H.; Park, H. H.; Jin, H. J. Nanocomposites of Polystyrene/Polystyrene-Grafted Graphene Oxides Synthesized by In-Situ Bulk Polymerization. *Journal of Nanoscience and Nanotechnology* **2013**, *13*, 1769-1772.

(372) Li, B. P.; Hou, W. P.; Sun, J. H.; Jiang, S. D.; Xu, L. L.; Li, G. X.; Memon, M. A.; Cao, J. H.; Huang, Y.; Bielawski, C. W.; Geng, J. X. Tunable Functionalization of Graphene Oxide Sheets through Surface-Initiated Cationic Polymerization. *Macromolecules* **2015**, *48*, 994-1001.

(373) Li, Y.; Wang, Z. Q.; Yang, L.; Gu, H.; Xue, G. Efficient coating of polystyrene microspheres with graphene nanosheets. *Chemical Communications* **2011**, *47*, 10722-10724.

(374) Li, Y. H.; Zhou, L. K.; Li, C. Q.: The preparation, morphology and electrical properties of polystyrene/graphene nanocomposite foams using supercritical carbon dioxide. In *Materials in Industry and Nanotechnology*; Xu, B., Li, H. Y., Eds.; Advanced Materials Research, 2013; Vol. 771; pp 51-54.

(375) Liu, Y. T.; Yang, J. M.; Xie, X. M.; Ye, X. Y. Polystyrene-grafted graphene with improved solubility in organic solvents and its compatibility with polymers. *Materials Chemistry and Physics* **2011**, *130*, 794-799.

(376) Nasirpour, F.; Pourmahmoudi, H.; Abbasi, F.; Littlejohn, S.; Chauhan, A. S.; Nogaret, A. Modification of Chemically Exfoliated Graphene to Produce Efficient Piezoresistive Polystyrene-Graphene Composites. *Journal of Electronic Materials* **2015**, *44*, 3512-3522.

(377) Oxfall, H.; Rondin, J.; Bouquey, M.; Muller, R.; Rigdahl, M.; Rychwalski, R. W. Elongational flow mixing for manufacturing of graphite nanoplatelet/polystyrene composites. *Journal of Applied Polymer Science* **2013**, *128*, 2679-2686.

(378) Park, W.; Hu, J. N.; Jauregui, L. A.; Ruan, X. L.; Chen, Y. P. Electrical and thermal conductivities of reduced graphene oxide/polystyrene composites. *Applied Physics Letters* **2014**, *104*.

(379) Pham, V. H.; Cuong, T. V.; Dang, T. T.; Hur, S. H.; Kong, B. S.; Kim, E. J.; Shin, E. W.; Chung, J. S. Superior conductive polystyrene - chemically converted graphene nanocomposite. *Journal of Materials Chemistry* **2011**, *21*, 11312-11316.

(380) Qi, X. Y.; Yan, D.; Jiang, Z. G.; Cao, Y. K.; Yu, Z. Z.; Yavari, F.; Koratkar, N. Enhanced Electrical Conductivity in Polystyrene Nanocomposites at Ultra-Low Graphene Content. *Acs Applied Materials & Interfaces* **2011**, *3*, 3130-3133.

(381) Ren, L. L.; Wang, X. Y.; Guo, S. Z.; Liu, T. X. Functionalization of thermally reduced graphene by in situ atom transfer radical polymerization. *Journal of Nanoparticle Research* **2011**, *13*, 6389-6396.

(382) Ren, P. G.; Yan, D. X.; Chen, T.; Zeng, B. Q.; Li, Z. M. Improved Properties of Highly Oriented Graphene/Polymer Nanocomposites. *Journal of Applied Polymer Science* **2011**, *121*, 3167-3174.

(383) Rissanou, A. N.; Harmandaris, V. Dynamics of various polymer-graphene interfacial systems through atomistic molecular dynamics simulations. *Soft Matter* **2014**, *10*, 2876-2888.

(384) Rissanou, A. N.; Harmandaris, V. Structural and Dynamical Properties of Polystyrene Thin Films Supported by Multiple Graphene Layers. *Macromolecules* **2015**, *48*, 2761-2772.

(385) Roghani-Mamaqani, H. Surface-initiated ATRP of styrene from epoxy groups of graphene nanolayers: twofold polystyrene chains and various graft densities. *Rsc Advances* **2015**, *5*, 53357-53368.

(386) Shen, B.; Zhai, W. T.; Chen, C.; Lu, D. D.; Wang, J.; Zheng, W. G. Melt Blending In situ Enhances the Interaction between Polystyrene and Graphene through pi-pi Stacking. *Acs Applied Materials & Interfaces* **2011**, *3*, 3103-3109.

(387) Steenackers, M.; Gigler, A. M.; Zhang, N.; Deubel, F.; Seifert, M.; Hess, L. H.; Lim, C.; Loh, K. P.; Garrido, J. A.; Jordan, R.; Stutzmann, M.; Sharp, I. D. Polymer Brushes on Graphene. *Journal of the American Chemical Society* **2011**, *133*, 10490-10498.

(388) Sun, S. T.; Cao, Y. W.; Feng, J. C.; Wu, P. Y. Click chemistry as a route for the immobilization of well-defined polystyrene onto graphene sheets. *Journal of Materials Chemistry* **2010**, *20*, 5605-5607.

(389) Syurik, J.; Ageev, O. A.; Cherednichenko, D. I.; Konoplev, B. G.; Alexeev, A. Non-linear conductivity dependence on temperature in graphene-based polymer nanocomposite. *Carbon* **2013**, *63*, 317-323.

(390) Syurik, Y. V.; Ghislandi, M. G.; Tkalya, E. E.; Paterson, G.; McGrouther, D.; Ageev, O. A.; Loos, J. Graphene Network Organisation in Conductive Polymer Composites. *Macromolecular Chemistry and Physics* **2012**, *213*, 1251-1258.

(391) Tang, L. C.; Wang, X.; Gong, L. X.; Peng, K.; Zhao, L.; Chen, Q.; Wu, L. B.; Jiang, J. X.; Lai, G. Q. Creep and recovery of polystyrene composites filled with graphene additives. *Composites Science and Technology* **2014**, *91*, 63-70.

(392) Tkalya, E.; Ghislandi, M.; Alekseev, A.; Koning, C.; Loos, J. Latex-based concept for the preparation of graphene-based polymer nanocomposites. *Journal of Materials Chemistry* **2010**, *20*, 3035-3039.

(393) Tkalya, E.; Ghislandi, M.; Otten, R.; Lotya, M.; Alekseev, A.; van der Schoot, P.; Coleman, J.; de With, G.; Koning, C. Experimental and Theoretical Study of the Influence of the State of Dispersion of Graphene on the Percolation Threshold of Conductive Graphene/Polystyrene Nanocomposites. *Acs Applied Materials & Interfaces* **2014**, *6*, 15113-15121.

(394) Wang, C.; Chiu, Y. C. Isothermal crystallization of syndiotactic polystyrene induced by graphene nanosheets and carbon nanotubes: a comparative study. *Journal of Polymer Research* **2015**, *22*.

(395) Wang, C.; Chiu, Y. C.; Huang, C. L. Electrical percolation and crystallization kinetics of semi-crystalline polystyrene composites filled with graphene nanosheets. *Materials Chemistry and Physics* **2015**, *164*, 206-213.

(396) Wang, H. N.; Chen, Z.; Xin, L. X.; Cui, J.; Zhao, S.; Yan, Y. H. Synthesis of pyrene-capped polystyrene by free radical polymerization and its application in direct

exfoliation of graphite into graphene nanosheets. *Journal of Polymer Science Part a-Polymer Chemistry* **2015**, *53*, 2175-2185.

(397) Wu, N.; She, X. L.; Yang, D. J.; Wu, X. F.; Su, F. B.; Chen, Y. F. Synthesis of network reduced graphene oxide in polystyrene matrix by a two-step reduction method for superior conductivity of the composite. *Journal of Materials Chemistry* **2012**, *22*, 17254-17261.

(398) Wu, X. L.; Liu, P. Facile preparation and characterization of graphene nanosheets/polystyrene composites. *Macromolecular Research* **2010**, *18*, 1008-1012.

(399) Xie, P. F.; Ge, X. P.; Fang, B.; Li, Z.; Liang, Y.; Yang, C. Z. Pickering emulsion polymerization of graphene oxide-stabilized styrene. *Colloid and Polymer Science* **2013**, *291*, 1631-1639.

(400) Yan, D. X.; Pang, H.; Li, B.; Vajtai, R.; Xu, L.; Ren, P. G.; Wang, J. H.; Li, Z. M. Structured Reduced Graphene Oxide/Polymer Composites for Ultra-Efficient Electromagnetic Interference Shielding. *Advanced Functional Materials* **2015**, *25*, 559-566.

(401) Yan, D. X.; Ren, P. G.; Pang, H.; Fu, Q.; Yang, M. B.; Li, Z. M. Efficient electromagnetic interference shielding of lightweight graphene/polystyrene composite. *Journal of Materials Chemistry* **2012**, *22*, 18772-18774.

(402) Yang, J. T.; Huang, L. Q.; Li, L. L.; Zhang, Y. F.; Chen, F.; Zhong, M. Q. Preparation of polystyrene/graphene oxide composites and their supercritical carbon dioxide foaming. *Journal of Polymer Research* **2013**, *20*.

(403) Yeole, N.; Kutcherlapati, S. N. R.; Jana, T. Polystyrene-graphene oxide (GO) nanocomposite synthesized by interfacial interactions between RAFT modified GO and core-shell polymeric nanoparticles. *Journal of Colloid and Interface Science* **2015**, *443*, 137-142.

(404) Yeom, H. Y.; Na, H. Y.; Lee, S. J. Influence of Graphene Oxide and Graphite Nanoplatelets on Rheological and Electrical Properties of Polystyrene Nanocomposites. *Polymer-Korea* **2014**, *38*, 502-509.

(405) Yin, G. N.; Zheng, Z.; Wang, H. T.; Du, Q. G.; Zhang, H. D. Preparation of graphene oxide coated polystyrene microspheres by Pickering emulsion polymerization. *Journal of Colloid and Interface Science* **2013**, *394*, 192-198.

(406) Yu, Y. H.; Lin, Y. Y.; Lin, C. H.; Chan, C. C.; Huang, Y. C. High-performance polystyrene/graphene-based nanocomposites with excellent anti-corrosion properties. *Polymer Chemistry* **2014**, *5*, 535-550.

- (407) Zhang, L. Y.; Shi, T. J.; Wu, S. L.; Zhou, H. O. Graphene/polystyrene nanocomposites synthesized via Pickering emulsion polymerization. *High Performance Polymers* **2014**, *26*, 156-165.
- (408) Zhao, P. F.; Luo, Y. Y.; Yang, J. L.; He, D. N.; Kong, L. X.; Zheng, P.; Yang, Q. Electrically conductive graphene-filled polymer composites with well organized three-dimensional microstructure. *Materials Letters* **2014**, *121*, 74-77.
- (409) Aldosari, M. A.; Othman, A. A.; Alsharaeh, E. H. Synthesis and Characterization of the in Situ Bulk Polymerization of PMMA Containing Graphene Sheets Using Microwave Irradiation. *Molecules* **2013**, *18*, 3152-3167.
- (410) Chang, K. C.; Ji, W. F.; Lai, M. C.; Hsiao, Y. R.; Hsu, C. H.; Chuang, T. L.; Wei, Y.; Yeh, J. M.; Liu, W. R. Synergistic effects of hydrophobicity and gas barrier properties on the anticorrosion property of PMMA nanocomposite coatings embedded with graphene nanosheets. *Polymer Chemistry* **2014**, *5*, 1049-1056.
- (411) Dai, J.; Lang, M. D. Preparation and Mechanical Properties of Graphene Oxide/PMMA and Surface-functionalized Graphene/PMMA Composites. *Acta Chimica Sinica* **2012**, *70*, 1237-1244.
- (412) Das, B.; Prasad, K. E.; Ramamurty, U.; Rao, C. N. R. Nano-indentation studies on polymer matrix composites reinforced by few-layer graphene. *Nanotechnology* **2009**, *20*.
- (413) Fan, Z.; Gong, F.; Nguyen, S. T.; Duong, H. M. Advanced multifunctional graphene aerogel - Poly (methyl methacrylate) composites: Experiments and modeling. *Carbon* **2015**, *81*, 396-404.
- (414) Feng, L.; Guan, G. H.; Li, C. C.; Zhang, D.; Xiao, Y. N.; Zheng, L. C.; Zhu, W. X. In situ Synthesis of Poly(methyl methacrylate)/Graphene Oxide Nanocomposites Using Thermal-initiated and Graphene Oxide-initiated Polymerization. *Journal of Macromolecular Science Part a-Pure and Applied Chemistry* **2013**, *50*, 720-727.
- (415) Goncalves, G.; Marques, P. A. A. P.; Barros-Timmons, A.; Bdkin, I.; Singh, M. K.; Emami, N.; Gracio, J. Graphene oxide modified with PMMA via ATRP as a reinforcement filler. *Journal of Materials Chemistry* **2010**, *20*, 9927-9934.
- (416) Heo, S.; Cho, S. Y.; Kim, D. H.; Choi, Y.; Park, H. H.; Jin, H. J. Improved Thermal Properties of Graphene Oxide-Incorporated Poly(methyl methacrylate) Microspheres. *Journal of Nanoscience and Nanotechnology* **2012**, *12*, 5990-5994.

(417) Hu, X. J.; Su, E. Q.; Zhu, B. C.; Jia, J. J.; Yao, P. H.; Bai, Y. X. Preparation of silanized graphene/poly(methyl methacrylate) nanocomposites in situ copolymerization and its mechanical properties. *Composites Science and Technology* **2014**, *97*, 6-11.

(418) Jang, J. Y.; Jeong, H. M.; Kim, B. K. Compatibilizing Effect of Graphite Oxide in Graphene/PMMA Nanocomposites. *Macromolecular Research* **2009**, *17*, 626-628.

(419) Ji, W. F.; Chang, K. C.; Lai, M. C.; Li, C. W.; Hsu, S. C.; Chuang, T. L.; Yeh, J. M.; Liu, W. R. Preparation and comparison of the physical properties of PMMA/thermally reduced graphene oxides composites with different carboxylic group content of thermally reduced graphene oxides. *Composites Part a-Applied Science and Manufacturing* **2014**, *65*, 108-114.

(420) Jiang, S. H.; Gui, Z.; Bao, C. L.; Dai, K.; Wang, X.; Zhou, K. Q.; Shi, Y. Q.; Lo, S. M.; Hu, Y. Preparation of functionalized graphene by simultaneous reduction and surface modification and its polymethyl methacrylate composites through latex technology and melt blending. *Chemical Engineering Journal* **2013**, *226*, 326-335.

(421) Ju, S. P.; Wang, Y. C.; Huang, G. J.; Chang, J. W. Miscibility of graphene and poly(methyl methacrylate) (PMMA): molecular dynamics and dissipative particle dynamics simulations. *Rsc Advances* **2013**, *3*, 8298-8307.

(422) Khezerlou, H.; Tahmasebipour, M. Molecular Dynamic Simulation of Graphene-Poly Methyl Methacrylate Nano-Composite. *Journal of Nanoelectronics and Optoelectronics* **2014**, *9*, 580-583.

(423) Kuila, T.; Bose, S.; Khanra, P.; Kim, N. H.; Rhee, K. Y.; Lee, J. H. Characterization and properties of in situ emulsion polymerized poly(methyl methacrylate)/graphene nanocomposites. *Composites Part a-Applied Science and Manufacturing* **2011**, *42*, 1856-1861.

(424) Kumar, M.; Chung, J. S.; Hur, S. H. Controlled atom transfer radical polymerization of MMA onto the surface of high-density functionalized graphene oxide. *Nanoscale Research Letters* **2014**, *9*.

(425) Li, X. G.; McKenna, G. B. Considering Viscoelastic Micromechanics for the Reinforcement of Graphene Polymer Nanocomposites. *Acs Macro Letters* **2012**, *1*, 388-391.

(426) Li, Y. L.; Kuan, C. F.; Chen, C. H.; Kuan, H. C.; Yip, M. C.; Chiu, S. L.; Chiang, C. L. Preparation, thermal stability and electrical properties of PMMA/functionalized graphene oxide nanosheets composites. *Materials Chemistry and Physics* **2012**, *134*, 677-685.

- (427) Liao, K. H.; Aoyama, S.; Abdala, A. A.; Macosko, C. Does Graphene Change T-g of Nanocomposites? *Macromolecules* **2014**, *47*, 8311-8319.
- (428) Liao, K. H.; Kobayashi, S.; Kim, H.; Abdala, A. A.; Macosko, C. W. Influence of Functionalized Graphene Sheets on Modulus and Glass Transition of PMMA. *Macromolecules* **2014**, *47*, 7674-7676.
- (429) Liu, F.; Hu, N.; Ning, H. M.; Liu, Y. L.; Li, Y.; Wu, L. K. Molecular dynamics simulation on interfacial mechanical properties of polymer nanocomposites with wrinkled graphene. *Computational Materials Science* **2015**, *108*, 160-167.
- (430) Meng, Q. S.; Kuan, H. C.; Araby, S.; Kawashima, N.; Saber, N.; Wang, C. H.; Ma, J. Effect of interface modification on PMMA/graphene nanocomposites. *Journal of Materials Science* **2014**, *49*, 5838-5849.
- (431) Mohamadi, S.; Sharifi-Sanjani, N.; Mahdavi, H. Functionalization of Graphene Sheets via Chemically Grafting of PMMA Chains Through in-situ Polymerization. *Journal of Macromolecular Science Part a-Pure and Applied Chemistry* **2011**, *48*, 577-582.
- (432) Pramoda, K. P.; Hussain, H.; Koh, H. M.; Tan, H. R.; He, C. B. Covalent Bonded Polymer-Graphene Nanocomposites. *Journal of Polymer Science Part a-Polymer Chemistry* **2010**, *48*, 4262-4267.
- (433) Rissanou, A. N.; Harmandaris, V. Structure and dynamics of poly(methylmethacrylate)/graphene systems through atomistic molecular dynamics simulations. *Journal of Nanoparticle Research* **2013**, *15*.
- (434) Roghani-Mamaqani, H.; Haddadi-Asl, V.; Sobhkhiz, Z.; Ghaderi-Ghahfarrokhi, M. Grafting poly (methyl methacrylate) from azo-functionalized graphene nanolayers via reverse atom transfer radical polymerization. *Colloid and Polymer Science* **2015**, *293*, 735-750.
- (435) Sheng, X. X.; Xie, D. L.; Cai, W. X.; Zhang, X. Y.; Zhong, L.; Zhang, H. P. In Situ Thermal Reduction of Graphene Nanosheets Based Poly(methyl methacrylate) Nanocomposites with Effective Reinforcements. *Industrial & Engineering Chemistry Research* **2015**, *54*, 649-658.
- (436) Skountzos, E. N.; Anastassiou, A.; Mavrantzas, V. G.; Theodorou, D. N. Determination of the Mechanical Properties of a Poly(methyl methacrylate) Nanocomposite with Functionalized Graphene Sheets through Detailed Atomistic Simulations. *Macromolecules* **2014**, *47*, 8072-8088.

(437) Song, J. L.; Zhang, J. X.; Lin, C. L. Influence of Graphene Oxide on the Tribological and Electrical Properties of PMMA Composites. *Journal of Nanomaterials* **2013**.

(438) Song, S. Q.; Wan, C. Y.; Zhang, Y. Non-covalent functionalization of graphene oxide by pyrene-block copolymers for enhancing physical properties of poly(methyl methacrylate). *Rsc Advances* **2015**, *5*, 79947-79955.

(439) Thomassin, J. M.; Trifkovic, M.; Alkarmo, W.; Detrembleur, C.; Jerome, C.; Macosko, C. Poly(methyl methacrylate)/Graphene Oxide Nanocomposites by a Precipitation Polymerization Process and Their Dielectric and Rheological Characterization. *Macromolecules* **2014**, *47*, 2149-2155.

(440) Tripathi, S. N.; Saini, P.; Gupta, D.; Choudhary, V. Electrical and mechanical properties of PMMA/reduced graphene oxide nanocomposites prepared via in situ polymerization. *Journal of Materials Science* **2013**, *48*, 6223-6232.

(441) Valles, C.; Kinloch, I. A.; Young, R. J.; Wilson, N. R.; Rourke, J. P. Graphene oxide and base-washed graphene oxide as reinforcements in PMMA nanocomposites. *Composites Science and Technology* **2013**, *88*, 158-164.

(442) Vo, N. H.; Dao, T. D.; Jeong, H. M. Electrically Conductive Graphene/Poly(methyl methacrylate) Composites with Ultra-Low Percolation Threshold by Electrostatic Self-Assembly in Aqueous Medium. *Macromolecular Chemistry and Physics* **2015**, *216*, 770-782.

(443) Vuluga, D.; Thomassin, J. M.; Molenberg, I.; Huynen, I.; Gilbert, B.; Jerome, C.; Alexandre, M.; Detrembleur, C. Straightforward synthesis of conductive graphene/polymer nanocomposites from graphite oxide. *Chemical Communications* **2011**, *47*, 2544-2546.

(444) Wang, G. R.; Liu, L. Q.; Dai, Z. H.; Liu, Q.; Miao, H.; Zhang, Z. Biaxial compressive behavior of embedded monolayer graphene inside flexible poly (methyl methacrylate) matrix. *Carbon* **2015**, *86*, 69-77.

(445) Wang, J. C.; Hu, H. T.; Wang, X. B.; Xu, C. H.; Zhang, M.; Shang, X. P. Preparation and Mechanical and Electrical Properties of Graphene Nanosheets-Poly(methyl methacrylate) Nanocomposites via In Situ Suspension Polymerization. *Journal of Applied Polymer Science* **2011**, *122*, 1866-1871.

(446) Wang, J. L.; Shi, Z. X.; Ge, Y.; Wang, Y.; Fan, J. C.; Yin, J. Solvent exfoliated graphene for reinforcement of PMMA composites prepared by in situ polymerization. *Materials Chemistry and Physics* **2012**, *136*, 43-50.

(447) Wang, W.; Jayatissa, A. H. Comparison study of graphene based conductive nanocomposites using poly(methyl methacrylate) and polypyrrole as matrix materials. *Journal of Materials Science-Materials in Electronics* **2015**, *26*, 7780-7783.

(448) Wang, W. L.; Jayatissa, A. H. Computational and experimental study of electrical conductivity of graphene/poly(methyl methacrylate) nanocomposite using Monte Carlo method and percolation theory. *Synthetic Metals* **2015**, *204*, 141-147.

(449) Yan, J. L.; Qi, G. Q.; Cao, J.; Luo, Y.; Yang, W.; Xie, B. H.; Yang, M. B. Study on Amino-functionalized Graphene Oxide/Poly(methyl methacrylate) Nanocomposites. *Chemistry Letters* **2012**, *41*, 683-685.

(450) Yang, J. T.; Yan, X. H.; Wu, M. J.; Chen, F.; Fei, Z. D.; Zhong, M. Q. Self-assembly between graphene sheets and cationic poly(methyl methacrylate) (PMMA) particles: preparation and characterization of PMMA/graphene composites. *Journal of Nanoparticle Research* **2012**, *14*.

(451) Yuan, X. Y.; Zou, L. L.; Liao, C. C.; Dai, J. W. Improved properties of chemically modified graphene/poly(methyl methacrylate) nanocomposites via a facile in-situ bulk polymerization. *Express Polymer Letters* **2012**, *6*, 847-858.

(452) Zeng, X. P.; Yang, J. J.; Yuan, W. X. Preparation of a poly(methyl methacrylate)-reduced graphene oxide composite with enhanced properties by a solution blending method. *European Polymer Journal* **2012**, *48*, 1674-1682.

(453) Zhang, H. B.; Zheng, W. G.; Yan, Q.; Jiang, Z. G.; Yu, Z. Z. The effect of surface chemistry of graphene on rheological and electrical properties of polymethylmethacrylate composites. *Carbon* **2012**, *50*, 5117-5125.

(454) Zhang, K.; Zhang, W. L.; Choi, H. J. Facile fabrication of self-assembled PMMA/graphene oxide composite particles and their electroresponsive properties. *Colloid and Polymer Science* **2013**, *291*, 955-962.

(455) Lin, C. Y.; Liu, T.; Zuo, M.; Li, H. H.; Chen, Q.; Zheng, Q. Effect of chemically reduced graphene oxide on the isothermal and non-isothermal phase separation behavior of poly(methyl methacrylate)/poly(styrene-co-acrylonitrile) binary polymer blends. *Rsc Advances* **2015**, *5*, 82259-82270.

(456) Ye, S. B.; Cao, Y. W.; Feng, J. C.; Wu, P. Y. Temperature-dependent compatibilizing effect of graphene oxide as a compatibilizer for immiscible polymer blends. *Rsc Advances* **2013**, *3*, 7987-7995.

(457) Mohamadi, S.; Sharifi-Sanjani, N.; Foyouhi, A. Evaluation of graphene nanosheets influence on the physical properties of PVDF/PMMA blend. *Journal of Polymer Research* **2013**, *20*.

- (458) Xing, Y.; Zhang, Y.; Zhang, H. M. Compatibilizing Effect of Graphene Oxide on Polyamide 6/Polystyrene Blends. *Acta Polymerica Sinica* **2015**, 706-712.
- (459) You, F.; Wang, D. R.; Li, X. X.; Liu, M. J.; Dang, Z. M.; Hu, G. H. Synthesis of Polypropylene- Grafted Graphene and Its Compatibilization Effect on Polypropylene/ Polystyrene Blends. *Journal of Applied Polymer Science* **2014**, 131.
- (460) Yu, Z. N. Thermal and Mechanical Properties of Smectic Main Chain Liquid Crystalline Networks. . Dissertation, Texas Tech University, 2015.
- (461) Li, T.; Zhou, C. L.; Jiang, M. UV ABSORPTION-SPECTRA OF POLYSTYRENE. *Polymer Bulletin* **1991**, 25, 211-216.
- (462) Zhang, H.-B.; Zheng, W.-G.; Yan, Q.; Jiang, Z.-G.; Yu, Z.-Z. The effect of surface chemistry of graphene on rheological and electrical properties of polymethylmethacrylate composites. *Carbon* **2012**, 50, 5117-5125.
- (463) Yang, Y.-K.; He, C.-E.; Peng, R.-G.; Baji, A.; Du, X.-S.; Huang, Y.-L.; Xie, X.-L.; Mai, Y.-W. Non-covalently modified graphene sheets by imidazolium ionic liquids for multifunctional polymer nanocomposites. *Journal of Materials Chemistry* **2012**, 22, 5666-5675.
- (464) Liu, N.; Luo, F.; Wu, H. X.; Liu, Y. H.; Zhang, C.; Chen, J. One-step ionic-liquid-assisted electrochemical synthesis of ionic-liquid-functionalized graphene sheets directly from graphite. *Advanced Functional Materials* **2008**, 18, 1518-1525.
- (465) Li, W.; Tang, X.-Z.; Zhang, H.-B.; Jiang, Z.-G.; Yu, Z.-Z.; Du, X.-S.; Mai, Y.-W. Simultaneous surface functionalization and reduction of graphene oxide with octadecylamine for electrically conductive polystyrene composites. *Carbon* **2011**, 49, 4724-4730.
- (466) Agnoli, S.; Granozzi, G. Second generation graphene: Opportunities and challenges for surface science. *Surface Science* **2013**, 609, 1-5.
- (467) Zhu, W.; Low, T.; Perebeinos, V.; Bol, A. A.; Zhu, Y.; Yan, H.; Tersoff, J.; Avouris, P. Structure and Electronic Transport in Graphene Wrinkles. *Nano Letters* **2012**, 12, 3431-3436.
- (468) Luo, J.; Jang, H. D.; Sun, T.; Xiao, L.; He, Z.; Katsoulidis, A. P.; Kanatzidis, M. G.; Gibson, J. M.; Huang, J. Compression and Aggregation-Resistant Particles of Crumpled Soft Sheets. *Acs Nano* **2011**, 5, 8943-8949.
- (469) Ma, X.; Zachariah, M. R.; Zangmeister, C. D. Crumpled Nanopaper from Graphene Oxide. *Nano Letters* **2012**, 12, 486-489.

(470) Zangmeister, C. D.; Ma, X.; Zachariah, M. R. Restructuring of Graphene Oxide Sheets into Monodisperse Nanospheres. *Chemistry of Materials* **2012**, *24*, 2554-2557.

(471) Wang, W.-N.; Jiang, Y.; Biswas, P. Evaporation-Induced Crumpling of Graphene Oxide Nanosheets in Aerosolized Droplets: Confinement Force Relationship. *Journal of Physical Chemistry Letters* **2012**, *3*, 3228-3233.

(472) Luo, J.; Jang, H. D.; Huang, J. Effect of Sheet Morphology on the Scalability of Graphene-Based Ultracapacitors. *Acs Nano* **2013**, *7*, 1464-1471.

(473) Mao, B. S.; Wen, Z.; Bo, Z.; Chang, J.; Huang, X.; Chen, J. Hierarchical Nanohybrids with Porous CNT-Networks Decorated Crumpled Graphene Balls for Supercapacitors. *Acs Applied Materials & Interfaces* **2014**, *6*, 9881-9889.

(474) Sohn, K.; Na, Y. J.; Chang, H.; Roh, K.-M.; Jang, H. D.; Huang, J. Oil absorbing graphene capsules by capillary molding. *Chemical Communications* **2012**, *48*, 5968-5970.

(475) Luo, J.; Zhao, X.; Wu, J.; Jang, H. D.; Kung, H. H.; Huang, J. Crumpled Graphene-Encapsulated Si Nanoparticles for Lithium Ion Battery Anodes. *Journal of Physical Chemistry Letters* **2012**, *3*, 1824-1829.

(476) Mao, S.; Wen, Z.; Kim, H.; Lu, G.; Hurley, P.; Chen, J. A General Approach to One-Pot Fabrication of Crumpled Graphene-Based Nanohybrids for Energy Applications. *Acs Nano* **2012**, *6*, 7505-7513.

(477) Chen, Y.; Guo, F.; Jachak, A.; Kim, S.-P.; Datta, D.; Liu, J.; Kulaots, I.; Vaslet, C.; Jang, H. D.; Huang, J.; Kane, A.; Shenoy, V. B.; Hurt, R. H. Aerosol Synthesis of Cargo-Filled Graphene Nanosacks. *Nano Letters* **2012**, *12*, 1996-2002.

(478) Chen, Y.; Guo, F.; Qiu, Y.; Hu, H.; Kulaots, I.; Walsh, E.; Hurt, R. H. Encapsulation of Particle Ensembles in Graphene Nanosacks as a New Route to Multifunctional Materials. *Acs Nano* **2013**, *7*, 3744-3753.

(479) Mao, S.; Wen, Z.; Huang, T.; Hou, Y.; Chen, J. High-performance bi-functional electrocatalysts of 3D crumpled graphene-cobalt oxide nanohybrids for oxygen reduction and evolution reactions. *Energy & Environmental Science* **2014**, *7*, 609-616.

(480) Guo, F.; Kim, F.; Han, T. H.; Shenoy, V. B.; Huang, J.; Hurt, R. H. Hydration-Responsive Folding and Unfolding in Graphene Oxide Liquid Crystal Phases. *Acs Nano* **2011**, *5*, 8019-8025.

- (481) Sen, D.; Bahadur, J.; Mazumder, S.; Verma, G.; Hassan, P. A.; Bhattacharya, S.; Vijai, K.; Doshi, P. Nanocomposite silica surfactant microcapsules by evaporation induced self assembly: tuning the morphological buckling by modifying viscosity and surface charge. *Soft Matter* **2012**, *8*, 1955-1963.
- (482) Cranford, S. W.; Buehler, M. J. Packing efficiency and accessible surface area of crumpled graphene. *Physical Review B* **2011**, *84*.
- (483) Tallinen, T.; Astrom, J. A.; Timonen, J. The effect of plasticity in crumpling of thin sheets. *Nature Materials* **2009**, *8*, 25-29.
- (484) Pereira, V. M.; Castro Neto, A. H.; Liang, H. Y.; Mahadevan, L. Geometry, Mechanics, and Electronics of Singular Structures and Wrinkles in Graphene. *Physical Review Letters* **2010**, *105*.
- (485) Vehring, R. Pharmaceutical particle engineering via spray drying. *Pharmaceutical Research* **2008**, *25*, 999-1022.
- (486) Nandiyanto, A. B. D.; Okuyama, K. Progress in developing spray-drying methods for the production of controlled morphology particles: From the nanometer to submicrometer size ranges. *Advanced Powder Technology* **2011**, *22*, 1-19.
- (487) Kho, K.; Hadinoto, K. Aqueous re-dispersibility characterization of spray-dried hollow spherical silica nano-aggregates. *Powder Technology* **2010**, *198*, 354-363.
- (488) Cheow, W. S.; Li, S.; Hadinoto, K. Spray drying formulation of hollow spherical aggregates of silica nanoparticles by experimental design. *Chemical Engineering Research & Design* **2010**, *88*, 673-685.
- (489) Parviz, D.; Metzler, S. D.; Das, S.; Irin, F.; Green, M. J. Tailored Crumpling and Unfolding of Spray-Dried Pristine Graphene and Graphene Oxide Sheets. *Small* **2015**.
- (490) Hu, H.; Xin, J. J.; Hu, H.; Wang, X.; Lu, X. Organic Liquids-Responsive β -Cyclodextrin-Functionalized Graphene-Based Fluorescence Probe: Label-Free Selective Detection of Tetrahydrofuran. *Molecules* **2014**, *19*, 7459-7479.
- (491) Huang, P.; Xu, C.; Lin, J.; Wang, C.; Wang, X. S.; Zhang, C. L.; Zhou, X. J.; Guo, S. W.; Cui, D. X. Folic Acid-conjugated Graphene Oxide loaded with Photosensitizers for Targeting Photodynamic Therapy. *Theranostics* **2011**, *1*, 240-250.
- (492) Wei, N.; Lv, C.; Xu, Z. Wetting of Graphene Oxide: A Molecular Dynamics Study. *Langmuir* **2014**, *30*, 3572-3578.

- (493) Irin, F.; Hansen, M. J.; Bari, R.; Parviz, D.; Metzler, S. D.; Bhattacharia, S. K.; Green, M. J. Adsorption and removal of graphene dispersants. *Journal of Colloid and Interface Science* **2015**, *446*, 282-289.
- (494) Tsapis, N.; Dufresne, E. R.; Sinha, S. S.; Riera, C. S.; Hutchinson, J. W.; Mahadevan, L.; Weitz, D. A. Onset of buckling in drying droplets of colloidal suspensions. *Physical Review Letters* **2005**, *94*.
- (495) Bahadur, J.; Sen, D.; Mazumder, S.; Bhattacharya, S.; Frieinghaus, H.; Goerigk, G. Origin of Buckling Phenomenon during Drying of Micrometer-Sized Colloidal Droplets. *Langmuir* **2011**, *27*, 8404-8414.
- (496) Bahadur, J.; Sen, D.; Mazumder, S.; Paul, B.; Bhatt, H.; Singh, S. G. Control of Buckling in Colloidal Droplets during Evaporation-Induced Assembly of Nanoparticles. *Langmuir* **2012**, *28*, 1914-1923.
- (497) Chang, C.; Song, Z.; Lin, J.; Xu, Z. How graphene crumples are stabilized? *Rsc Advances* **2013**, *3*, 2720-2726.
- (498) Stevens, B.; Dessiatova, E.; Hagen, D. A.; Todd, A. D.; Bielawski, C. W.; Grunlan, J. C. Low-Temperature Thermal Reduction of Graphene Oxide Nanobrick Walls: Unique Combination of High Gas Barrier and Low Resistivity in Fully Organic Polyelectrolyte Multilayer Thin Films. *ACS Applied Materials & Interfaces* **2014**, *6*, 9942-9945.
- (499) Jiang, D.-e.; Cooper, V. R.; Dai, S. Porous graphene as the ultimate membrane for gas separation. *Nano letters* **2009**, *9*, 4019-4024.
- (500) Biener, J.; Stadermann, M.; Suss, M.; Worsley, M. A.; Biener, M. M.; Rose, K. A.; Baumann, T. F. Advanced carbon aerogels for energy applications. *Energy & Environmental Science* **2011**, *4*, 656-667.
- (501) Lei, Z.; Lu, L.; Zhao, X. S. The electrocapacitive properties of graphene oxide reduced by urea. *Energy & Environmental Science* **2012**, *5*, 6391-6399.
- (502) Liu, Y.; Xie, B.; Zhang, Z.; Zheng, Q.; Xu, Z. Mechanical properties of graphene papers. *Journal of the Mechanics and Physics of Solids* **2012**, *60*, 591-605.
- (503) Wu, Z. S.; Winter, A.; Chen, L.; Sun, Y.; Turchanin, A.; Feng, X.; Müllen, K. Three-Dimensional Nitrogen and Boron Co-doped Graphene for High-Performance All-Solid-State Supercapacitors. *Advanced Materials* **2012**, *24*, 5130-5135.

(504) Cao, X.; Shi, Y.; Shi, W.; Lu, G.; Huang, X.; Yan, Q.; Zhang, Q.; Zhang, H. Preparation of novel 3D graphene networks for supercapacitor applications. *Small* **2011**, *7*, 3163-3168.

(505) Bai, H.; Li, C.; Wang, X.; Shi, G. On the gelation of graphene oxide. *The Journal of Physical Chemistry C* **2011**, *115*, 5545-5551.

(506) Worsley, M. A.; Kucheyev, S. O.; Mason, H. E.; Merrill, M. D.; Mayer, B. P.; Lewicki, J.; Valdez, C. A.; Suss, M. E.; Stadermann, M.; Pauzauskie, P. J. Mechanically robust 3D graphene macroassembly with high surface area. *Chemical Communications* **2012**, *48*, 8428-8430.

(507) Worsley, M. A.; Olson, T. Y.; Lee, J. R.; Willey, T. M.; Nielsen, M. H.; Roberts, S. K.; Pauzauskie, P. J.; Biener, J.; Satcher Jr, J. H.; Baumann, T. F. High surface area, sp²-cross-linked three-dimensional graphene monoliths. *The journal of physical chemistry letters* **2011**, *2*, 921-925.

(508) Worsley, M. A.; Pauzauskie, P. J.; Olson, T. Y.; Biener, J.; Satcher Jr, J. H.; Baumann, T. F. Synthesis of graphene aerogel with high electrical conductivity. *Journal of the American Chemical Society* **2010**, *132*, 14067-14069.

(509) Wang, J.; Ellsworth, M. Graphene aerogels. *Ecs Transactions* **2009**, *19*, 241-247.

(510) Wu, Y.; Yi, N.; Huang, L.; Zhang, T.; Fang, S.; Chang, H.; Li, N.; Oh, J.; Lee, J. A.; Kozlov, M.; Chipara, A. C.; Terrones, H.; Xiao, P.; Long, G.; Huang, Y.; Zhang, F.; Zhang, L.; Lepro, X.; Haines, C.; Lima, M. D.; Lopez, N. P.; Rajukumar, L. P.; Elias, A. L.; Feng, S.; Kim, S. J.; Narayanan, N. T.; Ajayan, P. M.; Terrones, M.; Aliev, A.; Chu, P.; Zhang, Z.; Baughman, R. H.; Chen, Y. Three-dimensionally bonded spongy graphene material with super compressive elasticity and near-zero Poisson's ratio. *Nature Communications* **2015**, *6*.

(511) Sudeep, P. M.; Narayanan, T. N.; Ganesan, A.; Shaijumon, M. M.; Yang, H.; Ozden, S.; Patra, P. K.; Pasquali, M.; Vajtai, R.; Ganguli, S.; Roy, A. K.; Anantharaman, M. R.; Ajayan, P. M. Covalently Interconnected Three-Dimensional Graphene Oxide Solids. *Acs Nano* **2013**, *7*, 7034-7040.

(512) Li, C.; Shi, G. Three-dimensional graphene architectures. *Nanoscale* **2012**, *4*, 5549-5563.

(513) Parviz, D.; Metzler, S. D.; Das, S.; Irin, F.; Green, M. J. Tailored Crumpling and Unfolding of Spray-Dried Pristine Graphene and Graphene Oxide Sheets. *Small* **2015**, *11*, 2661-2668.

(514) Lv, W.; Zhang, C.; Li, Z.; Yang, Q.-H. Self-Assembled 3D Graphene Monolith from Solution. *Journal of Physical Chemistry Letters* **2015**, *6*, 658-668.

(515) Yao, B.; Chen, J.; Huang, L.; Zhou, Q.; Shi, G. Base-Induced Liquid Crystals of Graphene Oxide for Preparing Elastic Graphene Foams with Long-Range Ordered Microstructures. *Advanced Materials* **2015**, n/a-n/a.

(516) Coluci, V. R.; Martinez, D. S. f. T.; Honório, J. G.; de Faria, A. i. F.; Morales, D. A.; Skaf, M. S.; Alves, O. L.; Umbuzeiro, G. A. Noncovalent interaction with graphene oxide: the crucial role of oxidative debris. *The Journal of Physical Chemistry C* **2014**, *118*, 2187-2193.

(517) Faria, A. F.; Martinez, D. S. T.; Moraes, A. C.; Maia da Costa, M. E.; Barros, E. B.; Souza Filho, A. G.; Paula, A. J.; Alves, O. L. Unveiling the role of oxidation debris on the surface chemistry of graphene through the anchoring of Ag nanoparticles. *Chemistry of Materials* **2012**, *24*, 4080-4087.

(518) Ruzicka, B.; Zaccarelli, E. A fresh look at the Laponite phase diagram. *Soft Matter* **2011**, *7*, 1268-1286.

(519) Wu, Q.; Meng, Y.; Wang, S.; Li, Y.; Fu, S.; Ma, L.; Harper, D. Rheological Behavior of Cellulose Nanocrystal Suspension: Influence of Concentration and Aspect Ratio. *Journal of Applied Polymer Science* **2014**, *131*.